UNIVERSITE DE STRASBOURG

Ecole Doctorale des Sciences de la Vie et de la Santé

THESE

présentée pour obtenir le grade de

Docteur de l'Université de Strasbourg

Discipline : Sciences du Vivant

Domaine : Aspects Moléculaires et Cellulaires de la Biologie

par

Oleksandr KUCHERAK

NOUVELLES SONDES FLUORESCENTES MEMBRANAIRES POUR ETUDIER L'APOPTOSE ET L'ORDRE LIPIDIQUE

Soutenue le 17 mai 2011 devant la commission d'examen :

Dr. Chantal ANDRAUD	**Rapporteur externe**
Dr. Laurence SALOME	**Rapporteur externe**
Pr. Line BOUREL	**Examinateur**
Dr. Jean-Claude CHAMBRON	**Examinateur**
Dr. Andrey KLYMCHENKO	**Examinateur**
Pr. Yves MELY	**Directeur de thèse**

UMR CNRS 7213, Faculté de Pharmacie, ILLKIRCH

First of all, I would like to thank Pr. Yves Mély for the opportunity to work in the Laboratory of Biophotonics and Pharmacology.

I would like to express my deepest gratitude and respect to Dr. Andrey Klymchenko, who has supported me throughout my thesis with his patience and knowledge whilst allowing me the space to work in my own way. One simply could not wish for a better and friendlier supervisor. I will always remember his jokes about “Prodan killer” when I joined the lab in 2007. I attribute the level of my skills to his encouragement and effort and without him this thesis, too, would not have been completed.

My work would not have been possible without the essential and gracious support of many people, who surrounded me by friendly and cheerful atmosphere in a daily life. My friends, it has been a real pleasure to work with all of you. Our communication has encouraged, supported and enlightened me. Without your willingness, suggestions and discussions, this thesis would never have been done. I cherish our time we spent together and hope that we will keep in touch despite the passing of time. I could not possibly name everyone who has contributed to this work (Guy Duportail, Sule Oncul, Viktoriia Postupalenko, Namrata Jain, Zeinab Darwich, Youri Arntz...), and I bag my apologies if I have not mentioned everyone to whom acknowledgement is due. I owe a great deal of gratitude to all of you!

Finally, I thank my family for their love and support throughout all my studies at the University of Strasbourg. I felt your presence right beside me all the time, and it helped me to accomplish this thesis.

Oleksandr Kucherak, Illkirch, May 2011

Abbreviation

3HC	3-Hyrdoxychromone
3HF	3-Hydroxyflavone
Chol	Cholesterol
DMF	Dimethylformamide
DMSO	Dimethylsulfoxide
DOPC	Dioleoylphosphatidylcholine
DOPS	Dioleoylphosphatidylserine
DPPC	Dipalmitoylphosphatidylcholine
ESIPT	Excited-State Intramolecular Proton Transfer
GUVs	Giant Unilamellar Vesicles
LUVs	Large Unilamellar Vesicles
Ld	Liquid Disordered phase
Lo	Liquid Ordered phase
NR	Nile Red
N*/T*	Intensity ratio of the N* and T* bands
QY	Quantum Yield of fluorescence
RT	Room Temperature
SM	Sphingomyelin
THF	Tetrahydrofuran
Tm	Melting (transition) temperature of lipid
λ_{abs}	Position of absorbtion maximum
λ_{fluo}	Position of fluorescence maximum (i.e. emission maximum)

Why fluorescence?

Fluorescence techniques have three major advantages over other instrumental methods: high sensitivity, high speed performance, and non-invasivity.

- Sensitivity - the most important issue since each molecule can emit thousands of photons that can be individually detected with modern detectors. Whereas absorbance measurements can reliably be used at concentrations down of several tenths of a micromolar, fluorescence can be used at concentrations thousands times smaller: pico- and even femtomolar.

- Using fluorescence one can monitor very rapid changes in concentration or conformation, since changes in fluorescence intensity on the order of picoseconds can be detected.

- The point of non-invasivity refers to the fact that samples are not affected or destroyed in the process, and usually no hazardous by-products are generated.

Due to its non-invasive character, fluorescence can be used in living cells and tissues with limited adverse effects. As a consequence, fluorescence has proven to be a versatile tool for a large range of applications as for instance:

- monitoring binding of ligands to biochemical species;
- measurement of distances within macromolecules and biological assemblies;
- study of the dynamics of protein folding;
- measurement of ion concentrations inside living cells;
- study of membrane structure and function;
- study of drug interactions with cell receptors, etc.

Fluorescence is a powerful technique for studying molecular interactions in analytical chemistry, biochemistry, cell biology, physiology, photochemistry, environmental science. In fact, fluorescence offers much more than mere signal-gathering capability. New developments in instrumentation, software, probes and applications have resulted in a burst of popularity for a technique that was firstly observed over 150 years ago.

CHAPTER 1

BIBLIOGRAPHICAL REVIEW

1. BIBLIOGRAPHICAL REVIEW

1.1. Fluorescence

1.1.1. Principles of fluorescence

Fluorescence belongs to the general photophysical phenomenon called luminescence, which corresponds to the emission of light from electronically excited states of atoms and molecules. Two types of molecular luminescence can be considered depending on the nature of their excited state. If the emission occurs from the singlet excited state, the process is called *fluorescence*. The emission rates of fluorescence are typically about 10^8-10^9 s^{-1}. If the emission occurs from the triplet excited state, the process is called *phosphorescence*. In this case, transitions to the ground state are forbidden and the emission rates are slow, about 10^6-$10\ s^{-1}$. Fluorescence occurs in a limited number of molecules (generally polyaromatic hydrocarbons or heterocycles) called fluorophores or fluorescent dyes. The process responsible for fluorescence is illustrated by the Jablonski diagram (Fig. 1.1). Three main steps are important in the fluorescence process: excitation, non-radiative relaxation and fluorescence emission (Lakowicz 2006).

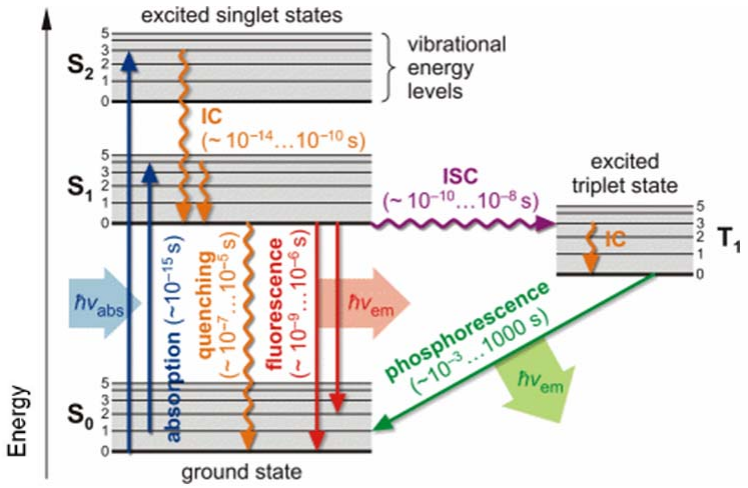

Figure 1.1. Jablonski diagram.

The fluorophore typically exists in the ground state (S_0). Upon excitation by light quantum ($h\nu_{abs}$) it is transferred to one of the excited vibrational states of the first electronic singlet state (S_1). The excess of vibrational energy is rapidly transferred to the solvent through collisions with the solvent molecules. Within state S_1 this nonradiative process is called *vibrational relaxation* (Fig. 1.1) and occurs in the sub-picosecond range. If the fluorophore is excited to the second electronic singlet state (S_2), it rapidly falls down to the S_1 state due to *internal conversion* (IC) that corresponds to a non-radiative transition between two isoenergetic vibrational states belonging to electronic states of the same spin multiplicity. Intersystem crossing (ISC) is another non-radiative transition that occurs between two isoenergetic vibrational levels belonging to electronic states of different multiplicities. Finally, other processes such as collisional quenching and fluorescence resonance energy transfer (FRET) may depopulate state S_1 and, together with internal conversion and intersystem crossing, compete with fluorescence.

Fluorescence emission is a radiative process in which a photon is emitted while the fluorophore is going back to its ground state S_0. The difference in energy or wavelength of the absorbed and emitted light is called the Stokes shift. The Stokes shift is an important parameter for the sensitivity of fluorescence techniques because it allows the detection of emission photons with a low background, as they are easily discriminated from the excitation photons. An important characteristic of fluorescence is the fluorescence quantum yield, which is the ratio of the number of fluorescence photons emitted to the number of photons absorbed. If no chemical degradation occurs, the same fluorophore can repeatedly emit photons under constant illumination. The fact that a single molecule can generate a large amount of photons is of main importance for the high sensitivity of fluorescence techniques. In solutions the fluorescent molecules are characterized by broad fluorescence excitation and emission spectra. The bandwidths of these spectra are important parameters in fluorescence assays where two or more different fluorophores are simultaneously detected.

1.1.2. Excited-state reactions

An excited-state reaction can be defined as a molecular process which occurs subsequent to excitation and which changes the structure of the excited-state fluorophore (Lakowicz 2006). An example of excited-state reaction is that of β-naphthol, which in neutral solution can loose its phenolic proton in the excited state (excitated state proton transfer). Deprotonation occurs more readily in the excited state because the electrons on the phenolic hydroxyl group are shifted to the aromatic ring making this hydroxyl group more acidic. Another interesting example is the excited-state intramolecular proton transfer (ESIPT) reaction. In this reaction, the proton is transfered between groups of the same molecule in the excited state. The ESIPT reaction is the basis of the probes developed in the present study. Its characteristics and applications will be described in the following chapters.

Another example of excited-state reaction is photoinduced charge transfer (PCT) that found a large range of applications in the construction of polarity sensitive fluorophores including labels for proteins. Among the well-known polarity sensitive probes are ANS (1-anilino-8-naphthalene sulfonate), TNS (p-toluidinyl-6-naphthalene sulfonate), Prodan (6-propionyl-2-dimethylamino naphthalene) and theirs derivatives. More details about them and their applications will be discussed in following chapters. PCT can be associated with twisted intramolecular charge transfer (TICT) due to internal rotation of the molecule in the excited state. TICT-dyes, or so-called molecular rotors, found numerous applications in the design of viscosity sensitive fluorescent probes. Examples of molecular rotors are DMABN (p-N,N-dimethylamino-benzylidene malononitrile) and its analogues.

Excimer and exciplex formation can also be considered as excited-state reactions, as for example pyrene excimer formation, or 2-phenylindole and anthracene exciplexes formed on interaction with dimethylaniline.

1.1.3. Solvatochromism

The fluorescence process described above does not take into consideration the influence of the solvent that can strongly modify the emission of a fluorophore. Such solvent effects shift the emission to still lower energies owing to a stabilization of the excited state by the solvent molecules. Typically, the fluorophore shows a larger dipole moment in the excited state (μ_e) than in the ground state (μ_g) due to a photoinduced charge transfer (PCT). Following excitation the solvent dipoles can reorient or relax around μ_e, which lowers the energy of the excited state thus leading to

a relaxation process called solvent relaxation (Fig. 1.2). This effect becomes larger with increasing solvent polarity, resulting in emission at lower energies (or longer wavelengths). The shift of the emission band in response to changes in solvent polarity is called fluorescence solvatochromism. In general, only fluorophores that have high dipole moment in the ground or excited state are able to display a large fluorescence solvatochromism. They are called solvatochromic or environment-sensitive dyes. Apolar molecules such as unsubstituted aromatic hydrocarbons, or symmetric molecules such as fluorescein, rhodamine and cyanine dyes are much less environmentally sensitive.

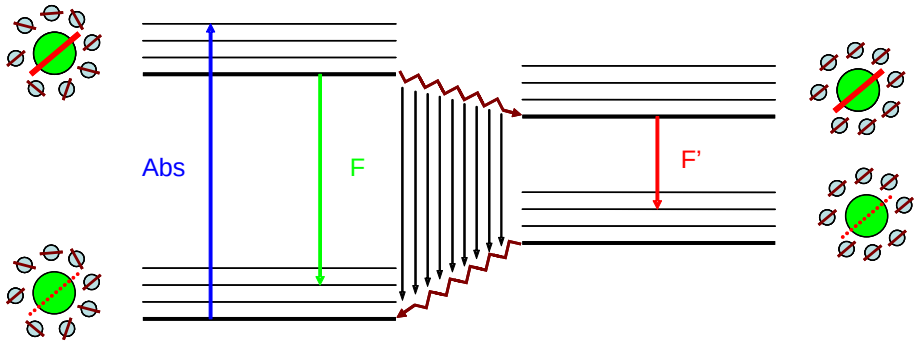

Figure 1.2. Solvent relaxation around a probe with a small dipole moment in its ground state and a large dipole moment in its excited state.

In the description of general (non-specific) solvent effects, the fluorophore is considered to be a dipole in a continuous medium of uniform dielectric constant. The interactions between the solvent and fluorophore affect the energy difference between the ground and the excited state. To a first approximation, this energy difference is a function of the refractive index (n) and dielectric constant (ε) of the solvent and is described by the Lippert-Mataga equation (Mataga and Kubota 1970; Lippert 1975):

$$\bar{\nu}_a - \bar{\nu}_f = \frac{2}{hc}(\mu_e - \mu_g)^2 a^{-3} \Delta f + const \quad (1)$$

where h is the Planck's constant, c is the velocity of light, $\mu_e - \mu_g$ is a change in dipole moment, a is the radius of the cavity in which the solute resides, *const* is a constant taking into account the non-radiative relaxation, and Δf is the orientation polarizability defined as:

$$\Delta f = f(\varepsilon) - f(n^2) = \frac{\varepsilon - 1}{2\varepsilon + 1} - \frac{n^2 + 1}{2n^2 + 1} \quad (2)$$

According to this equation, the Stokes shift of a dye is proportional to the square of its transition moment and the orientation polarizability of solvent. It is frequently used to measure the transition dipole moment of new fluorophores based on spectroscopic measurements in solvents of different polarity. However, it should be noted that specific solvent-fluorophore interactions, such as H-bonding, produce strong deviations from the theory. Thus, the fluorescence solvatochromism reflects usually both universal and specific interactions taking place between the emitting molecule and its microenvironment.

1.2. Synthetic fluorescent dyes

Fluorescent dyes are essential tools in biological research. The selection of an appropriate dye and of the corresponding fluorescence technique depends entirely on the biological system and the problem of study. Here we will highlight only the most important examples of chromophores and their applications. All known fluorophores could be divided into two main classes based on their origin: (1) natural fluorophores, which are synthesized by nature in living organisms as for example, aminoacids like tryptophan, tyrosine and phenylalanine (Demchenko 1986) or green fluorescent protein (Shaner et al., 2007; Chudakov et al., 2010); and (2) synthetic fluorophores, obtained artificially by chemical synthesis. The latter class could be further splitted into "classical" (environment-insensitive) and environment-sensitive dyes. Here only synthetic fluorophores are discussed.

1.2.1. "Classical" synthetic dyes

The most well-known and probably the most common dyes are fluorescein and rhodamine (Fig. 1.3). Fluorescein was first synthesized by Baeyer in 1871 and still remains one of the most popular dyes. Rhodamine is an amino-containing analog of fluorescein. It bears a positive charge delocalized between two amino groups through a conjugated aromatic system. Usually rhodamines are much more photostable and less pH-sensitive than fluoresceins.

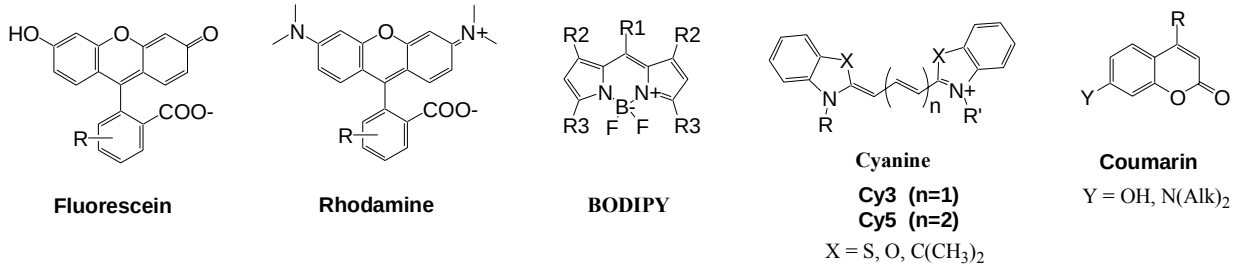

Figure 1.3. The most common synthetic fluorescent dyes.

Another common family of dyes is BODIPY derivatives, which were firstly discovered in 1968 by Treibs and Kreuzer. They are strongly absorbing small molecules that emit a relatively narrow fluorescence band with high quantum yields. BODIPY dyes are slightly sensitive to the polarity and pH of their environment and are reasonably stable in physiological conditions. Meantime, they have some disadvantages like poor water solubility and small Stokes shift. Nowadays, the chemistry and application of BODIPY dyes are increasingly developing (Loudet and Burgess 2007; Ulrich et al., 2008).

Cyanine dyes (Mishra et al., 2000) are based on a polymethine chain ended by two amino/imino groups. Most popular cyanine dyes contain heterocyclic rings that increase the stability and make their synthesis easier. This family of dyes is characterized by high extinction coefficients and red-shifted absorption maxima. Both parameters depend strongly on the length of the polymethine chain.

Coumarin dyes (Fig. 1.3) is a relative old class of dyes, which found a number of biological applications mainly due to the small size and good water solubility (Eggeling et al., 1997). However, its fluorescence properties, such as absorption in UV-region and low photostability are clear disadvantages compared to all other dyes mentioned above.

We also should mention other families of dyes such as Alexa, ATTO, DyLight, HiLyte Fluors, etc. These are recently developed fluorophores characterized by significantly improved spectroscopic properties.

1.2.2. Environment-sensitive dyes with single emission band

Unlike the "classical" fluorescent dyes, environment-sensitive dyes can change their fluorescence properties (fluorescence intensity or emission color) in response to changes in the physico-chemical properties of their molecular environment. Their response to the environment is driven by excited-state reactions in their fluorescent cores (conformational change or charge, electron and proton transfer, etc.) and their non-covalent interactions with surrounding, like universal interactions (van der Waals, dipole-dipole, dipole-external electric field, etc.) and specific H-bonding interactions. Here we do not consider pH- and ion-sensitive dyes as environment-sensitive, since the response of these dyes is associated with changes in their chemical structure: protonation/deprotonation or formation of a complex with an ion. Most of the environment-sensitive dyes can be classified into two types: molecular rotors and solvatochromic dyes.

The **molecular rotors** are fluorophores exhibiting a strong variation of their fluorescence quantum yields as a function of their intramolecular rotation. Therefore, the fluorescence intensity of these dyes depends on the environment viscosity. In more viscous media these rotations are slowed down, which increases the fluorescence intensity of the dye. Being incorporated into lipid membranes or proteins these fluorophores monitor the microviscosity of the surrounding at the sites of their location. Typical examples of these probes are DCVJ, its carboxy-analogue (Haidekker and Theodorakis 2007) and some recently developed analogues of Prodan (Kim et al., 2008) (Fig. 1.4).

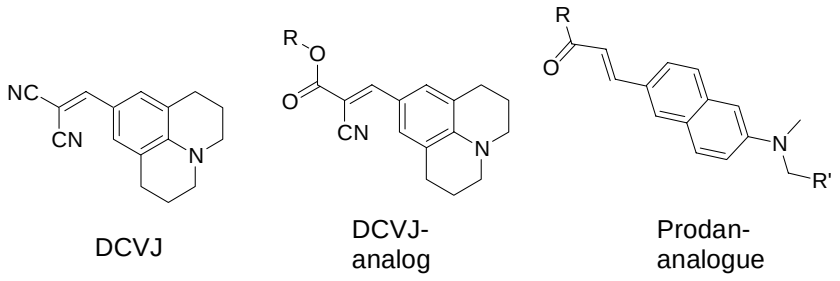

Figure 1.4. Representative examples of molecular rotors.

A more widely used class of environment-sensitive fluorophores is **solvatochromic dyes** exhibiting shifts in their emission spectra as a function of polarity and hydration of their environment. These dyes exhibit strong changes in dipole moments upon electronic excitation. Universal dipole-dipole and specific H-bonding interactions of these dyes with their surrounding change the energy of the electronic transition and, thus, shift the maxima of their excitation and emission spectra (Mataga and Kubota 1970; Lippert 1975). A typical example of such dye is Prodan (2-propionyl-6-dimethylaminonaphthalene) (Weber and Farris 1979). In this fluorophore, the dipole moment increases dramatically upon electronic excitation due to an intramolecular charge transfer (ICT) from the electron donor dialkylamino group to the electron acceptor carbonyl group (Fig.1.5). As a result, these dyes exhibit a red-shift of their emission spectrum in response to an increase in solvent polarity, and in relaxation rates of their surroundings (Parasassi et al., 1994a; Sykora et al., 2002; Lakowicz 2006). Moreover, an additional strong red-shift of the Prodan emission is connected to the interaction with H-bond donor molecules of the surrounding (Catalan et al., 1991; Samanta and Fessenden 2000; Cerezo et al., 2001). This specific effect is typical for environment-sensitive dyes containing H-bond acceptor groups (such as carbonyl) and is of particular interest for studying environment hydration (water is a strong H-bond donor). An additional important property of environment-sensitive dyes is their poor fluorescence intensity in water due to electron transfer to water. Therefore, incorporation of these dyes into proteins and lipid membranes usually results in strong increase of the fluorescence intensity due to efficient screening of these molecules from bulk water (Slavik 1982).

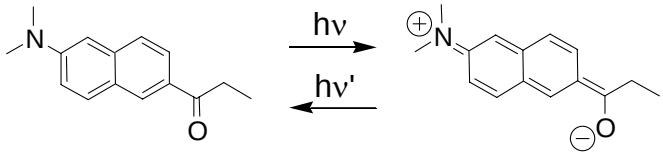

Figure 1.5. Typical solvatochromic fluorescent dye (Prodan) and its excited-state intramolecular charge transfer.

One of the first solvatochromic dyes used for protein and membrane studies was 1,8-ANS (Weber and Daniel 1966). This dye as well as its analogue 2,6-TNS (Fig. 1.6) are essential tools for protein and membrane investigations (Slavik 1982; Lakowicz 2006). In addition to their strong solvent-dependent shifts in the fluorescence spectrum, they show dramatic increase in fluorescence intensity on binding to biomolecules. In bulk water the fluorescence of these dyes is strongly quenched by an electron transfer to water, while being bound to proteins or lipid membranes they are efficiently screened from water resulting in a strong fluorescence increase. The other naphthalene sulfonic acid analogues, which found even more applications in biology, are dansyl-derivatives (Fig. 1.6). The reactive derivative dansyl chloride is a label for amino groups in proteins and lipids. Similarly to 1,8-ANS, the emission color and emission intensity of the dansyl moiety is highly sensitive to solvent polarity (Holmes-Farley and Whitesides 1986; Goncalves 2009).

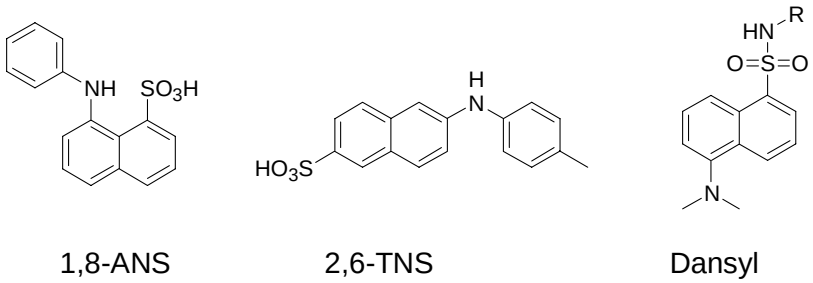

Figure 1.6. Commonly used naphthalene sulfonic acid derivatives.

As it was already mentioned, the most common solvatochromic fluorophore that displays sensitivity to the polarity of its local environment is Prodan (Weber and Farris 1979). Due to very strong fluorescence solvatochromism and high fluorescence quantum yield, this dye and its derivatives, found numerous applications in protein and membrane studies (Haskard and Li-Chan 1998; Moreno et al., 1999; Kaur and Horowitz 2004; Sykora et al., 2005; Bagatolli 2006). However, the key disadvantage of this dye is its absorption in the UV range (360 nm), which limits its applications in cellular studies. In order to shift the absorbance of Prodan to the red, Lu and coworkers (Lu et al., 2006) have synthesized its benzo-analogue 2-propionyl-6-dimethylaminoanthracene, Anthradan (Fig. 1.7). The main advantage of this red-shifted dye is the possibility to avoid interference from the autofluorescence of many biological components and allow a more favorable excitation wavelength for fluorescence microscopy applications. However, this dye showed decreased extinction coefficient compared to parent Prodan.

The other important family of environment-sensitive dyes, which recently attracted attention of biophysicists, is phthalimide-derivatives (Fig. 1.7). The smallest of them, 4-N,N-dimethylamino phthalimide (4DMP) can be considered as one of the first chromophores for polarity sensing. This relatively small and rigid molecule presents a very strong solvent sensitivity, namely its emission shifts from 440 nm in diethyl ether to 560 nm in water (Soujanya et al., 1996). However, it also shows absorption in the UV region (380-390 nm) and very low extinction coefficient. In order to improve these properties, the 4DMP fluorophore was extended to a new environment-sensitive dye 6-N,N-dimethylamino-2,3-naphthalimide (6DMN) (Vazquez et al., 2005). This fluorophore

exhibited interesting fluorescence properties with emission in the 500-600 nm range and complex (fluorescence intensity and position of the maximum) response to the changes of environment polarity, though its absorption properties were not considerably improved. In this respect, a recently developed analogue of 4DMP, 4-N,N-Dimethylamino-1,8-naphthalimide (4DMN), constitutes a significant improvement showing absorption maximum shifted to 440 nm. It should be noted that similarly to 1,8-ANS, 4DMP and all its analogues are nearly non-fluorescent in water and become highly fluorescent in aprotic media. These properties are important for intensiometric detection of molecular interactions (Loving and Imperiali 2008). However, their poor fluorescence in water makes them inefficient in cases where the label shows significant water exposure at all steps of interaction (for example, peptide-DNA interactions).

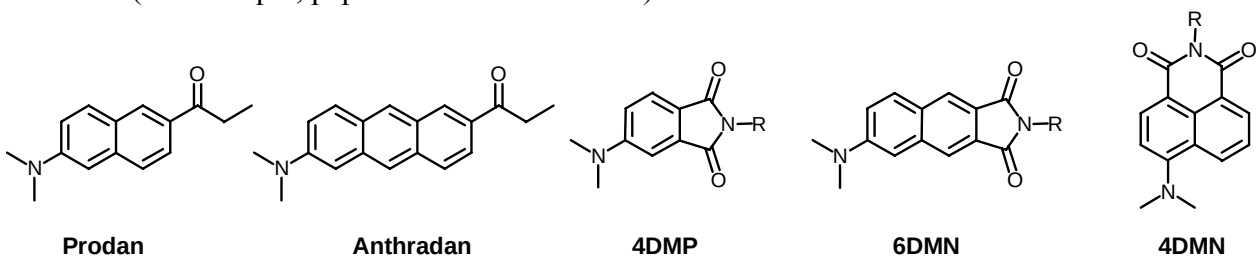

Figure 1.7. Prodan, its analogue Anthradan, phthalimide and naphthymide derivatives.

In the search of advanced environment-sensitive dyes a bichromophoric dye Fluoroprobe (Fig. 1.8) was developed (Mes et al., 1984). This dye exhibits a charge transfer through space, which generates an exceptional transition dipole moment (27 D) and showed high solvent sensitivity. For the moment, Fluoroprobe remains the most environment-sensitive dye (Table 1.1). However, this dye found no applications in biology, due to the extremely strong quenching of its fluorescence in polar media, UV absorption maximum (308 nm) and very low extinction coefficient.

It is also worth to mention a recently introduced Dapoxyl dye showing exceptionally high fluorescent solvatochromism (Diwu et al., 1997). This dye shows 200 nm red shift from hexane to water/acetonitrile (4/1) mixture. It presents strong a fluorescence quantum yield and high extinction coefficient, though its absorption in UV remains a disadvantage.

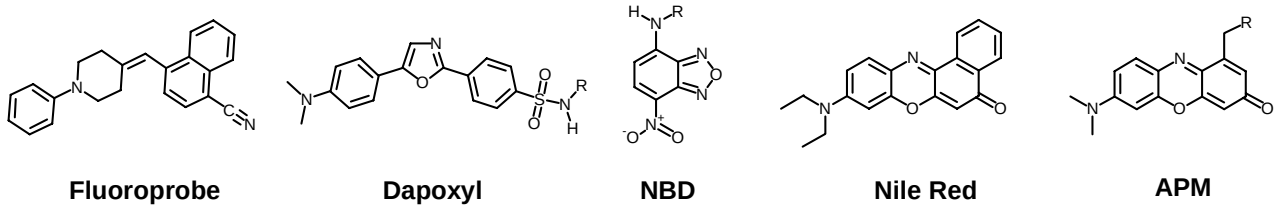

Figure 1.8. Advanced fluorescent solvatochromic dyes.

Remarkably, the vast majority of environment-sensitive dyes show absorption in the UV-region, while few dyes present significantly red shifted absorption and emission. These are NBD (Chattopadhyay 1990) and Nile Red (Diaz et al., 2008) dyes and their analogues (Fig. 1.8). Indeed, the absorption maximum of NBD derivatives is centred around 460-480 nm while for Nile Red (Greenspan et al., 1985) and its recently introduced analogue APM (Cohen et al., 2005) it is 530 and 560 nm, respectively. The extinction coefficient and the fluorescence quantum yields of these dyes are relatively good (Table 1.1). However, these favorable spectroscopic properties are compensated by a sever disadvantage: poor fluorescence solvatochromism, which makes them weakly sensitive in the applications where relatively small variations of the environment properties are expected.

Table 1.1. Properties of common solvatochromic fluorescent dyes.[a]

Dye	λ_{Abs}, nm (MeOH)	ε_{max} (MeOH)	Polar solvent (MeOH)		Apolar solvent (Toluene)		$\Delta\nu_{Fluo}$, cm^{-1}
			λ_{Fluo}, nm	QY, %	λ_{Fluo}, nm	QY, %	
Fluoroprobe	308 cyclohexane	12000	695 acetonitrile	<0.1 acetonitrile	476	46	6620
Dapoxyl SEDA	373	28000	584	39	457	86	4760
Prodan	361	18400	498	51	417	55	3900
6DMN	382	8000	589	1.2	491	21	3390
Anthradan	456	12100 (THF)	604	41	507	58	3170
DMAP	396	6500	534	12 acetonitrile	457 dioxane	62 dioxane	3160
Dansyl EDA	335	4600	526	49	471	81	2220
Coumarine 153	416	33500	556	-	495	-	2220
Nile Red	553	45000	632	38	569	90	1750
NBD	465	22000	541	-	529	-	420

[a] λ_{Abs} - absorption maximum, ε_{max} – extinction coefficient ($M^{-1}cm^{-1}$), λ_{Fluo} – fluorescence maximum, QY – fluorescence quantum yield, THF – tetrahydofuran, MeOH – methanol.

A special case of environment-sensitive dyes is the electrochromic dyes. They operate by the same photophysical principle as solvatochromic dyes, namely by a strong intramolecular charge transfer (ICT) upon electronic excitation. Electrochromic dyes are commonly rod-shaped molecules bearing electron donor and acceptor groups on the two opposite sides. Generally, any solvatochromic dye can work as an electrochromic dye, but the efficiency is dependent on the transition dipole moment and the geometry of molecule. Typical examples of electrochromic dyes are styryl pyridinium dyes (Fig. 1.9). The interaction of the ground- and excited-state dipoles with an external electric field results in electrochromic shifts of both absorption and emission bands (Loew and Simpson 1981; Bublitz and Boxer 1997). However, the shifts in emission spectra are distorted by solvent relaxation (polarity effects) and, therefore, shifts in excitation spectra are commonly used for evaluation of the electrochromic effects (Clarke and Kane 1997). Importantly, dyes showing strong electrochromic response by emission are still missing. The styryl pyridinium dyes represent good extinction coefficients and red shifted absorption, though their fluorescence quantum yields are relatively low in fluid media and become satisfactory only in rigid media like lipid membranes. Therefore, these dyes are mainly used in membranes studies (Loew et al., 1985; Clarke and Kane 1997).

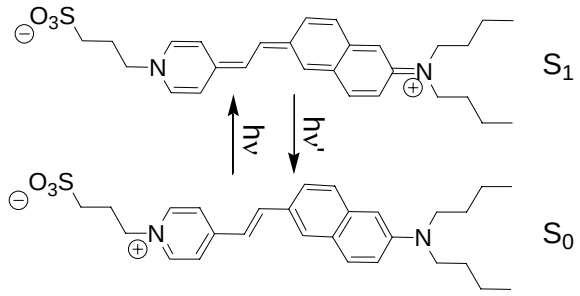

Figure 1.9. Typical example of styryl pyridinium dye and its transformation from the ground (S_0) to the excited (S_0) state.

The critical overview of the existing environment-sensitive dyes show that dyes with both strong fluorescence solvatochromism and good fluorescence properties are still missing. Thus, there is a strong need of improved solvent-sensitive fluorescent dyes.

1.2.3. Environment-sensitive dyes with two emission bands (ESIPT-dyes)

Excited-State Intramolecular Proton Transfer (ESIPT) reaction was observed and characterized for the first time in salicylic acid ester (Fig. 1.10) (Weller 1956). The methylsalicylate ion displays an unusual large Stokes shift in comparison to its methylated analog methyl 2-methoxybenzoate. This unusual spectral property was attributed to an excited-state proton transfer from the hydroxy- to the carbonyl-group that decreases the energy of the excited-state species, giving a red-shifted emission band. Later, similar spectroscopic properties were observed for different carbonyl and heterocyclic compounds.

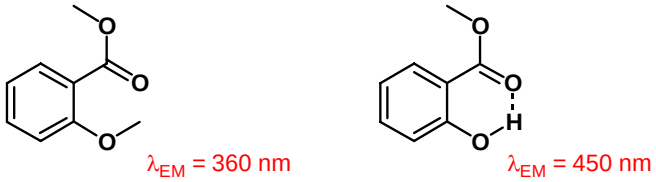

Figure 1.10. Methyl 2-methoxybenzoate (λ_{Fluo} = 360 nm) and methylsalicylate (λ_{Fluo} = 450 nm).

The main governing force for the ESIPT reaction is the change of the acidicity of the proton donor hydroxy-group and the basicity of the proton-acceptor carbonyl (Formosinho and Arnaut 1993). Due to the accompanying charge redistribution the carbonyl group becomes strongly basic, while the hydroxy-roup – strongly acidic, which leads to a proton transfer, giving the tautomer form (T*). Both the rate and the equilibrium constants of such process are controlled by the proton transfer energy barrier and the energy difference between the normal (N*) and tautomer (T*) forms of the excited molecule (Fig. 1.11).

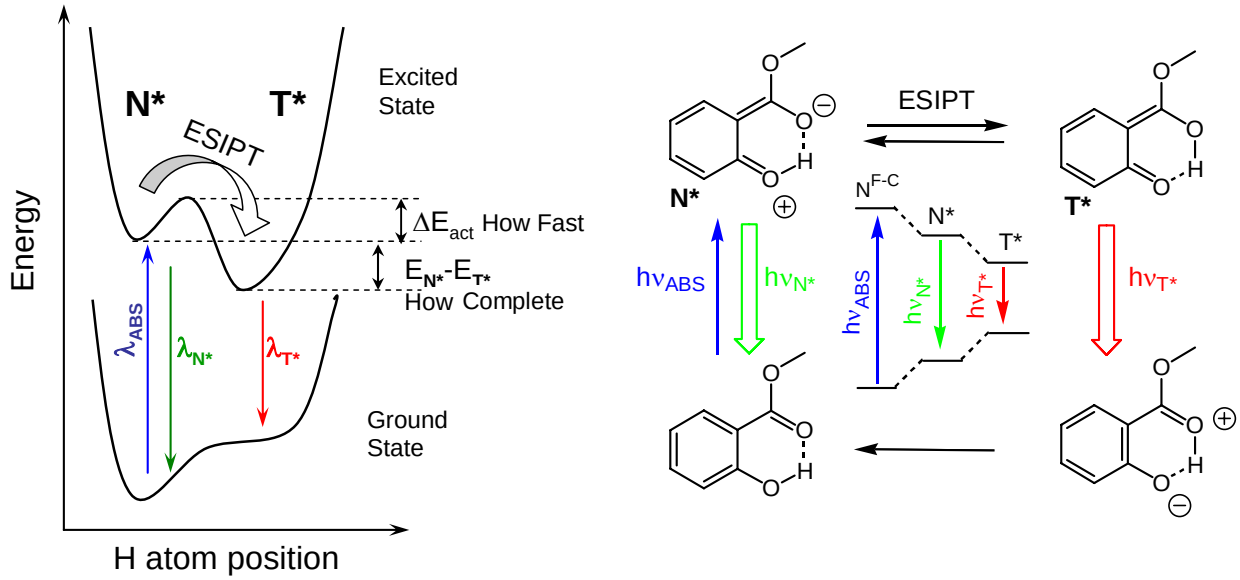

Figure 1.11. An energy diagram of the ESIPT reaction (left) and example of ESIPT in methyl salicylate (right). In the ground state the normal (N*) form is strongly favored. After excitation the tautomer (T*) form with a shifted proton may present lower energy and thus ESIPT reaction becomes favorable. ESIPT could be characterized by (a) its rate, which depends on the energy barrier (ΔE_{act}), and (b) its equilibrium constant, which depends on the energy level difference between the two excited states (E_{N^*}-E_{T^*}). If ΔE_{act} is too high, the ESIPT will not occur. In contrast, if ΔE_{act} is low enough, the equilibrium between the N* and T* forms can be reached within the excited-state lifetime, which is governed by E_{N^*}-E_{T^*}.

The ESIPT reaction is probably one of the fastest chemical processes described to date. Its rate can vary in a rather large time-scale range (from 10^{-14} to 10^{-8} s). Only in the 90s new instrumental methods have appeared that allowed studying such processes with enough precision, namely the so-called "ultra-fast laser spectroscopy" methods, including the ultra-fast transient absorption (TA) and the time-correlated single photon counting (TCSPC) approaches.

In most of cases described so far, the ESIPT reaction occurs between the hydroxyl group and the oxygen atom of the carbonyl (Legourrierec et al., 1994) or the sp^3-hybridized nitrogen atom (Ormson and Brown 1994). In salicylic acid the hydrogen bond results in the formation of a six-member cycle. The short length of this bond (~2 Å) is optimal for proton transfer, explaining the low energy barrier of the process (< 15.5 kJ/mol) and its very high rate (k~ 10^{13} s^{-1}) (Herek et al., 1992). In most cases, the salicylic acid derivatives exhibit only one fluorescence band that belongs to the tautomer form, due to the large energy difference between the two excited-state forms (~37 kJ/mol).

Ortho-hydroxyarylbenzoazines (Laemer et al., 1988) including *ortho*-hydroxybenzoazoles (Becker et al., 1987), correspond to a large class of compounds that exhibit an ESIPT reaction to a nitrogen atom (Fig. 1.12). Due to their relatively easy synthesis a variety of compounds of this family was obtained and thoroughly investigated (Heller and Williams 1970; Grabowska et al., 1990). The common feature of these molecules is their fast and irreversible ESIPT reaction in aprotic media resulting in the exclusive emission of tautomer (T*) form.

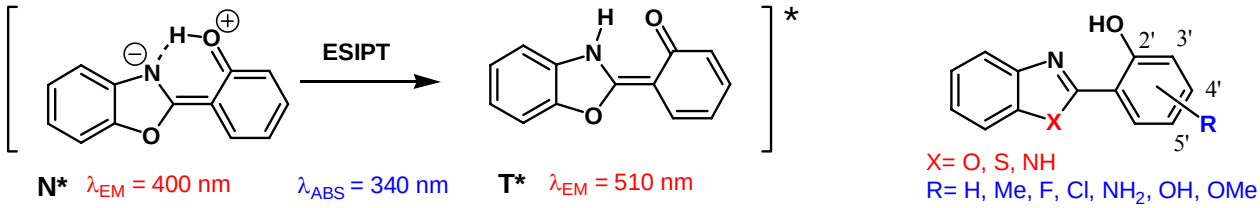

Figure 1.12. ESIPT in *Ortho*-hydroxyarylbenzoazole and main substitutions for this class of dyes.

In protic solvents the ESIPT reaction is blocked due to intermolecular hydrogen bonds, thus resulting in the emission of only the normal (N*) form. The normal and tautomer forms show their emission maxima around 400 nm and 510 nm, respectively. In most cases, the quantum yields do not exceed 20 %, with the only exception of benzimidazoles (Sinha and Dogra 1986) for which they reach 50-80 %.

The effect of substituents at the aryl ring of *ortho*-hydroxyarylbenzotriazols on the fluorescence properties was investigated (Heller and Williams 1970). The fluorescence was shown to depend on the position and electron donating properties of the substituent on the side ring of the dye. For example, an amino group in position 5' of the aromatic ring gives a bathochromic shift, while a dialkylamino group in position 4' induces a hypsochromic shift. Interestingly, the 4'-dialkylamino derivative exhibits a relatively slow ESIPT rate (~ 5.4×10^{11} s^{-1}) compared to the parent unsubstituted compound (> 2.9×10^{13} s^{-1}) (Cheng et al., 2006). Unfortunately, neither electron donating nor electron-withdrawing groups are inducing a high quantum yield of the chromophore which remains low in all cases.

Of particular interest are 3-hydroxychromones (3HC), which form an intramolecular H-bond through a 5-membered cycle (see Fig. 1.17) providing a pathway for the ESIPT reaction (Sengupta and Kasha 1979). In comparison with a 6-membered cycle (in dyes described above), the hydrogen bond in the 5-membered cycle is weaker and therefore can be easily perturbed by H-bonding interactions (McMorrow and Kasha 1984). As a result, the emission of both N* and T* forms can be observed in polar protic solvents.

3-Hydroxychromone dyes. Among ESIPT dyes of particular interest are 3-hydroxychromones (3HC). Chromones (chromen-4-ones) are natural dyes abondant in the vegetable kingdom. Most natural chromones containing phenyl (aryl) substituents in position 2 of the heterocycle are commonly called flavones (Fig. 1.13). The flavone derivatives bearing a hydroxyl group in position 3 of the heterocycle are called 3-hydroxyflavones (3HF). These compounds attracted the attention of spectroscopists after the discovery of their dual fluorescence by Frolov and co-workers (Frolov et al., 1974). Later, Sengupta and Kasha have explained this phenomenon by an excited-state intramolecular proton transfer (ESIPT) reaction (Sengupta and Kasha 1979). Importantly, the pathway for ESIPT in 3-hydroxychromones is provided by the intramolecular H-bond through a 5-membered cycle which is much weaker than 6-membered cycle presented by other ESIPT systems (see above). Therefore, it can be easily disrupted by H-bonding interactions with environment (McMorrow and Kasha 1984), so that 3HC dyes can exhibit two emission bands: the short-wavelength band corresponding to the normal excited state (N*) and the long-wavelength band – to the photo-tautomer product (T*) (Fig. 1.14).

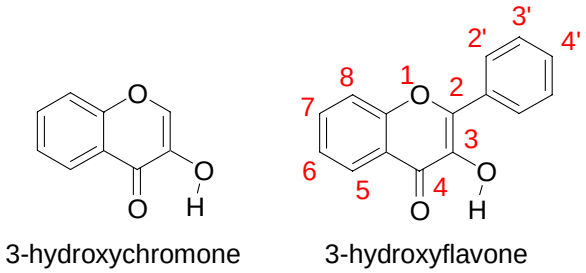

Figure 1.13. Chemical structure of 3-hydroxychromone and 3-hydroxyflavone.

While classical solvatochromic dyes shift their emission maximum and fluorescence intensity in response to changes of their environment such as polarity, 3HC dyes change also the ratio of their two emission bands intensities. Measuring the intensity ratio of the two emission bands is more precise and convenient than measuring absolute intensity, since this ratio is independent from dye concentration and instrumental settings. Moreover, due to two-band emission ESIPT dyes provide an additional channel of spectroscopic information for analysis of their environment, as compared to the one-band solvatochromic dyes. In a first step, the early studies on 3-hydroxychromones and their analogues will be presented.

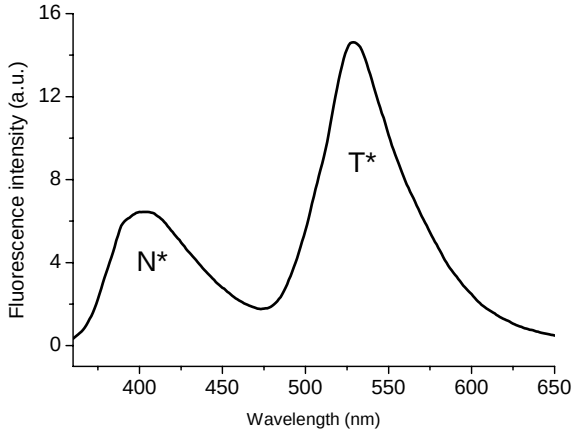

Figure 1.14. Fluorescence spectrum of 3-hydroxyflavone in methanol. Excitation wavelength was 350 nm.

Solvent effects on 3HC dyes. The non-substituted 3HF shows only T* band emission in aprotic solvents while a dual fluorescence is observed in protic environment (McMorrow and Kasha 1984) (Fig. 1.15). The intensity ratio of the two emission bands (N*/T*) is higher in more polar alcohols making possible to sense the environment polarity just by recording the fluorescence spectrum. Meanwhile, in aprotic media the N* band intensity is too low, thus rendering the environment sensing difficult to perform through ratiometric measurements.

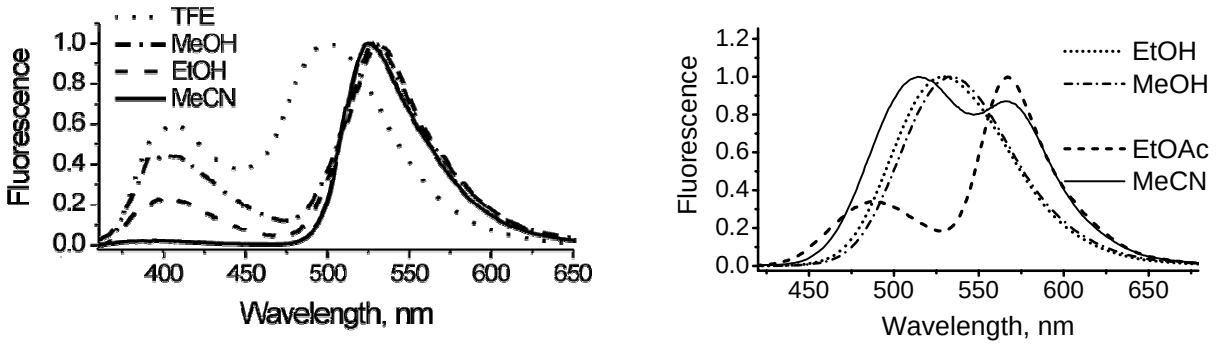

Figure 1.15. Fluorescence of 3HF (left) and its dimethylamino derivative (right) in protic and aprotic solvents.

A significant progress was done after the dialkylamino derivatives of 3HF were synthesized (Chou et al., 1993; Ormson et al., 1994) (Fig. 1.16). Due to the 4'-dialkylamino group the N* excited state in these compounds exhibit a very large dipole moment, where the electronic charge is transferred from the dialkylamino group to the chromone moiety (Chou et al., 1993; Swinney and Kelley 1993; Nemkovich et al., 2005). In contrast, the excited-state tautomer T* exhibits much lower charge separation (Fig. 1.17) and, thus, lower dipole moment (Chou et al., 2005; Yesylevskyy et al., 2005). Therefore the N* state, unlike the T* state, shows a significant solvatochromism. Indeed, on increase in the solvent polarity the N* band shifts to the red while the T* band remains almost unchanged (Fig. 1.18). An increase of solvent polarity results in an increase of the relative intensity of the N* emission band. Therefore, the ratio of intensities of the N* and T* bands in emission (N*/T*) is an important indicator of solvent polarity (Ercelen et al., 2002a; Klymchenko et al., 2002a; Ercelen et al., 2002b; Klymchenko et al., 2003a; Klymchenko et al., 2003b).

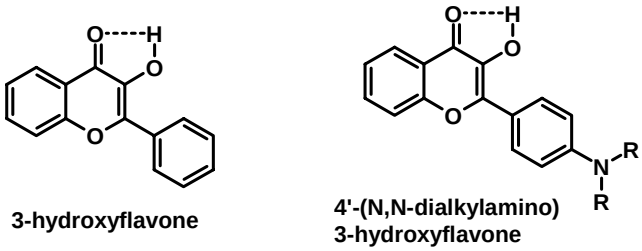

Figure 1.16. Structures of 3-hydroxyflavone (3HF) and 4'-(N,N-dialkylamino)-3-hydroxyflavone.

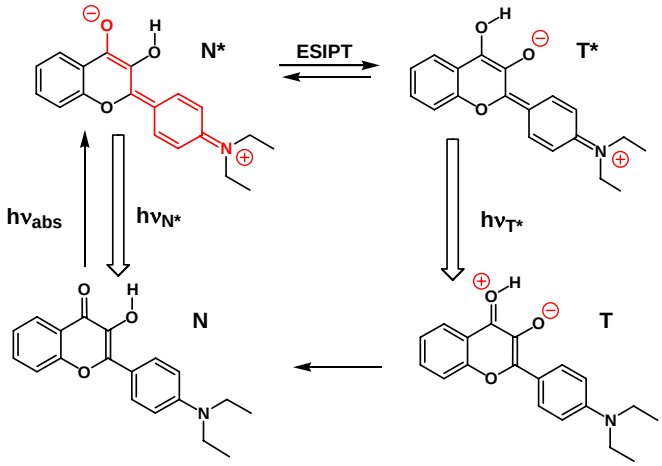

Figure 1.17. Photophysical cycle of 4'-(N,N-diethylamino)-3-hydroxyflavone dye.

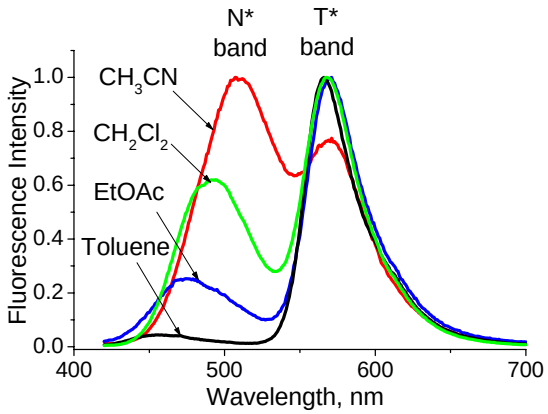

Figure 1.18. Fluorescence spectra of 4'-(N,N-diethylamino)-3-hydroxyflavone in aprotic solvents of different polarity.

It is important to note that these molecules allow the simultaneous determination of four parameters, ν_{abs}, ν_{N*}, ν_{T*} and N*/T*, which can differently characterize the physical properties of the microenvironment. An algorithm using these four spectroscopic parameters was proposed to simultaneously estimate three microenvironment characteristics: polarity, polarizability and H-bond donor ability (Klymchenko and Demchenko 2003). This algorithm was successfully applied in binary solvent mixtures, AOT reverse micelles and proteins.

Hydrogen Bonding. A particularly attractive feature of 3HFs is their high sensitivity to hydrogen bonding. The ESIPT reaction site is strictly localized between the 3-hydroxy and 4-carbonyl groups, which form an H-bond that closes a low-stable five-member ring (Sengupta and Kasha 1979). Therefore, this reaction shows an extreme sensitivity to intermolecular H-bond perturbation (McMorrow and Kasha 1984). 3HFs show two emission bands in alcohols, meanwhile in aprotic solvents of similar polarity the T* band strongly dominates. This effect could be better observed in dialkylamino derivatives of 3HCs, namely 4'-(N,N-diethylamino)-3-hydroxyflavone (FE) (Klymchenko and Demchenko 2003). The N*/T* ratio of FE was shown to be up to 10 times higher in protic solvents than in aprotic solvents of the same polarity. This high sensitivity was related to the H-bonding of solvent proton donors with the 4-carbonyl group of FE acting as an H-bond proton acceptor (Fig. 1.19).

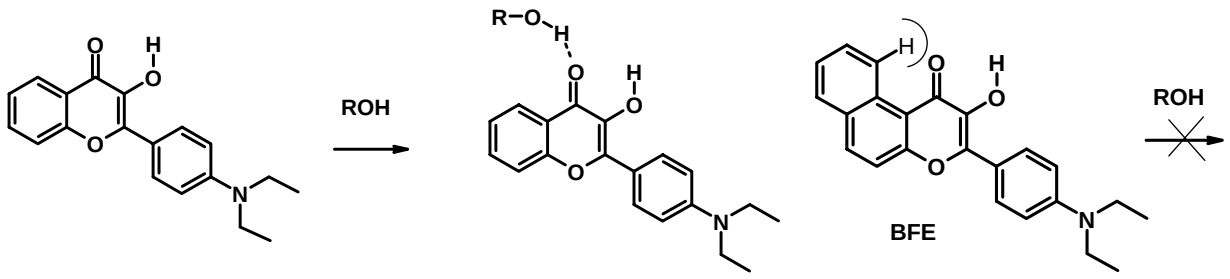

Figure 1.19. Formation of an H-bonding complex of FE with alcohol is blocked by the additional benzene ring in BFE.

Interestingly, a benzo-analogue of FE, 5,6-benzo-4'-diethylamino-3-hydroxyflavone (BFE), with a 4-carbonyl group sterically protected from the intermolecular H-bonding (Fig. 1.19) does not show any sensitivity of its dual emission to protic solvents. This result suggested that only one type of H-bonding (between protic solvents and the carbonyl group) affects the dual emission of dialkylamino substituted 3HFs, while H-bonding of the solvents with the 3-hydroxy group is not detected in the fluorescence spectra (Klymchenko et al., 2003a).

ESIPT kinetics in 3-hydroxyflavones. ESIPT in non substituted 3HFs was an object of intensive kinetic studies in the 1980s. The first dynamic studies of ESIPT in non-substituted 3HFs by picosecond time-resolved spectroscopy (Sengupta and Kasha 1979; Itoh et al., 1983) revealed that ESIPT occurs very rapidly, usually in less than 10 ps, and that the kinetic constants of the proton-transfer reaction are temperature-dependent. Moreover, McMorrow and coworkers observed that the ESIPT reaction time is less than 8 ps (McMorrow et al., 1984) in degassed ultra-dry hydrocarbon solutions at 293 K.

Kinetic two-state models were developed for describing excited-state processes, in particular intramolecular proton transfer. Pioneer works on the analysis of two-state excited-state reactions were from Birks (Birks 1970) and Brand et al. (Laws and Brand 1979). The latter focused on the time-resolved study of the intermolecular proton transfer in the excited state of naphthol molecules. In further research works (Woolfe and Thistlethwaite 1981; Itoh et al., 1982; Swinney and Kelley 1993) the excited-two-state model was applied for describing the intramolecular proton transfer in 3HF molecules. This became possible due to the development of ultrafast time-resolved fluorescence spectroscopy that allowed measuring the time constants of ESIPT processes (Marks et al., 1997). Brown et al. found that ESIPT for 3HF in methylcyclohexane and acetonitrile is extremely fast and irreversible, showing an estimated time constant of 35 fs (Ameer-Beg et al., 2001). In ethanol they found a time constant of irreversible ESIPT of 60 fs. The slower ESIPT in this solvent was attributed to the greater strength of the solute-solvent interactions. Introducing new techniques for measuring the decay curves and new methods for treating the lifetime data allowed revisiting the results of previous experiments and building new concepts. It is also remarkable that before 2003 no attempts have been made to study kinetics of 4'-(dialkylamino)-3-hydroxyflavones, which were of high potential interest for variety of applications. Later studies led to the discovery of a reversible ESIPT reaction in these compounds, which is rather rare for the ESIPT dyes (Shynkar et al., 2003).

Looking through the history of the ESIPT-dyes we can conclude that this class of compounds (especially 3-hydroxyflavones) is highly promising for the development of environment-sensitive fluorescent probes.

1.3. Cell plasma membrane

First membrane explorations were conducted by Overton in 1890s. Basing on the studies of how various molecules pass through the membrane, he published a preliminary hypothesis in which he proposed that there are some similarities between cell membranes and lipids such as olive oil, and that certain molecules (i.e., lipids) pass through the membrane by "dissolving" in the lipid interior of the membrane. Few years later Langmuir, a physical chemist, proposed the monolayer lipid structure (Langmuir 1917). He stated that the fatty acid molecules form a monolayer by orienting themselves vertically with the hydrocarbon chains away from the water and the carboxyl groups in contact with the surface of the water.

Later, Gorter and Grendel extracted the lipids from red blood cells by using organic solvents. They demonstrated that lipid molecules could form a double layer (bilayer) and, further, that the surface area of the lipids extracted from the red blood cells was about twice the surface area of the cells themselves. Using these two observations and performing analogous studies with red blood cells from several animals, these scientists suggested the bilayer structure for the membrane (Gorter and Grendel 1925). Within ten years Danielli and Davson proposed a new membrane model which was accepted by the majority of scientists. They stated that membrane is basically a "sandwich" of lipids (arranged in a bilayer structure) covered on both sides with proteins (Danielli and Davson 1935). The hydrophilic heads of the phospholipids are on the outside, while the hydrophobic tails are faced inward. It should be noted, that for many years this model was accepted by biologists as a basis for membrane structure. Another researcher, a physical chemist Robertson, came to a similar membrane model, which he called the "unit membrane" (Robertson 1957). Basing on electron microscope studies he found the "trilaminar" membrane appearance consisting of two darker outer lines and a lighter inner region. According to Robertson, the two outer (darker) lines were the protein layers and the inner region was the lipid bilayer.

However, many of the findings of later research were not clearly explainable within the proposed models. In the early 1970s, a new model of membrane structure was proposed by Singer and Nicolson (Singer and Nicolson 1972). The model retained the lipid bilayer structure firstly proposed by Gorter and Grendel, and consisted of two statements: 1) the core lipid bilayer exists in a fluid state capable of dynamic movement; 2) the proteins are thought to be globular and to float within the lipid bilayer penetrating it to varying degrees. In simple words, proteins form a mosaic of particles on the membrane surface. Since 1972, this theory known as “fluid mosaic model” was used as the prefered model of membrane structure.

Finally, in 1997 the Singer-Nicolson model was further revised by Simons and Ikonen, who took into account dynamic phase transitions of the cell membrane suggesting a theory of “lipid rafts” (Simons and Ikonen 1997).

1.3.1. Phase transitions in biomembranes

Cellular plasma membranes consist of a variety of molecules including lipids, cholesterol, and proteins. For decades, it has been considered that these materials exhibit liquid crystalline behavior (due to the presence of fluid phase with rapid lateral diffusion) and that the combination of oriented structure, fluidity and lability are important characteristics for optimal functioning of the plasma membrane (Bernal 1933; Stewart 1961). Indeed, these are key physical characteristics which were considered in the development of the fluid mosaic model of the cell plasma membrane (Singer and Nicolson 1972). Another intriguing property of biomembranes is that they are often just above the temperature for transition to the gel phase. This phase transition is likely of great significance in the homeostasis of phase-separated domains in the cell membrane called rafts (Simons and Ikonen 1997; Vereb et al., 2003). Lipid raft structures enriched with cholesterol, glycolipids, and sphingolipids (Simons and Vaz 2004) are proposed to play important role in a great variety of membrane trafficking and signaling events. It is known that gel phase membranes exhibit dramatically decreased permeability and that the rates of active transport events such as endo or exocytosis are decreased dramatically and frequently are ceased altogether (Chapman 1975; McElhaney 1984). The evidence that the membrane phase transitions are important has been gathering for over 70 years.

While Singer and Nicholson were developing the fluid mosaic model, Chapman was performing a series of experiments that focused on the phase transition characteristics of cell membranes (Chapman 1975). A remarkable correspondence was observed between the phase transition temperature of model lipid bilayer systems and that one observed for cells. Modulation of membrane fluidity was suggested to affect a number of important cell characteristics including membrane permeability and signaling.

The importance of phase transitions in cell membranes is underlined by the > 4000 articles published on “lipid rafts” since 1997. This particular aspect of phase transitions in cell membranes has garnered substantial attention because of the predicted role of lipid rafts in cell functions, particularly, in signal transduction and transport across the membrane. The combination of nanometer size, time dynamics, cell complexity and diversity has kept the study of lateral membrane phase heterogeneities very challenging. The importance of a fluid phase membrane for cell function is a central dogma of structural cell biology (Alberts et al., 2002; Vereb et al., 2003). However, might the transition of the cell plasma membrane to the gel state serve a useful biological function? This transition could provide an interesting cellular “switch” for vital membrane properties such as permeability, receptor clustering, and could modify the ratio between the surface area and volume of cell. In order to answer question, an effective approach for investigation of membrane phase state should be available.

1.3.2. Raft theory

In the last decade, a large interest was focused on the raft theory and its evolution (Coskun and Simons 2010; Lingwood and Simons 2010; Mongrand et al., 2010; Quinn 2010).

Indirect evidence of membrane heterogeneity was obtained by a row of experimental results. First data concerning lateral heterogeneity was reported as early as in 1973 (Yu and Steck 1973). Yu and Steck have studied the effect of non-ionic detergents on red blood cell membranes. Upon detergent treatment cell membranes were found to be not readily soluble, and detergent-resistant membranes (DRM) were observed (Schroeder et al., 1994; Patra et al., 1999; Brown and London 2000). Usually, DRMs are prepared by using the detergent Triton X-100. Action of this detergent on cell membranes at 4°C leads to the formation of small micelles (detergent-soluble fraction, containing unsaturated phosphatidylcholines and proteins) and larger particles, or DRMs (low-density fraction, containing sphingomyelin, cholesterol and proteins), that can be separated by centrifugation. DRMs were found to consist of a unique lipid composition, enriched 3- to 5-fold in cholesterol (Chol) and sphingolipids but relatively depleted in glycerophospholipids (Pike et al., 2002). Due to the fact that some lipids are found to be Triton insoluble within the gel phase (Ribeiro and Dennis 1973; Schroeder et al., 1998) it was suggested that DRMs are formed due to phase separation in the membrane.

At low temperatures phospholipid bilayers usually exist in a highly ordered gel phase. Above the melting temperature (**Tm**) that is characteristic of each lipid, the bilayer is present in a phase termed liquid-crystalline, in which the lipid acyl chains are disordered. In the case of bilayer formed of two lipids with different Tm (Fig. 1.20) transition from one state to another is smoothed, and coexistence of phases may occur. If it is so, two distinct states can be observed at a significant range of temperature. For these phases the corresponding terms, liquid-ordered (**Lo**) and liquid-disordered (**Ld**) phase should be used (Brown and London 1998). High temperatures favour the chaotic Ld phase while low temperatures favour the more viscous Lo phase. In the Lo phase the acyl chains of lipids are extended and ordered as in the gel phase, but have a bit higher lateral mobility (Mouritsen 1991). The properties of lipids in the Ld phase resemble those of the fluid (liquid-crystalline) state.

Biological glycerolipids generally have very low Tm values while sphingolipids (especially glycosphingolipids) have much higher Tm values. This disparity suggests that phase separation between glycerolipid- and sphingolipid-rich domains might occur, leading to the DRM formation upon detergent treatment. Consistent with this possibility the indications of glycosphingolipid clustering in the plasma membrane have sometimes been observed morphologically (Thompson and Tillack 1985). Importantly, the gel phase does not exist in biological membranes except in unusual cases (Parasassi et al., 1993). However, DRMs do not provide direct evidence for the existence of rafts, as detergents may artificially provoke phase separation and DRM formation (Kurzchalia et al., 1995). Further data indicated that the organization of the lipids in membranes is much more complex. It is now widely recognized that membranes are not homogenous but show lateral asymmetry (Tocanne et al., 1989; Glaser 1993; Tocanne et al., 1994) and transmembrane asymmetry (Devaux 1993; Zachowski 1993) (Fig. 1.21). The most striking demonstrations of heterogeneity of lipid organization are those that use immunofluorescence to show the discrete localization of proteins and lipids in living cells (Gomez-Mouton et al., 2001; Yamaji-Hasegawa and Tsujimoto 2006).

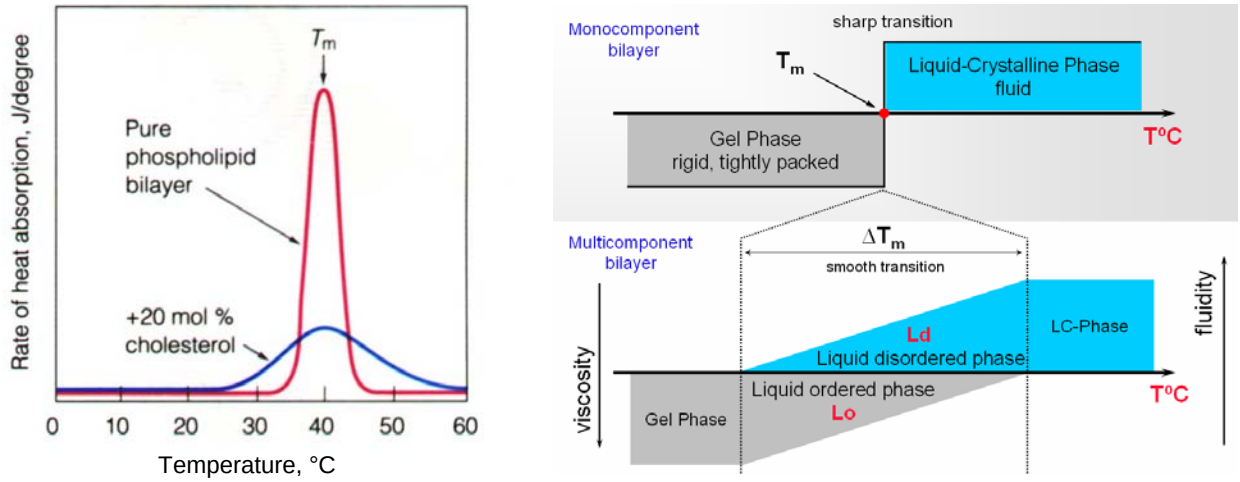

Figure 1.20. The impact of lipid composition on the physical properties of bilayer.

Raft definition. The raft theory was first proposed in 1997 (Simons and Ikonen 1997). This theory predicted the existence of lipid and protein microdomains ("rafts") that are enriched in cholesterol and sphingolipids and have a functional role in processes like signaling and membrane trafficking. Today lipid rafts are defined as small (10-200 nm), heterogeneous, dynamic domains that compartmentalize cellular processes and can be stabilized to form larger platforms (Pike 2006).

Since its original proposal, the raft concept has attracted an enormous interest with attempts to define what a raft actually is, and to implicate rafts in an ever growing list of cellular functions. Despite intensive research, the actual nature and functioning of lipid rafts are not completely understood. Moreover, the lack of simple tools to study rafts in intact cells has brought about caution and distrust towards its value (Munro 2003; Hancock 2006; Shaw 2006).

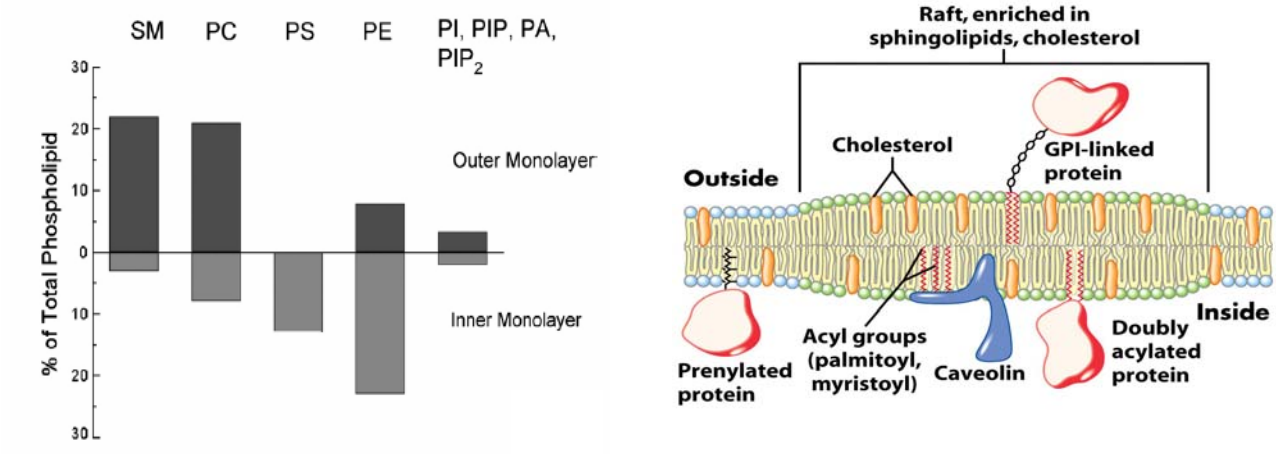

Figure 1.21. The distribution of lipids between inner and outer membrane leaflets (Hanshaw and Smith 2005). Schematic representation of raft-domain (Lodish et al., 2004). Sphingomyelin (SM), phosphatidylcholine (PC), phosphatidylethanolamine (PE), phosphatidylserine (PS), phosphatidylinositol (PI), phosphatidylinositol 4-phosphate (PIP), phosphatidylinositol 4,5-bisphosphate (PIP_2), phosphatidic acid (PA).

Formation of rafts. Experiments with artificial membranes have demonstrated that domains mimicking rafts in biological membranes have higher lipid ordering (liquid-ordered phase) than the surrounding non-raft area (liquid-disordered phase) (Sengupta et al., 2007). Such phase separation of lipid domains has been found to be induced by different forces such as specific lipid interactions, lipid immiscibility and line tension.

Sterol-acyl chain interactions can promote mutual immiscibility and lead to phase separation (Xu and London 2000). Cholesterol is critical for the structural integrity of raft domains and there have been numerous reports of the disruption of raft structure by agents which selectively deplete cholesterol from the plasma membrane (Westover et al., 2003). Its presence in mixtures of high melting point lipids such as dipalmitoylphosphatidylcholine (DPPC) and sphingomyelin (SM), induces the transition of both gel and liquid-disordered domains to a highly ordered structure that, however, maintained high lipid mobility. The non-ideal behavior of lipid mixtures and the ability of cholesterol to decrease the molecular volume of phospholipid and sphingolipid acyl chains (so called "condensing effect", see Fig. 1.22) continue to be explored (Greenwood et al., 2006). The condensing effect is promoted by extensive van der Waals interactions of the sterol skeleton along the length of the non-polar acyl chains, and is increased with the saturation and length of the chain. This effect may confer detergent-resistance and selective protein targeting to membrane microdomains and is believed to be one of the "driving forces" behind the formation of raft structures.

Some researches have suggested *specific interaction of charged groups* to be also a driving force of this process (Kojima and Hakomori 1991). Resultant domains thus exhibit altered mobility, dynamics and permeability reflective of either Ld or Lo domains, rather than homogenously dispersed lipid mixtures.

Finally, it was suggested that one more important driving force of domain formation is *line tension*. Line tension refers to the energy required to create the boundary between a domain (referred to hereafter as a raft) and the surrounding membrane. In practice, rafts are thicker than the surrounding membrane, and this hydrophobic mismatch contributes to the energy required to maintain rafts as a separate phase. Studies have shown that the greater the difference in thickness between the two phases, the higher the line tension that results in the formation of larger rafts (Garcia-Saez et al., 2007). Deformation of the lipids at the boundary of rafts, including changes in tilt and splay, helps to reduce the line tension (Kuzmin et al., 2005).

A) 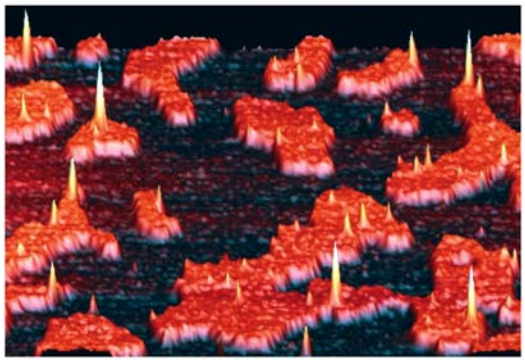

B) 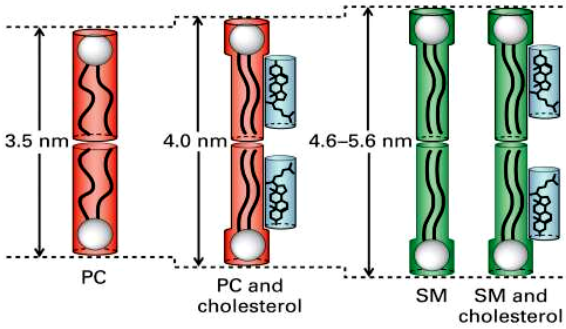

Figure 1.22. (A) Visualization of lipid rafts (orange) in supported lipid bilayer by atomic force microscopy (Saslowsky et al., 2002). (B) Condensing effect of cholesterol on phospholipids.

Attempts to prove rafts existence. The presence of membrane proteins which are approximately equal by mass to lipids (Takamori et al., 2006) create complications in studying the lipid phase behavior of biomembranes.

A simple model system for imaging lipid domains is giant vesicles (GUVs), composed of lipids forming liquid ordered and disordered phases (Fig. 1.23). Experimental data using fluorescence microscopy on GUVs showed for first time the images of temperature-dependent lateral structure of GUVs composed of different phospholipids, phospholipid binary mixtures, ternary lipid mixtures containing cholesterol, natural lipid extracts and native membranes (Bagatolli 2007).

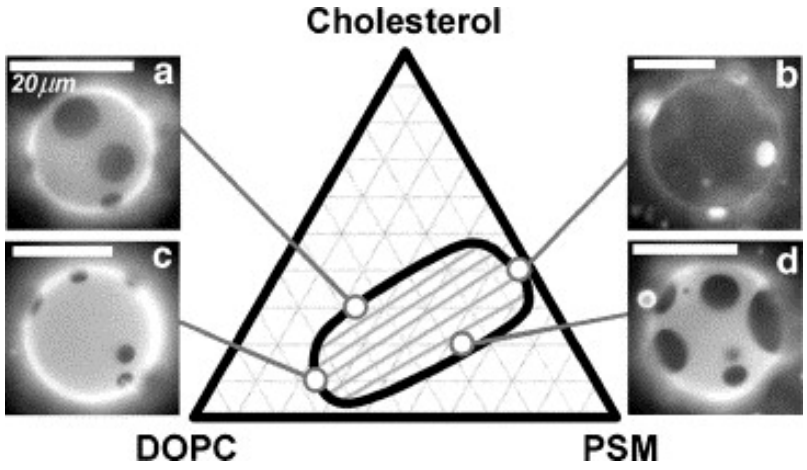

Figure 1.23. Phase diagram showing the coexistence of two phases in ternary mixture of Chol, DOPC and Palmitoyl-SM (PSM) at 25°C. Fluorescence microscopy images of GUVs with different membrane compositions: (a) 2:1 DOPC/PSM + 30 % Chol, (b) 1:19 DOPC/PSM + 40 % Chol, (c) 3:1 DOPC/PSM + 10% Chol, and (d) 1:2 DOPC/PSM + 20 % Chol. White regions represent Ld-phase rich in the unsaturated lipid DOPC, and the dark regions correspond to Lo-phase rich in the saturated lipid PSM and only slightly enriched in cholesterol (Veatch and Keller 2005).

Since the statement of raft theory one major question has arisen. If rafts are present in cells, it should be possible to detect them directly (Mukherjee and Maxfield 2004). One of the best ways for detection of hypothetic domains is fluorescence microscopy due to its non-invasivity and high spatio-temporal resolution. Fluorescence resonance energy transfer (FRET), scanning confocal microscopy, fluorescence correlation spectroscopy (FCS), image correlation spectroscopy (ICS), single-particle tracking (SPT) were intensively used for investigating lipid domains in live cells. They are summarized in recent reviews (Jacobson et al., 2007; Miersch and Mutus 2007). Among the reported approaches, atomic force microscopy (AFM) (Hinterdorfer and Dufrene 2006) and high resolution mass spectrometry (Miersch and Mutus 2007) were also applied. In addition to the named approaches, spectroscopy and thermodynamics related techniques such as differential scanning calorimetry, IR spectroscopy, NMR, and X-ray diffraction (Bagatolli 2007) were also used.

Despite this technical variety direct visualization of rafts in living cells appeared to be a complicated task. For example, GPI-anchored proteins were the first group of proteins reported to be enriched in lipid rafts (Brown and Rose 1992). GPI-anchored proteins and gangliosides, taken as raft markers because of their enrichment in DRMs, appeared uniformly distributed on the cell surface when detected microscopically. However, the distribution of these markers was changed dramatically upon clustering with antibodies or other agents. Detailed single-particle tracking

experiments in cells showed that a ganglioside and a GPI-anchored protein were transiently confined to domains of about 200–300 nm that were sensitive to a glycosphingolipid synthesis inhibitor (Jacobson and Dietrich 1999). One of the latest reports in raft detection was done by Eggeling and coworkers in 2009 (Eggeling et al., 2009). They used combination of advanced optical microscopy (STED technique) and fluctuation analysis (Celli and Gratton 2010). Their results allowed to suggest existence of complexes, formed by proteins and small cholesterol-dependent membrane domains (<20 nm) with a lifetime around 10-20 ms. These results are in accordance with previous data based on FRET or FCS approaches (Varma and Mayor 1998; Sharma et al., 2004; Lenne et al., 2006), which suggested the existence of clusters formed by sphingolipid and lipid-modified proteins (GPI-APs) in the outer membrane leaflet.

Thus, the size of rafts in cell membranes as well as their lifetime is a matter of debates. The lifetime value remains controversial, while their size seems to vary depending on the method employed to measure them (Jacobson et al., 2007). In contrast, model systems composed of a limited number of components reveal well defined phase separation. In this case raft-domains are stable and of sufficient size to be detected by traditional imaging fluorescence techniques (London 2005).

In conclusion, fluorescence microscopy techniques are of great importance for detailed investigations of the lipid phase behavior in membranes. These techniques rely on application of fluorescent membrane probes that are described in the next chapter.

1.3.3. Apoptosis and its effect on plasma membrane

Apoptosis is the process of programmed cell death (PCD) that occurs in multicellular organisms. It includes numerous biochemical events that lead to characteristic cell changes and, subsequently, to cell death. Research in and around apoptosis has increased substantially since the early 1990s. In addition to its importance as a biological phenomenon, defective apoptotic process has been implicated in an extensive variety of diseases. Excessive apoptosis causes atrophy such as in ischemic damage, whereas an insufficient amount results in uncontrolled cell proliferation such as cancer. Importantly, apoptosis is considered to be a regulated and controlled process.

In 1842 Carl Vogt was first to describe the principle of apoptosis. In 1885 Walther Flemming delivered a more precise description of the programmed cell death. However, it was not until 1965 that the topic was resurrected. While studying tissues using electron microscopy, J. F. R. Kerr was able to distinguish apoptosis from traumatic cell death (Greek: *apo* – from, off, without; *ptosis* – falling; *apoptosis* - "dropping off") (Kerr et al., 1972).

Apoptosis plays an important role in organism homeostasis. Tightly-controlled homeostatic mechanisms are required to regulate the balance between proliferation (increase in number of cells) and apoptosis (decrease in number of cells) in order that the functional and structural integrity of organs and tissues are maintained (Erickson 1997). Apoptosis is thus a highly regulated process that can be induced, stimulated and inhibited at different stages (Fig. 1.24). Although many of the key apoptotic proteins that are activated or inactivated in the apoptotic pathways have been identified, the molecular mechanisms of action or activation of these proteins are not fully understood and are the focus of continued research. The importance of understanding the mechanistic machinery of apoptosis is vital because programmed cell death is a component of both health and disease, being initiated by various physiologic and pathologic stimuli.

Mechanism of Apoptosis. The mechanisms of apoptosis are highly complex and sophisticated, involving an energy-dependent cascade of molecular events (Fig. 1.24). Briefly, apoptosis includes initiative and executive steps. The three main types of initiation are extrinsic (tumor necrosis factor TNF), intrinsic (non-receptor mediated stimuli) and perforin-granzyme pathways. Each one requires specific triggering signals to begin an energy-dependent cascade of molecular events. Each pathway activates its own initiator caspase (8, 9, 10) which in turn activates the executioner caspase-3. Like many other proteases, the caspases are formed as inactive proenzymes of 30-50 kDa. Basing on their function in apoptosis, the caspases are divided into two classes: the initiator caspases (caspases 8 and 9) and the effector caspases (caspases 3, 6 and 7). Unprogrammed activation of the caspases has serious consequences for the cell. Therefore, activation of caspases is strictly controlled. In the normal state of the cell the caspases are maintained in an inactive state, but they can be rapidly and extensively activated by a small inducing signal.

The executive step starts with the activation of the caspase-3. This step is an early apoptotic event and is followed by the translocation of phosphatidylserine located in the inner leaflet of the plasma membrane to the outer leaflet (Schlegel and Williamson 2001). Activation of caspase-3 is called the "point of no return" and results in the formation of the apoptosome. Since once activated, effector caspases cause variety of proteins to be degraded resulting in irreversible damage of the cell and its death. Importantly, apoptosis has characteristic cytomorphological features like cell shrinkage, dynamic membrane blebbing, chromatin condensation, nuclear fragmentation, and chromosomal DNA fragmentation. These events are followed by formation of apoptotic bodies and, finally, phagocytosis of the apoptotic bodies by adjacent parenchymal cells, neoplastic cells or macrophages. As a consequence, the apoptotic cell does not release intracellular components, thus avoiding inflammatory reactions (in contrary to necrosis). In fact, condensation of the chromatin, degradation of DNA, cell shrinkage, fragmentation of the cell nucleus and disassembly into

membrane-enclosed apoptotic vesicles are characteristics that clearly distinguish apoptosis from other forms of cell death. For details on apoptosis see recent reviews (Elmore 2007; Meulmeester and Jochemsen 2008; Salvesen and Riedl 2008; Taylor et al., 2008) or more early publications (Huppertz et al., 1999; Kiechle and Zhang 2002).

It is interesting to note that other forms of programmed cell death have been described. Three of the best-understood examples of non-apoptotic cell death are type II cell death, necroptosis and PARP1-mediated necrotic death while other forms of programmed cell death may yet be discovered (Degterev and Yuan 2008).

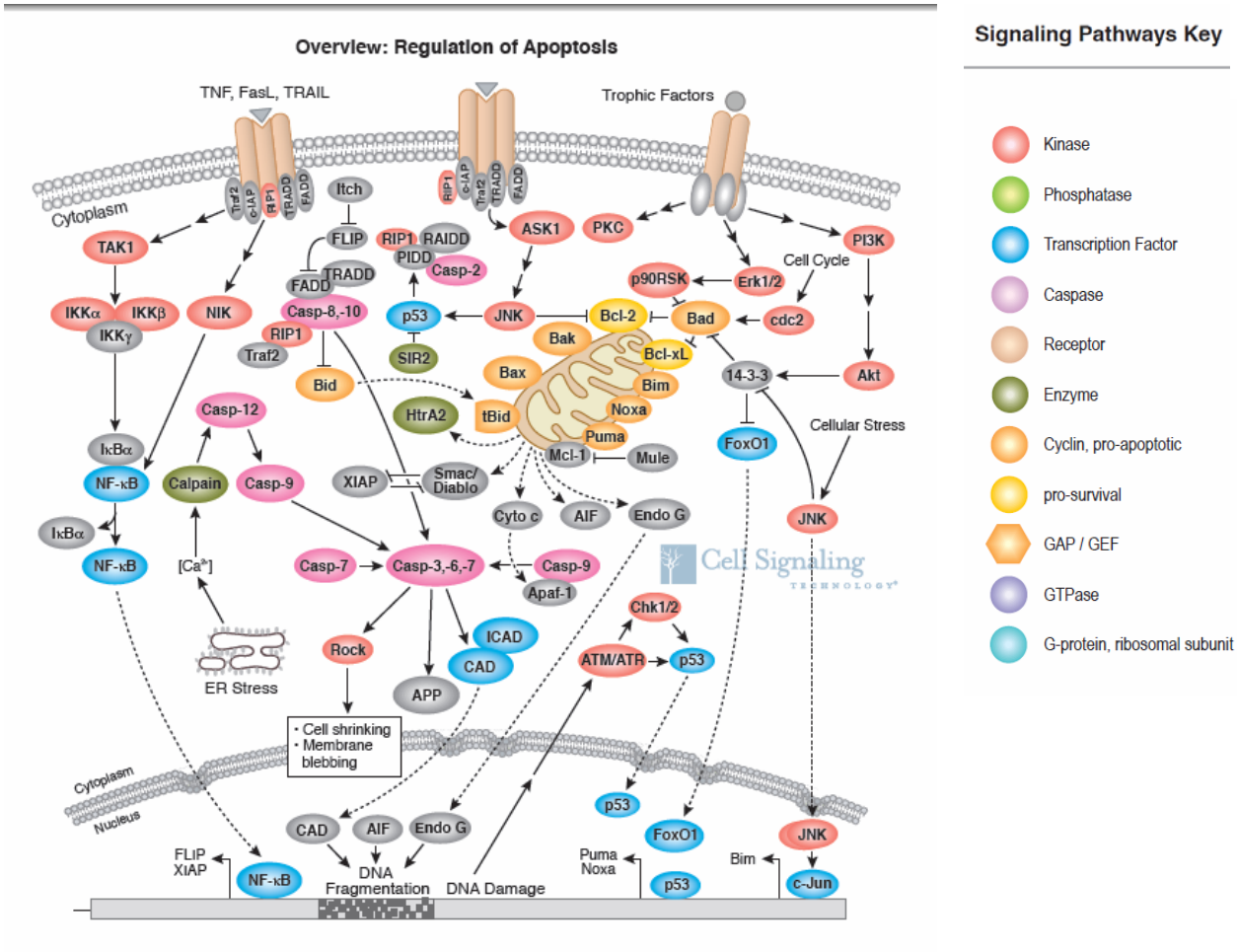

Figure 1.24. Apoptosis mediators (from www.cellsignal.com).

Membrane changes. The usually observed apoptosis membrane change is its morphologic modification (membrane blebbing). It is characterized by formation of "bubbles" and frequently culminates in the pinching off many blebs as small vesicles that have been named apoptotic bodies (Coleman et al., 2001). Another reported change is the decrease of lipid asymmetry that is in tight connection with changes of physical membrane parameters like fluidity, hydration, membrane potential, etc. Except the loss of membrane asymmetry, the changes include a decrease in lipid order (Tanaka and Ohnishi 1976) and packing (Williamson et al., 1982; Schlegel et al., 1993; Mower et al., 1994), an increase in fluidity (Morrot et al., 1986) and an increase in the hydrophobicity of the outer leaflet (McEvoy et al., 1986).

The plasma membrane lipid asymmetry in healthy cells is thought to be maintained by flipases which are membrane proteins that facilitate the translocation of lipid molecules from one leaflet to the other (Higgins 1994). In addition to the potency of maintaining PS asymmetrically at the inner membrane leaflet by the flippase activity, cells also possess the ability to translocate PS to

the outer leaflet of the plasma membrane (Bevers et al., 1982; Bevers et al., 1983; Connor et al., 1994). During apoptosis, PS is translocated to the outer membrane leaflet in response to pro-apoptotic stimuli (Fadok et al., 1992; Martin et al., 1995). This translocation is caspase dependent, but how caspases promote PS externalization is unclear (Martin et al., 1996). Importantly, it was shown that apoptotic exposure of PS is a tag for specific recognition by macrophages and for phagocytosis (Fadok et al., 1993; Hanayama et al., 2002). To date, the molecular machinery responsible for cell surface exposure of PS remains unidentified. Scramblases, which are responsible for the inward-out translocation of PS by scrambling the aminophospholipids over the inner and outer membrane leaflet, have been demonstrated to be responsible for PS exposure in platelets and erythrocytes (Diaz and Schroit 1996; Zwaal and Schroit 1997). Others claim a role for fodrin (nonerythroid spectrin) in maintaining an asymmetric phospholipid composition of the cytoplasmic membrane by anchoring PS at the cytofacial membrane. As a consequence of fodrin degradation by ICE-like proteases, PS would be exposed during apoptosis. PS exposure seems to last from the early execution phase of apoptosis until the final stage, at which the cell has broken up into apoptotic bodies.

Interestingly, recent works discussed the influence of lipid raft dynamics on cell apoptosis (Malorni et al., 2008). Another report proposed a mechanism of apoptosis induction due to membrane changes caused by GM1-ganglioside. It was found that incorporation of GM1 into a model membrane lead to an increase of the line tension. The latter resulted in the appearance of large domains followed by their shape transformation and final pinching out from vesicles forming their own homogeneous liposomes (Akimov et al., 2009).

Assays for Apoptosis detection. Since apoptosis occurs via a complex signaling cascade that is tightly regulated at multiple points, there are many opportunities to evaluate the activity of the proteins involved. As the activators, effectors and regulators of this cascade continue to be elucidated, a large number of apoptosis assays are devised to detect and count apoptotic cells. Apoptosis detection methods can be classified in the next way (Elmore 2007):

1. Cytomorphological alterations

2. DNA fragmentation (TUNEL - terminal transferase-mediated dUTP nick-end labeling)

3. Detection of caspases, cleaved substrates, regulators and inhibitors

4. Membrane alterations (Annexin V, F2N12S)

5. Mitochondrial assays

Each assay has advantages and disadvantages which may make it acceptable for one application but inappropriate for another application (Watanabe et al., 2002; Otsuki et al., 2003). A detailed description of each method mentioned above can be also found in reviews (Stadelmann and Lassmann 2000; Martinez et al., 2010). Aspects of the molecular machinery and biochemistry of apoptosis, relevant to the development of molecular imaging probes, are highlighed in reviews (Wolters et al., 2007; Tait 2008). Here we will only focus on the technique of apoptosis detection related to membrane changes. This technique includes two fluorescence assays.

Annexin V detection assay. Annexin V was first reported by Bohn and colleagues (Inaba et al., 1984) who isolated it from human placenta and called it placental protein 4 (PP4), and by Reutelingsperger et al. (Reutelingsperger et al., 1985), who isolated it from the umbilical cord by virtue of its anticoagulant activity and called it vascular-anticoagulant-α. The finding that annexin V specifically binds to PS in the presence of calcium (Tait et al., 1989; Andree et al., 1990) facilitated the investigation of the PS exposure at the outer membrane leaflet of cells. Koopman et al. (Koopman et al., 1994) were the first to describe a method using an extrinsically applied hapten (i.e., FITC or biotin) labeled annexin V to detect apoptosis. Annexin V is not able to bind to healthy cells since this protein is not able to penetrate the phospholipid bilayer.

Annexin V is a calcium-dependent protein that preferentially binds phosphatidylserine with high affinity. Once the apoptotic cells expose PS, they are bound with fluorescently-labeled annexin V and can be visualized. In dead cells the inner leaflet of the membrane is also available for annexin V binding, since the integrity of the plasma membrane is lost. To discriminate between dead and apoptotic cells, a membrane impermeable DNA stain (propidium iodide, PI) can be added simultaneously to the cell suspension. In this way healthy (no staining), apoptotic (single staining) and dead cells (double staining) are discriminated and analyzed either by flow cytometry or fluorescence microscopy. Annexin V affinity assay was further developed by labelling the protein with biotin or with several radionuclides to develop various protocols for measuring apoptosis both in vitro (van Engeland et al., 1998) and in vivo (Blankenberg et al., 1998; Dumont et al., 2001; Kenis et al., 2004; Murakami et al., 2004) in animal models. Today, the upgrade-version of annexin VI assay is described (Smith et al., 2010).

The advantages of the assay are its high sensitivity (can detect a single apoptotic cell) and the ability to confirm the activity of initiator caspases. Externalization of PS residues on the outer plasma membrane of apoptotic cells allows detection via annexin V in tissues, embryos or cultured cells (Bossy-Wetzel and Green 2000). The annexin V technique has several limitations. The first, a high extracellular concentration of Ca^{2+} ions (up to 2.5 mM) has to be provided for complete binding of annexin V to PS. Since Ca^{2+} ions activate the scramblase that randomizes the phospholipids distribution (Williamson et al., 1992), this enzyme can move PS to the cell surface in a calcium-dependent manner and lead to false positive results. Furthermore, annexin V can associate with membrane surfaces containing by-products of lipid peroxidation that modify amines by producing negative charges (Balasubramanian et al., 2001). Detergents in the medium can also change the annexin V lipid binding specificity (Meers and Mealy 1993).Routinely used cell harvesting techniques for adhering cells, such as trypsinization, can also produce false results in application of this method (van Engeland et al., 1998). Finally, for complete annexin V binding, pre-incubation times of up to 1 h are commonly needed making kinetic measurements problematic (Zweifach 2000).

F2N12S detection assay is based on the F2N12S, a molecular fluorescent probe (Shynkar et al., 2007). This dye exhibits an excited-state intramolecular proton transfer (ESIPT) reaction resulting in a dual fluorescence with two emission bands at 480 nm and 570 nm, producing a two-color ratiometric response to variations in the lipid composition of the cell outer leaflet. In combination with propidium iodide, which is capable of passing through the cell membrane only in late apoptotic or necrotic cells, it allows discrimination normal, dead and early apoptotic cells. F2N12S is a novel violet excitable dye for the detection of membrane asymmetry changes during apoptosis. It works well on adherent and suspension cells and correlates with other indicators of apoptosis, such as caspase detection or changes in mitochondrial membrane potential.

This assay provides an easy, efficient method for the detection of apoptosis with dead cell discrimination using a violet laser flow cytometer. Unlike annexin-based assays, this assay does not require special buffers or washing steps, and it is less susceptible to the cell membrane damages commonly found during the physical or chemical removal steps when assaying adherent cells, therefore, providing better data quality. Additional advantages include accurate apoptotic analysis on trypsinized cells and simple 5 minute staining protocol compatible with other blue-excited apoptotic stains. The main disadvantage of the assay is connected with the low photostability of F2N12S – insufficient for continuous fluorescence imaging. Moreover, the mechanism of the probe response is not clearly established, as PS exposure may not be the only reason for the observed emission response of the probe.

Alternative methods of apoptosis detection based on membrane changes. Alternative methods to detect the changes of the cell plasma membranes on apoptosis include application of monoclonal antibodies against negatively charged lipids (Miyazawa et al., 1992; Ran et al., 2002). These antibodies found limited applications, probably because of their lability, high cost and complex procedures for visualization of their binding. Moreover, it was shown that their binding inhibits the Na/K-ATPase activity (Stekhoven et al., 1994). Meantime, by mimicking the properties of antibodies some peptides were found to recognize PS (Igarashi et al., 1995) and PE (Emoto et al., 1997) and bind them specifically. Biotinilation of these peptides allows their conjugation with fluorescently labeled streptavidin in order to label apoptotic cells fluorescently.

Probing the exposure of PS on the cell surface can be also achieved with an organic molecule composed of a fluorophore and an artificial zinc-containing receptor (Koulov et al., 2003). However, this probe is still far from ideal mainly because of the requirement for chelating Zn^{2+} ions in the medium. Tracking of lipid exchange between leaflets can also be performed with fluorescently labeled lipids (Connor and Schroit 1988; Pomorski et al., 1995). But it has to be kept in mind that modification of the lipid distribution between leaflets is not well tolerated by the cells, and cell treatment with exogenic PS can itself induce apoptosis (Uchida et al., 1998). The increase of the negative charge of apoptotic cells due to PS exposure can also be used for sensing. Thus, apoptotic cells can be labeled with cationic liposomes containing fluorescent phospholipid analogs (Bose et al., 2004). Basing on the same principle of selective binding to negatively charged surface, positively charged nanoparticles have been used for apoptosis detection (Schellenberger et al., 2004).

Finally, the membrane-specific detection of apoptotic cells can be based on the decrease of lipid order and membrane rigidity that follows the randomization of the lipid content of the membrane. The small size of the lipid head of PE and the repulsion between negatively charged PS heads should increase hydration of the outer leaflet, and these changes can be detected by fluorescent dyes. There are many observations that apoptotic cells exhibit increased binding of not only cationic amphiphilic drugs, such as chlorpromazine and verapamil (Moreau et al., 1997), but also of the negatively charged lipophilic dye, merocyanine 540 (M540) (McEvoy et al., 1986; Frey 1995). This dye is known to bind most efficiently to structurally destabilized lipid bilayers (Williamson et al., 1983; Stillwell et al., 1993) and therefore can distinguish apoptotic cells. However, the approach based on M540 binding is rarely used because of its low specificity (Frey 1997). Other apoptotic reporters have been described, including small molecules, nanoparticles, cationic liposomes, and some other proteins that can recognize PS on the membrane surface (see review of Hanshaw and Smith 2005).

This short review of available methods of studying the cell plasma membrane alterations upon apoptosis demonstrates that simple, inexpensive and universal techniques have to be developed. These techniques should be fast in response and not depend on the presence of Ca^{2+} or other ions. They should be direct, with a minimum number of reaction steps and with sufficient sensitivity providing a broad range of comparative measurements in cell suspensions, cell-sorting conditions, single cells and tissue slices for microscopy.

1.3.4. Fluorescent membrane probes

A variety of fluorescent membrane probes have been synthesized during the last decades. Hundreds of them are commercially available. These probes provide a powerful approach to study membrane-related phenomena by fluorescence microscopy (which gives information on membrane lateral organization by direct visualization) and fluorescence spectroscopy (which gives information about molecular interactions, order and micro environment). The aim of this chapter is to give a general presentation and current state of fluorescent membrane probe development.

Classification. Due to the large variety of membrane probes, there is no universal criterion for their classification. All probes are usually characterized by high membrane affinity, i.e. a strong partitioning in favor of the lipidic apolar phase versus the aqueous bulk. Fluorescent membrane probes can be classified by numerous principles among which the most important are:

- presence of charged group – charged molecules (Patman, TMA-DPH) or structures without charge (Prodan, Nile Red);
- probe structure (Fig.1.25) – lipid-like molecules (NBD-lipids or labelled acids; with fluorophore attached to acyl chain or to the polar head group) or probes with original molecular design (Cyanines, F2N12S);
- origin of chromophore – environment-sensitive probes (NBD, 3-hydroxyflavones) or environment-insensitive (Rhodamine, Fluorescein, etc);
- target parameter – probes for polarity, viscosity, hydration, potential measurements;
- type of response – intentiometric probes or ratiometric ones;
- molecular mass – small molecules or macromolecules.

In order to choose the best-fitting membrane probe(s) when planning up the experiment, a few important points should be kept in mind:

- Membrane includes outer and inner leaflets. Each of them is composed of different lipids and proteins. Thus, the physical properties of the bilayer are different for both sides. Knowledge of orientation and location of the probe is important in order to avoid misleading conclusions. Dye molecules show heterogeneous distribution in the bilayer (Klymchenko et al., 2004a), and neutral probes can easily partition between the two membrane leaflets (Krasnowska et al., 1998) due to the relatively weak van der Waals interactions, resulting in detection of a mean value within the membrane.
- Physical membrane properties are not constant along the bilayer. The inhomogeneous nature of the lipid bilayer originates from localization of the phospholipids functional groups at different membrane depths (Wiener and White 1992) and results in strong gradients of polarity and hydration (Bartucci et al., 2003; Kurad et al., 2003).
- Finally, fluorescence properties of probes are sensitive to a number of parameters, such as polarity, hydration, viscosity, and so on (Valeur 2002). In this respect, it is very difficult to discriminate all these factors by using only the information based on the spectral shift of a single fluorescence band.

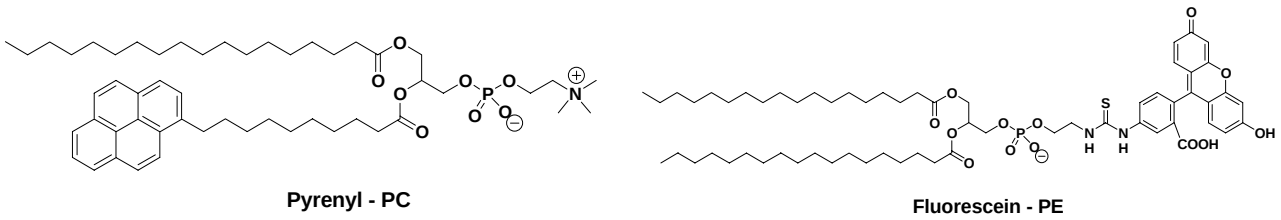

Figure 1.25. Fluorescent phospholipid probes with different attachment of fluorophore.

One of the most commonly used *neutral probes* is diphenylhexatriene (DPH). Addition of DPH to a membrane results in complete probe incorporation with no significant emission of the probe in aqueous environment. DPH, which is mainly used for the determination of membrane fluidity by fluorescence anisotropy (Lentz 1989), has no precise location in the membrane bilayer, in contrast to its cationic derivative TMA-DPH (Kuhry et al., 1983; Kuhry et al., 1985) which is localized near the membrane-water interface by trimethylammonium anchor group.

Among the popular voltage sensitive (potentiometric) dyes the most characterized are *transmembrane potential probes*. Transmembrane potential plays a major role in cell bioenergetics and membrane transport and is often measured by standard electrophysiological methods provided for cells that are large enough for the insertion of microelectrodes. The development of potentiometric dyes has been motivated by the needs for neuroscientists to monitor neuronal electrical activity when microelectrode measurements were inadequate. Now these dyes represent an approach alternative to classical microelectrodes.

The transmembrane potential fluorescent probes have been classified as either slow or fast (electrochromic) dyes (Fig. 1.26). There is a fundamental difference between these two families of dyes with regard to both the mechanism and speed of their response to membrane potentials. Three main classes of slow potential-sensitive dyes are carbocyanines, oxonols and rhodamine derivatives. Slow dyes monitor membrane potential through their Nernst equilibrium distribution between the cell interior and the exterior medium. The mechanism underlying the response of the fast dyes is known as electrochromism and relies on the interaction of an electric field with the ground-state and excited-state dipole moments of the chromophore. Fast dyes follow membrane potential changes in the nanosecond time scale. There are two main groups of fast-response dyes suitable for measuring membrane potential: ANEP-dyes (Amino Naphthyl Ethenyl Pyridinium dyes developed by L. Loew) and RH dyes originally synthesized by R. Hildesheim. Both classes belong to the sytryl-pyridinium family and their main representatives RH414 and di-4-ANEPPS (Grinvald et al., 1982; Fluhler et al., 1985) are shown in Fig.1.26. They were applied to measure membrane potentials in squid axon, red blood cells, pig and sheep heart, lipid vesicles and a variety of cells in culture (Montana et al., 1989; Bedlack et al., 1992; Loew et al., 1992). These dyes exhibit relatively low sensitivity to changes in transmembrane potential (~7% per 100 mV) and thus they are mostly used for investigation of systems which exhibit large changes in transmembrane potential (like neurons). Among ANEP-dyes the most promising probe is di-4-ANEPPDHQ. This dye exhibits very low cell internalization and good signal/noise ratio. It can be useful for neural network analysis and visualization of cholesterol-enriched lipid domains (Obaid et al., 2004; Jin et al., 2005; Obaid et al., 2005).

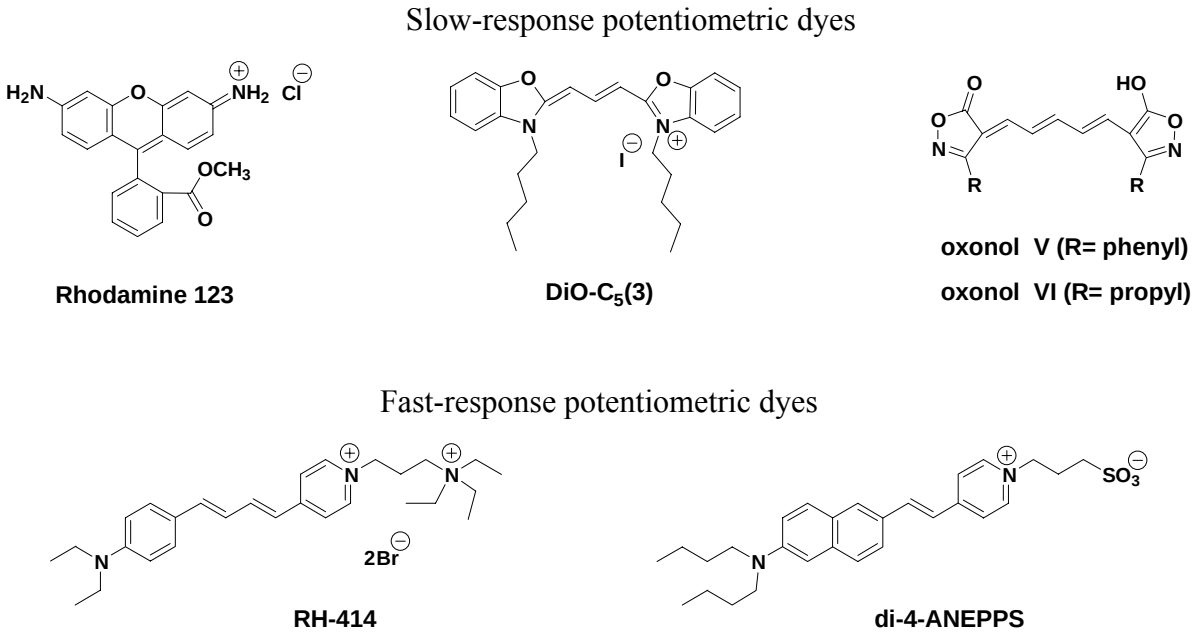

Figure 1.26. Structures of probes for transmembrane potential (Haugland 2002).

Recently, new potentiometric dyes were described (Fig. 1.27). ANNINE-6 (Hubener et al., 2003) contains six anellated benzene rings and exhibits a very high voltage-sensitivity that is exclusively based on a molecular Stark effect (Kuhn and Fromherz 2003). One serious problem with this dye is its extremely low solubility in water, thus intracellular staining of brain tissue is impossible (Dombeck et al., 2005). In contrast, its water soluble analogue ANNINE-6plus (Fromherz et al., 2008) exhibits a high solubility of around 1mM and displays a strong binding to lipid membranes. As compared to ANNINE-6, the novel dye can be used to stain cells directly from aqueous solution without surfactants or organic solvents.

In our laboratory a voltage sensitive dye based on 3-hydroxychromone was developed. It is characterized by deep insertion of its fluorophore into the lipid bilayer allowing two-color ratiometric response to transmembrane potential up to 15% per 100 mV (Klymchenko et al., 2006). Although this probe is more sensitive than ANEP-dyes, its sensitivity is lower than that of ANINE-dyes.

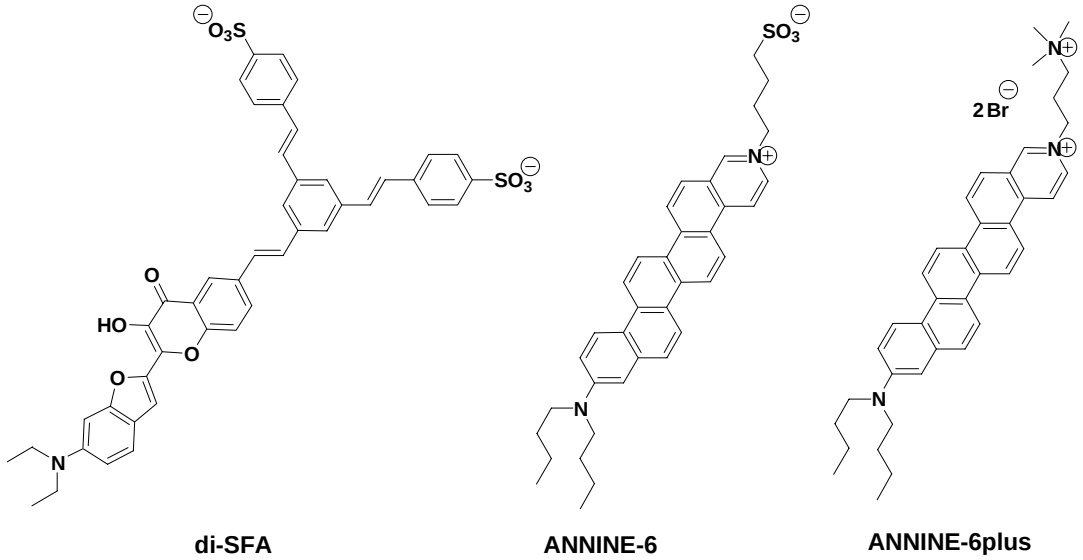

Figure 1.27. Structures of new potentiometric dyes.

The most developed and popular *solvatochromic membrane probes* are 6-propionyl-2-dimethylamino-naphthalene (PRODAN), 6-lauroyl-2-dimethylaminonaphthalene (Laurdan), Nile Red and derivatives of 7-nitro-2,l,3-benzoxadiazol-4-amine (NBD). These probes respond to changes of their environment by shifts of their fluorescence emission and/or excitation spectra (Loew 1988; Reichardt 1994; Valeur 2002). Prodan is highly sensitive to various structural changes not only in proteins but also in lipid bilayers. For instance, a strong red shift of its emission is observed on transition from liquid crystalline phase to gel phase (Krasnowska et al., 1998). Strong changes in the emission color are also observed on addition of cholesterol (Massey 1998; Bondar and Rowe 1999) and under high pressure, or upon addition of local anesthetics and alcohols (Chong 1988; Zeng and Chong 1995). A similar response to phase transition and cholesterol is reported for the more hydrophobic Prodan analog, Laurdan (Parasassi et al., 1990; Parasassi et al., 1994).

Our laboratory had also shown that solvatochromic dyes based on 3-hydroxychromone are highly sensitive to variety of membrane properties, particularly hydration, polarity, lipid order and electrostatics (Klymchenko et al., 2004a; Klymchenko et al., 2004b).

The sensitivity of environment-sensitive probes to the membrane lipid phase has been used to visualize rafts in model membranes (Dietrich et al., 2001; Bagatolli, 2006; Jin et al., 2006). According to Prodan and Laurdan data, the hydration in the Lo phase is much lower than in fluid phase, being close to that of the gel phase (Parasassi et al., 1994). An environment sensitive dye of the styrylpiridinium family, di-ANEPPQ, also shows a blue-shifted emission in the Lo phase with respect to the fluid phase (Jin et al., 2006), suggesting a decreased water relaxation. In contrast to the fluid phase, the Lo phase stained with the probe shows strong second harmonic generation (SHG) signal, suggesting that the probe adopts a vertical orientation.

The Lo phase was also characterized by using both DPH (Gidwani et al., 2001) and molecular rotor probes. Since the Lo phase demonstrates high lipid order and slow dynamics, the corresponding domains can be visualized using the enhanced fluorescence intensity of a molecular rotor based on a Prodan analogue (Kim et al., 2008). Due to the response to membrane hydration probes Laurdan and di-ANEPPQ allow color-imaging of the lipid domains (Bagatolli, 2006; Jin et al., 2006). Remarkably, the last approach is independent from the partition of the probe between the different phases and provides a direct assignment of the phases according to their hydration. Recently a Prodan-based fatty acid was introduced, which having higher specificity to cell plasma membranes, is probably more suitable than other Prodan derivatives for cellular studies of lipid domains (Kim et al., 2007). Also, several membrane probes of the 3-hydroxychromone family showed strong changes in the two-color emission when Lo and Ld phases were compared. This property was used to visualize lipid domains in giant vesicles (Klymchenko et al., 2009).

During last decade a great number of research articles were dedicated to the development of new fluorescent molecules (Cairo et al., 2010; Demchenko et al., 2009; Lavis and Raines 2008) as well as of new fluorescent approaches (Wu et al., 2011; Demchenko 2010), indicating that these problems are still of actuality. However, despite a great variety of available probes for visualizing biological membranes, only few of them can be used for quantitative measurements of membrane-related parameters. The lack of simple tools is the main obstacle for further membrane investigation. In this context, the present thesis is aimed on developing new fluorescent membrane probes allowing effective visualisation and analytic measurement of lipid organization both in model systems and live cells.

CHAPTER 2

RESULTS AND DISCUSSION

2. RESULTS AND DISCUSSION

2.1. Probes based on 3-hydroxyflavone (3HF) fluorophore

2.1.1. Mechanism of F2N12S response to apoptosis

Previously, our laboratory developed the probe F2N12S, that is able to detect apoptosis by changes of its emission spectrum due to the loss of transmembrane asymmetry (Shynkar et al., 2007). However, only one possible factor of the probe response was mentioned (PS exposure), and no clear mechanism of the probe response to apoptosis was proposed.

In order to clarify the mechanism of the probe response we performed a set of experiments. Through the spectroscopic analysis of F2N12S response, we characterized the membranes in terms of hydration and polarity (electrostatics). The hydration parameter value in cell membranes was found in between the values obtained in model membranes with liquid ordered (Lo) and liquid disordered (Ld) phases, suggesting that cell plasma membranes exhibit a significant fraction of Lo phase at the outer leaflet. Moreover, two-photon fluorescence microscopy showed that cell membranes labeled with this probe exhibits a homogeneous lipid distribution, suggesting that the putative domains with Lo phase are distributed all over the membrane and are highly dynamic. Cholesterol depletion affected dramatically the fluorescence spectrum of the probe suggesting the disappearance of the Lo phase in cell membranes. This conclusions were corroborated with the viscosity-sensitive diphenylhexatriene derivative TMA-DPH, showing membrane fluidity in intact cells intermediate between those for Lo and Ld phases in model membranes, as well as a significant increase in fluidity after cholesterol depletion. Moreover, we observed that cell apoptosis increases strongly the hydration parameter, suggesting that, similarly to the cholesterol extraction process, apoptosis results in the loss of Lo phase at the outer leaflet of cell membranes. This loss of Lo phase could be attributed to a flip of sphingomyelin from the outer to the inner leaflet of the plasma membrane due to apoptosis-driven lipid scrambling. Some increase in the membrane polarity was also observed, suggesting some increase in the negative surface charge due to PS exposure in apoptotic cells. Thus, these studies showed that the response of F2N12S to apoptosis is not a simple answer to the PS exposure, but a combination of effects, where the main one is probably the loss of Lo phase at the outer leaflet. All these results were recently published (Publication 1).

This study further stimulated the development of new membrane probes with improved sensitivity to lipid order and to surface charge, as it will be presented in the next chapters.

2.1.2. First generation of 3HF probes

Molecular design. The first generation of 3HF probes is shown in Fig. 2.1. These molecules are the long chain analogues of F2N12S, and they were designed in order to find the optimal configuration of lipophilic chains in the probe structure. Thus, probes **1** and **2**, resemble the structure of the original probe and consist of a fluorophore and an anchoring part, formed by long alkyl chain and zwitterionic group, connected together by a linker (simple methylene-group). As compared to the original F2N12S, probe **1** bears longer lipophilic groups on the fluorophore moiety (dibutylamino group), while probe **2** bears extended alkyl chain (octadecyl-group) in the anchoring part.

Other molecules of the 1st generation, probes **3-6**, feature a more flexible propyloxy-group as a linker between a fluorophore and an anchoring part of the molecule (Fig. 2.2). This linker confers to the fluorophore an additional freedom of orientation and localization in the lipid bilayer.

For probes **3-6**, the presence of an electron donor alkyloxy-group in the 7-position of 3HF core affects the emission spectra and reduces the N* band intensity. probes **3** and **4** bear a donor dibutylamino group in the 4'-position of the 3HF core, while **5** and **6** bear stronger donor diphenylamino group and thus are expected to show higher intensity of the N* band, as it is known for flavones, the stronger donor in 4'-position – the more intensive N* band in the emission spectrum. Finally, structures of probes **3** and **4** differ only by the presence of a methyl-group in the 8-position on the flavone core, and the same difference is seen for probes **5** and **6**.

Chemical synthesis. In order to obtain the long-chain analogues probes **1** and **2**, Br-methyl flavone derivatives were synthesized as described before (Klymchenko et al., 2002c). Further, they were coupled with dodecylmethylamine (for probe **1**) or octadecylmethylamine (for probe **2**) in THF (see Scheme 4.3 in chapter Materials and Methods). Reaction proceeded at RT with excellent yield. Obtained tertiary amines were quaternized with an excess of 1,3-propanesultone in toluene/acetonitrile mixture (1:1) to give the final dyes (probes **1** and **2**) in good yields.

Synthesis of linker-modified analogues **3-6** consists of two parts: (a) introduction of tertiary amino group into acetophenone molecule (see Scheme 4.2); and (b) synthesis of 3-hydroxy-flavone by modified Algar-Flynn-Oyamada (AFO) reaction, followed by quaternization of the tertiary amine with 1,3-propanesultone (see Scheme 4.4). Firstly, 2,4-dihydroxy-acetophenone (or its 3-methyl homologue) was reacted with 1-bromo-3-chloropropane under basic conditions. Obtained (3-chloropropyloxy)-derivative was coupled with dodecylmethylamine in the presence of potassium carbonate to give the desired acetophenone with tertiary amino group. Secondly, condensation of the prepared acetophenone with 4-dibutylamino-benzaldehyde (or 4-diphenylamino-benzaldehyde) was done in the presence of sodium methoxide in DMF. Reaction proceeded at RT and resulted in chalcone derivatives, which were further transformed into 3-hydroxyflavones by boiling in ethanol with hydrogen peroxide and excess of sodium methoxide. Obtained flavones with tertiary amino moiety were reacted with 1,3-propanesultone to yield the final products (probes **3-6**).

Structures of all obtained substances were elucidated by NMR spectroscopy and Mass spectrometry. All the final probes were purified by column chromatography (or preparative TLC) and were pure according to NMR and LCMS data, flash TLC analysis and their absorption spectra. Detailed synthetic schemes, procedures and related information are presented in chapter Materials and Methods.

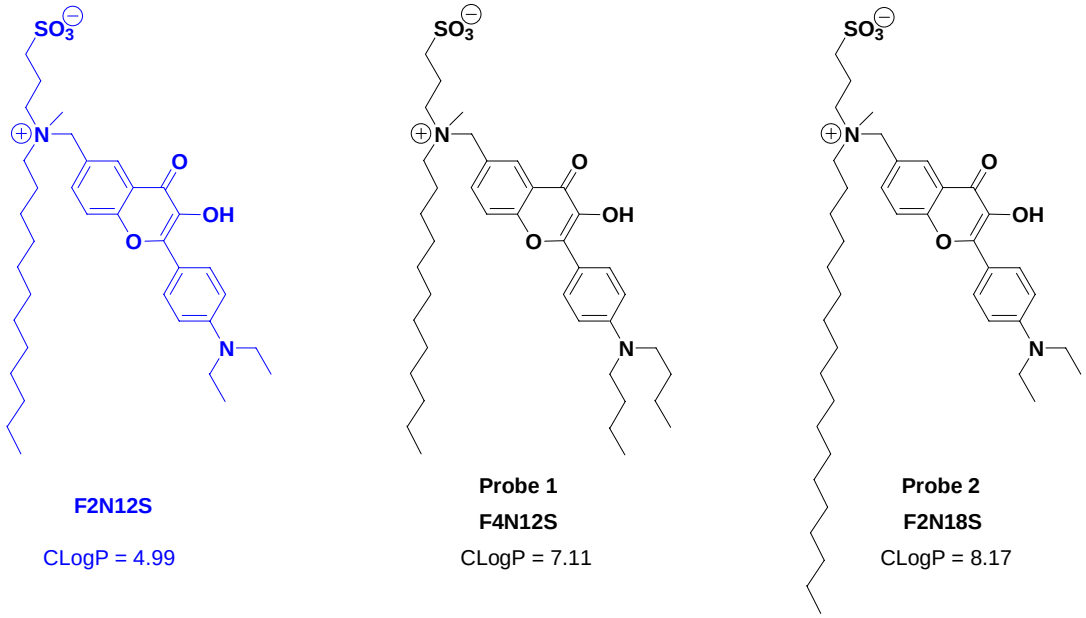

Figure 2.1. Chemical structures of original probe F2N12S and its long-chain analogues. ClogP values were calculated using the software ChemDraw Ultra 6.0, Cambridgesoft Corporation.

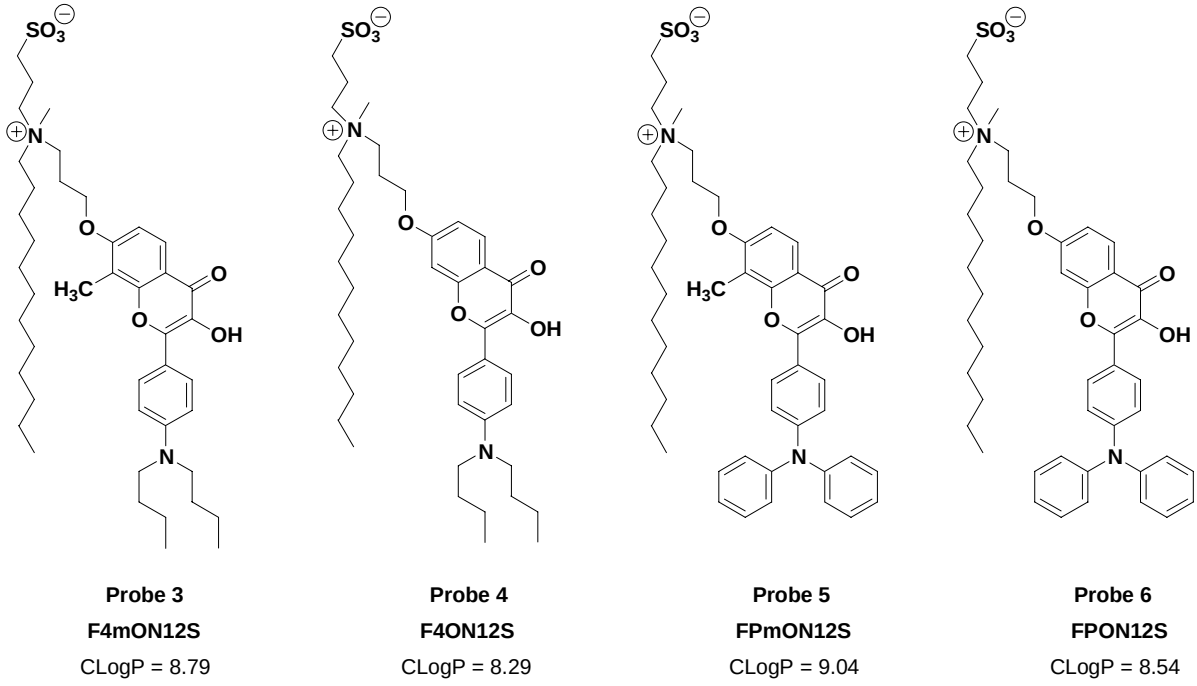

Figure 2.2. Chemical structures of linker-modified analogues of F2N12S.

Binding to model membranes. Similarly to the original probe F2N12S, the new dyes are not emissive in buffer solution, but upon their binding to lipid membrane they become highly fluorescent. In order to explore their binding properties, titration of lipid vesicles with increasing probe concentration was performed (Fig. 2.3). Importantly, only probes **1** and **4** have comparable fluorescence intensities with respect to F2N12S, while other dyes showed lower values in the same experimental conditions. Upon binding to lipid membranes probe **2** showed much lower fluorescence intensity than probe **1**. We could speculate that probe **2** is too hydrophobic and prefers self-aggregation rather than incorporation into the lipid bilayer. This fact has limited the detailed investigation of probe **2**.

Interestingly, probes **3** and **5** revealed lower fluorescence intensity in respect to their non-methylated analogues **4** and **6**. Our suggestion on the origin of this effect is that 8-methyl group disfavors free rotation around C-O bond in 7-position of the flavone core due to steric hindrance. The reduced rotational freedom of fluorophore may impose unfavorable orientation of the probes in the bilayers, and thus decrease the fluorescence intensity (i.e. membrane affinity). Interestingly, butyl derivative probe **4**, reveals two times higher fluorescence in DOPC-vesicles as compared to its phenyl-analogue probe **6**, where donor group is more rigid and bulky.

In order to access the binding kinetics we compared the fluorescence intensity of the probes at different incubation times. Binding of F2N12S was fast as the intensity remained invariant after 3min of incubation. In contrast, the 1st generation showed slow membrane incorporation. For example, complete binding of probes **4** and **6** to DOPC vesicles was observed in 30 min.

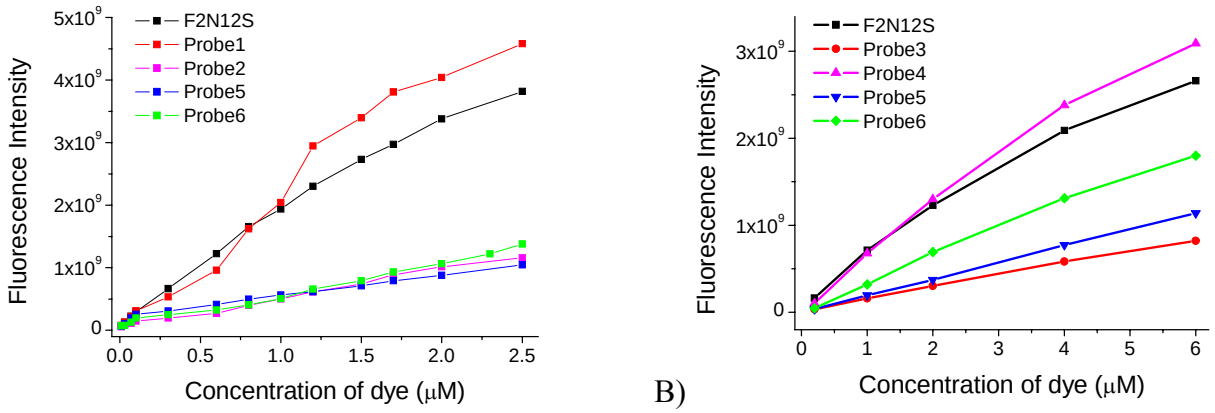

Figure 2.3. Emission intensities of the 1st generation of 3HF probes and F2N12S in DOPC vesicles. Lipid concentration was 200 μM in phosphate buffer 20 mM, pH 7.4. Incubation time was 5 min (A) and 30 min (B) at 20°C.

Table 2.1. Spectroscopic properties of the 1st generation of 3HF probes in model membranes.[a)]

Probe	Lipid vesicles	λ_{abs}, nm	N* band, nm	T* band, nm	N*/T*	QY, %
F2N12S	DOPC	418	514	571	1.00	30.0
	DOPS	419	503	568	1.46	20.5
	DPPC-Chol	422	476	571	0.19	22.0
	Sm-Chol	425	472	573	0.70	26.5
Probe 1 F4N12S	DOPC	421	506	574	1.07	25.0
	DOPS	418	507	570	1.51	17.5
	DPPC-Chol	422	473	573	0.23	24.0
	Sm-Chol	419	484	576	0.79	20.5
Probe 3 F4mON12S	DOPC	390	478	569	0.26	4.5
	DOPS	384	488	571	0.93	3.0
	DPPC-Chol	382	490	567	0.27	2.0
	Sm-Chol	384	485	569	0.29	4.0
Probe 5 FPmON12S	DOPC	386	482	575	1.29	3.0
	DOPS	384	484	576	1.40	5.0
	DPPC-Chol	385	485	574	1.28	6.5
	Sm-Chol	387	482	577	1.56	6.5
Probe 6 FPON12S	DOPC	396	495	575	0.50	2.5
	DOPS	392	499	571	1.00	3.5
	DPPC-Chol	392	503	573	0.23	5.5
	Sm-Chol	398	498	573	0.46	5.0

[a)] Binary lipid mixtures correspond to DPPC-Chol (2:1) and Sm-Chol (2:1). Dye concentration was 1 μM; total lipid concentration was 200 μM in phosphate buffer 20 mM, pH 7.4. Incubation time was 5 min at 20°C.

Sensitivity to lipid composition. The new probes were studied in vesicles formed by different lipids in order to evaluate their sensitivity to membrane physico-chemical properties, which are dependent on membrane composition. Lipids DOPC and DOPS form membranes with Ld phase, while lipid mixtures of DPPC-Chol and Sm-Chol correspond to membranes with Lo phase. Moreover, DOPS is an anionic lipid and therefore, forms negatively charged membrane, in contrast to the neutral DOPC one.

Spectroscopic properties of new probes in various membranes are summarized in Table 2.1. It is worth to note, ratio N*/T* is a very important and convenient criterion for characterization of dual emission of 3HF probes. Usually emission spectra are presented in normalized form, where the intensity of T* band is equal to 1, while the intensity value of the N* band corresponds to the ratio of emission intensities and is called N*/T* ratio.

Spectral profiles of probes **1**, **3**, **6** and parent F2N12S are shown in Fig. 2.4. It is clear that probe **1** exhibits very similar emission behavior to that of F2N12S in vesicles of different lipid composition. This result is expected since differences of structure are minimal between these probes. In contrast, probe **3** does not show any variation of the fluorescence spectra in vesicles with Ld phase (DOPC) or Lo phase (Sm-Chol and DPPC-Chol). On the other hand, probe **3** exhibited significant fluorescence changes in respect to negative charge, as N*/T* ratio increased drastically in DOPS vesicles compared to DOPC ones. This indicates that probe **3** is not sensitive to lipid order, and it is exclusively sensitive to surface charge, in contrast to F2N12S and probe **1**, which emission depends on both parameters. It should be noted that probes **4** and **6** also showed some specific sensitivity to the surface charge, though some heterogeneity in N*/T* values for neutral Ld and Lo phases was observed for these molecules. probe **5** exhibited the lowest fluorescence intensity in all lipid membranes together with poor changes of N*/T* that has limited further exploration of this probe.

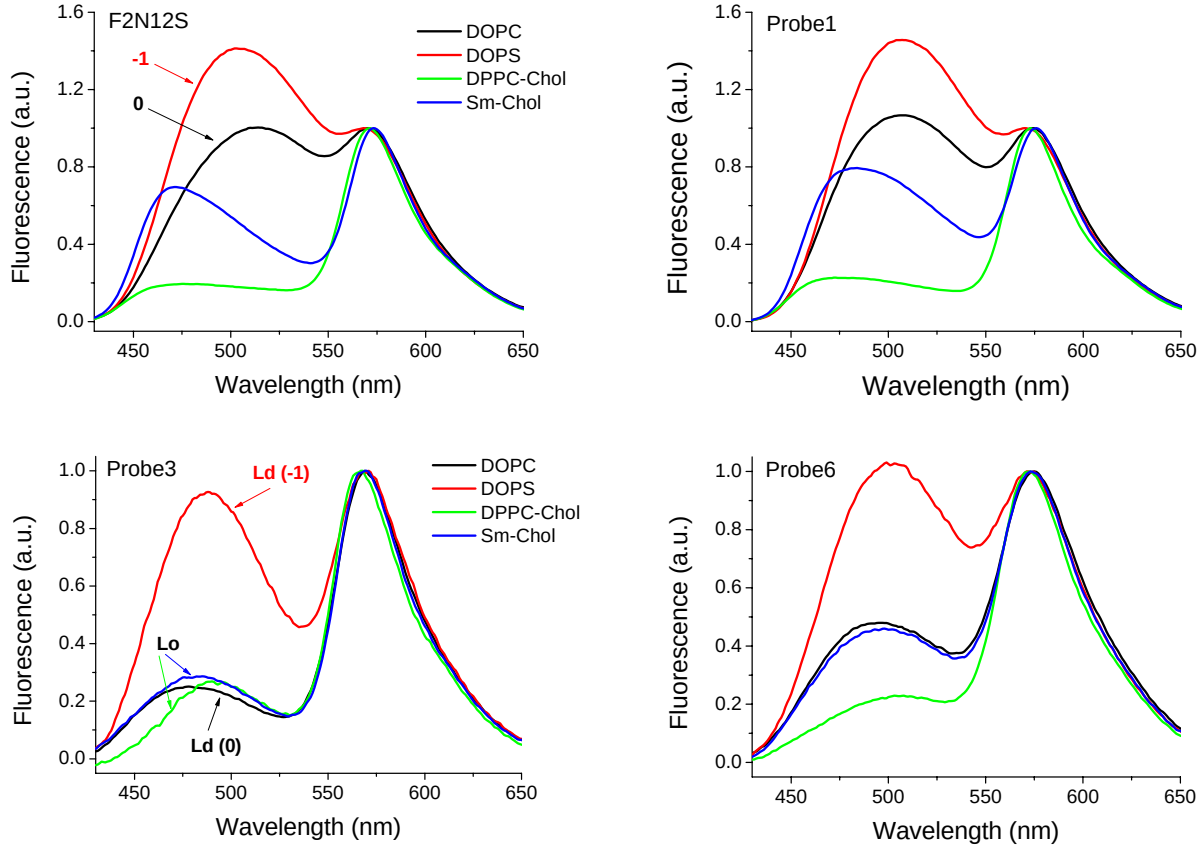

Figure 2.4. Emission spectra of parent F2N12S and probes **1**, **3** and **6** in different lipid vesicles. Dye concentration was 1 μM, lipid concentration was 200 μM in phosphate buffer 20 mM, pH 7.4. Incubation time was 5 min at 20°C.

Sensitivity to surface charge. Further, we explored thoroughly the sensitivity of our probes to the negative surface charge. Emission spectra of the probes were measured in vesicles, composed of DOPC with various contents of DOPS, a negatively charged lipid (Fig. 2.5). The response (%) of the probes vs. content of PS revealed an almost linear dependence for all the dyes, while for probes **3** and **6** the slope of the curve is clearly higher than for F2N12S, confirming their higher sensitivity to the surface charge. Importantly, the variation of N*/T* ratio calculated as $2(a-b)/(a+b)\times 100$ % for probe **3** was 110 % when pure DOPC and DOPS vesicles are compared. This response is 3-fold higher than only 33 % value observed for probe F2N12S.

Several reasons could explain the observed results. Firstly, for probe **3** the localization of the fluorophore is closer to the membrane surface as compared to F2N12S (Fig. 2.6). The surface localization of probe **3** is probably caused by the methyl group, which plays an important role. Such localization could explain also the absence of lipid order effect on the fluorescence of probe **3**, because changes in lipid order take place in regions much deeper than the location of the probe. Secondly, an additional improvement could be connected with the presence of 7-alkoxygroup in our dyes, which was previously shown to increase the sensitivity to surface charge (M'Baye et al., 2007). Thus, probe **3** showed a strongly improved sensitivity to the surface charge together with no sensitivity to the lipid order. This unique profile makes probe **3** very attractive for selective monitoring of surface charge in cell membranes, in particular, on apoptosis transformation.

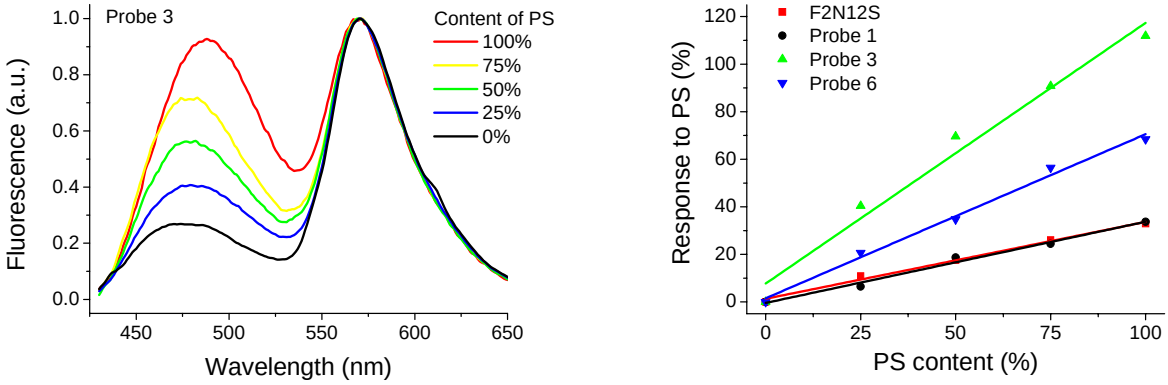

Figure 2.5. Response of selected 3HF probes to DOPS content in DOPC vesicles. Dye concentration was 1 μM, lipid concentration was 200 μM in phosphate buffer 20 mM, pH 7.4. Response was calculated on the base of N*/T* values as *2(a-b)/(a+b)×100%*.

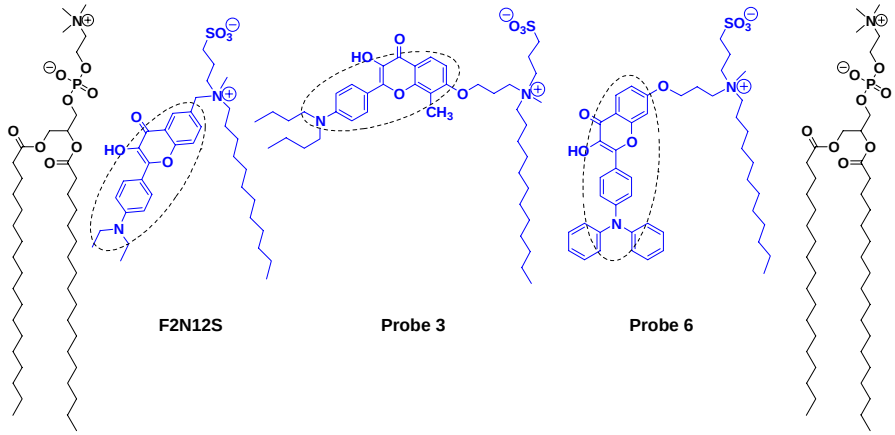

Figure 2.6. Hypothetic localization of the 1st generation probes in the lipid membrane (only monolayer is shown). Dotted lines show the position of fluorophore (tilted, horizontal and vertical).

Cellular studies. After experiments with lipid vesicles, we investigated our probes in plasma membranes. For this purpose, U87MG human malign astrocytes were used. Titrations with increasing dye concentration were performed to determine optimal conditions. Probes were applied for detection of apoptosis induced by Actinomycin D (Fig. 2.7). Probe **1** behaved similarly to F2N12S, showing the same fluorescence intensity on binding to living cells. For this probe, the changes of N*/T* values between normal and apoptotic cells were close to those of F2N12S, confirming their similar behavior, as it was observed in lipid vesicles. Probes **2** and **5** were not studied in cells because of poor membrane binding.

For probes **3**, **4** and **6**, titration studies showed that incubation at 37 °C was needed to reach complete binding equilibrium and stable emission spectrum. Indeed, after temperature increase from 20 to 37°C, the fluorescence intensity of probe **6** in intact cells increased 3-fold and reached a value similar to the F2N12S one. The observed temperature effect suggested that these dyes aggregate rapidly in aqueous solutions at 20°C, while heating prevents fast aggregation favoring the membrane binding. Interesting to note, for probes **3**, **4** and **6** intensities in apoptotic cells were 1.5 times higher then that of intact cells. This can be explained by an increased number of binding sites for these molecules in apoptotic membranes, due to decrease in the lipid order (as shown before). Unfortunately, named dyes showed almost no response to apoptosis, as their difference of N*/T* values in intact and apoptotic cells did not exceed 0.05.

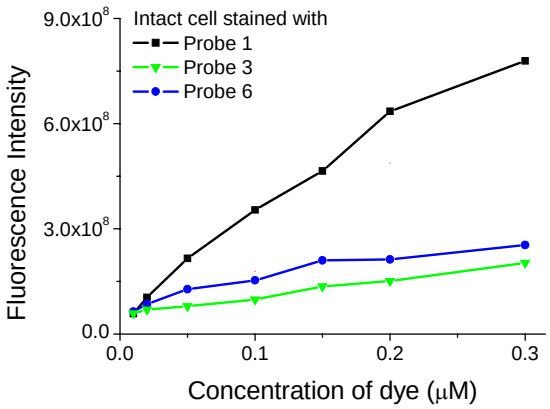

A)

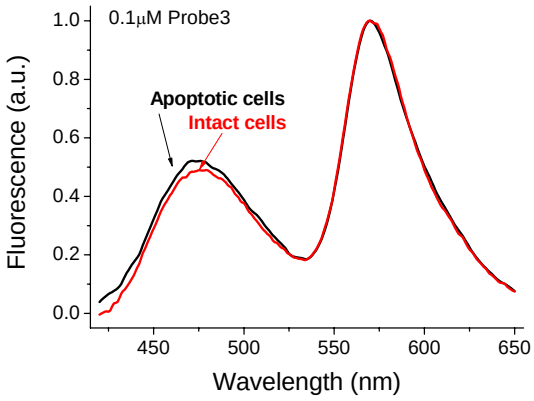

B)

Figure 2.7. Titration of cellular membranes with the 1st generation of 3HF probes (A). Incubation time was 7 min at 20°C. Response of probe **3** to apoptosis in U87MG human malign astrocytes (B). Apoptosis was induced by 18 h incubation with 0.5 μg/mL Actinomycin D.

Why probes **3**, **4** and **6** were not able to detect apoptotic appearance of PS on the outer membrane leaflet? To evaluate the possible change of N*/T* we choose probe **3** due to its unique sensitivity profile. We assumed that dye molecule is localized only on the outer membrane leaflet and responds only to PS exposure upon apoptosis. Using a linear dependence of the probe response to the amount *x* of PS in % (*N*/T*= 0.0065*x+0.260*) and value of PS content in cell plasma membrane (15 %), we calculated an expected change of N*/T* of 0.310-0.260 = 0.050. It should be mentioned that this value can be observed only in the case of 100% amount of apoptotic cells and equal redistribution of PS between inner to outer membrane leaflet (7.5 % of PS at the outer leaflet). Therefore, the real response of the probe to PS exposure should be <0.05, which is in line with a negligible response of probe **3** to apoptosis. This result suggests that the originally observed response of F2N12S may be also driven by factors other than surface charge, namely by changes in the lipid order.

Conclusion. In this chapter, synthesis and properties of the 1st generation of flavone probes were described, and they were compared with original probe F2N12S. Examination of long chain analogues indicated that F2N12S exhibits an optimal structure and that no significant improvements can be achieved by simple extension of alkyl chains at the different parts of the molecule. Higher hydrophobicity of the probes increased their aggregation in buffer and disfavored dye binding to model and cell plasma membranes.

A remarkable feature of several new probes is their high sensitivity to negatively charged lipids (PS content), together with strongly diminished sensitivity to lipid order. Despite this improvement, the probes showed almost no response to apoptosis. Therefore, we conclude that the response of 3HF dyes to apoptosis may be mainly related to the changes of lipid order in cell plasma membrane, in line with results presented in chapter 2.1.1.

Thus, by favoring surface localization of the fluorophore we obtained a unique sensitivity to surface charge, but it was not useful for apoptosis detection. Taking this into account, we decided to develop new molecules with vertical (deep) localization in the lipid bilayer in order to obtain probes with high sensitivity to lipid order. This approach was realized in the 2nd generation of 3HF probes and is described in the next chapter.

2.1.3. Second generation of 3HF probes

Molecular design. The 2nd generation of flavone probes includes five molecules, displayed in Fig.2.8. Their structure combines a zwitterionic group and long alkyl chains attached to opposite sides of the fluorophore moiety. Such molecular design favors vertical dye orientation in the membrane. It should be noted that the probes exhibit a propyloxy-linker, attached at 6- or 7-position of the flavone core. One can expect lower N*/T* values for probes **7** and **8**, due to the donating effect of oxygen conjugated with 4-carbonyl group (Klymchenko et al., 2003c). In addition, 7-substituted molecules have angular (curved, banana-like) geometry, while 6-substituted flavones are linear molecules (probes **9-11**), and one can expect different membrane binding behavior. The length of N,N-dialkyl chains was also varied.

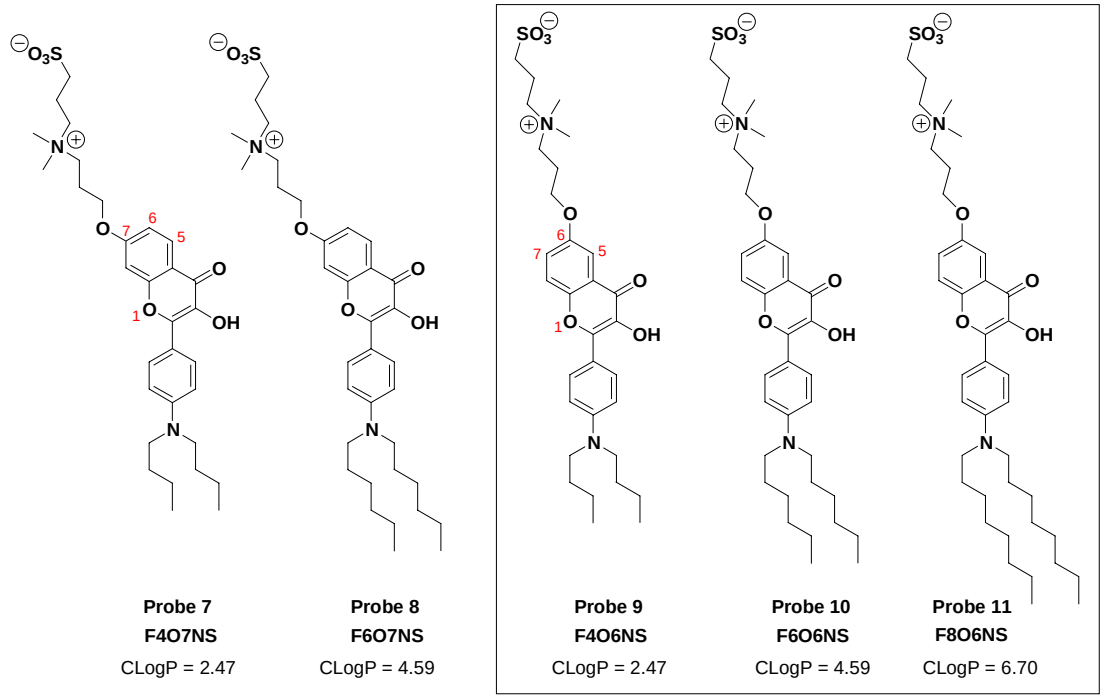

Figure 2.8. Chemical structures of the 2nd generation of 3HF probes ("vertical" probes).

Chemical synthesis. Synthesis of probes was started from 2,4-dihydroxy-acetophenone (or isomeric 2,5-substituted derivative), which was alkylated with 1-bromo-3-chloropropane under basic conditions (see Scheme 4.2 in chapter Materials and Methods). Obtained product was activated by NaJ in acetone (Finkelstein reaction) and was subsequently coupled with dimethyl-amine in THF to produce the acetophenone with a tertiary amino group. In the second part of synthesis, aniline was reacted with hexyl iodide (or octyl iodide) in the presence of potassium carbonate in DMF, and the formed intermediate was formylated by Vilsmeier reaction to produce corresponding 4-dialkylamino-benzaldehyde (see Scheme 4.1). Finally, oxidative cyclization of obtained 4-dialkylamino-benzaldehydes with previously prepared acetophenone was done by their treatment with excess of sodium methoxide in DMF. Resulted chalcone intermediates were further transformed into 3-hydroxyflavones by reaction with hydrogen peroxide and excess of sodium methoxide. Obtained flavones with tertiary amino moiety were reacted with 1,3-propanesultone to yield the desired products (see Scheme 4.5).

Structures of all obtained substances were elucidated by NMR spectroscopy and Mass spectrometry. All the final probes were purified by column chromatography (or preparative TLC) and were pure according to NMR and LCMS data, TLC analysis and their absorption spectra. Detailed synthetic schemes, procedures and related information are presented in chapter Materials and Methods.

Binding to model membranes. Investigation of binding properties of new dyes was started with titration experiments, where the concentration of lipid vesicles was varied (probe concentration remained constant). The new probes showed emission intensities comparable with that of F2N12S. The information about binding affinity was obtained by comparing the steepness of the fluorescence curves. The intensity changes were not so steep for the butyl-derivative probe **7** (red line, Fig. 2.9). It has "banana like" (angular) structure, and its binding to lipid bilayer is less favorable. In addition, lower affinity of probe **7** to lipid membrane is supported by its higher solubility in water: its fluorescence quantum yield in water reaches 2%, while for F2N12S and other dyes (probes **8-11**) it is around 0.5 %.

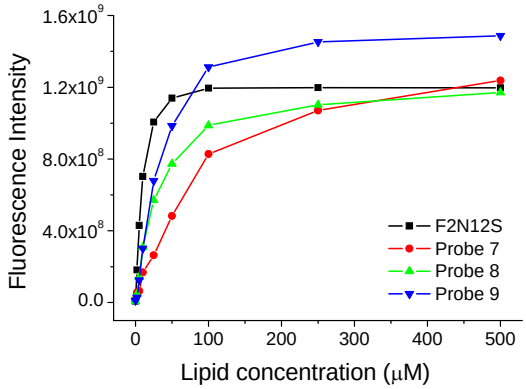

Figure 2.9. Titration of dyes with increasing amount of DOPC vesicles in phosphate buffer 20 mM, pH 7.4. Dye concentration was 0.5 μM. Incubation time at 20°C was 3 min and 7 min (for probe **8**).

Absorption properties of new dyes were found to be similar, in line with the minor structural changes in their fluorophores. For example, in DOPC absorption maximum of probes **7** and **8** was 410 nm and for probes **9-11** it was 417 nm. As F2N12S, all new probes showed well separated two bands in the emission spectrum. The position of the N* band and the N*/T* ratio in various lipid vesicles are collected in Table 2.2. Interestingly, probes **7** and **8** systematically showed twice as low N*/T* value compared to their 6-substituted analogues **9-11**. As it was mentioned before, this is due to donating effect of the O-atom in the 7-position of flavone core (Klymchenko et al., 2003c).

Table 2.2. Spectroscopic properties of the 2nd generation of 3HF probes in model membranes.[a)]

	Probe 7 F4O7NS		**Probe 8 F6O7NS**		**Probe 9 F4O6NS**		**Probe 10 F6O6NS**		**Probe 11** [b)] **F8O6NS**	
T* band, nm	571		571		561		561		561	
Lipid vesicle	**N* band, nm**	**N*/T***	**N* band, nm**	**N*/T***	**N* band, nm**	**N*/T***	**N* band, nm**	**N*/T***	**N* band, nm**	**N*/T***
DOPS (Ld)	488	0.78	479	0.85	487	1.75	489	1.55	-	-
DOPC (Ld)	500	0.51	491	0.43	485	1.05	492	1.00	484	1.05
DOPC-Chol (2:1) (Ld)	496	0.32	482	0.27	477	0.78	479	0.72	475	0.76
DOPC-Chol-Sm (1:1:1) (Ld+Lo)	493	0.34	484	0.29	477	0.83	480	0.75	476	0.84
Sm-Chol (2:1) (Lo)	480	0.25	482	0.31	470	0.67	463	0.56	462	0.72

[a)] Dye concentration was 1 μM, lipid concentration was 200 μM in phosphate buffer 10 mM, pH 7.0. Incubation time was 5 min at 20°C. [b)] Incubation time was 30 min at 20°C.

It is interesting to note the difference in the incorporation times of the new probes. Similarly to F2N12S, butyl derivatives (probes **7** and **9**) need only 3 min to incorporate into lipid membranes, while hexyl derivatives **8** and **10** reach total equilibrium in 6 min. For the octyl analogue (probe **11**), incubation time was found to be very long at 20°C (about 30 min), but an equilibrated emission spectrum was reached in 10 min upon heating at 37°C. The emission intensity of probe **11** in model vesicles was the lowest between presented dyes that has limited its detailed investigation.

Sensitivity to surface charge. DOPC and DOPS vesicles represent Ld phase with neutral and negative surface charge respectively. By analyzing the emission spectra of new probes, we revealed high N*/T* ratio in negatively charged membranes, showing the probe sensitivity to the surface charge. The response of the probes to PS content was calculated as *2(a-b)/(a+b)×100%*, and it was equal to 42, 66, 50 and 43 % for probes **7**, **8**, **9**, **10** respectively, which is significantly higher than that of F2N12S, but lower than that of probe **3** from the 1st generation.

Sensitivity to lipid order. Further experiments were aimed to explore the effect of lipid order on the probe behavior. For this purpose, lipid vesicles composed of various lipids were titrated with increasing dye concentration (Fig. 2.10). Titration was started from 0.2μM dye, and it was continued up to saturation, where no increase of fluorescence upon dye addition was observed. In Ld phase (presented by DOPC and DOPC-Chol membranes) probes **7-10** showed emission intensities similar to F2N12S, but significant differences were observed for membranes with Lo phase.

In vesicles composed of sphingomyelin and cholesterol, which are known to exist in Lo phase, one can observe two interesting effects (Fig. 2.10). At first, butyl derivatives (probes **7** and **9**) exhibited somewhat higher fluorescence intensity than corresponding hexyl analogues (probes **8** and **10**). At second, linear molecules (probes **9** and **10**) showed higher fluorescence intensity as compared to their banana-like analogues **7** and **8**. Thus, tight packing of lipids in Lo phase disfavors binding of molecules with angular structure and too long alkyl chains. Additional influence of lipid phase on fluorescence behavior can be followed by comparison of emission intensities of probe **10**, taken as an example, in various membrane types. In line with increasing fraction of Lo phase, one can see the decrease of integral intensity, and the lowest value is observed in Sm-Chol vesicles, where the number of binding sites is minimal due to tight lipid packing.

Similarly to F2N12S, the new probes showed a significantly decreased N*/T* ratio in Lo phase (Sm-Chol) as compared to Ld phase (DOPC). However, we found a low N*/T* ratio for Ld phase in the presence of cholesterol (DOPC-Chol), which is close to that for membranes with Lo phase. Thus, in contrast to F2N12S, the emission of new probes is sensitive to the presence of cholestero in Ld phase (see Table 2.2).

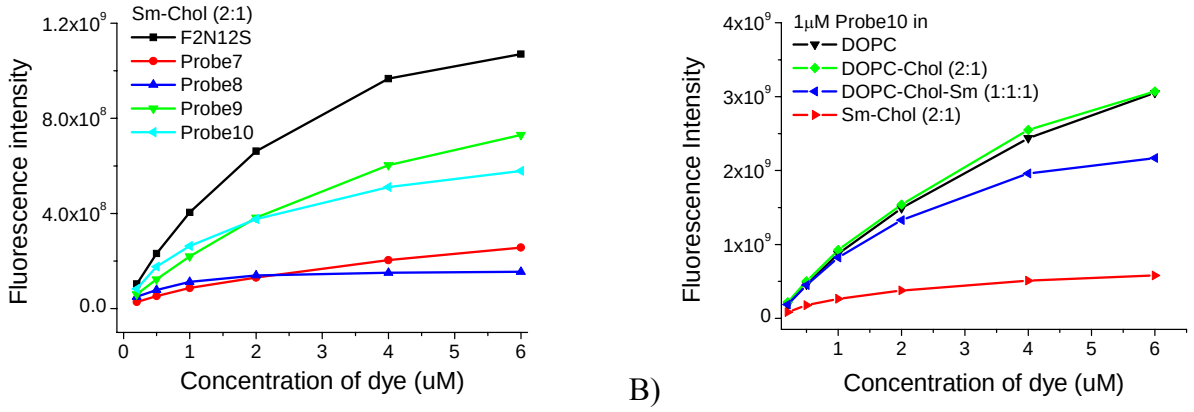

Figure 2.10. Titration of Lo phase vesicles with the 2nd generation of 3HF probes (A). Integral intensity of probe **10** in various lipid vesicles (B). Lipid concentration was 200 μM in phosphate buffer 20 mM, pH 7.4. Incubation time was 5 min at 20°C.

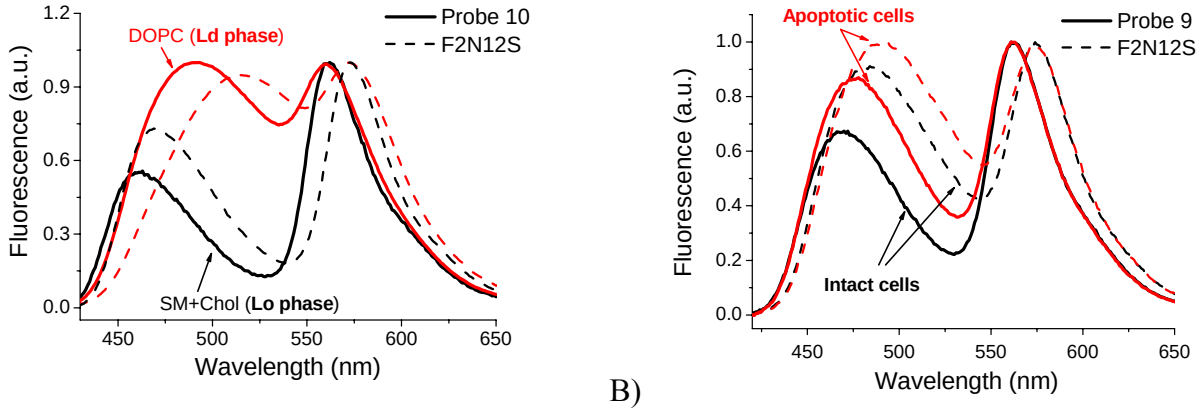

Figure 2.11. Comparison of the emission properties of the 2nd generation of 3HF probes (solid line) and parent F2N12S (dot line) in model (A) and cell membranes (B).

Finally, we were able to compare behavior of F2N12S and the 2nd generation probes in model membranes (Fig. 2.11). In addition to the pronounced advantage of vertical probes (higher response to PS content), one can also find better separation of emission bands and higher response to lipid phase state and the presence of cholesterol.

Cellular studies. Our cellular studies were mainly focused on two types of experiments: (a) cholesterol depletion with methyl-β-cyclodextrin; and (b) detection of apoptosis induced by 18h incubation with Actinomycin D.

For experiments with cholesterol depletion, we choose two linear molecules (probes **9** and **10**) because of their high affinity to lipid membranes. Both probes showed improved response to cholesterol content compared to F2N12S (Fig. 2.12). Indeed, the response to cholesterol extraction calculated as *2(a-b)/(a+b)×100%* was 60 and 48 % for probes **9** and **10** respectively, while for F2N12S it was only 27 %. Importantly, ratios N*/T* observed in intact cells and in model Lo-membranes (see Table 2.2) were of similar value (around 0.6-0.7).

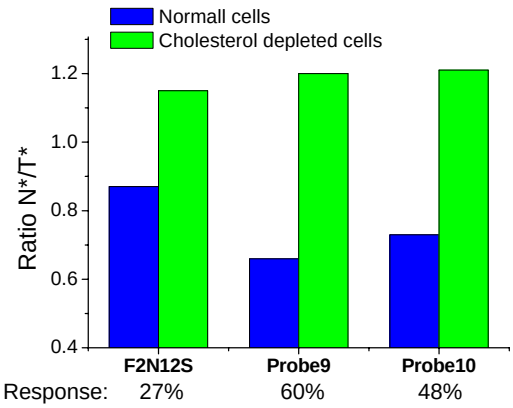

Figure 2.12. Sensitivity of the 2nd generation of 3HF probes to cholesterol content in plasma membrane. Cholesterol was depleted by 5 mM methyl-β-cyclodextrin for 2 h at 37°C.

Results of experiments with apoptosis detection are presented in Fig. 2.13. Firstly, we analyzed the integral fluorescence intensity of the new probes bound to the cell membranes. Probes **8** and **10** (with hexyl chains) showed 2-fold higher fluorescence intensity with respect to F2N12S, while their butyl analogues **7** and **9** showed lower fluorescence intensity in plasma membranes. Also, the low intensity was observed for probe **11**. Thus, one can follow the tendency of growing ClogP-value in the row **9-10-11**, which firstly leads to the increase in probe membrane affinity (probe **10**), and

finally results in the domination of self-aggregation process and poor membrane binding (probe **11**). Secondly, we analyzed the N*/T* changes of probes **7-11** bound to the cell membranes. For all new probes, the N*/T* values were higher in apoptotic cells than in intact cells, indicating a clear response of the new probes to apoptosis. Response to apoptosis calculated as $2(a-b)/(a+b)\times 100\%$ was 18-26 % that was higher as compared to original probe F2N12S. Though probes **7** and **8** showed response close to that of probes **9** and **10**, they are much less convenient for apoptosis detection because of the rather low intensity of the N* band (i.e. signal/noise ratio is low).

It is important to note that the higher sensitivity of probes **9** and **10** to apoptosis correlates well with their improved sensitivity to both membrane lipid order and surface charge as compared to F2N12S.

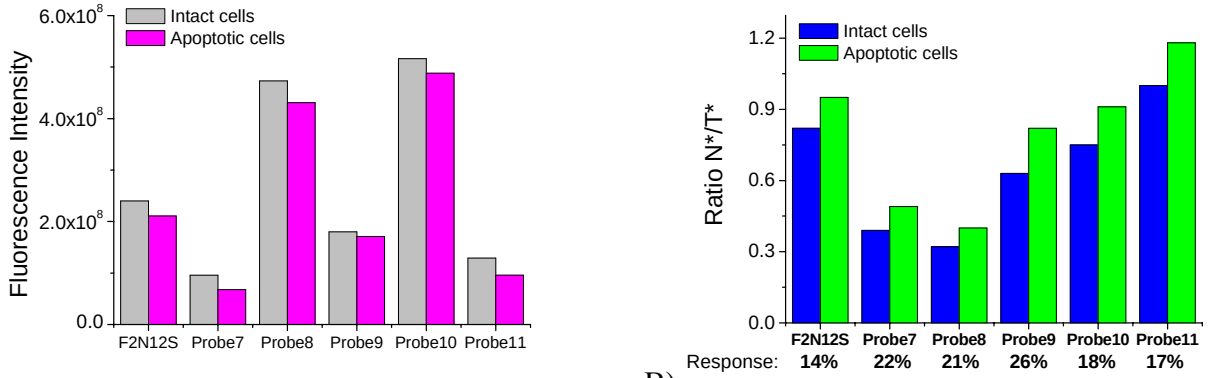

Figure 2.13. Emission intensities of the 2nd generation of 3HF probes in cell membranes (A) and their response to apoptosis (B). Dye concentration was 0.1 μM. Incubation time was 7 min at 20°C; no intensity changes after 20 min of incubation were observed. For probe **11** incubation time was 30 min at 37°C.

Conclusion. In this chapter, the synthesis and properties of 2nd generation of 3HF probes were described. These dyes were considered to have strictly vertical orientation in lipid membrane due to their molecular design. They exhibited improved sensitivity to surface charge and lipid order as well as higher fluorescence intensity in model and cell plasma membranes. In cells, the new probes show stronger variation of their dual emission in response to cholesterol extraction and apoptosis. Thus, the 2nd generation of 3-HF probes constitute a significant improvement in respect to the parent probe F2N12S.

Basing on the properties of the 1st and the 2nd generation of 3HF probes we propose three important statements for the molecular design of fluorescent membrane probes:

1) A typical membrane probe should contain an amphiphilic anchor group and a fluorophore. The anchor group should include a long hydrophobic chain, responsible for membrane incorporation, and a zwitterion group, responsible for specific localization at the certain depth in the membrane. The fluorophore should be environment-sensitive in order to monitor the changes of local membrane properties by the emission spectrum.

2) Vertical orientation and sufficiently deep location of the fluorophore in the membranes are important parameters govering the probe affinity to lipid membrane, the sensitivity to the lipid order and to the surface charge.

3) For apoptosis detection, the sensitivity to the lipid order appears to be more important that the sensitivity to the surface charge.

Basing on the obtained results we decided to use another fluorophore for the development of membrane probes. For this purpose, we selected Nile Red, which is a well know environment-sensitive dye with attractive spectroscopic properties.

2.2. Probes based on Nile Red (NR) fluorophore

2.2.1. First generation of NR probes

Molecular design. For the development of membrane probes based on Nile Red fluorophore, we choose 2-hydroxy Nile Red as a basic structure. As it was reported previously, 2-hydroxy Nile Red (Nagy et al., 2004) exhibits the same solvatochromic properties as parent Nile Red (Golini et al., 1998). The presence of hydroxy-group allowed us to conjugate the fluorophore with additional functionalities (Fig. 2.14). As one can see, probes **12** and **13** are composed of a fluorophore, a long alkyl chain and a zwitterionic group, connected together by a linker (flexible propyloxy-group). The structure of probe **12** is closely related to F2N12S, while probe **13** is similar to probe **2** from the 1st generation of 3HF probes (see Fig. 2.1).

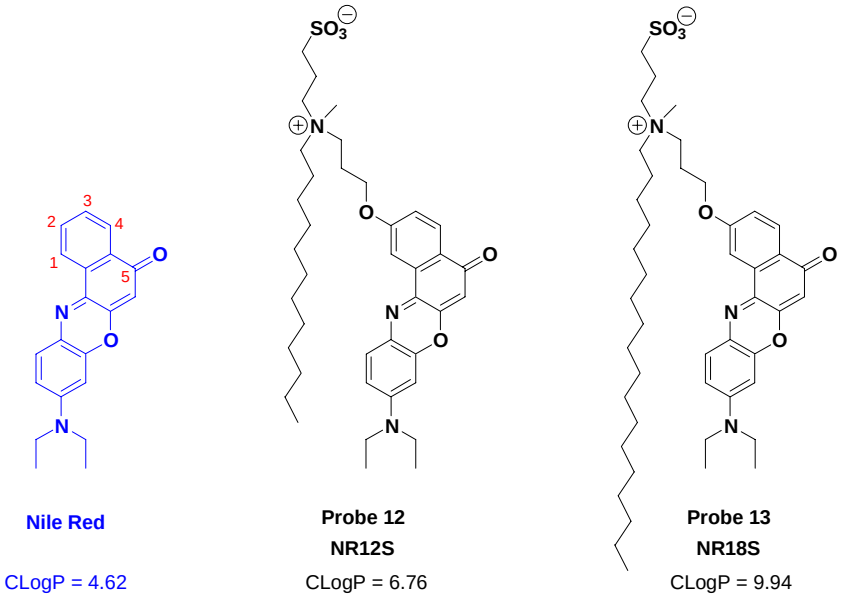

Figure 2.14. Chemical structures of the 1st generation of NR probes.

Chemical synthesis. Probes **12** and **13** were synthesized in 3 steps starting from 2-hydroxy Nile Red. It was alkylated with 1-bromo-3-chloroporpane under basic conditions, followed by coupling with dodecyl-methyl-amine (or octadecyl-methyl amine). Obtained tertiary amines were reacted with 1,3-propanesultone to yield the final probes (see Scheme 4.6 in Materials and Methods).

Spectroscopic properties of new probes in organic solvents resemble the ones of parent Nile Red (Table 2.3). One can see analogous changes of absorption and emission maxima, QY values. Interestingly, Nile Red shows significant fluorescence in water, while the more lipophilic probes **12** and **13** exhibit negligible QY in aqueous medium. In addition, the blue-shifted position of the absorption maxima indicates the formation of aggregated species for probes **12** and **13** in water.

Binding to model membranes. We found that probe **13** binds poorly to lipid membranes as it was evidenced from the corresponding titration experiments in DOPC vesicles (Fig. 2.15). Once again, similarly to long-chain 3HF probe **2**, too high CLogP value resulted in self-aggregation that prevents the membrane binding. In contrary, probe **12** (further referred as NR12S) showed very good binding to lipid membranes, which results in >100-fold increase in its fluorescence intensity. Importantly, an "on-off" switching of Nile Red fluorophore in the presence of dithionite-ions was

discovered. It allowed us to demonstrate that in aqueous solutions, NR12S binds only the outer membrane leaflet and exhibits slow flip-flop at room temperature. In model vesicles studies, variation of surface charge did not modify the emission spectrum of NR12S, but a significant blue shift (up to 50nm) of its fluorescence maximum was observed upon transition from liquid disordered phase towards liquid ordered phase. These two phases were clearly visualized in NR12S-stained giant vesicles by fluorescence microscopy imaging.

Microscopy studies of cells revealed that NR12S binds exclusively the plasma membrane. Using cholesterol depletion/enrichment experiments with methyl-β-cyclodextrin, we showed that the emission color of this probe correlates well with the cholesterol content in cell membranes. In addition, our preliminary data showed that NR12S is sensitive to apoptosis. The response of this dye to apoptosis is similar to the effect of cholesterol extraction. The same phenomenon was observed for F2N12S and the 2nd generation of flavone probes, confirming that the loss of the lipid order in apoptotic cells can be used for apoptosis detection. The described results were recently published (Publication 2).

Basing on the properties of NR12S and F2N12S, we can state that the proposed theory of membrane probe design is universal and does not depend on the fluorophore structure.

Table 2.3. Spectroscopicl properties of the 1st generation of NR probes in organic solvents.[a)]

Solvent	Nile Red			Probe 12 (NR12S)			Probe 13 (NR18S)		
	λ_{abs}, nm	λ_{fluo}, nm	QY, %	λ_{abs}, nm	λ_{fluo}, nm	QY, %	λ_{abs}, nm	λ_{fluo}, nm	QY, %
$CHCl_3$	540	595	88	547	599	79	547	598	82
EtOH	550	626	52	550	626	52	550	626	52
MeOH	553	632	38	555	631	40	555	631	39
DMF	544	618	63	544	615	69	544	616	66
H_2O	591	657	3.5	522	657	0.2	519	-	<0.1

[a)] Dye concentration was 1 μM.

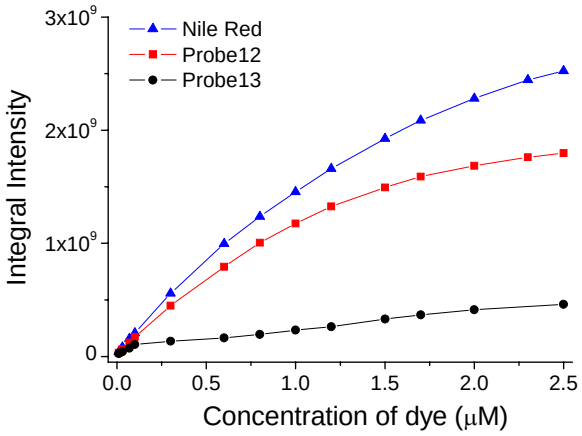

Figure 2.15. Titration of DOPC vesicles with the 1st generation of NR probes. Lipid concentration was 200 μM in phosphate buffer 20 mM, pH 7.4. Incubation time was 5 min at 20°C.

2.2.2. Second generation of NR probes

Molecular design. The 2nd generation of NR-based probes is presented by five molecules (Fig. 2.16). Their structures consist of zwitterionic group and long alkyl chains attached to the opposite side of Nile Red fluorophore. Such molecular design favors strictly vertical dye orientation in the membrane, similarly to the 2nd generation of 3HF probes (see Fig. 2.8). It should be noted that the linker is presented by a propyloxy-group attached at 2- or 3-position of benzo[a]phenoxazine ring. Probes **14-16** exhibit some angular (curved, banana-like) geometry, while 3-substituted probes **17** and **18** represent linear molecules, and one can expect some differences in their membrane binding. The membrane affinity should increase with the growing length of alkyl chains. As ClogP value of probe **14** is below unity, this molecule is expected to be soluble in water and exhibit poor membrane binding.

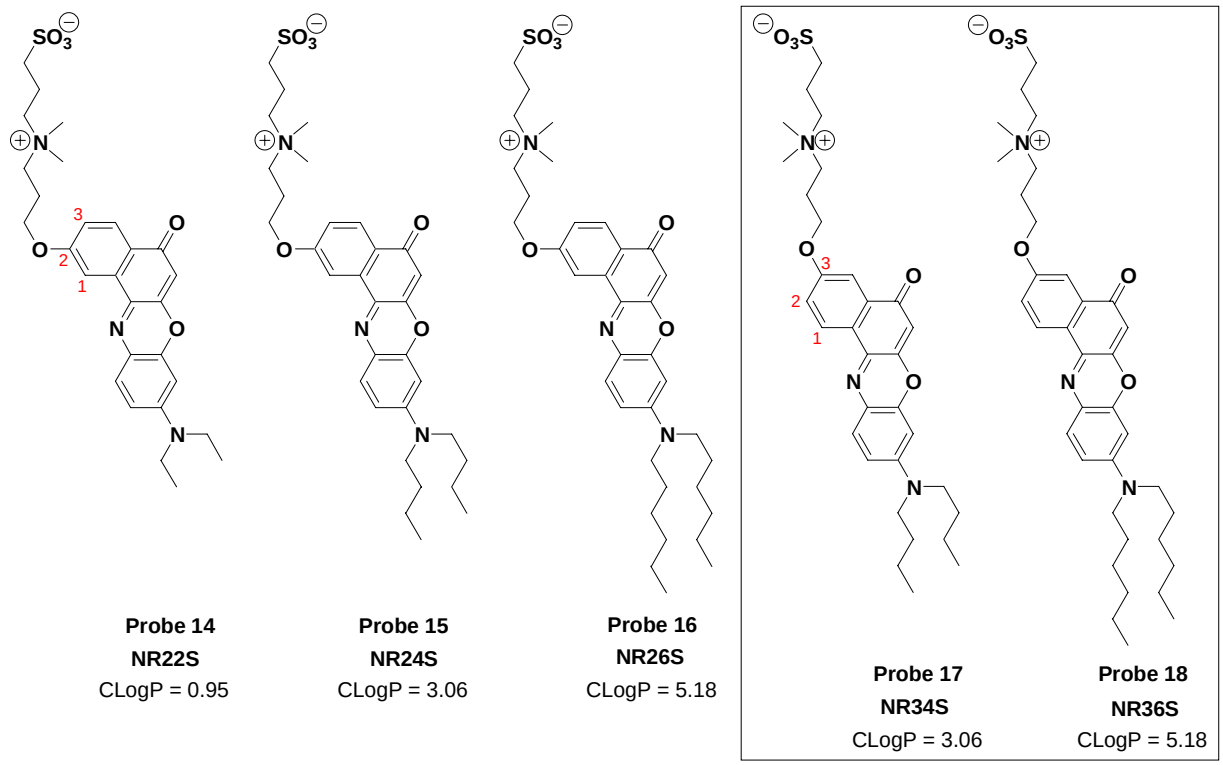

Figure 2.16. Chemical structures of the 2nd generation of NR probes.

Chemical synthesis. Synthesis of probes was started from the preparation of 2- and 3-hydroxy-Nile Red derivatives with long alkyl chains (see Scheme 4.7 in Materials and Methods). For this purpose, 3-methoxyaniline was alkylated by butyl iodide (or hexyl iodide) in DMF under basic conditions, and the methoxy group was removed by boiling with aqueous HBr. Obtained 3-(dibutylamino)-phenol was nitrosylated by sodium nitrite in acidic medium, and the formed product was isolated in the form of its hydrochloric salt. It was further reacted with 1,6-dihydroxynaphtalene at 160°C in DMF affording the 2-hydroxy-Nile Red with butyl (or hexyl) chains. Analogous treatment of the obtained hydrochloric salt with 1,7-dihydroxynaphtalene resulted in the formation of isomeric 3-hydroxy-Nile Red derivatives. Purified hydroxy-NR compounds were further alkylated with 1-bromo-3-chloropropane under basic conditions (see Scheme 4.8). Obtained products were activated by treatment with NaJ in acetone (Finkelstein reaction), followed by coupling with dimethylamine in THF. Resulted tertiary amines were quaternized with 1,3-propanesultone to yield the final products (probes **14-18**).

Structures of all obtained substances were elucidated by NMR spectroscopy and Mass spectrometry. All the final probes were purified by column chromatography (or preparative TLC) and were pure according to NMR and LCMS data, TLC analysis and their absorption spectra. Detailed synthetic schemes, procedures and related information are presented in chapter Materials and Methods.

Spectroscopic properties of the 2nd generation Nile Red probes were studied in different organic solvents (Table 2.4). The absorption and fluorescence spectra of all five dyes were highly similar, and the new molecules show strong red shift of their emission peak on increase of solvent polarity. High fluorescence QY was observed in most organic solvents. However, some differences were observed for aqueous solutions: probes **16** and **18** (with hexyl chains) are almost non-fluorescent in water (QY = 0.1 %), whereas probes **14**, **15** and **17** are considerably fluorescent in aqueous medium. The low QY can be explained by the formation of oligomers or micelles, where the fluorophore is probably self-quenched. The existence of oligomers for hexyl derivatives in water is also supported by the strongly blue-shifted absorption maxima as compared to that in organic solvents.

Table 2.4. Spectroscopic properties of the 2nd generation of NR probes in various organic solvents.[a)]

Solvent	Probe 14 NR22S			Probe 15 NR24S			Probe 16 NR26S			Probe 17 NR34S			Probe 18 NR36S		
	λ_{abs}, nm	λ_{fluo}, nm	QY,%	λ_{abs}, nm	λ_{fluo}, nm	QY,%	λ_{abs}, nm	λ_{fluo}, nm	QY,%	λ_{abs}, nm	λ_{fluo}, nm	QY,%	λ_{abs}, nm	λ_{fluo}, nm	QY,%
Dioxane	521	588	49.0	528	588	74.0	528	588	72.0	533	589	78.0	533	589	84.0
THF	524	591	54.5	531	593	66.0	531	593	69.0	534	594	75.0	534	594	72.0
CH_2Cl_2	542	601	45.0	546	604	58.5	546	604	56.0	548	609	59.0	548	609	63.5
CH_3CN	535	610	85.5	539	613	84.5	539	613	81.0	540	618	80.5	540	618	81.0
DMF	543	615	70.5	546	618	68.0	546	618	66.0	547	623	66.6	547	623	67.0
DMSO	551	623	60.0	554	627	58.0	554	627	56.0	555	632	54.0	555	632	54.0
EtOH	550	626	54.0	552	630	50.0	552	630	49.0	553	636	43.0	553	636	43.5
MeOH	554	632	41.0	557	636	36.5	557	636	36.0	557	642	30.0	557	642	31.0
Water	594	655	5.0	596	662	3.0	516	655	0.1	594	669	2.0	508	650	0.1

[a)] Dye concentration was 1 μM.

Binding to model membranes. On binding to DOPC vesicles probes **15-18** showed about 100-fold increase in the fluorescence intensity accompanied with some blue shift of emission maximum. In contrast, probe **14** showed only 2-fold increase of fluorescence intensity, which is evidently connected with its affinity to lipid membrane. The latter is clearly connected with the insufficient ClogP value of this probe (below unity).

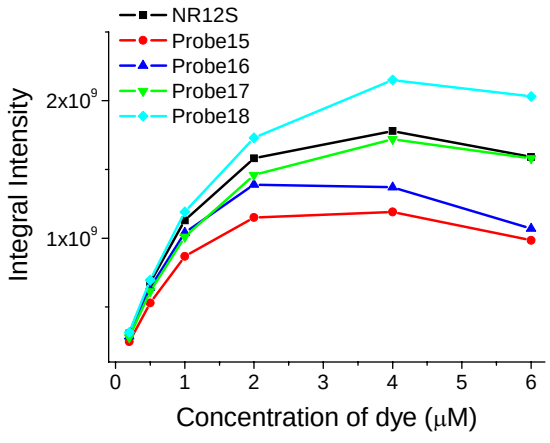

Figure 2.17. Titration of DOPC vesicles with the 2nd generation of NR probes. Lipid concentration was 200 μM in phosphate buffer 20 mM, pH 7.4.

When the titration curves in DOPC vesicles are considered (Fig. 2.17), we could notice that probes **16** and **18** (with hexyl chains) showed higher fluorescence intensity as compared to their butyl-chain analogues **15** and **17**. On the other hand, linear molecules **17** and **18** exhibited higher fluorescence intensity compared to their angular analogues, probes **15** and **16**. Thus, similarly to the 2nd generation of 3HF probes, the linear geometry of molecule and the presence of sufficiently long alkyl chains favor the membrane binding. Probe **18** showed the highest fluorescence intensity among the studied probes, including NR12S.

Investigation of probe binding to lipid vesicles revealed the difference in incubation times. For probes **16** and **18** it was 5 min while corresponding butyl derivatives **17** and **18** showed reproducible emission spectra just after 2min of incubation at 20°C. In the case of hexyl derivatives the presence of aggregated species in aqueous solutions slows down the probe incorporation into lipid bilayer, similarly to the observations made for 3HF probes.

Sensitivity to lipid order. We studied the spectroscopic properties of the new dyes in membranes composed of different lipids and analyzed them with respect to parent molecules, Nile Red and NR12S (Table 2.5). Remarkably, the QY of the dyes depends on the membrane phase. Thus, all probes showed comparable QY in Ld phase, while in Lo phase linear probes **17** and **18** showed about 5-fold higher values. Further, in Lo phase angular probes **15** and **16** showed the fluorescence peak at 660 nm, which correspond to the emission of non-bound molecules surrounded by water. Also, the presence of non-bound fluorescent species is confirmed by absorption spectra, where the dominating band corresponding to the absorption of "free" probe was observed (Fig. 2.18).

Table 2.5. Spectroscopic properties of the 2nd generation of NR probes in various lipid vesicles.[a)]

Probe	Sm-Chol (2:1) *Lo phase*			DPPC-Chol (2:1) *Lo phase*			DOPC *Ld phase*			DOPS *Ld phase*		
	λ_{abs}, nm	λ_{fluo}, nm	QY, %	λ_{abs}, nm	λ_{fluo}, nm	QY, %	λ_{abs}, nm	λ_{fluo}, nm	QY, %	λ_{abs}, nm	λ_{fluo}, nm	QY, %
NR	528	586	40	532 552	594	54	550	627	44	554	629	39
NR12S	522	571	28	521	558 585	30	531	609	34	534	605	42
Probe 15	590	572	6	591	559	7	537	618	30	538	611	32
Probe 16	516	572	7	516	561	10	532	609	36	534	603	35
Probe 17	543 590	568	38	531 590	560	48	537	609	32	541	611	42
Probe 18	519 534	571	51	527	562	55	536	600	34	540	604	47

[a)] Dye concentration was 1 μM; lipid concentration was 200 μM in phosphate buffer 20 mM, pH 7.4.

This drastic difference in the QY of the dyes in Lo phase is clearly connected with the much more efficient incorporation of the linear probes **17** and **18** into tightly packed lipid assemblies as compared to the angular molecules **15** and **16**. Moreover, linear probe **18** exhibited more efficient incorporation than corresponding butyl analogue **17**, as the QY of the former was higher. Thus, in Lo phase probe **18** showed superior brightness compared to all NR-baser probes including NR12S.

Similarly to NR12S, variation of surface charge did not affect the emission spectrum of new probes (DOPC vs. DOPS), while a significant blue shift (up to 50nm) of fluorescence maximum was observed upon transition from Ld to Lo phase (Fig. 2.19). To analyze the sensitivity of the new probes to lipid order, we calculated the intensity ratio of the green and red parts of the emission spectrum and evaluated the response of all NR dyes as $2(a-b)/(a+b)\times 100\%$. It was found NR12S and probe **17** to be the most sensitive to lipid order.

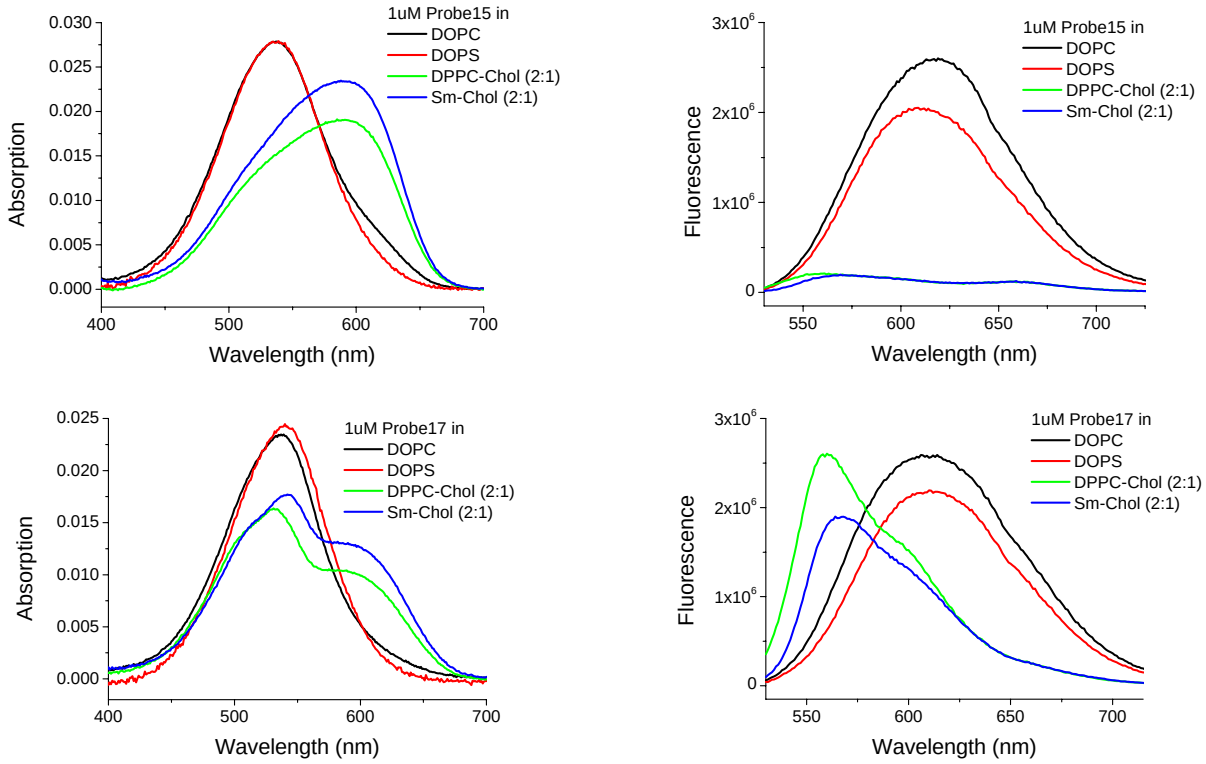

Figure 2.18. Absorption and emission spectra of probes **15** and **17** in various lipid vesicles. Lipid concentration was 200 μM in phosphate buffer 20 mM, pH 7.4.

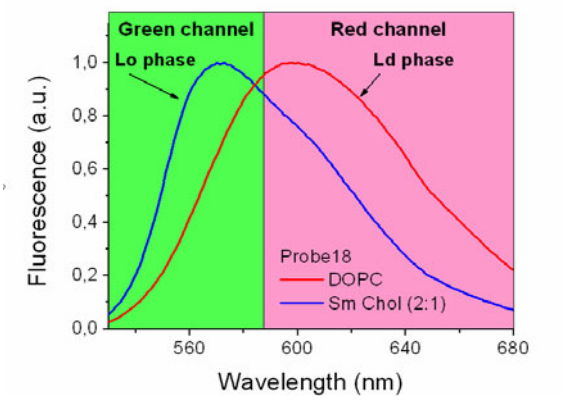

Probe	Ratio Green/Red		Response, %
	Lo phase	Ld phase	
NR12S	0.91	0.26	111
Probe **15**	0.54	0.23	80
Probe **16**	0.82	0.30	93
Probe **17**	0.98	0.28	111
Probe **18**	0.88	0.32	93

Figure 2.19. Ratiometric approach for multicolor imaging with the 2nd generation of NR probes and their sensitivity to lipid order. Channels correspond to 530-585 mn (green) and 585-700 nm (red) spectral regions. Response was calculated as *2(a-b)/(a+b)×100%* on the base of Green/Red values.

Cellular studies. For cellular studies U87MG human malign astrocytes were used. In line with the data obtained from lipid vesicles, the integral fluorescence intensity in normal and apoptotic cells was the highest for probe **18**, which has a linear structure with two hexyl chains (Fig. 2.20). Importantly, all the explored probes **15-18**, as well as NR12S, were sensitive to apoptosis, and their emission bands were red shifted in the case of apoptotic cells. In order to evaluate the amplitude of probe response, we applied the ratiometric approach and calculated the ratio of emission intensities for two parts of the emission spectrum. For the new dyes, the spectroscopic response to apoptosis was 15-22 % while NR12S showed the highest sensitivity to apoptosis. The observed red shift (i.e. reduced value Green/Red) indicated the loss of lipid order in the membranes of apoptotic cells, in line with our previous results with 3HF probes.

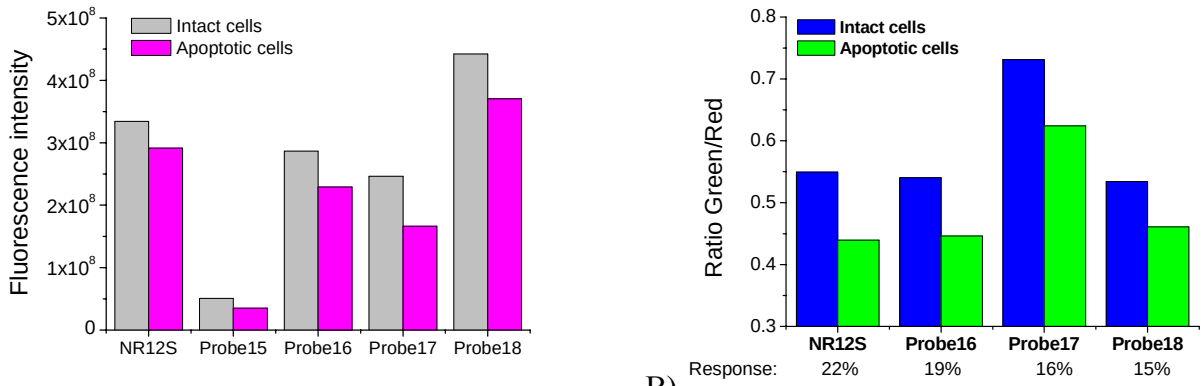

A) B)

Figure 2.20. Emission intensities of the 2nd generation of NR probes in plasma membranes (A) and their response to apoptosis (B).

Conclusion. Generally, the 2nd generation of NR probes showed fluorescent properties similar to NR12S, though one of the new probes showed superior fluorescence intensity in model and cellular membranes. All Nile Red-based probes were sensitive to lipid order by changing the position of their emission bands. We found that probes with linear geometry and hexyl chains showed superior fluorescence quantum yields in Lo phase, suggesting their high affinity to the tightly packed phase. Moreover, all the probes were sensitive to apoptosis, and their spectroscopic response confirmed the loss of the lipid order in apoptotic membranes, that is in line with the data obtained previously with 3HF probes.

As compared to existing membranes probes, the key advantages of the Nile Red-based probes arise from their fluorophore. High brightness, red-shifted absorption and emission maxima, high photostability and valuable on/off switching capability of Nile Red core present these dyes as powerful fluorescent tools which can be used in biology for monitoring cholesterol content and membrane lipid order, and for detection of apoptosis.

2.3. Development of new environment-sensitive fluorophores

In previous chapters we developed the theory of design of fluorescent membrane probes and approbated it on two different fluorophores, 3-hydroxyflavone and Nile Red, which showed the general applicability of this theory. Obtainer results inspired us to look through the existing fluorophores in order to find the most attractive molecules with the aim to transform them into new fluorescent membrane probes. To our surprise, only limited number of fluorescent compounds exhibited good solvatochromism supported with other important spectroscopic properties (i.e. absorption in visible spectral region, large extinction coefficient and Stokes shifts, high photostability and sufficient two-photon absorption cross section). Moreover, Prodan is still considered as ideal polarity (environment-sensitive) probe (Valeur 2002). That is why we directed our research to the development of new classes of fluorescent compounds with improved spectroscopic characteristics.

2.3.1. Solvatochromic dyes on the base of 2-dialkylamino-7-carbonyl-fluorene

In a search for environmentally sensitive dyes with superior properties, we extended the electronic conjugation of one of the best solvatochromic dyes, Prodan, by substituting its naphthalene core with fluorene. The newly synthesized fluorene derivatives, probes **19** and **20** (see Scheme 4.9 in Materials and Methods) bearing strong electron-donor (dialkylamino) and electron-acceptor (carbonyl) groups at the 2 and 7 positions showed a red-shifted absorption (close to 400 nm), twice as large an extinction coefficients (43 000 M^{-1} cm^{-1}), and a manifold larger two-photon absorption cross section (~400 GM) as compared to Prodan. Studies in solvents revealed much stronger fluorescence solvatochromism of the new dyes, which is connected with their twice as large transition dipole moment (14.0 D). Similarly to Prodan, they exhibit high fluorescence quantum yields, while their photostability is largely improved. Thus, substitution of the naphthalene core in Prodan with fluorene resulted in new fluorophores with advanced spectroscopic and solvatochromic properties. We expect them to find a variety of applications in future as environmentally sensitive probes and fluorescent labels for biology. The results of our findings on this topic were recently published (Publication 3).

2.3.2. Solvatochromic dyes on the base of 3-methoxychromone

In a search for solvatochromic dyes with superior properties, we developed three environment-sensitive fluorescent dyes on the base of a strong electron acceptor 3-methoxychromone unit with varied electron-donor (aryl substituent) at its 2-position (see Scheme 4.10 in Materials and Methods). All three dyes showed remarkable polarity-dependent shifts of the emission maximum, which were increased with extension of the dye conjugation (Fig. 2.21). For the compound bearing a diethylamino-fluorenyl donor group, the difference between the excited and the ground-state dipole moments reached 20D, which is among the largest reported for neutral dipolar fluorophores. Moreover, the new dyes were characterized by significant two-photon absorption cross-section (up to 450 GM) and large fluorescence quantum yields. In comparison to the parent 3-hydroxychromone derivatives, the new dyes showed the improved photostability, which confirms that photodegradation of 3-hydroxychromones occurs from a product of the excited-state intramolecular proton transfer. Described class of 3-methoxychromone dyes may serve as attractive building block for the development of environment-sensitive fluorescent probes. The results of our findings are presented in the manuscript (Publication 4).

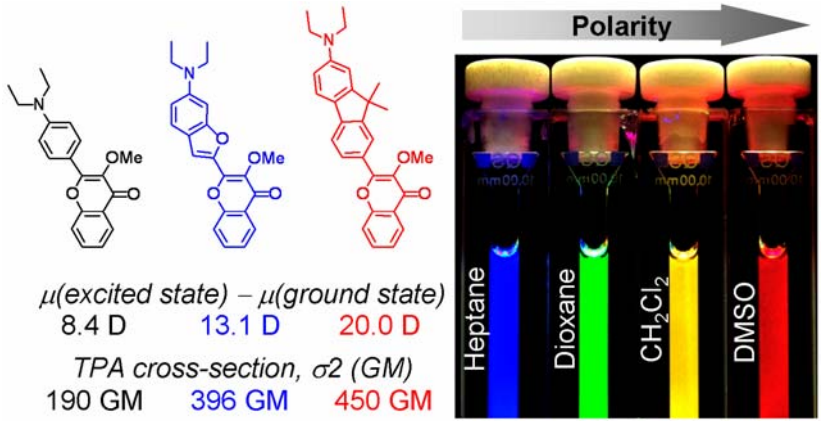

Fig. 2.21. Fluorescence solvatochromism of 3-methoxychromones.

2.4. Current development of membrane probes

Prodan and Laurdan are among the most popular fluorescent probes for investigation of membrane polarity and visualization of lipid order (Bagatolli 2006). In lipid vesicles Prodan shows emission changes in the range of 50 nm (Krasonwka et al., 1998). Basing on structure similarity, we assumed that the described above fluorene-based molecules, probe **19** (FR0) and **20** (FR8), can substitute Prodan and Laurdan in membrane studies due to their red-shifted absorption maxima (around 390 nm) and much higher sensitivity to environment (Fig. 2.22).

For this purpose, we investigated the spectroscopic behavior of FR0 and FR8 in lipid vesicles (Fig. 2.23). At low concentrations, FR0 showed a blue emission maximum at 465nm, indicating deeply incorporated fluorophore into membrane bilayer. Upon increasing the dye concentration a dramatic red shift (75 nm) of the emission band was observed. Probably, at higher concentration the probe molecules bind at the more polar interface of the lipid membrane. For FR8, a strong blue emission was observed along the whole studied range of concentration.

The observed blue fluorescence suggests a deeper location of FR0 and FR8 in lipid bilayer as compared to Prodan and Laurdan. This can be explained by a higher lipophilicity of the fluorene core as compared to the naphthalene one. In addition, the strong dependence of the fluorescence spectra of FR0 on the concentration limits its application as a membrane probe.

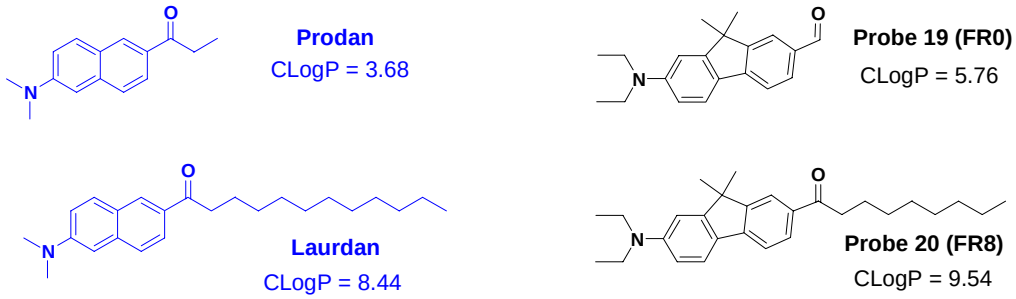

Figure 2.22. Probes **19** and **20** as fluorescent membrane probes.

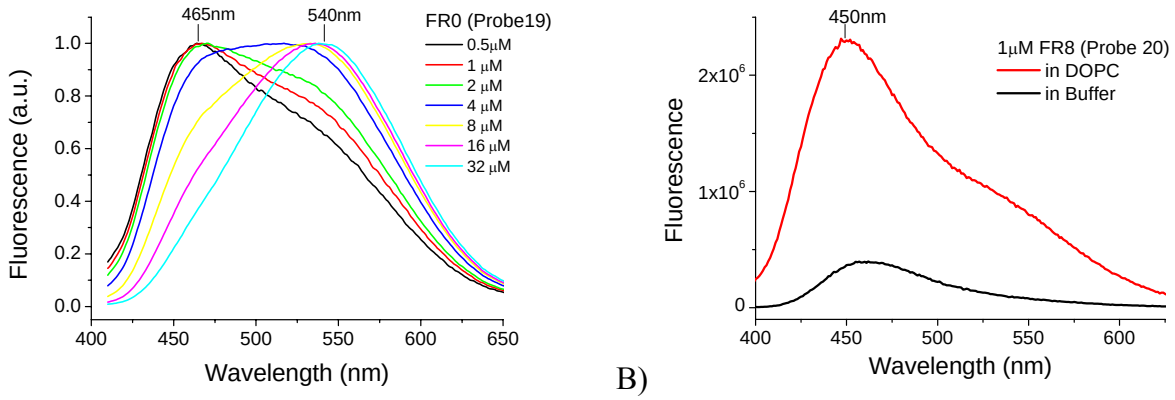

Figure 2.23. Titration of DOPC vesicles with increasing concentration of FR0 (A). Emission spectrum of FR8 in DOPC vesicles (B). Lipid concentration was 200 μM, incubation time was 10 min at 20°C.

To overcome the mentioned problems, the fluorophore should be placed closer to the surface of the lipid bilayer. Therefore, four fluorene molecules were synthesized (Fig. 2.24), where we wanted to localize the fluorophore at different depths and orientations in the lipid membrane.

Chemical synthesis. Synthesis of probe **21** was started from 2-amino-7-bromo-9,9-dimethylfluorene (see Scheme 4.11 in Materials and Methods), which was alkylated with butyl iodide. Obtained substance was transformed into Grignard reagent and further reacted with succinic anhydride in THF to afford the final product. In the synthesis of probe **22** we used 2-dibutylamino-7-bromofluorene derivative (see Scheme 4.12), which was reacted with butyl lithium and obtained intermediate was coupled with specially prepared methyl ester of 2-dimethylamino-2-methyl-propionic acid. Formed product with tertiary amino group failed the reaction with 1,3-propanesultone (probably due to steric hindrance), but it was successfully quaternized with methyl iodide resulting in probe **22**. Analogous strategy was used for synthesis of probe **23**. Synthesis of probe **24** was started from 2-amino-7-bromo-9,9-dimethylfluorene, which was monoalkylated by octyl iodide (see Scheme 4.13). Second alkylation was done with 1-bromo-3-chloropropane. Obtained product, bearing N-(3-chloropropyl)-N-octyl-amino group, was activated with NaJ in acetone (Finkelstein reaction) and coupled with dimethylamine in THF. Remaining aromatic Br-substituent was transformed into formyl group via Li-organics. The resulting fluorescent molecule with tertiary amino group was quaternized with 1,3-propanesultone to yield the final product, probe **24**. Structures of all obtained substances were elucidated by NMR spectroscopy and Mass spectrometry. All the final probes were purified by column chromatography (or preparative TLC) and were pure according to NMR and LCMS data, TLC analysis and their absorption spectra. Detailed synthetic schemes, procedures and related information are presented in chapter Materials and Methods.

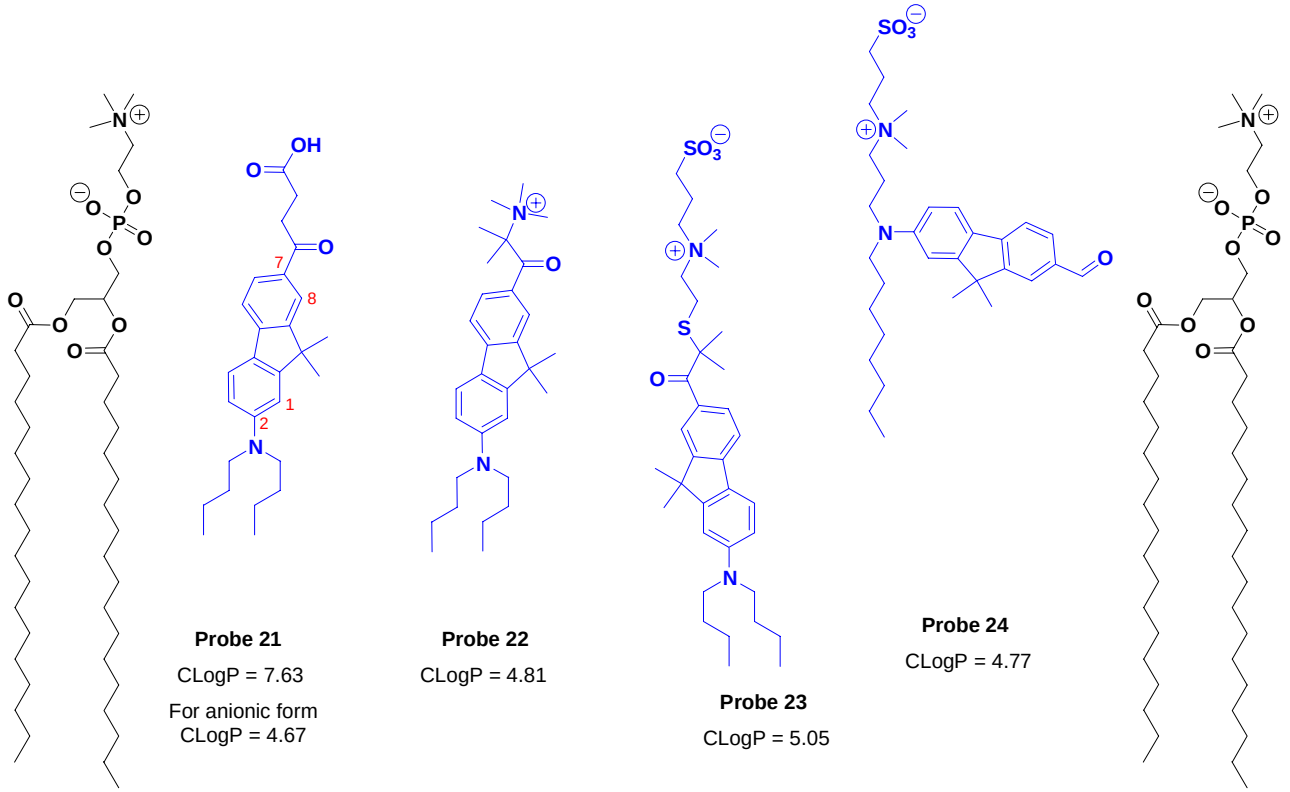

Figure 2.24. Chemical structures of fluorene-based probes **21-24** and their hypothetic position in lipid membrane.

Binding to model membranes. Firstly, the fluorescent properties of new dyes in aqueous buffer and lipid vesicles were investigated. All the fluorene probes showed poor emission in phosphate buffer while a strong increase in emission intensity was observed upon binding to lipid membranes. Observed fluorescence spectra are displayed in Fig. 2.25. It should be noted, that within the membrane, the emission of our fluorene dyes is governed by the penetration depth of 7-carbonyl group, which is able to create hydrogen bonds with aqueous media. Deep penetration disfavors H-bond interaction and results in blue shifted emission of the probe. In contrary, low penetration of the carbonyl results in a red shifted emission maximum.

Let us firstly consider probes **22** and **23**, which showed similar emission maxima at 475 nm. It is suggested that these are molecules with vertical orientation in the membrane, and this may impose their deep insertion into bilayer. It was surprising that probes **22** and **23** exhibited similar position of fluorescence maxima, as probe **22** was expected to be localized much shallower than probe **23** in the membrane. However, in the structure of probe **22** a high steric hindrance around the 7-carbonyl group prevents probably the H-bond formation with water and leads to the same emission maximum as for probe **23**.

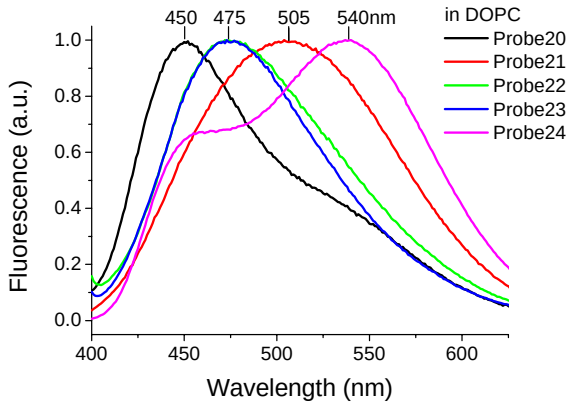

Figure 2.25. Normalized emission spectra of probes **20-24** in DOPC vesicles. Dye concentration was 1 μM.

The emission maxima of probes **21** and **24** in lipid bilayers were significantly shifted to the red with respect to probes **22** and **23**. Importantly, probe **21** presents a sterically available carbonyl group, and therefore it can form H-bonds with water within the membrane leading to the observed red shift. Analyzing the structure of probe **24** it can be seen that the fluorophore is directly attached to anchoring group, which imposed its horizontal shallow localization within the membrane (as it is shown in Fig. 2.24). Remarkably this dye shows clearly two emission bands, which may indicate two populations of the probe: shallow horizontal (long-wavelength band) and deep vertical (short-wavelength band).

Sensitivity to lipid order. Fluorescent properties of probe **24** were explored in vesicles composed of different lipids (Fig. 2.26), and our main attention was focused on the shape of its emission spectrum. In model membranes with Ld phase we found two fluorescence maxima at 455 and 540 nm, while the long-wavelength band was dominant. In Lo-membranes, the emission spectrum was found to be completely different, as emission of the short-wavelength band was mainly observed. Evidently, in the tightly packed Lo phase, the fluorophore attains probably vertical orientation, where the CO-group is localized in highly apolar environment.

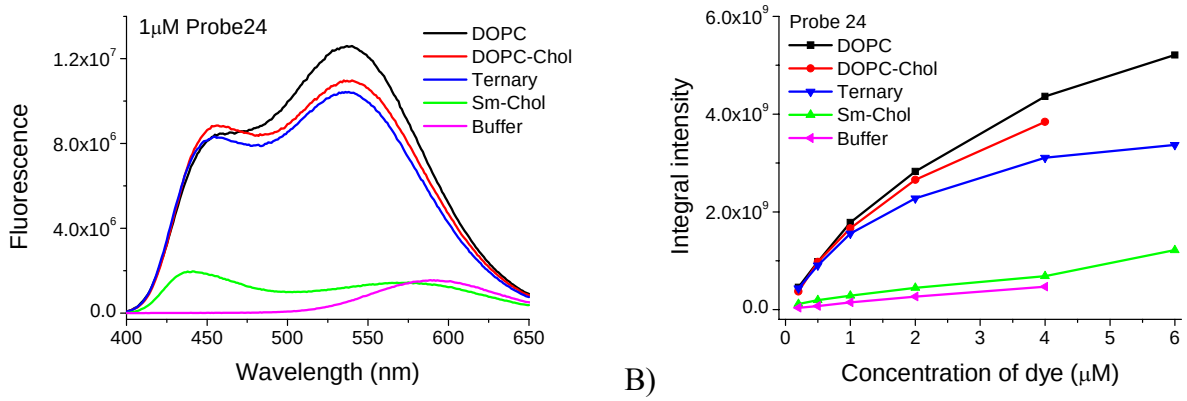

Figure 2.26. Emission spectra of probe **24** in different vesicles (A). Titration of various vesicles with probe **24** (B). Lipid concentration was 200 μM in phosphate buffer 20 mM, pH 7.4. Incubation time was 3 min at 20°C. Ternary vesicles are composed of lipid mixture DOPC, Sm and Chol (1:1:1).

The observed long-wavelength band in Lo phase vesicles corresponds well to the emission of the fluorophore in water, indicating that the probe is only partially bound to membrane. This poor affinity to Lo phase is probably connected with the bulky geometry of probe **24**, which disfavors its co-assembly with tightly packed lipids. Such a conclusion is further supported by relatively low fluorescence intensity of the probe **24** in membranes with Lo phase (Fig. 2.26). Moreover, when ternary lipid mixture containing both phases was tested, probe **24** showed emission intensity comparable to Ld phase, thus confirming its strong preference to disordered phase. Despite this negative result on affinity to Lo phase, we should note that the spectroscopic response of probe **24** to lipid order is enormous. Its spectrum shifts by about 80 nm when Lo and Ld phases are compared. This effect is larger than the response of well-known solvatochromic dyes to lipid order, Prodan or di-ANEPPQ (from aminostyryl piridinium family), and can be explained by the presence of fluorene core with its improved sensitivity to environment, as shown above.

Conclusion. At the moment no optimal membrane probe based on fluorene was obtained. The majority of presented fluorene dyes exhibit blue-shifted emission yet in the disordered phase while the other dyes bind poorly to the ordered phase. Currently we are working on the design of new fluorene-based molecule, which is expected to have two emission bands in fluorescence spectrum (as probe **24**), together with stronger affinity to membrane with Lo phase.

CHAPTER 3

CONCLUSIONS AND PERSPECTIVES

3. CONCLUSIONS AND PERSPECTIVES

Conclusions

The aim of this work was to develop molecular fluorescent tools for studying biomembrane properties (phase state, surface charge, polarity, etc.) and to relate these properties to biological questions related to apoptosis and membrane lipid order. In particular, this work was focused on the development of new membrane fluorescent probes that could overcome the drawbacks of the parent F2N12S due to improved sensitivity and brightness, more convenient excitation wavelength and higher photostability.

Firstly, we clarified the mechanism of response of F2N12S, the first ratiometric probe for apoptosis detection, which was previously developed in our laboratory. We showed that the main driving force making probe to change its emission spectrum upon apoptosis is the transition of plasma membrane from Lo towards to Ld phase state.

Secondly, more than 20 molecular fluorescent probes were designed, synthesized, purified and identified by NMR and HRMS techniques. Exploration of the fluorescent properties in organic solvents of different polarity clearly showed the solvatochromic behavior of these probes. By applying fluorescence spectroscopy and microscopy, we examined their binding to membranes and revealed their sensitivity profiles in model systems (LUVs and GUVs) and cell plasma membranes. Finally, all the probes were applied in cellular studies for detection of apoptosis and for sensing cholesterol content. According to obtained results, all the probes were classified into 3 types:

1) Probes sensitive only to surface charge. This type is represented by flavone derivatives of the 1st generation. They showed nearly no sensitivity to the phase state, while their sensitivity to the surface charge was much higher (3-fold) than that of F2N12S. Unfortunately, cellular studies revealed that this type of probes did not show any sensitivity to apoptosis.

2) Probes sensitive both to surface charge and to phase state, presented by flavone derivatives of the 2nd generation. This type of dyes, expected to present vertical orientation in lipid bilayer, preserved their high sensitivity to the negative surface charge, while their sensitivity to the phase state of the lipid membranes was significantly improved. In cellular studies, these dyes showed an about 2-fold increased response to cholesterol extraction and to apoptosis as compared to F2N12S.

3) Probes sensitive only to the phase state, presented by Nile Red derivatives of the 1st and the 2nd generations. These dyes showed identical emission peaks in charged and neutral membranes, but revealed strong blue shift (up to 50nm) in the presence of Lo phase. Cellular studies showed their significant response to apoptosis. Further, these dyes were applied for visualization of Ld-Lo phase domains and quantification of cholesterol content in cell membranes. Finally, we developed a methodology of reversible redox switching of Nile Red fluorophore using sodium dithionite. This method allowed us to show that new probes, in contrast to parent Nile Red, bind exclusively the outer membrane leaflet of lipid bilayer with negligible flip-flop process.

Thirdly, basing on the obtained data we analyzed the effect of the molecular structure on the probe behavior and proposed an approach for the design of fluorescent membrane probes. Fluorophore orientation and localization in the membrane are the key features governing the optimal fluorescence response. A typical membrane probe should contain a long hydrophobic chain, a zwitterion group and a fluorophore, which are responsible for probe incorporation into membrane, its specific localization at a certain depth in the membrane and for sensing the local membrane properties.

Finally, our research was directed to the development of advanced environment-sensitive fluorophores for designing new membranes probes. In this respect two classes of compounds were discovered on the basis of fluorene and 3-methoxychromone units, both bearing strong electron donor (dialkylamino) and acceptor (carbonyl) groups at the opposite ends of the conjugation core. As compared to the classical solvatochromic dye Prodan, these fluorophores feature extended electronic conjugation and exhibited red-shifted absorption, larger extinction coefficients and two-photon absorption cross-sections, high fluorescence quantum yields and improved photostabilities. Studies in organic solvents revealed much stronger fluorescence solvatochromism of these new dyes, which is connected with their larger change in the dipole moment on electronic excitation. Thus, these new fluorophores exhibited attractive spectroscopic properties, and we expect them to find variety of applications as building blocks for advanced fluorescent probes and labels in biology.

Perspectives

We expect that synthesized molecules will find numerous applications in the future. The first perspective is to study the effects of cholesterol extraction and apoptosis induced by different agents in various cell lines. These studies will provide us with information about the applicability and universality of the approach to apoptosis detection based on the monitoring membrane phase changes. In addition, our probes can be used for quantitative measurements of apoptosis by flow cytometry. It will give a new knowledge about this important biological process.

Presented probes can be used for studies of membrane waves originated from actin-myosin interactions. It is known that these interactions stiffen the plasma membrane, and take part in endocytosis, exocytosis, release of extracellular vesicles, and the regulation of tension between membrane and the cytoskeleton. Currently, the biological mechanism resulting in wave formation is not clear (Tyska et al., 2010). The new probes can be applied in studies of membrane changes during physiological adaptation (Hazel and Williams 1990). For instance, some animal cells do not have physiological thermoregulation and must control membrane properties by varying membrane composition (Durairaj and Vijayakumar 1984). In addition to apoptosis, membrane trafficking and variation of membrane composition, other membrane-related events can be explored by our probes (for instance signal transduction), and the connection between these events and membrane physical properties can be established. Finally, an interesting application of new probes is to develop the approach for *in vivo* imaging of cellular membranes directly in animals by using fluorescence tomography.

Application of new instrumental techniques, such as fluorescence correlation spectroscopy, single molecule microscopy and super-resolution microscopy in combination with our probes could be of significant interest for investigation of nanoscopic organization of biological membranes, and particularly for imaging membrane domains (rafts). Thus, presented probes can be useful in biomedical applications for studies of membrane phase changes related to numerous diseases (Maxfield and Tabas 2005). Recent reports indicated that alcohol consumption reduces immunity to infection by disruption of lipid rafts (Szabo et al., 2007). The infection of human erythrocytes by the malarial parasite causes membrane sorting and signaling events that rely on proteins present in lipid rafts (Murphy et al., 2006). Lipid rafts have been implicated in prion disease as the location of the post-translational conformation conversion of the normal prion protein to the infectious form (Taylor and Hooper, 2006). Lipid rafts are suggested to play a role in Alzheimer's disease (Cordy et al., 2006), prostate cancer (Freeman et al., 2005) in hypertension (Callera et al., 2007), etc.

Except the monitoring membrane domains, the new probes can be also used in classical fluorescence applications as FRET partner. For instance NR12S can be useful as FRET acceptor due to its absorption around 530 nm, where common fluorophores (such as fluorescein) emit. Both facts, FRET and co-localization of our probes with other fluorescent molecules (for instance labeled membrane proteins, etc), could facilitate the studies of interactions taking place at the membrane surface.

Last but not least, the proposed theory of membrane probe design can be useful for development of novel sensors for various membrane physical properties. Thus, the newly described classes of fluorophores, based on fluorene and 3-methoxychromone units both presenting improved spectroscopic properties, can be further transformed into advanced membrane probes. Also, this approach can be used in design of new dyes bearing classical environment-insensitive fluorophores for the applications where the high fluorescence brightness, photostability and/or long lifetime are required (single molecule microscopy, lifetime imaging, etc). Moreover, the fluorophore could be substituted with a quencher molecule. This design would allow obtaining the quenching probes with high specificity to plasma membrane, and could be used for selective quenching of fluorescent molecules bound to lipid membranes.

Generally speaking, the theory and the new probes described in this work should stimulate the research on biological membranes and the development of new molecular fluorescent tools for membrane imaging.

CHAPTER 4

MATERIALS AND METHODS

4. MATERIALS AND METHODS

4.1. Synthetic procedures

All the solvents and chemicals were purchased from Alfa Aesar, Fluka, Sigma-Aldrich, or TCI Europe. The solvents were of analytical grade. NMR spectra were recorded on a Bruker spectrometer at frequency 300 or 400 MHz. Mass spectra measurements were performed using an Agilent 6520 Accurate Mass QToF and an Agilent 1200 RRLC (Agilent Technologies, Santa Clara USA).

General procedure for synthesis of 3-hydroxyflavones:

2-Hydroxyacetophenone derivative (200 mg, 1.00 eq) was mixed with corresponding aldehyde (1.05 eq) in 2mL of DMF. To the obtained solution sodium methoxide (4 eq) was added. Reaction mixture became dark orange. It was stirred at RT overnight and then diluted with 10mL of ethanol. New portion of sodium methoxide (12 eq) and 30 % aqueous H_2O_2 (10 eq) were added. Resulted solution was refluxed for 3 min, cooled and poured into 100mL of water. After neutralizing with 10% HCl formed precipitate was filtered off. If the precipitate was not formed the product was extracted with an organic solvent (2 times). Combined organic layers were dried with Na_2SO_4 and evaporated under vacuum. Obtained residue was purified by preparative TLC or column chromatography (usual eluent was CH_2Cl_2/MeOH = 9/1 unless indicated).

General procedure for quaternization of amines with 1,3-propanesultone:

Tertiary amine (1eq) and 1,3-propanesultone (2eq) were mixed together in dry acetonitrile. Reaction mixture was refluxed overnight at 90°C. After cooling it was stirred at RT for additional 1h. Organic solvent was removed by vacuum evaporation. Obtained residue was purified by preparative TLC (usual eluent was CH_2Cl_2/MeOH = 85/15 unless indicated) to give the final product.

4.1.1. Synthesis of 3HF-based membrane probes

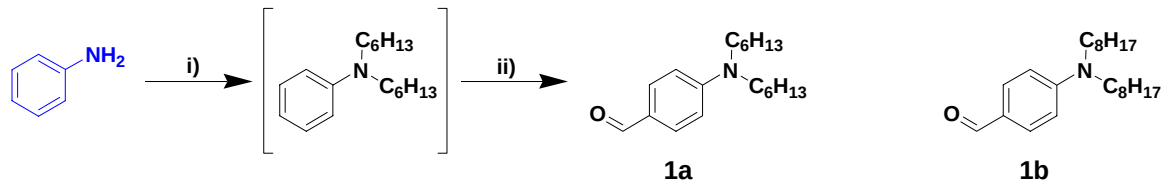

i) DMF, n-hexyl iodide, K_2CO_3, 120°C 4h; ii) DMF, $POCl_3$, 0°C, then 65°C 3h (overall yield 82%).

Scheme 4.1. Synthesis of benzaldehydes with long alkyl chains.

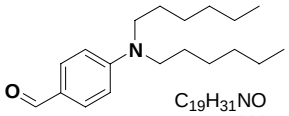

$C_{19}H_{31}NO$
Exact Mass: 289,2406

Compound 1a
4-Dihexylamino-benzaldehyde

In a round-bottom flask aniline (3.53g, 0.038mol) was dissolved in 20mL of DMF. Then *n*-hexyl iodide (14.1mL, 0.095mol) and potassium carbonate (15.73g, 0.114mol) were added. Reaction mixture was stirred upon heating at 120°C for 4h. After cooling it was poured into 200mL of water and extracted with chloroform. Organic layer was dried with sodium sulfate and evaporated under vacuum to give crude N,N-dihexyl aniline. Obtained brown oil was used directly in the next step.

Dry DMF (14.7mL, 0.190mol) was placed in the round-bottom flask, and then $POCl_3$ (5.2mL, 0.057mol) was added dropwise at 0°C under vigorous stirring. After the addition was completed (about 10 min) a clear colourless solution was formed. Reaction mixture was stirred for additional 5min, and previously obtained N,N-dihexyl aniline was added dropwise. Ice bath was replaced with oil bath, and the solution was heated at 65°C for 3h. After cooling it was poured into 100g of ice water and stirred at RT for 30min. After neutralization with aq. K_2CO_3 the solution was extracted with $CHCl_3$ (2 times). Combined organic layers were dried with sodium sulfate. Inorganic salt was filtered off and chloroform was removed by vacuum evaporation. Obtained dark oil was purified by column chromatography (eluent EtOAc/Heptane = 1/9) to produce the desired aldehyde **1a** as a colourless oil. Yield 9.0g (82%). **^{1}H NMR** (400MHz, $CDCl_3$): δ 9.68 (s, 1H), 7.68 (d, 2H), 6.62 (d, 2H), 3.32 (t, 4H), 1.59 (m, 4H), 1.40-1.20 (m, 12H), 0.89 (t, 6H). **LCMS** (m/z): MM-ES+APCI, found $[M+1]^+$ 290.2 (calcd for $C_{19}H_{32}NO^+$ 290.2).

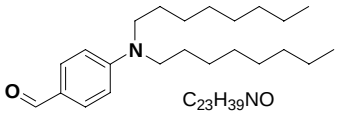

$C_{23}H_{39}NO$
Exact Mass: 345,3032

Compound 1b
4-Dioctylamino-benzaldehyde

It was synthesized analogously to previous compound starting from aniline and *n*-octyl iodide. Colourless oil, yield 80%. **^{1}H NMR** (300MHz, $CDCl_3$): δ 9.68 (s, 1H), 7.68 (d, 2H), 6.62 (d, 2H), 3.32 (t, 4H), 1.59 (m, 4H), 140-1.15 (m, 20H), 0.88 (t, 6H). **LCMS** (m/z): MM-ES+APCI, found $[M+1]^+$ 346.3 (calcd for $C_{23}H_{40}NO^+$ 346.3).

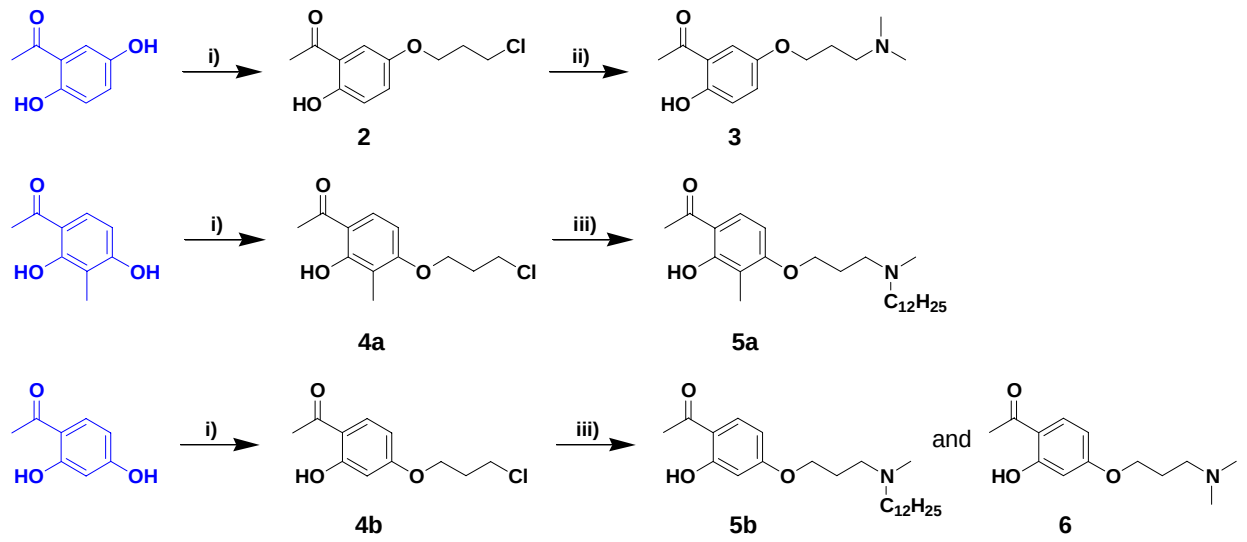

Scheme 4.2. Synthesis of acetophenones with tertiary aminogroups.

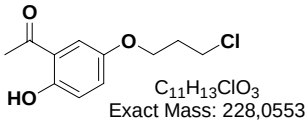

Compound 2
5-(3-Chloro-propoxy)-2-hydroxy-acetophenone

In a round-bottom flask 2,5-dihydroxy-acetophenone (3.05g, 0.020mol) was dissolved in 20mL of DMF. Then 1-bromo-3-chloro-propane (2.36mL, 0.022mol) and potassium carbonate (5.54g, 0.040mol) were added. Reaction mixture was stirred upon heating at 80°C for 4h. Solution became dark. After cooling it was poured into 200mL of water, neutralized with 10% aq. HCl and extracted with $CHCl_3$ (2 times). Combined organic layers were dried with sodium sulfate. Inorganic salt was filtered off and chloroform was removed by vacuum evaporation. Obtained dark oil was purified by column chromatography (eluent CH_2Cl_2) to produce compound **2** as colourless oil. Yield 2.55g (56%). **^{1}H NMR** (400MHz, $CDCl_3$): δ 11.84 (s, 1H), 7.18 (d, 1H), 7.09 (dd, 1H), 6.90 (d, 1H), 4.08 (t, 2H), 3.74 (t, 2H), 2.59 (s, 3H), 2.21 (m, 2H). **LCMS** (m/z): MM-ES+APCI, found $[M+1]^+$ 229.1 (calcd for $C_{11}H_{14}ClO_3^+$ 229.1).

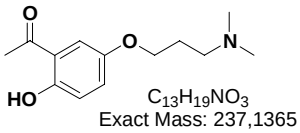

Compound 3
5-(3-Dimethylamino-propoxy)-2-hydroxy-acetophenone

Compound **2** (2.55g, 0.011mol) was dissolved in small amount of acetone. Then 5mL of saturated solution of NaJ in acetone were added. After 2 min of stirring white precipitate of NaCl has appeared. Stirring was continued at RT 1h. Inorganic salt was filtered off, and resulted solution was evaporated under vacuum. Obtained iodo-derivative was treated with 2M solution of dimethylamine in THF (17.0mL, 0.033mol). Reaction mixture warmed up, and white residue was formed in 2min. It was stirred at RT for 2h. Organic solvent was removed by vacuum evaporation. Residue was treated with aq. Na_2CO_3 in order to decompose ammonium salt. Free amine was extracted with $CHCl_3$ (2 times). Combined organic layers were dried with sodium sulfate. Inorganic salt was filtered off and chloroform was removed by vacuum evaporation. Obtained dark oil was purified by

column chromatography (eluent CH_2Cl_2/MeOH = 9/1) to produce compound **3** as white solid. Yield 1.10g (41%). **^{1}H NMR** (400MHz, $CDCl_3$): δ 11.82 (s, 1H), 7.16 (d, 1H), 7.07 (dd, 1H), 6.87 (d, 1H), 3.96 (t, 2H), 2.58 (s, 3H), 2.48 (t, 2H), 2.26 (s, 6H), 1.94 (m, 2H). **LCMS** (m/z): ESI, found $[M+1]^+$ 238.1 (calcd for $C_{13}H_{20}NO_3^+$ 238.1).

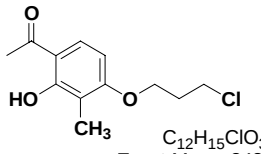

$C_{12}H_{15}ClO_3$
Exact Mass: 242,0710

Compound 4a
4-(3-Chloro-propoxy)-2-hydroxy-3-methyl-acetophenone

It was synthesized analogously to compound **2** starting from 2,4-dihydroxy-3-methyl-acetophenone. Colourless oil, yield 53%. **^{1}H NMR** (300MHz, $CDCl_3$): δ 12.75 (s, 1H), 7.58 (d, 1H), 6.44 (d, 1H), 4.19 (t, 2H), 3.76 (t, 2H), 2.56 (s, 3H), 2.27 (m, 2H), 2.09 (s, 3H). **LCMS** (m/z): MM-ES+APCI, found $[M+1]^+$ 243.1 (calcd for $C_{12}H_{16}ClO_3^+$ 243.1).

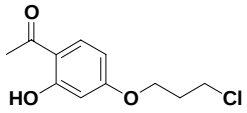

$C_{11}H_{13}ClO_3$
Exact Mass: 228,0553

Compound 4b
4-(3-Chloro-propoxy)-2-hydroxy-acetophenone

It was synthesized analogously to compound **2** starting from 2,4-dihydroxy-acetophenone. Colourless oil, yield 55%. **^{1}H NMR** (300MHz, CDCl3): δ 12.71 (s, 1H), 7.62 (d, 1H), 6.43 (dd, 1H), 6.41 (d, 1H), 4.15 (t, 2H), 3.72 (t, 2H), 2.55 (s, 3H), 2.24 (m, 2H). **LCMS** (m/z): MM-ES+APCI, found $[M+1]^+$ 229.1 (calcd for $C_{11}H_{14}ClO_3^+$ 229.1).

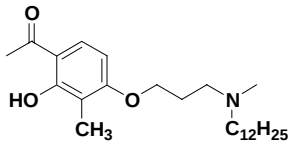

$C_{25}H_{43}NO_3$
Exact Mass: 405,3243

Compound 5a
4-(3-Dodecylmethylamino-propoxy)-2-hydroxy-3methyl-acetophenone

Acetophenone derivative **4a** (2.70g, 0.011mol) was dissolved in 20mL of acetonitrile. Then dodecylmethylamine (5.60mL, 0.022mol), potassium carbonate (4.63g, 0.033mol) and potassium iodide (1.00g, 0.006mol) were added. Reaction mixture was stirred upon heating at 80°C for 4h. Organic solvent was removed by vacuum evaporation. Obtained residue was purified by column chromatography (eluent CH_2Cl_2/MeOH = 95/5) to produce compound **5a** as white solid. Yield 1.60g (35%). **^{1}H NMR** (200MHz, $CDCl_3$): δ 12.74 (s, 1H), 7.54 (d, 1H), 6.41 (d, 1H), 4.07 (t, 2H), 2.53 (s, 3H), 2.50 (m, 2H), 2.32 (m, 2H), 2.21 (s, 3H), 2.08 (s, 3H), 1.95 (m, 2H), 1.42 (m, 2H), 1.35-1.15 (m, 18H), 0.86 (t, 3H). **LCMS** (m/z): MM-ES+APCI, found $[M+1]^+$ 406.3 (calcd for $C_{25}H_{44}NO_3^+$ 406.3).

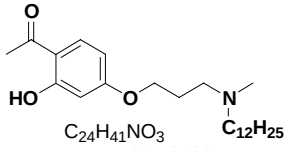

$C_{24}H_{41}NO_3$
Exact Mass: 391,3086

Compound 5b
4-(3-Dodecylmethylamino-propoxy)-2-hydroxy-acetophenone

It was synthesized analogously to previous compound starting from acetophenone derivative **4b**. White solid, yield 31%. **^{1}H NMR** (300MHz, $CDCl_3$): δ 12.66 (s, 1H), 7.61 (d, 1H), 6.38 (dd, 1H), 6.35 (d, 1H), 4.09 (t, 2H), 3.19 (m, 2H), 2.99 (m, 2H), 2.77 (s, 3H), 2.53 (s, 3H), 2.38 (m, 2H), 1.81 (m, 2H), 1.40-1.15 (m, 18H), 0.85 (t, 3H). **LCMS** (m/z): MM-ES+APCI, found $[M+1]^+$ 392.3 (calcd for $C_{24}H_{42}NO_3^+$ 392.3).

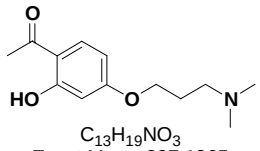

Compound 6
4-(3-Dimethylamino-propoxy)-2-hydroxy-acetophenone

It was synthesized analogously to compound **3** starting from acetophenone derivative **4b**. White solid, yield 35%. **^{1}H NMR** (300MHz, $CDCl_3$): δ 12.67 (s, 1H), 7.63 (d, 1H), 6.43 (dd, 1H), 6.37 (d, 1H), 4.14 (t, 2H), 3.34 (dd, 2H), 2.88 (s, 6H), 2.54 (s, 3H), 2.44 (m, 2H). **LCMS** (m/z): ESI, found $[M+1]^+$ 238.1 (calcd for $C_{13}H_{20}NO_3^+$ 238.1).

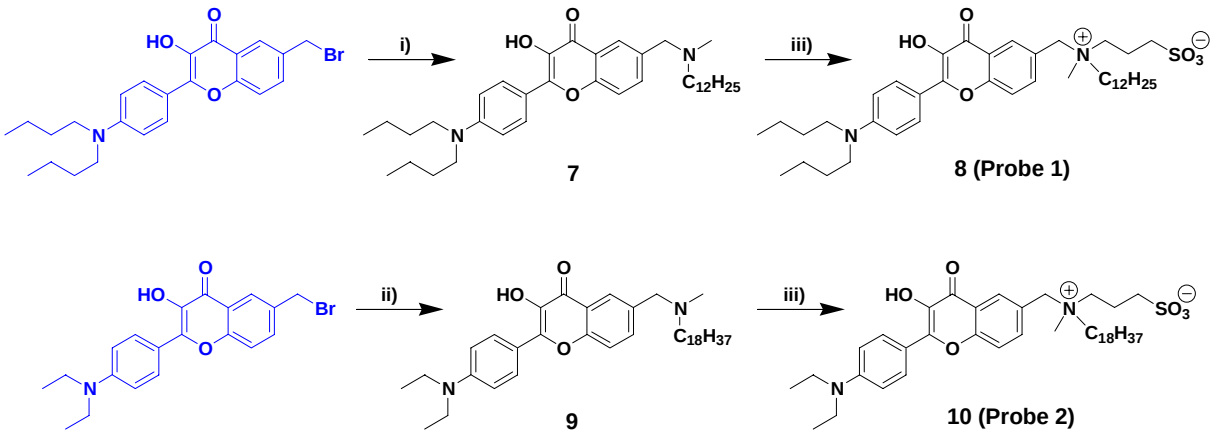

i) THF, dodecylmethylamine, RT 3h; ii) THF, methyloctadecylamine, RT 3h;
iii) CH_3CN, 1,3-propanesultone, 90°C overnight.

Scheme 4.3. Synthesis of long chain analogues of F2N12S.

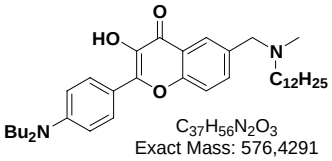

Compound 7
N-[(4'-Dibutylamino-3-hydroxy-6-flavonyl)-methyl]-N-methyl-dodecylamine

6-Bromomethyl-4'-dibutylamino-3-hydroxyflavone (obtained as described by Klymchenko et al., 2002c) (100mg, 0.25mmol) was dissolved in dry THF. Dodecylmethylamine (165µL, 0.75mmol) was added, and reaction mixture was stirred at RT for 3h. Organic solvent was removed by vacuum evaporation. Obtained residue was purified by column chromatography (eluent CH_2Cl_2/MeOH = 95/5) to give compound **7** as yellow solid, yield 110mg (88%). **^{1}H NMR** (300MHz, $CDCl_3$): δ 8.14 (d, 2H), 8.07 (d, 1H), 7.68 (dd, 1H), 7.48 (d, 1H), 6.73 (d, 2H), 3.58 (s, 2H), 3.34 (t, 4H), 2.38 (m, 2H), 2.19 (s, 3H), 1.61 (m, 4H), 1.51 (m, 2H), 1.37 (m, 4H), 1.30-1.15 (m, 18H), 0.96 (t, 6H), 0.86 (t, 3H). **LCMS** (m/z): MM-ES+APCI, found $[M+1]^+$ 577.4 (calcd for $C_{37}H_{57}N_2O_3^+$ 577.4).

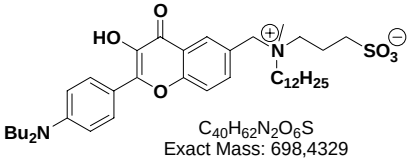

Compound 8 (Probe 1)
N-[(4'-Dibutylamino-3-hydroxy-6-flavonyl)-methyl]-N-methyl-N-(3-sulfopropyl)-1-dodecanaminium, inner salt

It was synthesized according to general procedure for quaternization of amines with 1,3-propanesultone starting from 50mg of previously obtained compound **7**. The product was purified by preparative TLC (eluent CH_2Cl_2/MeOH = 85/15). Yellow solid, yield 25mg (41%). **^{1}H NMR** (300MHz, $CDCl_3$): δ 8.10 (s, 1H), 7.97 (d, 2H), 7.80 (d, 1H), 7.43 (d, 1H), 6.61 (d, 2H), 4.82 (s,

2H), 3.75 (m, 2H), 3.31 (m, 4H), 3.20-2.90 (m, 7H), 2.43 (m, 2H), 1.75 (m, 2H), 1.59 (m, 4H), 1.37 (m, 4H), 1.30-1.10 (m, 18H), 0.97 (t, 6H), 0.83 (t, 3H). **LCMS** (m/z): MM-ES+APCI, found $[M+1]^+$ 699.4 (calcd for $C_{40}H_{63}N_2O_6S^+$ 699.4).

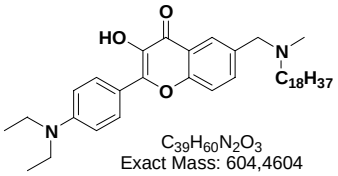

Compound 9
N-[(4'-Diethylamino-3-hydroxy-6-flavonyl)-methyl]-N-methyl-octadecylamine

6-Bromomethyl-4'-diethylamino-3-hydroxyflavone (obtained as described by Klymchenko et al., 2002c) (100mg, 0.25mmol) was dissolved in dry THF. Methyloctadecylamine (211mg, 0.75mmol) was added and reaction mixture was stirred at RT for 3h. Organic solvent was removed by vacuum evaporation. Obtained residue was purified by column chromatography (eluent CH_2Cl_2/MeOH = 95/5) to give compound **9** as yellow solid, yield 120mg (80%). **^{1}H NMR** (300MHz, $CDCl_3$): δ 8.16 (d, 2H), 8.07 (d, 1H), 7.68 (dd, 1H), 7.50 (d, 1H), 6.76 (d, 2H), 3.56 (s, 2H), 3.44 (q, 4H), 2.37 (m, 2H), 2.18 (s, 3H), 1.50 (m, 2H), 1.35-1.15 (m, 36H), 0.87 (t, 3H). **LCMS** (m/z): MM-ES+APCI, found $[M+1]^+$ 605.5 (calcd for $C_{39}H_{61}N_2O_3^+$ 605.5).

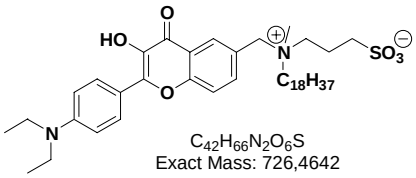

Compound 10 (Probe 2)
N-[(4'-Diethylamino-3-hydroxy-6-flavonyl)-methyl]-N-methyl-N-(3-sulfopropyl)-1-octadecanaminium, inner salt

It was synthesized according to general procedure for quaternization of amines with 1,3-propanesultone starting from 50mg of previously obtained compound **9**. The product was purified by preparative TLC (eluent CH_2Cl_2/MeOH = 85/15). Yellow solid, yield 20mg (33%). **^{1}H NMR** (300MHz, $CDCl_3$): δ 8.10 (s, 1H), 7.97 (d, 2H), 7.80 (d, 1H), 7.43 (d, 1H), 6.61 (d, 2H), 4.82 (s, 2H), 3.75 (m, 2H), 3.31 (m, 4H), 3.20-2.90 (m, 7H), 2.43 (m, 2H), 1.75 (m, 2H), 1.40-1.15 (m, 36H), 0.85 (t, 3H). **LCMS** (m/z): MM-ES+APCI, found $[M+1]^+$ 727.5 (calcd for $C_{42}H_{67}N_2O_6S^+$ 727.5).

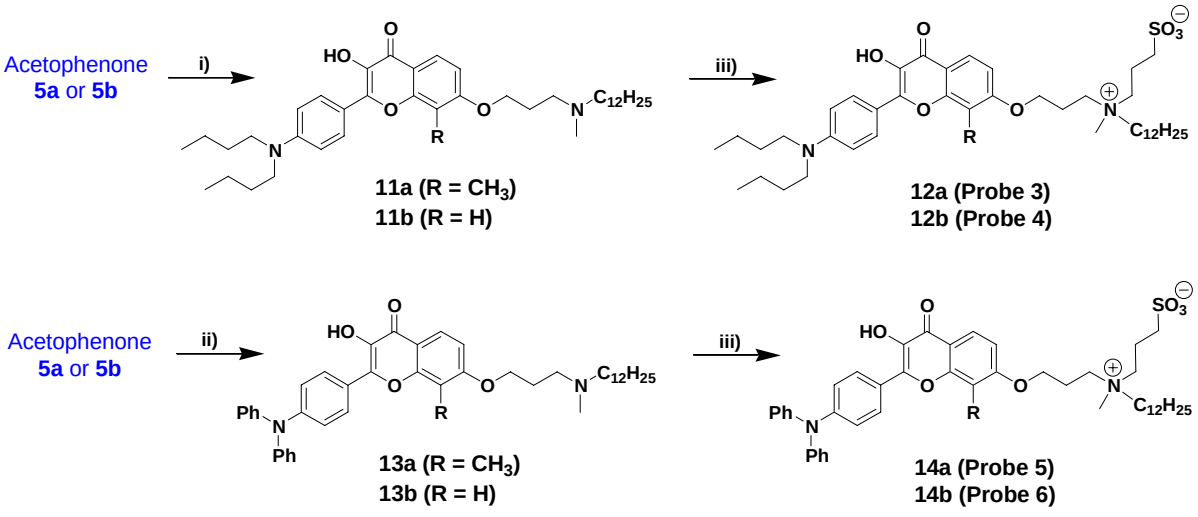

i) DMF, 4-dibutylamino-benzaldehyde, MeONa, then EtOH, 30% H_2O_2, MeONa, reflux 3min;
ii) DMF, 4-diphenylamino-benzaldehyde, MeONa, then EtOH, 30% H_2O_2, MeONa, reflux 3min;
iii) CH_3CN, 1,3-propanesultone, 90°C overnight.

Scheme 4.4. Synthesis of linker-modified analogues of F2N12S.

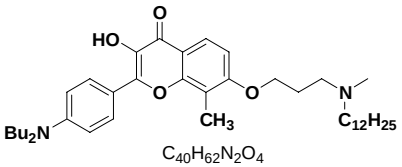

$C_{40}H_{62}N_2O_4$
Exact Mass: 634,4710

Compound 11a
4'-Dibutylamino-7-[3-dodecylmethylamino-propoxy]-3-hydroxy-8-methyl-flavone

It was synthesized according to general procedure for synthesis of 3-hydroxyflavones starting from 4-dibutylamino-benzaldehyde and compound **5a** (200mg, 0.50mmol). The product was purified by preparative TLC (eluent CH_2Cl_2/MeOH = 9/1). Yellow solid, yield 70mg (22%). **^{1}H NMR** (300MHz, $CDCl_3$): δ 8.13 (d, 2H), 8.00 (d, 1H), 6.88 (d, 1H), 6.73 (d, 2H), 4.19 (m, 2H), 3.34 (t, 4H), 2.85 (m, 2H), 2.63 (m, 2H), 2.47 (s, 3H), 2.38 (s, 3H), 2.16 (m, 2H), 1.65 (m, 2H), 1.58 (m, 4H), 1.45-1.15 (m, 22H), 0.95 (t, 6H), 0.86 (t, 3H). **LCMS** (m/z): MM-ES+APCI, found $[M+1]^+$ 635.5 (calcd for $C_{40}H_{63}N_2O_4^+$ 635.5).

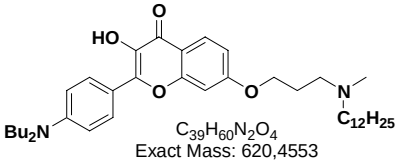

$C_{39}H_{60}N_2O_4$
Exact Mass: 620,4553

Compound 11b
4'-Dibutylamino-7-[3-dodecylmethylamino-propoxy]-3-hydroxy-flavone

It was synthesized according to general procedure for synthesis of 3-hydroxyflavones starting from 4-dibutylamino-benzaldehyde and compound **5b** (200mg, 0.50mmol). The product was purified by preparative TLC (eluent CH_2Cl_2/MeOH = 9/1). Yellow solid, yield 80mg (25%). **^{1}H NMR** (400MHz, $CDCl_3$): δ 8.08 (d, 2H), 8.04 (d, 1H), 6.80-6.70 (m, 2H), 6.69 (d, 2H), 4.11 (m, 2H), 3.32 (t, 4H), 2.90 (m, 2H), 2.70 (m, 2H), 2.53 (s, 3H), 2.22 (m, 2H), 1.65 (m, 2H), 1.58 (m, 4H), 1.40-1.20 (m,22H), 0.95 (t, 6H), 0.84 (t, 3H). **LCMS** (m/z): MM-ES+APCI, found $[M+1]^+$ 621.5 (calcd for $C_{39}H_{61}N_2O_4^+$ 621.5).

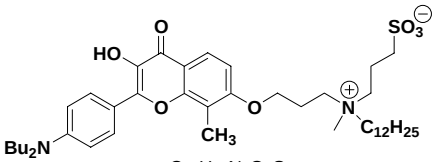

$C_{43}H_{68}N_2O_7S$
Exact Mass: 756,4747

Compound 12a (Probe 3)
N-[3-(4'-Dibutylamino-3-hydroxy-8-methyl-flavonyl-7-oxy)-propyl]-N-methyl-N-(3-sulfopropyl)-1-dodecanaminium, inner salt

It was synthesized according to general procedure for quaternization of amines with 1,3-propanesultone starting from 40mg of previously obtained compound **11a**. The product was purified by preparative TLC (eluent CH_2Cl_2/MeOH = 85/15). Yellow solid, yield 12mg (25%). **^{1}H NMR** (300MHz, $CDCl_3$): δ 8.06 (d, 2H), 8.00 (d, 1H), 6.80 (d, 1H), 6.66 (d, 2H), 4.15 (m, 2H), 3.74 (m, 2H), 3.64 (m, 2H), 3.28 (t, 4H), 3.18 (s, 3H), 3.05-2.85 (m, 4H), 2.40-2.15 (m, 4H), 2.11 (s, 3H), 1.67 (m, 2H), 1.56 (m, 4H), 1.45-1.10 (m, 22H), 0.94 (t, 6H), 0.84 (t, 3H). **LCMS** (m/z): MM-ES+APCI, found $[M+1]^+$ 757.5 (calcd for $C_{43}H_{69}N_2O_7S^+$ 757.5).

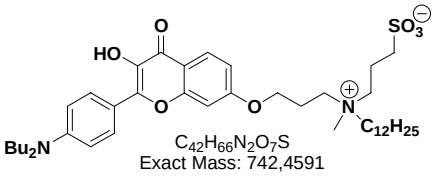

$C_{42}H_{66}N_2O_7S$
Exact Mass: 742,4591

Compound 12b (Probe 4)
N-[3-(4'-Dibutylamino-3-hydroxy-flavonyl-7-oxy)-propyl]-N-methyl-N-(3-sulfopropyl)-1-dodecanaminium, inner salt

It was synthesized according to general procedure for quaternization of amines with 1,3-propanesultone starting from 40mg of previously obtained compound **11b**. The product was purified by preparative TLC (eluent CH_2Cl_2/MeOH = 85/15). Yellow solid, yield 18mg (38%). **^{1}H NMR** (300MHz, $CDCl_3$): δ 8.05 (m, 3H), 6.88 (m, 2H), 6.66 (d, 2H), 4.15 (m, 2H), 3.74 (m, 2H), 3.64 (m, 2H), 3.28 (t, 4H), 3.18 (s, 3H), 3.05-2.85 (m, 4H), 2.40-2.15 (m, 4H), 1.67 (m, 2H), 1.56 (m, 4H), 1.45-1.10 (m, 22H), 0.94 (t, 6H), 0.84 (t, 3H). **LCMS** (m/z): MM-ES+APCI, found $[M+1]^+$ 743.5 (calcd for $C_{42}H_{67}N_2O_7S^+$ 743.5).

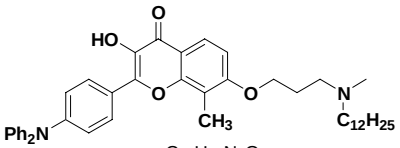

$C_{44}H_{54}N_2O_4$
Exact Mass: 674,4084

Compound 13a
4'-Diphenylamino-7-[3-dodecylmethylamino-propoxy]-3-hydroxy-8-methyl-flavone

It was synthesized according to general procedure for synthesis of 3-hydroxyflavones starting from 4-diphenylamino-benzaldehyde and compound **5a** (200mg, 0.50mmol). The product was purified by preparative TLC (eluent CH_2Cl_2/MeOH = 9/1). Yellow solid, yield 80mg (24%). **^{1}H NMR** (300MHz, $CDCl_3$): δ 8.11 (d, 2H), 8.02 (d, 1H), 7.35-7.20 (m, 4H), 7.20-7.05 (m, 8H), 6.95 (d, 1H), 4.16 (m, 2H), 2.83 (m, 2H), 2.61 (m, 2H), 2.46 (s, 3H), 2.37 (s, 3H), 2.16 (m, 2H), 1.59 (m, 2H), 1.40-1.15 (m, 18H), 0.85 (t, 3H). **LCMS** (m/z): MM-ES+APCI, found $[M+1]^+$ 675.4 (calcd for $C_{44}H_{55}N_2O_4^+$ 675.4).

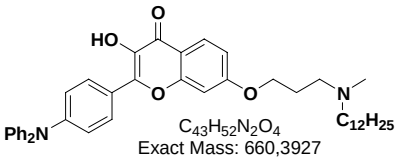

$C_{43}H_{52}N_2O_4$
Exact Mass: 660,3927

Compound 13b
4'-Diphenylamino-7-[3-dodecylmethylamino-propoxy]-3-hydroxy-flavone

It was synthesized according to general procedure for synthesis of 3-hydroxyflavones starting from 4-diphenylamino-benzaldehyde and compound **5b** (200mg, 0.50mmol). The product was purified by preparative TLC (eluent CH_2Cl_2/MeOH = 9/1). Yellow solid, yield 85mg (25%). **^{1}H NMR** (300MHz, $CDCl_3$): δ 8.11 (d, 2H), 8.05 (d, 1H), 7.35-7.25 (m, 4H), 7.20-7.10 (m, 8H), 6.92 (m, 2H), 4.14 (m, 2H), 2.74 (m, 2H), 2.54 (m, 2H), 2.41 (s, 3H), 2.12 (m, 2H), 1.55 (m, 2H), 1.40-1.15 (m, 18H), 0.86 (t, 3H). **LCMS** (m/z): MM-ES+APCI, found $[M+1]^+$ 661.4 (calcd for $C_{43}H_{53}N_2O_4^+$ 661.4).

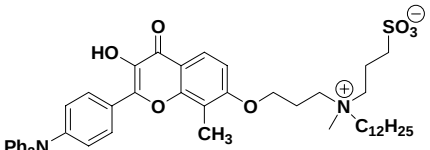

$C_{47}H_{60}N_2O_7S$
Exact Mass: 796,4121

Compound 14a (Probe 5)
N-[3-(4'-Diphenylamino-3-hydroxy-8-methyl-flavonyl-7-oxy)-propyl]-N-methyl-N-(3-sulfopropyl)-1-dodecanaminium, inner salt

It was synthesized according to general procedure for quaternization of amines with 1,3-propanesultone starting from 40mg of previously obtained compound **13a**. The product was purified by preparative TLC (eluent CH_2Cl_2/MeOH = 85/15). Yellow solid, yield 20mg (42%). **^{1}H NMR** (300MHz, $CDCl_3$): δ 7.93 (d, 2H), 7.85 (d, 1H), 7.30-7.20 (m, 4H), 7.15-7.00 (m, 8H), 6.92 (d, 1H), 4.15 (m, 2H), 3.74 (m, 2H), 3.64 (m, 2H), 3.26 (s, 3H), 3.00 (m, 2H), 2.82 (m, 2H), 2.40-2.15 (m, 4H), 2.10 (s, 3H), 1.67 (m, 2H), 1.35-1.10 (m, 18H), 0.81 (t, 3H). **LCMS** (m/z): MM-ES+APCI, found $[M+1]^+$ 797.4 (calcd for $C_{47}H_{61}N_2O_7S^+$ 797.4).

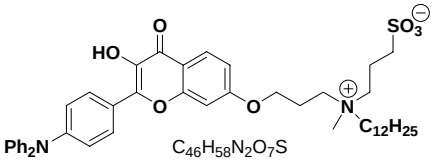

$C_{46}H_{58}N_2O_7S$
Exact Mass: 782,3965

Compound 14b (Probe 6)
N-[3-(4'-Diphenylamino-3-hydroxy-flavonyl-7-oxy)-propyl]-N-methyl-N-(3-sulfopropyl)-1-dodecanaminium, inner salt

It was synthesized according to general procedure for quaternization of amines with 1,3-propanesultone starting from 40mg of previously obtained compound **13b**. The product was purified by preparative TLC (eluent CH_2Cl_2/MeOH = 85/15). Yellow solid, yield 11mg (23%). **^{1}H NMR** (300MHz, $CDCl_3$): δ 7.93 (d, 2H), 7.85 (d, 1H), 7.30-7.20 (m, 4H), 7.15-7.05 (m, 8H), 7.00 (m, 2H), 4.15 (m, 2H), 3.74 (m, 2H), 3.64 (m, 2H), 3.20 (s, 3H), 3.00 (m, 2H), 2.82 (m, 2H), 2.40-2.15 (m, 4H), 1.67 (m, 2H), 1.35-1.10 (m, 18H), 0.82 (t, 3H). **LCMS** (m/z): MM-ES+APCI, found $[M+1]^+$ 783.4 (calcd for $C_{46}H_{59}N_2O_7S^+$ 783.4).

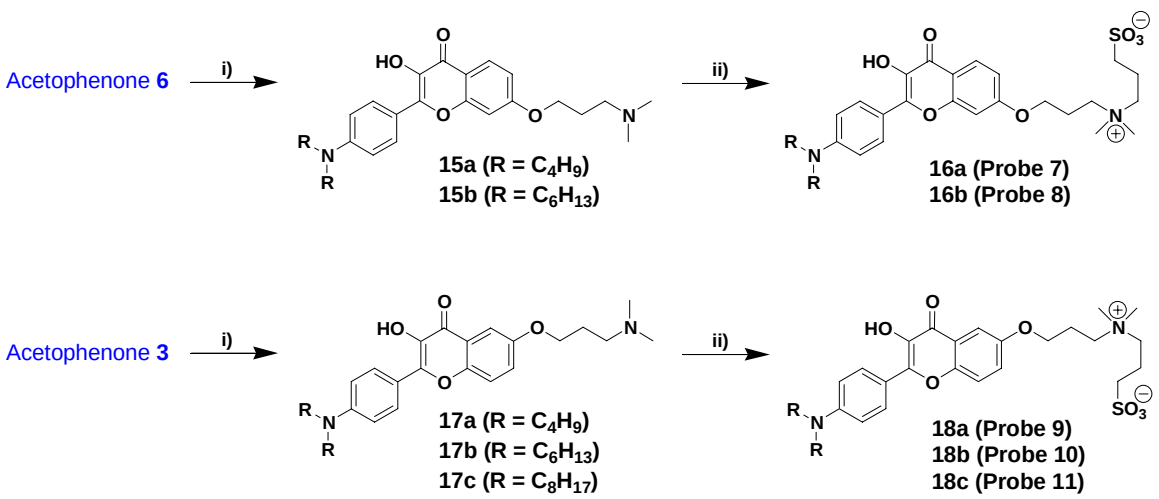

i) DMF, 4-dibutylamino-benzaldehyde (or aldehydes **1a-b**), MeONa, then EtOH, 30% H_2O_2, MeONa, reflux 3min; ii) CH_3CN, 1,3-propanesultone, 90°C overnight.

Scheme 4.5. Synthesis of the 2nd generation of 3HF probes.

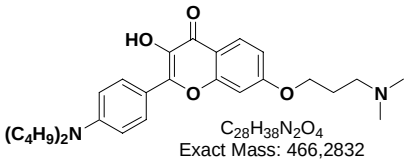

Compound 15a
4'-Dibutylamino-7-(3-dimethylamino-propoxy)-3-hydroxy-flavone

It was synthesized according to general procedure for synthesis of 3-hydroxyflavones starting from 4-dibutylamino-benzaldehyde and compound **6** (200mg, 0.84mmol). The product was purified by preparative TLC (eluent CH_2Cl_2/MeOH = 9/1). Yellow solid, yield 90mg (22%). **^{1}H NMR** (400MHz, $CDCl_3$): δ 8.09 (d, 2H), 8.01 (d, 1H), 6.82 (m, 2H), 6.70 (d, 2H), 4.16 (t, 2H), 3.52 (m, 2H), 3.31 (m, 4H), 3.26 (s, 6H), 2.47 (m, 2H), 1.58 (m, 4H), 1.36 (m, 4H), 0.96 (t, 6H). **LCMS** (m/z): MM-ES+APCI, found $[M+1]^+$ = 467.3 (calcd for $C_{28}H_{39}N_2O_4^+$ 467.3).

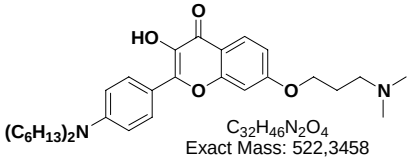

Compound 15b
4'-Dihexylamino-7-(3-dimethylamino-propoxy)-3-hydroxy-flavone

It was synthesized according to general procedure for synthesis of 3-hydroxyflavones starting from 4-dihexylamino-benzaldehyde **1a** and compound **6** (200mg, 0.84mmol). The product was purified by preparative TLC (eluent CH_2Cl_2/MeOH = 9/1). Yellow solid, yield 100mg (23%). **^{1}H NMR** (400MHz, $CDCl_3$): δ 8.10 (d, 2H), 8.08 (d, 1H), 6.92 (d, 1H), 6.91 (s, 1H), 6.71 (d, 2H), 4.13 (t, 2H), 3.32 (m, 4H), 2.71 (m, 2H), 2.43 (s, 6H), 2.12 (m, 2H), 1.60 (m, 4H), 1.40-1.20 (m, 12H), 0.90 (t, 6H). **LCMS** (m/z): MM-ES+APCI, found $[M+1]^+$ 523.4 (calcd for $C_{32}H_{47}N_2O_4^+$ 523.4).

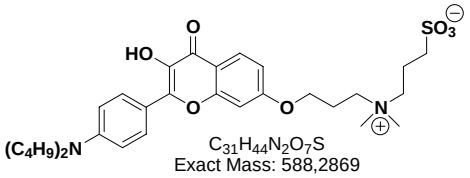

Compound 16a (Probe 7)
N-[3-(4'-Dibutylamino-3-hydroxy-flavonyl-7-oxy)-propyl]-N,N-dimethyl-N-(3-sulfopropyl)-aminium, inner salt

It was synthesized according to general procedure for quaternization of amines with 1,3-propanesultone starting from 30mg of previously obtained compound **15a**. The product was purified

by preparative TLC (eluent CH_2Cl_2/MeOH = 85/15). Yellow solid, yield 20mg (52%). **^{1}H NMR** (400MHz, $CDCl_3$): δ 7.98 (m, 3H), 6.86 (m, 2H), 6.60 (m, 2H), 3.98 (m, 2H), 3.65 (m, 2H), 3.55 (m, 2H), 3.25 (m, 4H), 3.15 (s, 6H), 3.00 (m, 2H), 2.30 (m, 2H), 2.20 (m, 2H), 1.50 (m, 4H), 1.35 (m, 4H), 0.87 (t, 6H). **HRMS** (m/z): ESI, found $[M+1]^+$ 589.29 (calcd for $C_{31}H_{45}N_2O_7S^+$ 589.29).

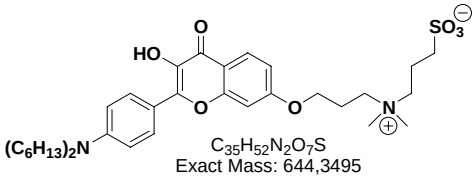

Compound 16b (Probe 8)
N-[3-(4'-Dihexylamino-3-hydroxy-flavonyl-7-oxy)-propyl]-N,N-dimethyl-N-(3-sulfopropyl)-aminium, inner salt

It was synthesized according to general procedure for quaternization of amines with 1,3-propanesultone starting from 30mg of previously obtained compound **15b**. The product was purified by preparative TLC (eluent CH_2Cl_2/MeOH = 85/15). Yellow solid, yield 22mg (59%). **^{1}H NMR** (400MHz, $CDCl_3$): δ 7.92 (m, 3H), 6.86 (m, 2H), 6.50 (m, 2H), 3.98 (m, 2H), 3.65 (m, 2H), 3.55 (m, 2H), 3.25 (m, 4H), 3.15 (s, 6H), 3.00 (m, 2H), 2.30 (m, 2H), 2.20 (m, 2H), 1.50 (m, 4H), 1.35-1.15 (m, 12H), 0.85 (t, 6H). **HRMS** (m/z): ESI, found $[M+1]^+$ 645.35 (calcd for $C_{35}H_{53}N_2O_7S^+$ 645.35).

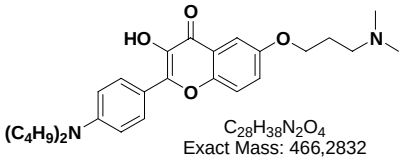

Compound 17a
4'-Dibutylamino-6-(3-dimethylamino-propoxy)-3-hydroxy-flavone

It was synthesized according to general procedure for synthesis of 3-hydroxyflavones starting from 4-dibutylamino-benzaldehyde and compound **3** (200mg, 0.84mmol). The product was purified by preparative TLC (eluent CH_2Cl_2/MeOH = 9/1). Yellow solid, yield 100mg (25%). **^{1}H NMR** (300MHz, $CDCl_3$): δ 8.12 (d, 2H), 7.52 (d, 1H), 7.42 (d, 1H), 7.20 (dd, 1H), 6.71 (d, 2H), 4.08 (t, 2H), 3.32 (t, 4H), 2.44 (t, 2H), 2.24 (s, 6H), 1.96 (m, 2H), 1.60 (m, 4H), 1.36 (m, 4H), 0.96 (t, 6H). **LCMS** (m/z): MM-ES+APCI, found $[M+1]^+$ 467.3 (calcd for $C_{28}H_{39}N_2O_4^+$ 467.3).

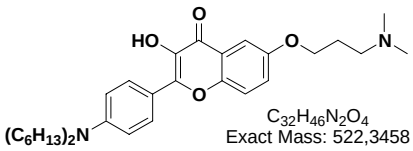

Compound 17b
4'-Dihexylamino-6-(3-dimethylamino-propoxy)-3-hydroxy-flavone

It was synthesized according to general procedure for synthesis of 3-hydroxyflavones starting from 4-dihexylamino-benzaldehyde **1a** and compound **3** (200mg, 0.84mmol). The product was purified by preparative TLC (eluent CH_2Cl_2/MeOH = 9/1). Yellow solid, yield 170mg (38%). **^{1}H NMR** (400MHz, $CDCl_3$): δ 8.12 (d, 2H), 7.51 (d, 1H), 7.42 (d, 1H), 7.20 (dd, 1H), 6.70 (d, 2H), 4.09 (t, 2H), 3.31 (t, 4H), 2.57 (t, 2H), 2.33 (s, 6H), 2.03 (m, 2H), 1.60 (m, 4H), 1.40-1.20 (m, 12H), 0.89 (t, 6H). **LCMS** (m/z): MM-ES+APCI, found $[M+1]^+$ 523.3 (calcd for $C_{32}H_{47}N_2O_4^+$ 523.3).

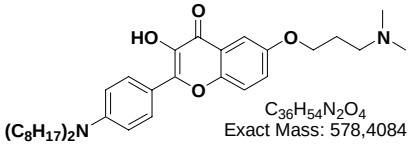

Compound 17c
4'-Dioctylamino-6-(3-dimethylamino-propoxy)-3-hydroxy-flavone

It was synthesized according to general procedure for synthesis of 3-hydroxyflavones starting from 4-dioctylamino-benzaldehyde **1b** and compound **3** (200mg, 0.84mmol). The product was purified by preparative TLC (eluent CH_2Cl_2/MeOH = 9/1). Yellow solid, yield 100mg (20%). **^{1}H NMR** (300MHz, $CDCl_3$): δ 8.12 (d, 2H), 7.52 (d, 1H), 7.42 (d, 1H), 7.22 (dd, 1H), 6.71 (d, 2H), 4.11 (t, 2H), 3.32 (t, 4H), 2.50 (t, 2H), 2.28 (s, 6H), 2.00 (m, 2H), 1.61 (m, 4H), 1.40-1.20 (m, 20H), 0.88 (t, 6H). **LCMS** (m/z): ESI, found $[M+1]^+$ 579.4 (calcd for $C_{36}H_{55}N_2O_4^+$ 579.4).

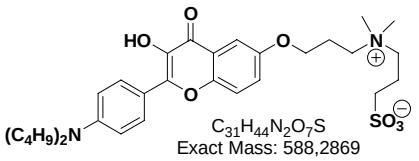

Compound 18a (Probe 9)
N-[3-(4'-Dibutylamino-3-hydroxy-flavonyl-6-oxy)-propyl]-N,N-dimethyl-N-(3-sulfopropyl)-aminium, inner salt

It was synthesized according to general procedure for quaternization of amines with 1,3-propanesultone starting from 30mg of previously obtained compound **17a**. The product was purified by preparative TLC (eluent CH_2Cl_2/MeOH = 85/15). Yellow solid, yield 27mg (70%). **^{1}H NMR** (300MHz, $CDCl_3$): δ 8.05 (d, 2H), 7.40 (d, 1H), 7.38 (d, 1H), 7.15 (dd, 1H), 6.66 (d, 2H), 4.10 (t, 2H), 3.67 (m, 2H), 3.53 (m, 2H), 3.30 (m, 4H), 3.14 (s, 6H), 2.91 (m, 2H), 2.38 (m, 2H), 2.24 (m, 2H), 1.56 (m, 4H), 1.33 (m, 4H), 0.93 (t, 6H). **HRMS** (m/z): ESI, found $[M+1]^+$ 589.29 (calcd for $C_{31}H_{45}N_2O_7S^+$ 589.29).

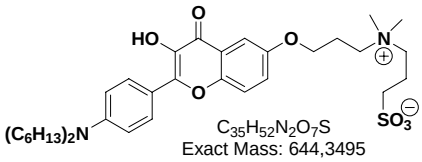

Compound 18b (Probe 10)
N-[3-(4'-Dihexylamino-3-hydroxy-flavonyl-6-oxy)-propyl]-N,N-dimethyl-N-(3-sulfopropyl)-aminium, inner salt

It was synthesized according to general procedure for quaternization of amines with 1,3-propanesultone starting from 30mg of previously obtained compound **17b**. The product was purified by preparative TLC (eluent CH_2Cl_2/MeOH = 85/15). Yellow solid, yield 30mg (80%). **^{1}H NMR** (300MHz, $CDCl_3$): δ 7.86 (d, 2H), 7.14 (d, 1H), 7.03 (d, 1H), 6.88 (dd, 1H), 6.49 (d, 2H), 3.90 (t, 2H), 3.65 (m, 2H), 3.55 (m, 2H), 3.30 (m, 4H), 3.15 (s, 6H), 3.05 (m, 2H), 2.33 (m, 2H), 2.20 (m, 2H), 1.50 (m, 4H), 1.40-1.15 (m, 12H), 0.86 (t, 6H). **HRMS** (m/z): ESI, found $[M+1]^+$ 645.35 (calcd for $C_{35}H_{53}N_2O_7S^+$ 645.35).

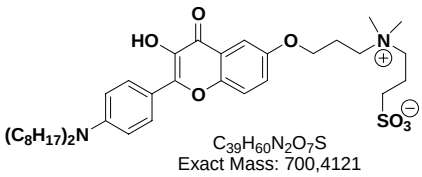

Compound 18c (Probe 11)
N-[3-(4'-Dioctylamino-3-hydroxy-flavonyl-6-oxy)-propyl]-N,N-dimethyl-N-(3-sulfopropyl)-aminium, inner salt

It was synthesized according to general procedure for quaternization of amines with 1,3-propanesultone starting from 30mg of previously obtained compound **17c**. The product was purified by preparative TLC (eluent CH_2Cl_2/MeOH = 85/15). Yellow solid, yield 24mg (66%). **^{1}H NMR** (200MHz, $CDCl_3$): δ 7.87 (d, 2H), 7.17 (d, 1H), 7.05 (d, 1H), 6.88 (dd, 1H), 6.49 (d, 2H), 3.90 (t, 2H), 3.65 (m, 2H), 3.55 (m, 2H), 3.30 (m, 4H), 3.15 (s, 6H), 3.05 (m, 2H), 2.33 (m, 2H), 2.20 (m, 2H), 1.50 (m, 4H), 1.40-1.10 (m, 20H), 0.86 (t, 6H). **HRMS** (m/z): ESI, found $[M+1]^+$ 701.42 (calcd for $C_{39}H_{61}N_2O_7S^+$ 701.42).

4.1.2. Synthesis of NR-based membrane probes

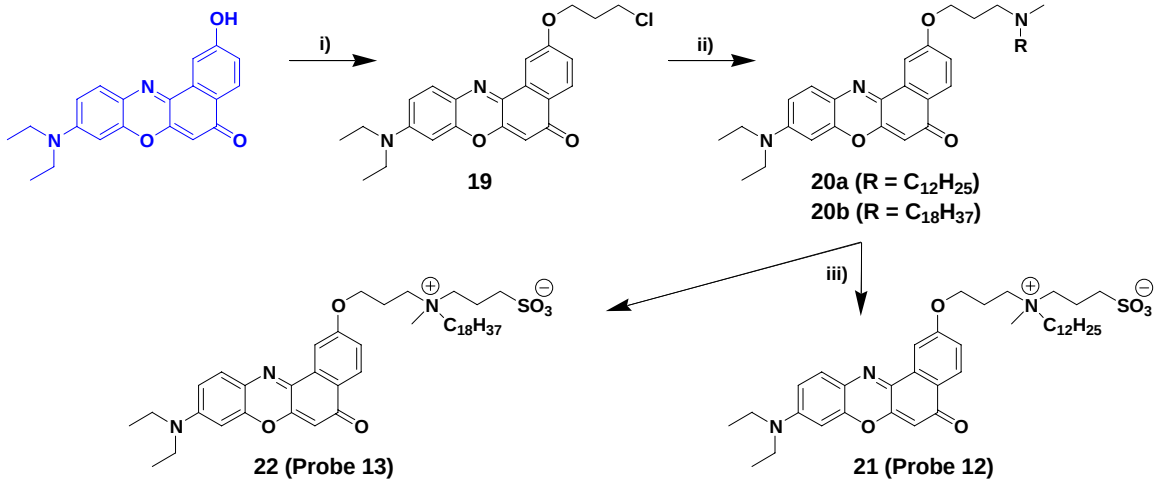

i) DMF, 1-bromo-3-chloropropane, K_2CO_3, 80°C 3h; ii) 2-butanone, dodecylmethylamine or methyloctadecylamine, K_2CO_3, KJ, reflux 48h; iii) CH_3CN, 1,3-propanesultone, 90°C overnight.

Scheme 4.6. Synthesis of the 1st generation of NR probes.

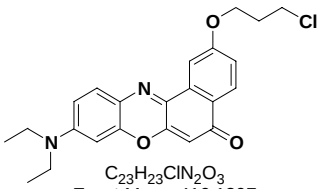

Compound 19
2-(3-Chloropropoxy)-9-diethylamino-benzo[a]phenoxazin-5-one

9-(Diethylamino)-2-hydroxy-benzo[a]phenoxazin-5-one (obtained as described by Briggs et al., 1997, Martin-Brown et al., 2005) (0.500g, 1.5mmol) was dissolved in dry DMF and cooled to 5°C. Then potassium carbonate (1.035g, 7.5mmol) and 1-bromo-3-chloropropane (1.60mL, 15.0mmol) were added to this solution. The reaction mixture was stirred at 80°C for 3h. Then the solvent was evaporated and the residue was treated with water. The precipitate was filtered off and washed with water and heptane to give compound **19** as a dark-violet solid. Yield 0.600g (96%). **^{1}H NMR** (300MHz, $CDCl_3$): δ 8.22 (d, 1H), 8.06 (d, 1H), 7.60 (d, 1H), 7.16 (dd, 1H), 6.66 (dd, 1H), 6.46 (d, 1H), 6.30 (s, 1H), 4.33 (t, 2H), 3.80 (t, 2H), 3.46 (q, 4H), 2.32 (m, 2H), 1.26 (t, 6H). **LCMS** (m/z): ESI, found $[M+1]^+$ 411.1 (calcd for $C_{23}H_{24}ClN_2O_3^+$ 411.1).

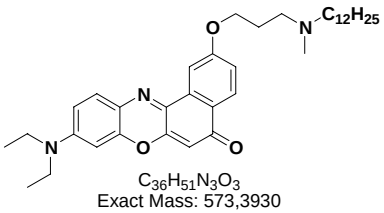

Compound 20a
9-Diethylamino-2-[3-(dodecylmethylamino)-propoxy]-benzo[a]phenoxazin-5-one

The Nile Red derivative **19** (150mg, 0.365mmol) was mixed with dodecylmethylamine (0.366mL, 1.460mmol) in butanone-2 in the presence of K_2CO_3 (126mg, 0.913mmol) and KI (60mg, 0.183mmol). The reaction mixture was refluxed for 48h. The solvent was evaporated under reduced pressure and the residue was purified by column chromatography (eluent CH_2Cl_2/MeOH = 95/5) to give compound **20a** as a dark-violet solid. Yield 200mg (95%). **^{1}H NMR** (300MHz, $CDCl_3$): δ 8.20 (d, 1H), 8.03 (d, 1H), 7.60 (d, 1H), 7.13 (dd, 1H), 6.66 (dd, 1H), 6.45 (d, 1H), 6.29 (s, 1H), 4.27 (t, 2H), 3.47 (q, 4H), 2.99 (m, 2H), 2.76 (m, 2H), 2.57 (s, 3H), 2.32 (m, 2H), 1.71 (m, 2H), 1.40-1.20 (m, 24H), 0.86 (t, 3H). **LCMS** (m/z): ESI, found $[M+1]^+$ 574.4 (calcd for $C_{36}H_{52}N_3O_3^+$ 574.4).

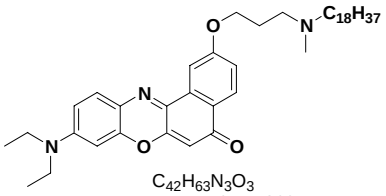

$C_{42}H_{63}N_3O_3$
Exact Mass: 657,4869

Compound 20b
9-Diethylamino-2-[3-(methyloctadecylamino)-propoxy]-benzo[a]phenoxazin-5-one

It was synthesized analogously to previous compound starting from 200mg of compound **19** (200mg, 49mmol) and methyloctadecylamine. The product was purified by column chromatography (eluent CH_2Cl_2/MeOH = 95/5) to give compound **20b** as dark red solid, yield 290mg (90%). **^{1}H NMR** (300MHz, $CDCl_3$): δ 8.16 (d, 1H), 8.00 (d, 1H), 7.52 (d, 1H), 7.11 (dd, 1H), 6.60 (dd, 1H), 6.41 (d, 1H), 6.25 (s, 1H), 4.25 (m, 2H), 3.45 (q, 4H), 2.65 (m, 2H), 2.50-2.25 (m, 5H), 2.10 (m, 2H), 1.51 (m, 2H), 1.40-1.15 (m, 36H), 0.88 (t, 3H). **LCMS** (m/z): MM-ES APCI, found $[M+1]^+$ 658.5 (calcd for $C_{42}H_{64}N_3O_3^+$ 658.5).

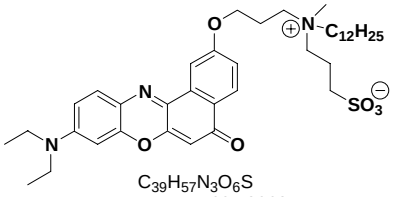

$C_{39}H_{57}N_3O_6S$
Exact Mass: 695,3968

Compound 21 (Probe 12)
N-[3-(9-Diethylamino-5-oxo-benzo[a]phenoxazin-2-yloxy)-propyl]-N-methyl-N-(3-sulfopropyl)-1-dodecanaminium, inner salt

It was synthesized according to general procedure for quaternization of amines with 1,3-propanesultone starting from 40mg of previously obtained compound **20a**. The product was purified by column chromatography (eluent CH_2Cl_2/MeOH=85/15). Dark violet solid, yield 67mg (33%). **^{1}H NMR** (400MHz, $CDCl_3$): δ 8.05 (d, 1H), 7.71 (d, 1H), 7.35 (d, 1H), 7.09 (dd, 1H), 6.44 (dd, 1H), 6.20 (d, 1H), 6.01 (s, 1H), 4.15 (m, 2H), 3.66 (m, 2H), 3.57 (m, 2H), 3.36 (q, 4H), 3.28 (s, 3H), 3.10 (m, 2H), 3.01 (m, 2H), 2.38 (m, 2H), 2.25 (m, 2H), 1.67 (m, 2H), 1.40-1.10 (m, 24H), 0.82 (t, 3H). **LCMS** (m/z): ESI, found $[M+1]^+$ 696.4 (calcd for $C_{39}H_{58}N_3O_6S^+$ 696.4).

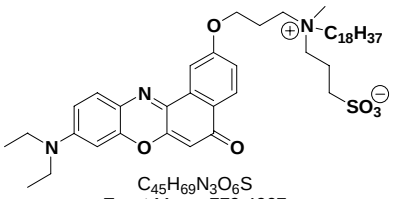

$C_{45}H_{69}N_3O_6S$
Exact Mass: 779,4907

Compound 22 (Probe 13)
N-[3-(9-Diethylamino-5-oxo-benzo[a]phenoxazin-2-yloxy)-propyl]-N-methyl-N-(3-sulfopropyl)-1-octadecanaminium, inner salt

It was synthesized according to general procedure for quaternization of amines with 1,3-propanesultone starting from 40mg of previously obtained compound **20b**. The product was purified by preparative TLC (eluent CH_2Cl_2/MeOH = 85/15). Red solid, yield 21mg (44%). **^{1}H NMR** (300MHz, $CDCl_3$): δ 8.03 (d, 1H), 7.72 (d, 1H), 7.37 (d, 1H), 7.05 (dd, 1H), 6.45 (dd, 1H), 6.22 (d, 1H), 6.03 (s, 1H), 4.16 (m, 2H), 3.74 (m, 2H), 3.58 (m, 2H), 3.36 (q, 4H), 3.21 (s, 3H), 3.05-2.80 (m, 4H), 2.40-2.15 (m, 4H), 1.69 (m, 2H), 1.35-1.10 (m, 36H), 0.83 (t, 3H). **LCMS** (m/z): MM-ES APCI, found $[M+1]^+$ 780.5 (calcd for $C_{45}H_{70}N_3O_6S^+$ 780.5).

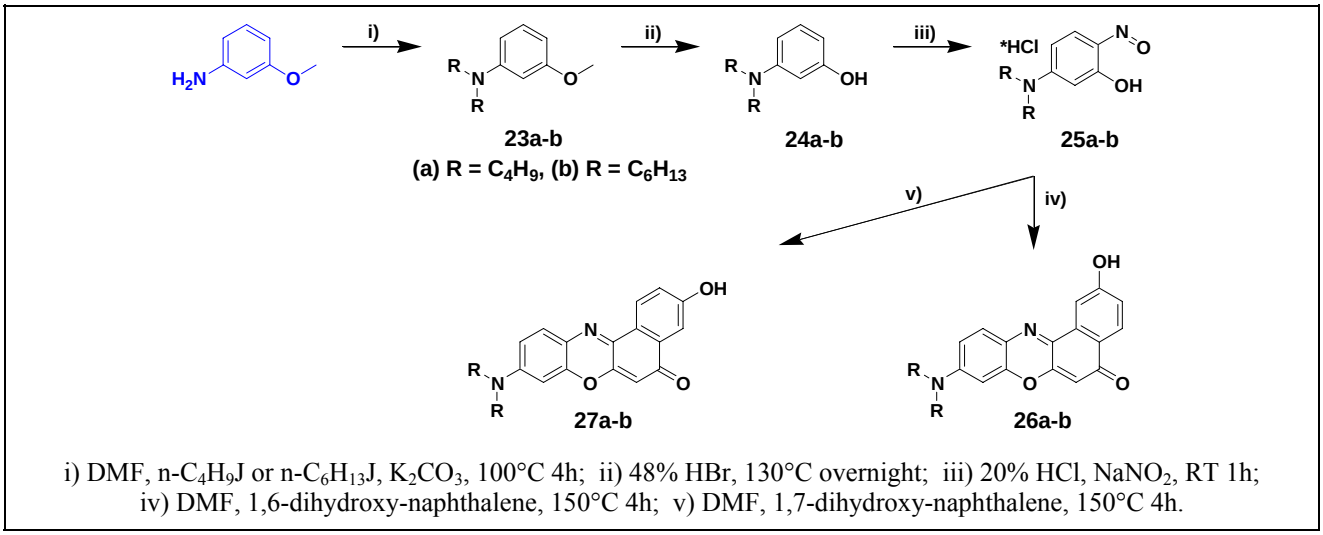

Scheme 4.7. Synthesis of 2- and 3-hydroxy Nile Red derivatives with long alkyl chains.

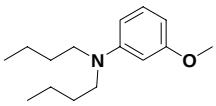

Compound 23a
Dibutyl-(3-methoxyphenyl)-amine

In a round-bottom flask 3-methoxyaniline (3.00g, 24mmol) was dissolved in 20mL of DMF. Then *n*-butyl iodide (6.17mL, 54mmol) and potassium carbonate (8.41g, 61mmol) were added. Reaction mixture was stirred upon heating at 100°C for 4h. After cooling it was poured into 200mL of water, neutralized with 10% aq. HCl and extracted with $CHCl_3$ (2 times). Combined organic layers were dried with sodium sulfate. Inorganic salt was filtered off and chloroform was removed by vacuum evaporation. Obtained dark oil was purified by column chromatography (eluent CH_2Cl_2/Heptane = 3/7) to give compound **23a** as colourless liquid. Yield 5.0g (87%). Crude product was used directly in the next step. **^{1}H NMR** (300 MHz, $CDCl_3$): δ 7.09 (t, 1H), 6.27 (dd, 1H), 6.20 (dd, 1H), 6.19 (d, 1H), 3.78 (s, 3H), 3.24 (t, 4H), 1.56 (m, 4H), 1.34 (m, 4H), 0.94 (t, 6H).

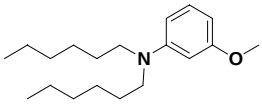

Compound 23b
Dihexyl-(3-methoxyphenyl)-amine

It was synthesized analogously to previous compound starting from 3-methoxyaniline and *n*-hexyl iodide. Colourless liquid, yield 85%. Crude product was used directly in the next step. **^{1}H NMR** (300 MHz, $CDCl_3$): δ 7.10 (t, 1H), 6.26 (dd, 1H), 6.20 (dd, 1H), 6.18 (d, 1H), 3.78 (s, 3H), 3.22 (t, 4H), 1.56 (m, 4H), 1.40-1.20 (m, 12H), 0.89 (t, 6H).

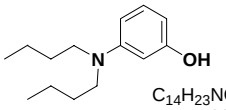

Compound 24a
3-Dibutylamino-phenol

Compound **23a** (5g, 21mmol) was treated with 48% aq. HBr (18mL). Reaction mixture was refluxed at 130°C overnight (till complete hydrolysis). Then it was cooled to RT and extracted with EtOAc (2 times). Combined organic layers were washed with saturated solution of aq. $NaHCO_3$, dried with sodium sulfate and evaporated under vacuum. Product **24a** is a white solid, which became slightly violet upon standing. Yield 4.6g (99%). Crude product was used directly in the next step. **^{1}H NMR** (300 MHz, $CDCl_3$): δ 7.10 (t, 1H), 6.50-6.30 (m, 3H), 3.24 (t, 4H), 1.56 (m, 4H), 1.31 (m, 4H), 0.90 (t, 6H). **LCMS** (m/z): MM-ES+APCI, found $[M+1]^+$ 222.2 (calcd for $C_{14}H_{24}NO^+$ 222.2).

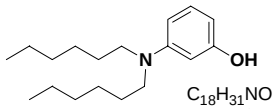

$C_{18}H_{31}NO$
Exact Mass: 277,2406

Compound 24b
3-Dihexylamino-phenol

It was synthesized analogously to previous compound starting from compound **23b**. White solid, yield 98%. Crude product was used directly in the next step. **^{1}H NMR** (300 MHz, $CDCl_3$): δ 11.67 (s, 1H), 7.49 (t, 1H), 7.31 (t, 1H), 7.13 (dd, 1H), 7.09 (dd, 1H), 3.48 (m, 2H), 3.25 (q, 2H), 1.94 (m, 2H), 1.40-1.10 (m, 14H), 0.78 (t, 6H). **LCMS** (m/z): MM-ES+APCI, found $[M+1]^+$ 278.2 (calcd for $C_{18}H_{32}NO^+$ 278.2).

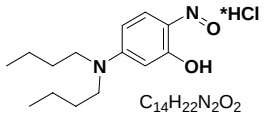

$C_{14}H_{22}N_2O_2$
Exact Mass: 250,1681

Compound 25a
5-Dibutylamino-2-nitrosophenol hydrochloride

Aminophenol **24a** (4.60g, 21mmol) was mixed with 30mL of 20% aq. HCl. Methanol was added to complete dissolution. Then aqueous solution of $NaNO_2$ (1.44g, 21mmol) was added dropwise at 0°C upon vigorous stirring. After 10-15min addition was completed, and solution became dark red. It was stirred at RT for 1h, and the formed precipitate was filtered off to give compound **25a** as orange solid, yield 5.4g (90%). After drying it was used directly in the next step. **^{1}H NMR** (300MHz, DMSO-d_6): δ double peaks 7.54 and 7.28 (d, 1H), 7.20 and 6.87 (dd, 1H), 6.65 and 5.72 (d, 1H), 3.75 (m, 4H), 1.63 (m, 4H), 1.35 (m, 4H), 0.91 (t, 6H). **LCMS** (m/z): MM-ES+APCI, found $[M+1]^+$ 251.2 (calcd for $C_{14}H_{23}N_2O_2^+$ 251.2).

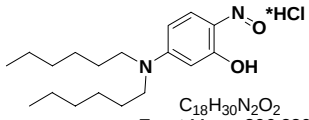

$C_{18}H_{30}N_2O_2$
Exact Mass: 306,2307

Compound 25b
5-Dihexylamino-2-nitrosophenol hydrochloride

It was synthesized analogously to previous compound starting from compound **24b**. Orange solid, yield 90%. **^{1}H NMR** (300 MHz, DMSO-d_6): δ double peaks 7.54 and 7.28 (d, 1H), 7.20 and 6.87 (dd, 1H), 6.36 and 5.70 (d, 1H), 3.75 (m, 4H), 1.63 (m, 4H), 1.45-1.20 (m, 12H), 0.86 (t, 6H). **LCMS** (m/z): MM-ES+APCI, found $[M+1]^+$ 307.2 (calcd for $C_{18}H_{31}N_2O_2^+$ 307.2).

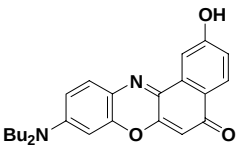

$C_{24}H_{26}N_2O_3$
Exact Mass: 390,1943

Compound 26a
9-Dibutylamino-2-hydroxy-benzo[a]phenoxazin-5-one

Hydrochloride **25a** (2.00g, 7.0mmol) and 1,6-dihydroxy-naphthalene (1.12g, 7.0mmol) were dissolved in 15mL of DMF. Reaction mixture was heated at 150°C for 4h. After cooling, DMF was removed by vacuum evaporation. Obtained residue was purified by column chromatography (eluent CH_2Cl_2/MeOH = 95/5) to give the title compound as dark green solid, yield 1.30g (48%). **^{1}H NMR** (300MHz, DMSO-d_6): δ 10.39 (s, 1H), 7.96 (d, 1H), 7.86 (d, 1H), 7.55 (d, 1H), 7.07 (dd, 1H), 6.75 (dd, 1H), 6.60 (d, 1H), 6.14 (s, 1H), 3.40 (t, 4H), 1.54 (m, 4H), 1.35 (m, 4H), 0.92 (t, 6H). **LCMS** (m/z): MM-ES+APCI, found $[M+1]^+$ 391.2 (calcd for $C_{24}H_{27}N_2O_3^+$ 391.2).

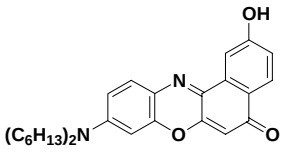

$C_{28}H_{34}N_2O_3$
Exact Mass: 446,2569

Compound 26b
9-Dihexylamino-2-hydroxy-benzo[a]phenoxazin-5-one

It was synthesized analogously to previous compound starting from compound **25b**. Dark green solid, yield 50%. **^{1}H NMR** (300MHz, DMSO-d_6): δ 10.38 (s, 1H), 7.95 (d, 1H), 7.86 (d, 1H), 7.55 (d, 1H), 7.07 (dd, 1H), 6.74 (dd, 1H), 6.56 (d, 1H), 6.13 (s, 1H), 3.40 (t, 4H), 1.54 (m, 4H), 1.40-1.20 (m, 12H), 0.86 (t, 6H). **LCMS** (m/z): MM-ES+APCI, found $[M+1]^+$ 447.2 (calcd for $C_{28}H_{35}N_2O_3^+$ 447.2).

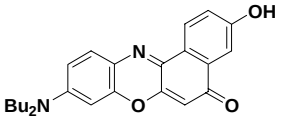

$C_{24}H_{26}N_2O_3$
Exact Mass: 390,1943

Compound 27a
9-Dibutylamino-3-hydroxy-benzo[a]phenoxazin-5-one

It was synthesized analogously to previous compound starting from 1,7-dihydroxy-naphthalene and compound **25a**. Bright red solid, yield 40%. **^{1}H NMR** (300MHz, DMSO-d_6): δ 10.35 (s, 1H), 8.40 (d, 1H), 7.58 (d, 1H), 7.44 (d, 1H), 7.20 (dd, 1H), 6.78 (dd, 1H), 6.60 (d, 1H), 6.26 (s, 1H), 3.40 (t, 4H), 1.55 (m, 4H), 1.35 (m, 4H), 0.92 (t, 6H). **LCMS** (m/z): MM-ES+APCI, found $[M+1]^+$ 391.2 (calcd for $C_{24}H_{27}N_2O_3^+$ 391.2).

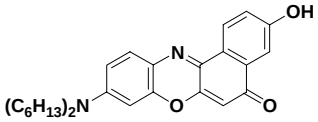

$C_{28}H_{34}N_2O_3$
Exact Mass: 446,2569

Compound 27b
9-Dihexylamino-3-hydroxy-benzo[a]phenoxazin-5-one

It was synthesized analogously to previous compound starting from 1,7-dihydroxy-naphthalene and compound **25b**. Bright red solid, yield 48%. **^{1}H NMR** (300MHz, DMSO-d_6): δ 10.35 (s, 1H), 8.40 (d, 1H), 7.57 (d, 1H), 7.44 (d, 1H), 7.20 (dd, 1H), 6.78 (dd, 1H), 6.58 (d, 1H), 6.25 (s, 1H), 3.38 (t, 4H), 1.55 (m, 4H), 1.40-1.20 (m, 12H), 0.87 (t, 6H). **LCMS** (m/z): MM-ES+APCI, found $[M+1]^+$ 447.2 (calcd for $C_{28}H_{35}N_2O_3^+$ 447.2).

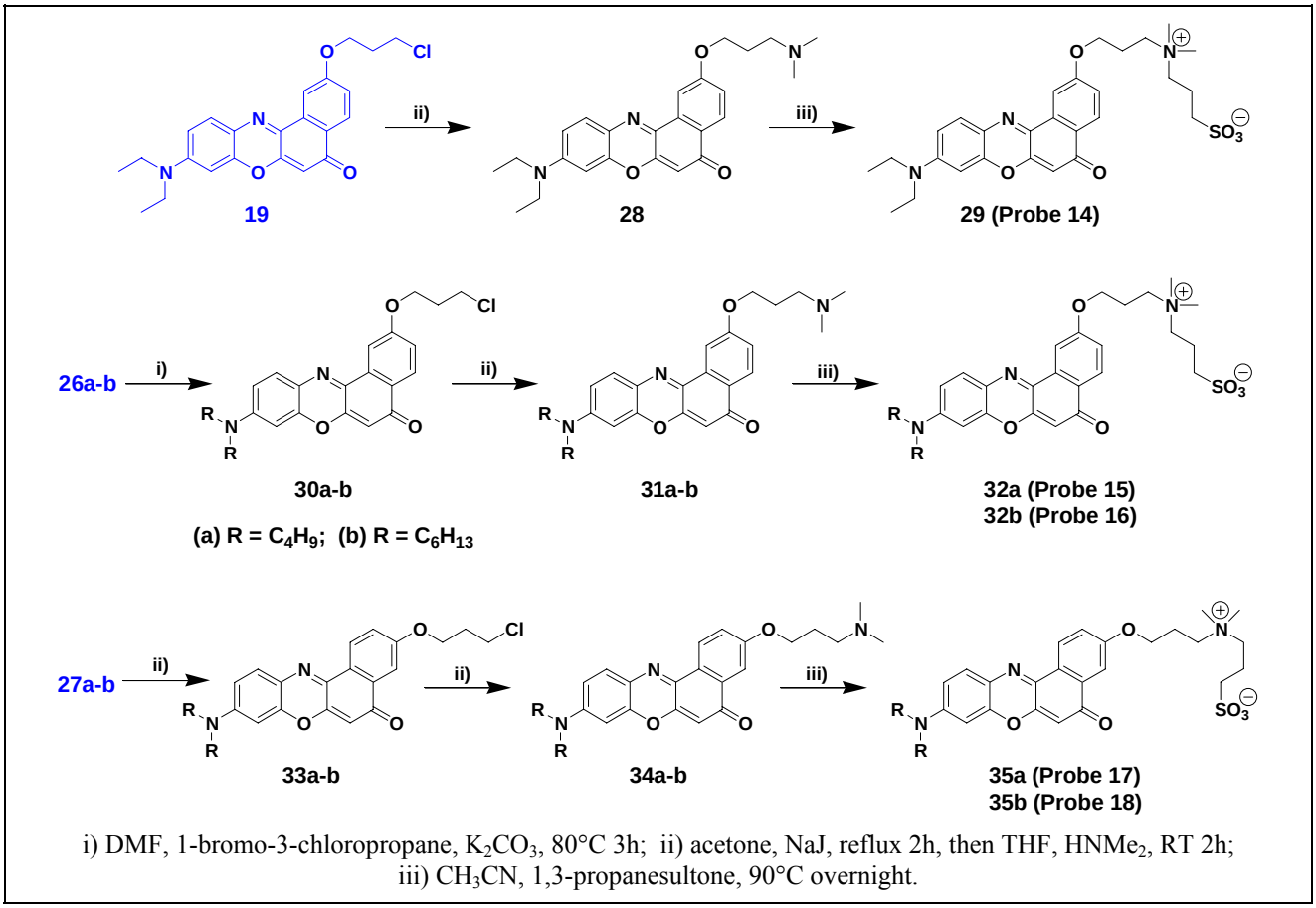

i) DMF, 1-bromo-3-chloropropane, K_2CO_3, 80°C 3h; ii) acetone, NaJ, reflux 2h, then THF, $HNMe_2$, RT 2h; iii) CH_3CN, 1,3-propanesultone, 90°C overnight.

Scheme 4.8. Synthesis of the 2nd generation of NR probes.

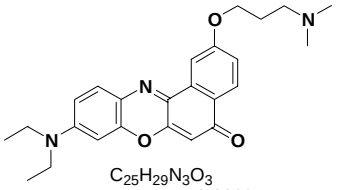

$C_{25}H_{29}N_3O_3$
Exact Mass: 419,2209

Compound 28
9-Diethylamino-2-(3-dimethylamino-propoxy)-benzo[a]phenoxazin-5-one

Compound **19** (205mg, 0.50mmol) was dissolved in small amount of acetone. Then 3mL of saturated solution of NaJ in acetone were added. Reaction mixture was boiled for 2h. Organic solvent was evaporated under vacuum. Residue was treated with $CHCl_3$ and washed with 0.5% aqueous solution of sodium dithionite. Organic layer was dried with sodium sulfate and evaporated. Crude iodo-derivative was treated with 2M solution of dimethylamine in THF (1mL, 4.0mmol). Reaction mixture was stirred at RT for 2h. Organic solvent was removed by vacuum evaporation. Residue was treated with aq. Na_2CO_3 in order to decompose ammonium salt. Free amine was extracted with $CHCl_3$ (2 times). Combined organic layers were dried with sodium sulfate. Inorganic salt was filtered off and chloroform was removed by vacuum evaporation. Obtained residue was purified by column chromatography (eluent CH_2Cl_2/MeOH = 95/5) to produce compound **28** as dark red solid, yield 100mg (48%). **^{1}H NMR** (400MHz, $CDCl_3$): δ 8.20 (d, 1H), 8.05 (d, 1H), 7.59 (d, 1H), 7.14 (dd, 1H), 6.64 (dd, 1H), 6.45 (d, 1H), 6.28 (s, 1H), 4.24 (t, 2H), 3.46 (q, 4H), 2.66 (t, 2H), 2.38 (s, 6H), 2.12 (m, 2H), 1.25 (t, 6H). **LCMS** (m/z): MM-ES+APCI, found $[M+1]^+$ 420.2 (calcd for $C_{25}H_{30}N_3O_3^+$ 420.2).

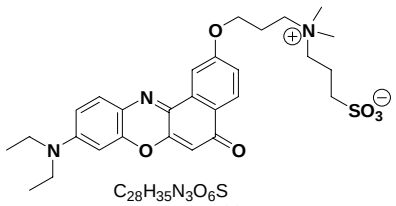

$C_{28}H_{35}N_3O_6S$
Exact Mass: 541,2247

Compound 29 (Probe 14)
N-[3-(9-Diethylamino-5-oxo-benzo[a]phenoxazin-2-yloxy)-propyl]-N,N-dimethyl-N-(3-sulfopropyl)-aminium, inner salt

It was synthesized according to general procedure for quaternization of amines with 1,3-propanesultone starting from 20mg of previously obtained compound **28**. Crude product was purified by preparative TLC (eluent CH_2Cl_2/MeOH = 7/3). Dark red solid, yield 21mg (80%). **^{1}H NMR** (400MHz, Methanol-d_4): δ 7.95 (d, 1H), 7.83 (d, 1H), 7.38 (d, 1H), 7.08 (dd, 1H), 6.68 (dd, 1H), 6.42 (d, 1H), 6.07 (s, 1H), 4.19 (t, 2H), 3.60 (m, 4H), 3.45 (m, 2H), 3.17 (s, 6H), 2.89 (t, 2H), 2.83 (m, 2H), 2.34 (m, 2H), 1.95 (m, 2H), 1.20 (t, 6H). **LCMS** (m/z): MM-ES+APCI, found $[M+1]^+$ 542.2 (calcd for $C_{28}H_{36}N_3O_6S^+$ 542.2).

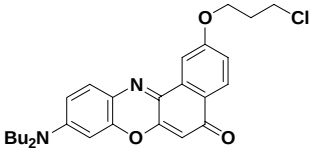

$C_{27}H_{31}ClN_2O_3$
Exact Mass: 466,2023

Compound 30a
2-(3-Chloropropoxy)-9-dibutylamino-benzo[a]phenoxazin-5-one

In a round-bottom flask 2-hydroxy-NR derivative **26a** (1.00g, 2.6mmol) was mixed with 1-bromo-3-chloropropane (0.55mL, 5.2mmol) potassium carbonate (0.71g, 5.2mmol) and 15mL of acetonitrile. Reaction mixture was stirred upon heating at 80°C for 3h. Organic solvent was removed by vacuum evaporation. Obtained residue was purified by column chromatography (eluent CH_2Cl_2/MeOH = 95/5) to give the title compound as dark green solid, yield 1.10g (92%). **^{1}H NMR** (300MHz, $CDCl_3$): δ 8.20 (d, 1H), 8.06 (d, 1H), 7.58 (d, 1H), 7.16 (dd, 1H), 6.62 (dd, 1H), 6.41 (d, 1H), 6.30 (s, 1H), 4.33 (t, 2H), 3.80 (t, 2H), 3.37 (t, 4H), 2.32 (m, 2H), 1.64 (m, 4H), 1.40 (m, 4H), 0.99 (t, 6H). **LCMS** (m/z): MM-ES+APCI, found $[M+1]^+$ 467.2 (calcd for $C_{27}H_{32}ClN_2O_3^+$ 467.2).

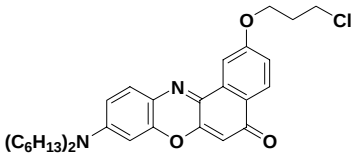

$C_{31}H_{39}ClN_2O_3$
Exact Mass: 522,2649

Compound 30b
2-(3-Chloropropoxy)-9-dihexylamino-benzo[a]phenoxazin-5-one

It was synthesized analogously to previous compound starting from compound **26b**. Dark green solid, yield 90%. **^{1}H NMR** (300 MHz, $CDCl_3$): δ 8.22 (d, 1H), 8.05 (d, 1H), 7.57 (d, 1H), 7.15 (dd, 1H), 6.61 (dd, 1H), 6.40 (d, 1H), 6.30 (s, 1H), 4.33 (t, 2H), 3.80 (t, 2H), 3.35 (t, 4H), 2.31 (m, 2H), 1.64 (m, 4H), 1.40-1.20 (m, 12H), 0.91 (t, 6H). **LCMS** (m/z): MM-ES+APCI, found $[M+1]^+$ 523.2 (calcd for $C_{31}H_{40}ClN_2O_3^+$ 523.2).

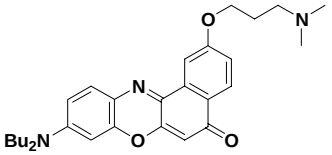

$C_{29}H_{37}N_3O_3$
Exact Mass: 475,2835

Compound 31a
9-Dibutylamino-2-(3-dimethylamino-propoxy)-benzo[a]phenoxazin-5-one

It was synthesized analogously to compound **28** starting from 3-chloropropoxy derivative **30a**. Dark red solid, yield 125mg (60%). **^{1}H NMR** (300MHz, $CDCl_3$): δ 8.20 (d, 1H), 8.06 (d, 1H), 7.58 (d, 1H), 7.16 (dd, 1H), 6.62 (dd, 1H), 6.41 (d, 1H), 6.30 (s, 1H), 4.24 (t, 2H), 3.37 (t, 4H), 2.60 (t, 2H), 2.35 (s, 6H), 2.10 (m, 2H), 1.64 (m, 4H), 1.40 (m, 4H), 0.99 (t, 6H). **LCMS** (m/z): MM-ES+APCI, found $[M+1]^+$ 476.3 (calcd for $C_{29}H_{38}N_3O_3^+$ 476.3).

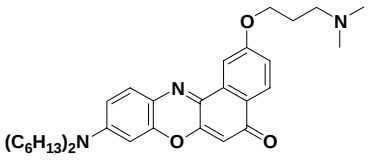

$C_{33}H_{45}N_3O_3$
Exact Mass: 531,3461

Compound 31b
9-Dihexylamino-2-(3-dimethylamino-propoxy)-benzo[a]phenoxazin-5-one

It was synthesized analogously to compound **28** starting from 3-chloropropoxy derivative **30b**. Dark red solid, yield 40%. **^{1}H NMR** (300MHz, $CDCl_3$): δ 8.22 (d, 1H), 8.06 (d, 1H), 7.58 (d, 1H), 7.16 (dd, 1H), 6.62 (dd, 1H), 6.41 (d, 1H), 6.30 (s, 1H), 4.24 (t, 2H), 3.36 (t, 4H), 2.62 (t, 2H), 2.36 (s, 6H), 2.10 (m, 2H), 1.64 (m, 4H), 1.40-1.20 (m, 12H), 0.91 (t, 6H). **LCMS** (m/z): MM-ES+APCI, found $[M+1]^+$ 532.4 (calcd for $C_{33}H_{46}N_3O_3^+$ 532.4).

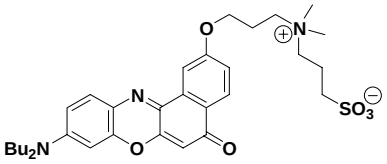

$C_{32}H_{43}N_3O_6S$
Exact Mass: 597,2873

Compound 32a (Probe 15)
N-[3-(9-Dibutylamino-5-oxo-benzo[a]phenoxazin-2-yloxy)-propyl]-N,N-dimethyl-N-(3-sulfopropyl)-aminium, inner salt

It was synthesized according to general procedure for quaternization of amines with 1,3-propanesultone starting from 20mg of previously obtained compound **31a**. Crude product was purified by preparative TLC (eluent CH_2Cl_2/MeOH = 8/2). Dark red solid, yield 18mg (71%). **^{1}H NMR** (300MHz, $CDCl_3$): δ 7.74 (d, 1H), 7.21 (s, 1H), 6.97 (d, 1H), 6.86 (d, 1H), 6.10 (d, 1H), 5.73 (s, 1H), 5.61 (s, 1H), 3.90 (m, 2H), 3.66 (m, 2H), 3.42 (t, 4H), 3.29 (s, 6H), 3.06 (m, 4H), 2.33 (m, 2H), 2.15 (m, 2H), 1.40 (m, 4H), 1.25 (m, 4H), 0.86 (t, 6H). **HRMS** (m/z): ESI, found $[M+1]^+$ 598.295 (calcd for $C_{32}H_{44}N_3O_6S^+$ 598.295).

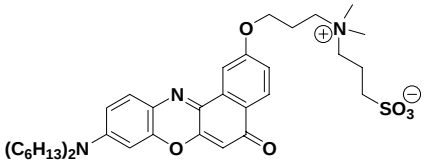

$C_{36}H_{51}N_3O_6S$
Exact Mass: 653,3499

Compound 32b (Probe 16)
N-[3-(9-Dihexylamino-5-oxo-benzo[a]phenoxazin-2-yloxy)-propyl]-N,N-dimethyl-N-(3-sulfopropyl)-aminium, inner salt

It was synthesized according to general procedure for quaternization of amines with 1,3-propanesultone starting from 20mg of previously obtained compound **31b**. Crude product was purified by preparative TLC (eluent CH_2Cl_2/MeOH = 8/2). Dark red solid, yield 20mg (80%). **^{1}H NMR** (300MHz, $CDCl_3$): δ 7.86 (d, 1H), 7.39 (s, 1H), 7.14 (d, 1H), 6.97 (d, 1H), 6.20 (d, 1H), 5.86 (s, 1H), 5.78 (s, 1H), 3.93 (m, 2H), 3.72 (m, 2H), 3.57 (t, 4H), 3.30 (s, 6H), 3.05 (m, 4H), 2.34 (m, 2H), 2.20 (m, 2H), 1.46 (m, 4H), 1.35-1.15 (m, 12H), 0.86 (t, 6H). **HRMS** (m/z): ESI, found $[M+1]^+$ 654.358 (calcd for $C_{36}H_{52}N_3O_6S^+$ 654.358).

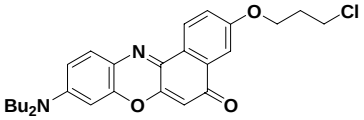

$C_{27}H_{31}ClN_2O_3$
Exact Mass: 466,2023

Compound 33a
3-(3-Chloropropoxy)-9-dibutylamino-benzo[a]phenoxazin-5-one

It was synthesized analogously to compound **30a** starting from 3-hydroxy-NR derivative **27a**. Bright red solid, yield 94%. **^{1}H NMR** (300MHz, $CDCl_3$): δ 8.57 (d, 1H), 7.74 (d, 1H), 7.58 (d, 1H), 7.26 (dd, 1H), 6.64 (dd, 1H), 6.44 (d, 1H), 6.40 (s, 1H), 4.29 (t, 2H), 3.77 (t, 2H), 3.37 (t, 4H), 2.30 (m, 2H), 1.64 (m, 4H), 1.40 (m, 4H), 0.99 (t, 6H). **LCMS** (m/z): MM-ES+APCI, found $[M+1]^+$ 467.2 (calcd for $C_{27}H_{32}ClN_2O_3^+$ 467.2).

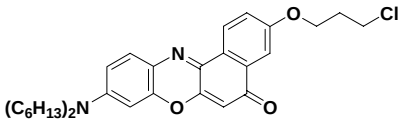

$C_{31}H_{39}ClN_2O_3$
Exact Mass: 522,2649

Compound 33b
3-(3-Chloropropoxy)-9-dihexylamino-benzo[a]phenoxazin-5-one

It was synthesized analogously to compound **30a** starting from 3-hydroxy-NR derivative **27b**. Bright red solid, yield 95%. **^{1}H NMR** (300MHz, $CDCl_3$): δ 8.57 (d, 1H), 7.74 (d, 1H), 7.58 (d, 1H), 7.26 (dd, 1H), 6.64 (dd, 1H), 6.44 (d, 1H), 6.40 (s, 1H), 4.29 (t, 2H), 3.77 (t, 2H), 3.36 (t, 4H), 2.29 (m, 2H), 1.64 (m, 4H), 1.40-1.20 (m, 12H), 0.91 (t, 6H). **LCMS** (m/z): MM-ES+APCI, found $[M+1]^+$ 523.3 (calcd for $C_{31}H_{40}ClN_2O_3^+$ 523.3).

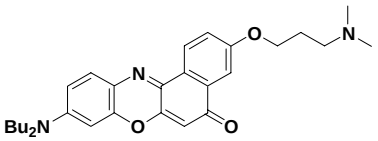

$C_{29}H_{37}N_3O_3$
Exact Mass: 475,2835

Compound 34a
9-Dibutylamino-3-(3-dimethylamino-propoxy)-benzo[a]phenoxazin-5-one

It was synthesized analogously to compound **28** starting from 3-chloropropoxy derivative **33a**. Dark red solid, yield 45%. **^{1}H NMR** (300MHz, $CDCl_3$): δ 8.57 (d, 1H), 7.72 (d, 1H), 7.58 (d, 1H), 7.26 (dd, 1H), 6.64 (dd, 1H), 6.44 (d, 1H), 6.39 (s, 1H), 4.19 (t, 2H), 3.37 (t, 4H), 2.55 (t, 2H), 2.32 (s, 6H), 2.05 (m, 2H), 1.64 (m, 4H), 1.40 (m, 4H), 0.99 (t, 6H). **LCMS** (m/z): MM-ES+APCI, found $[M+1]^+$ 476.3 (calcd for $C_{29}H_{38}N_3O_3^+$ 476.3).

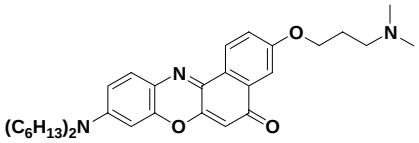

$C_{33}H_{45}N_3O_3$
Exact Mass: 531,3461

Compound 34b
9-Dihexylamino-3-(3-dimethylamino-propoxy)-benzo[a]phenoxazin-5-one

It was synthesized analogously to compound **28** starting from 3-chloropropoxy derivative **33b**. Dark red solid, yield 50%. **^{1}H NMR** (300MHz, $CDCl_3$): δ 8.57 (d, 1H), 7.72 (d, 1H), 7.58 (d, 1H), 7.26 (dd, 1H), 6.64 (dd, 1H), 6.44 (d, 1H), 6.39 (s, 1H), 4.19 (t, 2H), 3.36 (t, 4H), 2.58 (t, 2H), 2.34 (s, 6H), 2.05 (m, 2H), 1.64 (m, 4H), 1.40-1.20 (m, 12H), 0.91 (t, 6H). **LCMS** (m/z): MM-ES+APCI, found $[M+1]^+$ 532.4 (calcd for $C_{33}H_{46}N_3O_3^+$ 532.4).

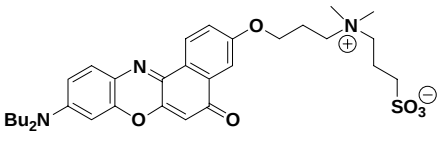

$C_{32}H_{43}N_3O_6S$
Exact Mass: 597,2873

Compound 35a (Probe 17)
N-[3-(9-Dibutylamino-5-oxo-benzo[a]phenoxazin-3-yloxy)-propyl]-N,N-dimethyl-N-(3-sulfopropyl)-aminium, inner salt

It was synthesized according to general procedure for quaternization of amines with 1,3-propanesultone starting from 20mg of previously obtained compound **34a**. Crude product was purified by preparative TLC (eluent CH_2Cl_2/MeOH = 8/2). Dark red solid, yield 18mg (71%). **^{1}H NMR** (300MHz, $CDCl_3$): δ 7.88 (d, 1H), 7.06 (s, 1H), 7.02 (d, 1H), 6.87 (d, 1H), 6.17 (d, 1H), 5.90 (s, 1H), 5.75 (s, 1H), 3.90 (m, 2H), 3.60 (m, 2H), 3.33 (t, 4H), 3.03 (m, 4H), 2.81 (s, 6H), 2.34(m, 2H), 2.20 (m, 2H), 1.43 (m, 4H), 1.25 (m, 4H), 0.89 (t, 6H). **HRMS** (m/z): ESI, found $[M+1]^+$ 598.295 (calcd for $C_{32}H_{44}N_3O_6S^+$ 598.295).

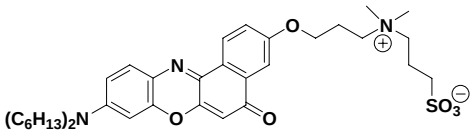

$C_{36}H_{51}N_3O_6S$
Exact Mass: 653,3499

Compound 35b (Probe 18)
N-[3-(9-Dihexylamino-5-oxo-benzo[a]phenoxazin-3-yloxy)-propyl]-N,N-dimethyl-N-(3-sulfopropyl)-aminium, inner salt

It was synthesized according to general procedure for quaternization of amines with 1,3-propanesultone starting from 20mg of previously obtained compound **34b**. Crude product was purified by preparative TLC (eluent CH_2Cl_2/MeOH = 8/2). Dark red solid, yield 20mg (80%). **^{1}H NMR** (300MHz, $CDCl_3$): δ 7.96 (d, 1H), 7.12 (m, 2H), 6.92 (d, 1H), 6.28 (d, 1H), 6.02 (s, 1H), 5.93 (s, 1H), 3.95 (m, 2H), 3.76 (m, 2H), 3.35 (t, 4H), 3.09 (m, 4H), 2.31 (m, 8H), 2.20 (m, 2H), 1.48 (m, 4H), 1.28 (m, 12H), 0.88 (t, 6H). **HRMS** (m/z): ESI, found $[M+1]^+$ 654.358 (calcd for $C_{36}H_{52}N_3O_6S^+$ 654.358).

4.1.3. Synthesis of 2-dialkylamino-7-carbonyl-fluorene dyes

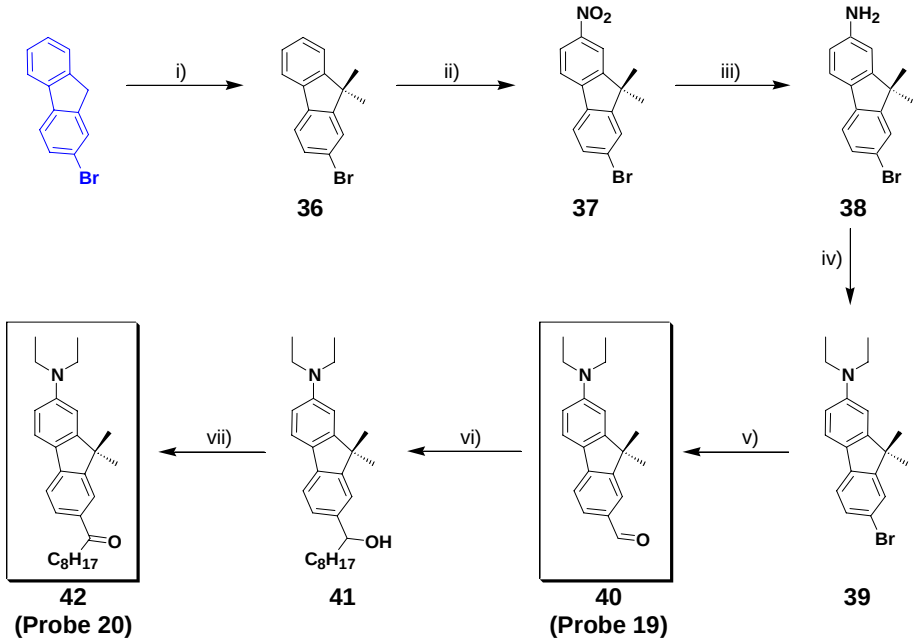

i) DMSO, MeJ, KOH and KJ, RT overnight; ii) 15% HNO_3 in acetic acid, RT 100min; iii) EtOH/H_2O, NH_4Cl, iron powder, reflux 2h; iv) DMF, EtJ, K_2CO_3, 80°C 5h; v) THF, BuLi -78°C 1h, then DMF -78°C 2h; vi) THF, octyl magnesium chloride, 0°C 1h; vii) dioxane, DDQ, RT 1h.

Scheme 4.9. Synthesis of fluorene-based solvatochromic dyes.

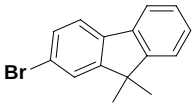

$C_{15}H_{13}Br$
Exact Mass: 272,0201

Compound 36
2-Bromo-9,9-dimethylfluorene

2-Bromofluorene (39.2g, 160.0mmol) was dissolved in 300 mL of DMSO at 60°C. Potassium iodide (2.7g, 16.0mmol) and iodomethane (51.1g, 360.0mmol) were then added; finally, powdered potassium hydroxide (36.0g, 640.0mmol) was slowly added. The mixture was stirred at room temperature overnight. Then the mixture was poured into 2000 mL of water, and a light yellow precipitate was formed. The solid was filtered, washed with water, and dried under vacuum. The light yellow solid was purified by crystallization from methanol to give product **36** as white crystals. Yield 40.3g (92%). NMR is in good correspondence with literature data (Zhan et al., 2005; Xie et al., 2006). **^{1}H NMR** (300 MHz, $CDCl_3$): δ 7.72-7.65 (m, 1H), 7.60-7.54 (m, 2H), 7.48-7.39 (m, 2H), 7.37-7.30 (m, 2H), 1.47 (s, 6H). **LCMS** (m/z): ESI, found $[M]^+$ 272.0 (calcd for $C_{15}H_{13}Br$ 272.0).

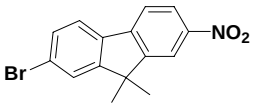

$C_{15}H_{12}BrNO_2$
Exact Mass: 317,0051

Compound 37
2-Bromo-9,9-dimethyl-7-nitrofluorene

2-Bromo-9,9-dimethylfluorene **36** (5.00g, 18.3mmol) was dissolved in 100mL of glacial acetic acid. To the formed solution, 15mL of fuming nitric acid were added dropwise at 0°C upon vigorous stirring. After addition was completed (about 10 min), reaction mixture was further stirred at RT. Reaction was monitored by TLC (eluent EtOAc/Heptane = 1/9). In 30min, yellow-green residue appeared. After appearance of the spot of dinitroproduct (~100 min, Rf ≈ 25%), the mixture was poured into 600mL of water. Formed residue was filtered off, washed with water and recrystallized from 200mL acetonitrile to give compound **37** as slightly-green needle crystals. Yield 4.2g (72%). NMR is in good correspondence with literature data (Saroja et al., 2004). **^{1}H NMR** (400 MHz, $CDCl_3$): δ 8.27-8.23 (m, 2H), 7.78 (dd, 1H), 7.65 (d, 1H), 7.62 (d, 1H), 7.53 (dd, 1H), 1.53 (s, 6H). **LCMS** (m/z): ESI, found $[M+1]^+$ 318.0 (calcd for $C_{15}H_{13}BrNO_2^+$ 318.0).

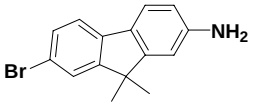

$C_{15}H_{14}BrN$
Exact Mass: 287,0310

Compound 38
7-Bromo-9,9-dimethylfluorenyl-2-amine

A mixture of nitrofluorene **37** (2.00g, 6.23mmol), iron powder (1.00g, 18.7 mmol), and NH_4Cl (740mg, 12.46 mmol) was refluxed in aqueous ethanol (90mL of alcohol and 25mL of water) at 85°C for 2h under inert atmosphere. Reaction was monitored by TLC, eluent EtOAc/Heptane = 9/1. After complete transformation of initial compound, the reaction mixture was treated with 50mL of aqueous saturated sodium bicarbonate and filtered through paper filter. Transparent solution was concentrated under reduced pressure in order to remove organic solvent. Formed residue was filtered off to yield compound **38** as transparent plates. Yield 1.72g (95%). The crude product was used directly in the next step. **^{1}H NMR** (200 MHz, $CDCl_3$): δ 7.47 (s, 1H), 7.45 (d, 1H), 7.42-7.38 (m, 2H), 6.72 (d, 1H), 6.64 (dd, 1H), 3.70 (br s, 2H), 1.42 (s, 6H). **LCMS** (m/z): ESI, found $[M+1]^+$ 288.0 (calcd for $C_{15}H_{15}BrN^+$ 288.0).

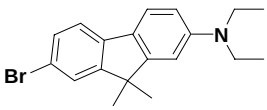

$C_{19}H_{22}BrN$
Exact Mass: 343,0936

Compound 39
(7-Bromo-9,9-dimethylfluorenyl)-2-diethylamine

To the solution of aminofluorene **38** (1.00g, 3.5mmol) in DMF, iodethane (1.37g, 8.75mmol) and K_2CO_3 (1.45g, 10.5mmol) were subsequently added. The resulting mixture was heated at 80°C for 5h. After cooling, it was poured into water, neutralized with 10% aqueous HCl and extracted with chloroform (2 times). Organic layer was dried with Na_2SO_4 and evaporated in vacuum. Residue was purified by column chromatography (eluent CH_2Cl_2/Heptane = 1/9) to obtain product **39** as a light-yellow powder. Yield 0.90g (75%). **^{1}H NMR** (200 MHz, $CDCl_3$): δ 7.55-7.30 (m, 4H), 6.70-6.60 (m, 2H), 3.41 (q, 4H), 1.44 (s, 6H), 1.20 (t, 6H). **LCMS** (m/z): ESI, found $[M+1]^+$ 344.1 (calcd for $C_{19}H_{23}BrN^+$ 344.1).

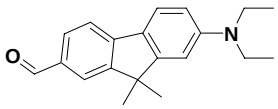

$C_{20}H_{23}NO$
Exact Mass: 293,1780

Compound 40 (Probe 19, FR0)
7-Diethylamino-9,9-dimethylfluorene-2-carbaldehyde

(7-Bromo-9,9-dimethylfluorenyl)-2-diethylamine **39** (500mg, 1.45mmol) was dissolved in dry THF. To the resulted clear yellow solution, BuLi (640µL of 2.5M solution in Hexane, 1.1eq) was added dropwise at -78°C under inert atmosphere. Reaction mixture was stirred for 1h, and yellow precipitate was formed. Then DMF (160mg, 2.18mmol, 1.5eq) was added dropwise and the formed solution was stirred for additional 2h at -78°C. Reaction mixture was allowed to heat to room temperature for 1h, quenched with 1M aqueous HCl and extracted with EtOAc (2 times). Organic layer was dried with Na_2SO_4 and evaporated in vacuum. Residue was purified by column chromatography (eluent EtOAc/Heptane = 1/9) to produce compound **40** as a yellow powder with melting point 106-107°C. Yield 256mg (60%). **^{1}H NMR** (400 MHz, $CDCl_3$): δ 9.96 (s, 1H), 7.86 (d, 1H), 7.76 (dd, 1H), 7.62 (d, 1H), 7.60 (dd, 1H), 6.72-6.64 (m, 2H), 3.45 (q, 4H), 1.48 (s, 6H), 1.22 (t, 6H). **^{13}C NMR** (100 MHz, $CDCl_3$): δ 12.59, 27.24, 44.72, 46.62, 105.14, 110.95, 118.12, 122.37, 122.46, 125.27, 131.21, 133.48, 146.90, 149.05, 153.23, 157.35, 191.97. **HRMS** (m/z): ESI, found $[M+1]^+$ 294.185 (calcd for $C_{20}H_{24}NO^+$ 294.185).

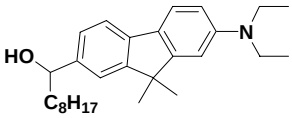

$C_{28}H_{41}NO$
Exact Mass: 407,3188

Compound 41
1-(7-Diethylamino-9,9-dimethylfluorenyl-2)-nonanol-1

Carbaldehyde **40** (50mg, 0.170mmol) was dissolved in 5mL of dry THF. To the resulted yellow solution, octyl magnesium chloride (94µL of 2M solution in THF, 1.1eq) was added dropwise at 0°C under inert atmosphere. Then, reaction mixture was stirred for 1h at RT. To decompose excess of Grignard reagent, one drop of water was added. Formed solution was concentrated in vacuum, treated with water and extracted with EtOAc (2 times). Organic layer was dried with Na_2SO_4 and evaporated in vacuum. Residue was purified by column chromatography (eluent CH_2Cl_2/Heptane = 1/1) to obtain compound **41** as a slightly-green oil. Yield 48mg (70%). **^{1}H NMR** (300 MHz, $CDCl_3$): δ 7.54 (d, 1H), 7.50 (d, 1H), 7,34 (d, 1H), 7.22 (dd, 1H), 6.73 (d, 1H), 6.66 (dd, 1H), 4.70 (t, 1H), 3.43 (q, 4H), 1.85-1.75 (m, 2H), 1.47 (s, 6H), 1.45-1.24 (m, 12H), 1.22 (t, 6H), 0.88 (t, 3H). **LCMS** (m/z): ESI, found $[M+1]^+$ 408.3 (calcd for $C_{28}H_{42}NO^+$ 408.3).

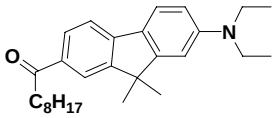

$C_{28}H_{39}NO$
Exact Mass: 405,3032

Compound 42 (Probe 20, FR8)
1-(7-Diethylamino-9,9-dimethylfluorenyl-2)-nonanon-1

Previously obtained alcool **41** (20mg, 0.049mmol) was dissolved in 1mL of dioxane. Resulted solution was added dropwise to the solution of DDQ (17mg, 0.074mmol, 1.5eq) in 1 mL dioxane. Initially, the solution turned red, and in 1h a precipitate was formed. It was filtered off and clear yellow solution was evaporated in vacuum. Residue was purified by preparative TLC (eluent EtOAc/Heptane = 1/9) to give of the desired product **42** as a yellow powder. Yield 2mg (10%). **^{1}H NMR** (300 MHz, $CDCl_3$): δ 7.96 (d, 1H), 7.89 (dd, 1H), 7,58 (d, 1H), 7.55 (dd, 1H), 6.71-6.63 (m, 2H), 3.44 (q, 4H), 2.97 (t, 2H), 1.81-1.69 (m, 2H), 1.47 (s, 6H), 1.34-1.24 (m, 10H), 1.22 (t, 6H), 0.87 (t, 3H). **HRMS** (m/z): ESI, found $[M+1]^+$ 406.310 (calcd for $C_{28}H_{40}NO^+$ 406.310).

4.1.4. Synthesis of 3-methoxychromone dyes

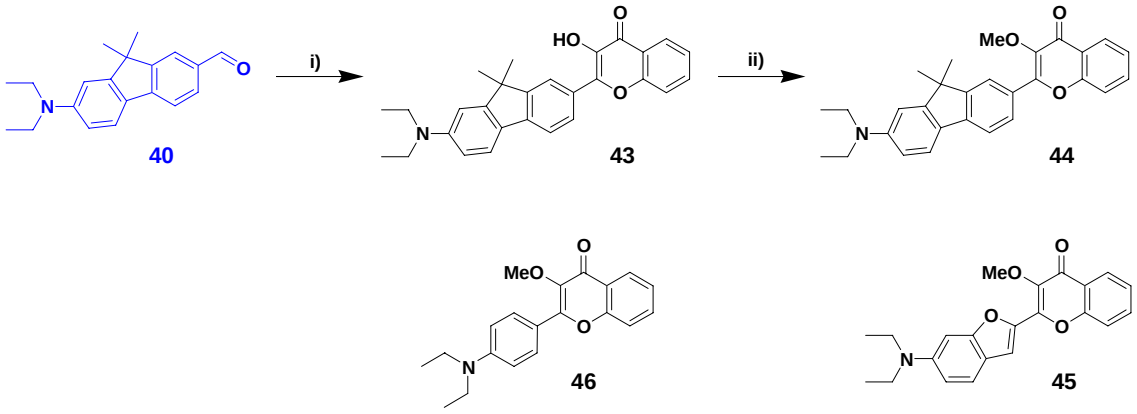

i) DMF, 2-hydroxy acetophenone, MeONa, then EtOH, 30% H_2O_2, MeONa, reflux 3min;
ii) MeOH, excess MeJ, K_2CO_3, RT 24h.

Scheme 4.10. Synthesis of 3-methoxychromone-based solvatochromic dyes.

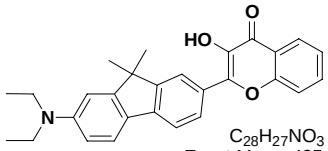

$C_{28}H_{27}NO_3$
Exact Mass: 425,1991

Compound 43
2-(7-Diethylamino-9,9-dimethylfluoren-2-yl)-3-hydroxychromone

Procedure is adapted from (Klymchenko et al., 2002a). 2-hydroxyacetophenone (31mg, 0.23mmol) was mixed with aldehyde **40** (65mg, 0.22mmol) and sodium methoxide (50mg, 0.88mmol) in 3mL of DMF. Reaction mixture became dark orange. Reaction mixture was stirred overnight at RT, and then it was diluted with 10mL of ethanol and more sodium methoxide (145mg, 2.64mmol) and 30% aqueous H_2O_2 (230µL, 2.20mmol) were added. Resulted solution was refluxed for 2-3 min, cooled and poured into 100mL of water. After neutralizing with 10% HCl the formed precipitate was filtered off and purified by preparative TLC (eluent CH_2Cl_2/Heptane = 1/1) to produce the desired chromone **43** as orange powder. Yield 30mg (32%). **^{1}H NMR** (300MHz, $CDCl_3$): δ 8.30-8.20 (m, 3H), 7.75-7.55 (m, 4H), 7.40 (t, 1H), 6.80-6.65 (m, 2H), 3.45 (q, 4H), 1.55 (s, 6H), 1.24 (t, 6H). **LCMS** (m/z): ESI, found $[M+1]^+$ 426.2 (calcd for $C_{28}H_{28}NO_3^+$ 426.2).

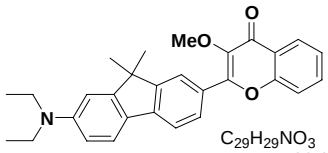

$C_{29}H_{29}NO_3$
Exact Mass: 439,2147

Compound 44
2-(7-Diethylamino-9,9-dimethylfluoren-2-yl)-3-methoxychromone

3-Hydroxychromone **43** (15mg, 0.035mmol) was mixed with an excess of methyl iodide (44µL, 0.700mmol) and potassium carbonate (10mg, 0.070mmol) in methanol. If necessary, some DMF was added to complete dissolution. Reaction mixture was stirred for 24h at RT. Organic solvent was removed under vacuum and the residue was purified by preparative TLC (eluent CH_2Cl_2/MeOH = 98/2, 2nd fraction) to give compound **44** as a yellow-orange solid, yield 12mg (77%). **^{1}H NMR** (400MHz, $CDCl_3$): δ 8.28 (dd, 1H), 8.13 (s, 1H), 8.07 (dd, 1H), 7.70-7.55 (m, 4H), 7.39 (m, 1H), 6.73 (d, 1H), 6.69 (dd, 1H), 3.91 (s, 3H), 3.45 (q, 4H), 1.53 (s, 6H), 1.23 (t, 6H). **^{13}C NMR** (100MHz, $CDCl_3$): δ 12.63, 27.40, 44.71, 46.84, 59.92, 105.37, 110.82, 117.93, 118.12, 121.82, 122.37, 124.29, 124.46, 125.77, 125.91, 126.89, 127.78, 133.15, 141.07, 143.02, 148.58, 152.70, 155.23, 156.60, 156.68, 174.95. **HRMS** (m/z): ESI, found $[M+1]^+$ 440.22 (calcd for $C_{29}H_{30}NO_3^+$ 440.22).

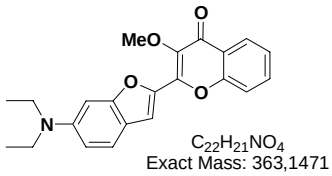

Compound 45
2-(6-Diethylaminobenzo[b]furan-2-yl)-3-methoxychromone

It was synthesized analogously to compound **44** starting from 10mg of 2-(6-diethylamino-benzo[b]furan-2-yl)-3-hydroxychromone (obtained as described by Klymchenko et al., 2003c). Orange solid, yield 6mg (58%). **^{1}H NMR** (400MHz, $CDCl_3$): δ 8.25 (dd, 1H), 7.70-7.58 (m, 3H), 7.47 (d, 1H), 7.38 (t, 1H), 6.83 (s, 1H), 6.76 (d, 1H), 4.07 (s, 3H), 3.45 (q, 4H), 1.23 (t, 6H). **HRMS** (m/z): ESI, found $[M+1]^+$ 364.15 (calcd for $C_{22}H_{22}NO_4^+$ 364.15).

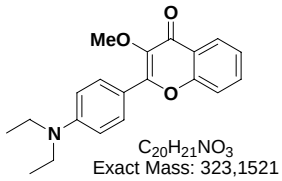

Compound 46
2-(4-Diethylaminophenyl)-3-methoxychromone

It was synthesized analogously to compound **44** starting from 15mg of 2-(diethylaminophenyl)-3-hydroxychromone (obtained as described by Chou et al., 1993). Yellow solid, yield 8mg (50%). **^{1}H NMR** (400MHz, $CDCl_3$): δ 8.25 (dd, 1H), 8.09 (d, 2H), 7.62 (m, 1H), 7.49 (d, 1H), 7.35 (t, 1H), 6.80-6.70 (br s, 2H), 3.89 (s, 3H), 3.45 (q, 4H), 1.23 (t, 6H). **HRMS** (m/z): ESI, found $[M+1]^+$ 324.16 (calcd for $C_{20}H_{22}NO_3^+$ 324.16).

4.1.5. Synthesis of fluorene-based membrane probes

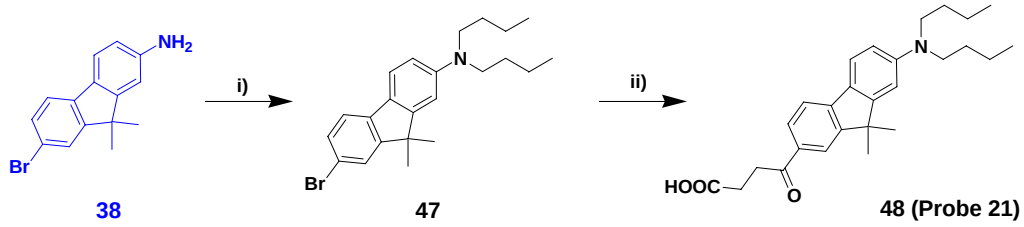

i) DMF, n-C_4H_9J, K_2CO_3, 100°C 4h; ii) THF, Mg, reflux, then succinic anhydride, 0°C 2h.

Scheme 4.11. Synthesis of fluorene-based probe **21**.

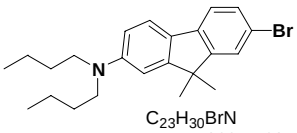

$C_{23}H_{30}BrN$
Exact Mass: 399,1562

Compound 47
7-Bromo-2-dibutylamino-9,9-dimethyl-fluorene

To the solution of aminofluorene **38** (1.00g, 3.5mmol) in DMF, *n*-butyl iodide (1.00mL, 8.7mmol) and K_2CO_3 (1.45g, 10.5mmol) were subsequently added. The resulting mixture was heated at 100°C for 4h. After cooling it was poured into water, neutralized with 10% aqueous HCl and extracted with chloroform (2 times). Combined organic layers were dried with Na_2SO_4 and evaporated under vacuum. Residue was purified by column chromatography (eluent CH_2Cl_2/Heptane = 1/9) to obtain product **47** as a light-yellow oil. Yield 1.2g (86%). **^{1}H NMR** (300MHz, $CDCl_3$): δ 7.48 (d, 1H), 7.44 (d, 1H), 7.39 (d, 1H), 7.35 (dd, 1H), 6.65 (d, 1H), 6.62 (dd, 1H), 3.33 (t, 4H), 1.61 (m, 4H), 1.44 (s, 6H), 1.40 (m, 4H), 0.98 (t, 6H). **LCMS** (m/z): MM-ES+APCI, found $[M+1]^+$ 400.2 (calcd for $C_{23}H_{31}BrN^+$ 400.2).

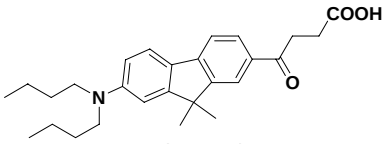

$C_{27}H_{35}NO_3$
Exact Mass: 421,2617

Compound 48 (Probe 21)
4-(7-Dibutylamino-9,9-dimethylfluoren-2-yl)-4-oxo-butyric acid

Procedure is adapted from (Kooistra et al., 2007). Grignard reagent, obtained from bromofluorene **47** (400mg, 1.00mmol) and magnesium turnings (25mg, 1.05mmol) upon heating at 50°C in dry THF, was added dropwise to the solution of succinic anhydride (200mg, 2.00mmol) in THF at -78°C under argon. After addition was completed reaction mixture was allowed to heat to room temperature and it was stirred for additional 4h. Reaction was quenched with water and extracted with chloroform (2×30mL). Combined organic layers were dried with Na_2SO_4 and evaporated under vacuum. Residue was purified by column chromatography (eluent CH_2Cl_2/MeOH = 95/5) to produce the final compound **48** as a yellow powder. Yield 150mg (36%). **^{1}H NMR** (400MHz, $CDCl_3$): δ 7.98 (d, 1H), 7.92 (dd, 1H), 7.58 (d, 1H), 7.56 (d, 1H), 6.67 (d, 1H), 6.64 (dd, 1H), 3.36 (m, 6H), 2.83 (t, 2H), 1.62 (m, 4H), 1.48 (s, 6H), 1.40 (m, 4H), 0.99 (t, 6H). **^{13}C NMR** (100MHz, $CDCl_3$): δ 13.98, 20.33, 27.28, 28.38, 29.39, 33.11, 46.67, 51.02, 105.27, 110.87, 117.74, 121.83, 122.07, 125.34, 128.13, 132.90, 145.56, 149.17, 152.76, 157.00, 197.40. **HRMS** (m/z): ESI, found $[M+1]^+$ 422.270 (calcd for $C_{27}H_{36}NO_3^+$ 422.270)

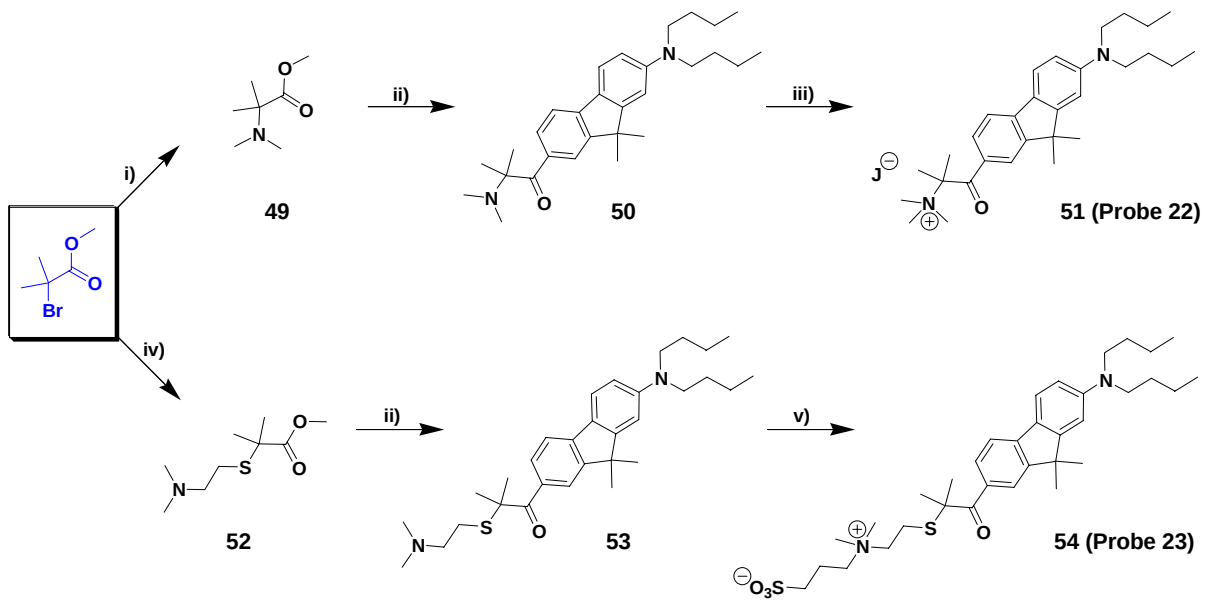

i) THF, $HNMe_2$, RT 2h; ii) THF, BuLi, compound **47**, -78°C 2h; iii) MeOH, MeJ, 60°C 24h;
iv) CH_3CN, $Me_2NCH_2CH_2SH$*HCl, K_2CO_3, 80°C 4h; v) CH_3CN, 1,3-propanesultone, 90°C overnight.

Scheme 4.12. Synthesis of probes **22** and **23**.

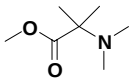

$C_7H_{15}NO_2$
Exact Mass: 145,1103

Compound 49
2-Dimethylamino-2-methyl-propionic acid methyl ester

2-Bromo-2-methyl-propionic acid methyl ester (4.00g, 22mmol) was treated with 2M solution of dimethylamine in THF (27mL, 55mmol). Reaction mixture warmed up and white residue was formed in 2min. It was stirred at RT for 2h. Organic solvent was removed by vacuum evaporation. Residue was purified by column chromatography (eluent CH_2Cl_2/MeOH = 95/5) to produce the title compound as colourless liquid, yield 1.1g (34%). **^{1}H NMR** (300MHz, $CDCl_3$): δ 3.72 (s, 3H), 2.32 (s, 6H), 1.32 (s, 6H).

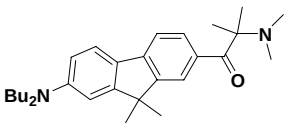

$C_{29}H_{42}N_2O$
Exact Mass: 434,3297

Compound 50
1-(7-Dibutylamino-9,9-dimethyl-fluoren-2-yl)-2-dimethylamino-2-methyl-propan-1-one

Bromofluorene **47** (200mg, 0.50mmol) was dissolved in dry THF, and butyl lithium (220µL of 2.5M solution in hexane, 0.55mmol) was added dropwise at -78°C under inert atmosphere. Reaction mixture was stirred for 1h, and then solution of previously obtained ester **49** (95mg, 0.65mmol) in THF was added dropwise. Formed solution was stirred for 2h at -78°C, and then it was allowed to heat to room temperature. After stirring for additional 1h reaction was quenched with 1M aqueous HCl (100µL). Organic layer was dried with Na_2SO_4 and evaporated under vacuum. Residue was purified by column chromatography (eluent EtOAc/Heptane = 9/1) to produce compound **50** as yellow solid, yield 50mg (23%). **^{1}H NMR** (400MHz, $CDCl_3$): δ 8.69 (d, 1H), 8.35 (s, 1H), 7.57 (d, 1H), 7.50 (d, 1H), 6.67 (d, 1H), 6.63 (dd, 1H), 3.15 (m, 4H), 2.30 (s, 6H), 1.64 (m, 4H), 1.47 (s, 6H), 1.40 (m, 4H), 1.34 (s, 6H), 0.99 (t, 6H). **LCMS** (m/z): MM-ES+APCI, found $[M+1]^+$ 435.3 (calcd for $C_{29}H_{43}N_2O^+$ 435.3).

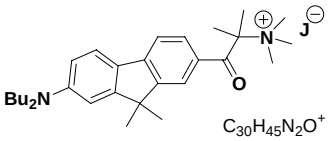

$C_{30}H_{45}N_2O^+$
Exact Mass: 449,3532

Compound 51 (Probe 22)
[2-(7-Dibutylamino-9,9-dimethyl-fluoren-2-yl)-1,1-dimethyl-2-oxo-ethyl]-trimethyl-ammonium iodide

Fluorene derivative **50** (50mg, 0.11mmol) was mixed with methyliodide (140µL, 2.20mmol) in methanol. Reaction mixture was closed with glass stopper and stirred at 60°C for 24h. Organic solvent was evaporated under vacuum, crude product was purified by preparative TLC (eluent CH_2Cl_2/MeOH = 95/5). Yellow solid, yield 20mg (30%). **^{1}H NMR** (300 MHz, $CDCl_3$): δ 7.75-7.70 (m, 2H), 7.59 (d, 1H), 7.56. (d, 1H), 6.65-6.60 (m, 2H), 3.62 (s, 9H), 3.35 (t, 4H), 2.10 (s, 6H), 1.62 (m, 4H), 1.48 (s, 6H), 1.40 (m, 4H), 0.98 (t, 6H). **HRMS** (m/z): ESI, found $[M]^+$ 449.361 (calcd for $C_{30}H_{45}N_2O^+$ 449.361).

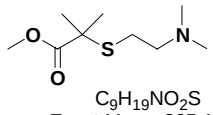

$C_9H_{19}NO_2S$
Exact Mass: 205,1136

Compound 52
2-(2-Dimethylamino-ethylsulfanyl)-2-methyl-propionic acid methyl ester

In a round-bottom flask 2-bromo-2-methyl-propionic acid methyl ester (4.00g, 22mmol) was mixed with 2-(dimethylamino)-ethanethiol hydrochloride (3.13g, 22mmol), potassium carbonate (9.15g, 66mmol) and 40mL of acetonitrile. Reaction mixture was boiled at 80°C for 4h. Organic solvent was removed by vacuum evaporation. Obtained residue was purified by column chromatography (eluent CH_2Cl_2/MeOH = 95/5) to give the title compound as a colourless liquid, yield 2.25g (50%). **^{1}H NMR** (300 MHz, $CDCl_3$): δ 3.69 (s, 3H), 2.70 (t, 2H), 2.45 (t, 2H), 2.21 (s, 6H), 1.49 (s, 6H). **LCMS** (m/z): MM-ES+APCI, found $[M+1]^+$ 206.1 (calcd for $C_9H_{20}NO_2S^+$ 206.1).

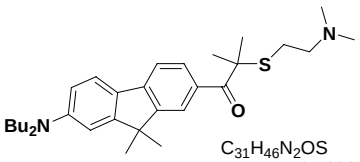

$C_{31}H_{46}N_2OS$
Exact Mass: 494,3331

Compound 53
1-(7-Dibutylamino-9,9-dimethyl-fluoren-2-yl)-2-(2-dimethylamino-ethylsulfanyl)-2-methyl-propan-1-one

It was synthesized analogously to compound **50** starting from bromofluorene **47** and ester **52**. The product was purified by preparative TLC (eluent CH_2Cl_2/MeOH = 9/1).Yellow solid, yield 45%. **^{1}H NMR** (300 MHz, $CDCl_3$): δ 8.23 (dd, 1H), 8.14 (d, 1H), 7.55 (d, 1H), 7.48 (d, 1H), 6.65 (d, 1H), 6.62 (dd, 1H), 3.34 (t, 4H), 2.62 (t, 2H), 2.47 (t, 2H), 2.19 (s, 6H), 1.62 (m, 10H), 1.46 (s, 6H), 1.38 (m, 4H), 0.97 (t, 6H). **LCMS** (m/z): MM-ES+APCI, found $[M+1]^+$ 495.3 (calcd for $C_{31}H_{47}N_2OS^+$ 495.3).

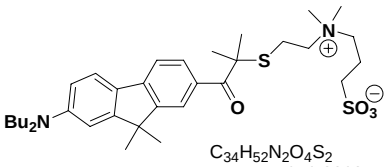

$C_{34}H_{52}N_2O_4S_2$
Exact Mass: 616,3368

Compound 54 (Probe 23)
N-{2-[2-(7-Dibutylamino-9,9-dimethyl-fluoren-2-yl)-1,1-dimethyl-2-oxo-ethylsulfanyl]-ethyl}-N,N-dimethyl-N-(3-sulfopropyl)-aminium, inner salt

It was synthesized according to general procedure for quaternization of amines with 1,3-propanesultone starting from 40mg of previously obtained compound **53**. The product was purified by preparative TLC (eluent CH_2Cl_2/MeOH = 85/15). Yellow solid, yield 40mg (80%). **^{1}H NMR** (300 MHz, $CDCl_3$): δ 8.05 (dd, 1H), 7.92 (d, 1H), 7.50 (d, 1H), 7.45 (d, 1H), 6.62 (s, 1H), 6.58 (d, 1H), 3.55 (t, 2H), 3.45-3.25 (m, 6H), 3.11 (s, 6H), 2.93 (m, 2H), 2.87 (m, 2H), 2.13 (m, 2H), 1.58 (m, 10H), 1.42 (s, 6H), 1.35 (m, 4H), 0.95 (t, 6H). **HRMS** (m/z): ESI, found $[M+1]^+$ 617.345 (calcd for $C_{34}H_{53}N_2O_4S_2^+$ 617.345).

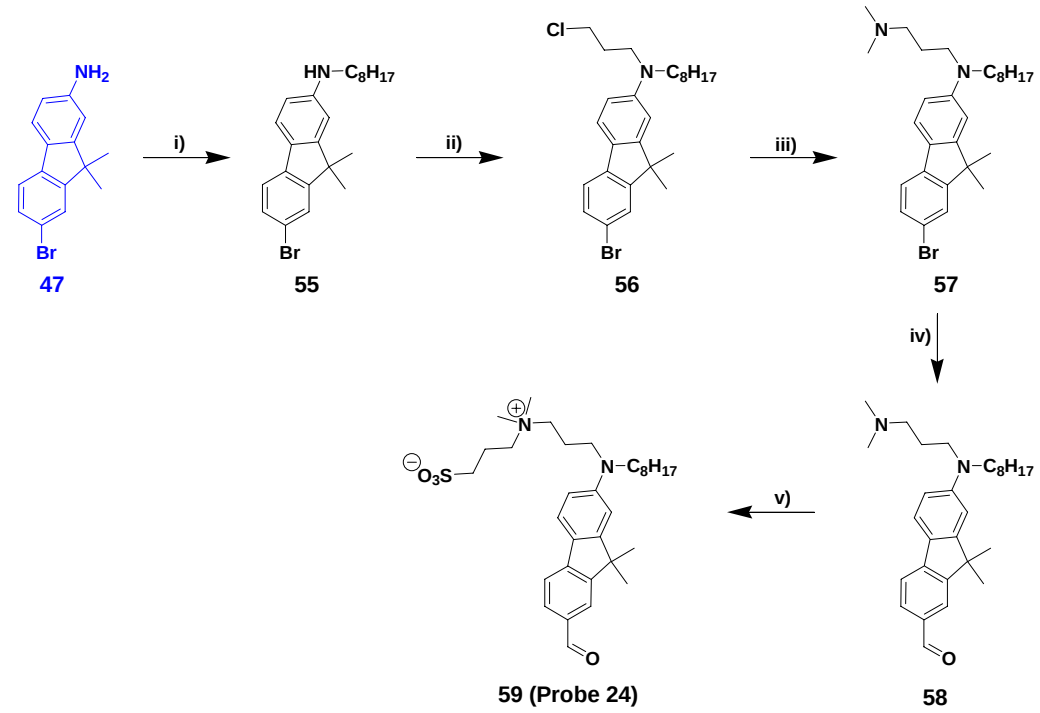

i) DMF, n-$C_8H_{17}J$, K_2CO_3, 100°C 4h; ii) DMF, 1-bromo-3-chloro-propane, K_2CO_3, 100°C 4h; iii) acetone, NaJ, RT 2h, then THF, $HNMe_2$, RT 2h; iv) THF, BuLi, -78°C, then DMF, -78°C 2h; v) CH_3CN, 1,3-propanesultone, 90°C overnight.

Scheme 4.13. Synthesis of probe **24**.

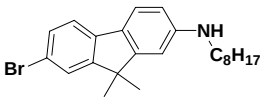

$C_{23}H_{30}BrN$
Exact Mass: 399,1562

Compound 55
2-Bromo-7-octylamino-9,9-dimethyl-fluorene

Aminofluorene **38** (1.00g, 3.5mmol), *n*-octyl iodide (630µL, 3.5mmol) and K_2CO_3 (0.96g, 7mmol) mixed together in DMF. The resulting mixture was heated at 80°C for 4h. After cooling, it was poured into water, neutralized with 10% aqueous HCl and extracted with chloroform (2 times). Combined organic layers were dried with Na_2SO_4 and evaporated under vacuum. Residue was purified by column chromatography (eluent CH_2Cl_2/Heptane = 1/1) to obtain product **55** as a white solid. Yield 0.77g (56%). **^{1}H NMR** (300MHz, $CDCl_3$): δ 7.47 (d, 1H), 7.45 (d, 1H), 7.40 (d, 1H), 7.36 (dd, 1H), 6.66 (d, 1H), 6.60 (dd, 1H), 3.16 (t, 2H), 1.66 (m, 2H), 1.42 (s, 6H), 1.40-1.20 (m, 10H), 0.88 (t, 3H). **LCMS** (m/z): MM-ES+APCI, found $[M+1]^+$ 400.2 (calcd for $C_{23}H_{31}BrN^+$ 400.2).

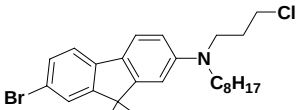

$C_{26}H_{35}BrClN$
Exact Mass: 475,1641

Compound 56
2-Bromo-7-[(3-chloropropyl)-octylamino]-9,9-dimethyl-fluorene

Previously obtained compound **55** (0.77g, 2.0mmol), 1-bromo-3-chloropropane (1.10mL, 10.0mmol) and K_2CO_3 (0.55g, 4.0mmol) were mixed together in DMF. The resulting mixture was heated at 100°C for 4h. After cooling, it was poured into water, neutralized with 10% aqueous HCl and extracted with chloroform (2 times). Combined organic layers were dried with Na_2SO_4 and evaporated under vacuum. Residue was purified by column chromatography (eluent CH_2Cl_2/Heptane = 1/1) to obtain product **56** as a white solid. Yield 0.40g (43%). **^{1}H NMR** (400MHz, $CDCl_3$): δ 7.50 (d, 1H), 7.45 (d, 1H), 7.40 (d, 1H), 7.36 (dd, 1H), 6.71 (d, 1H), 6.64 (dd,

1H), 3.63 (t, 1H), 3.54 (t, 2H), 3.32 (m, 3H), 2.09 (m, 2H), 1.62 (m, 2H), 1.43 (s, 6H), 1.40-1.20 (m, 10H), 0.88 (t, 3H). **HRMS** (m/z): ESI, found $[M+1]^+$ 476.17 (calcd for $C_{26}H_{36}BrClN^+$ 476.17).

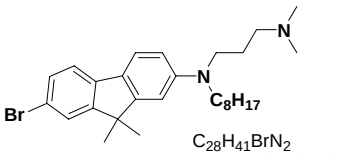

$C_{28}H_{41}BrN_2$
Exact Mass: 484,2453

Compound 57
2-Bromo-7-[(3-dimethylamino-propyl)-octylamino]-9,9-dimethyl-fluorene

Compound **56** (400mg, 0.84mmol) was dissolved in small amount of acetone. Then 5mL of saturated solution of NaJ in acetone were added. After 2 min of stirring white precipitate of NaCl has appeared. Stirring was continued at RT 2h. Inorganic salt was filtered off and resulted solution was evaporated under vacuum. Crude iodo-derivative was treated with 2M solution of dimethylamine in THF (1mL, 2.10mmol). Reaction mixture was stirred at RT for 2h. Organic solvent was removed by vacuum evaporation. Residue was treated with aq. Na_2CO_3 in order to decompose ammonium salt. Free amine was extracted with $CHCl_3$ (2 times). Combined organic layers were dried with sodium sulfate. Inorganic salt was filtered off and chloroform was removed by vacuum evaporation. Obtained residue was purified by column chromatography (eluent CH_2Cl_2/MeOH = 95/5) to produce compound **57** as white solid. Yield 220mg (54%). **^{1}H NMR** (300MHz, CDCl3): δ 7.48 (d, 1H), 7.44 (s, 1H), 7.38 (d, 1H), 7.35 (d, 1H), 6.66 (d, 1H), 6.62 (dd, 1H), 3.39 (t, 2H), 3.32 (t, 2H), 2.39 (t, 2H), 2.29 (s, 6H), 1.82 (m, 2H), 1.61 (m, 2H), 1.43 (s, 6H), 1.40-1.20 (m, 10H), 0.88 (t, 3H). **HRMS** (m/z): ESI, found $[M+1]^+$ 485.25 (calcd for $C_{28}H_{42}BrN_2^+$ 485.25).

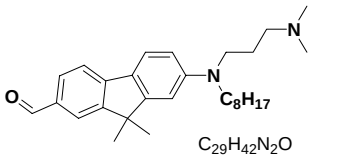

$C_{29}H_{42}N_2O$
Exact Mass: 434,3297

Compound 58
2-Formyl-7-[(3-dimethylamino-propyl)-octylamino]-9,9-dimethyl-fluorene

Compound **57** (220mg, 0.45mmol) was dissolved in dry THF. To the resulted clear yellow solution, BuLi (400µL of 2.5M solution in Hexane, 1.00mmol) was added dropwise at -78°C under inert atmosphere. Reaction mixture was stirred for 1h and yellow precipitate was formed. Then DMF (100µL, 1.35mmol) was added dropwise and the formed solution was allowed to heat to room temperature. Then reaction mixture was stirred at 40°C for 2h, quenched with 1M aqueous HCl and extracted with EtOAc (2 times). Organic layer was dried with Na_2SO_4 and evaporated under vacuum. Residue was purified by column chromatography (eluent CH_2Cl_2/MeOH = 9/1) to produce compound **58** as a yellow powder. Yield 100mg (51%). **^{1}H NMR** (300MHz, $CDCl_3$): δ 9.96 (s, 1H), 7.86 (d, 1H), 7.76 (dd, 1H), 7.62 (d, 1H), 7.60 (d, 1H), 6.68 (s, 1H), 6.65 (d, 1H), 3.43 (t, 2H), 3.35 (t, 2H), 2.43 (t, 2H), 2.31 (s, 6H), 1.84 (m, 2H), 1.62 (m, 2H), 1.47 (s, 6H), 1.40-1.20 (m, 10H), 0.88 (t, 3H). **HRMS** (m/z): ESI, found $[M+1]^+$ 435.338 (calcd for $C_{29}H_{43}N_2O^+$ 435.338).

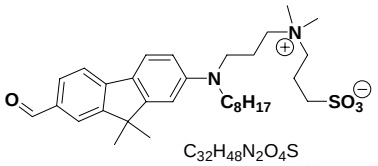

$C_{32}H_{48}N_2O_4S$
Exact Mass: 556,3335

Compound 59 (Probe 24)
N-{3-[(7-Formyl-9,9-dimethyl-fluoren-2-yl)-octylamino]-propyl}-N,N-dimethyl-N-(3-sulfopropyl)-aminium, inner salt

It was synthesized according to general procedure for quaternization of amines with 1,3-propanesultone starting from 40mg of previously obtained compound **58**. The product was purified by preparative TLC (eluent CH_2Cl_2/MeOH = 85/15). Yellow solid, yield 46mg (90%). **^{1}H NMR** (300MHz, $CDCl_3$): δ 9.90 (s, 1H), 7.81 (s, 1H), 7.69 (d, 1H), 7.57 (d, 2H), 6.69 (s, 1H), 6.65 (d, 1H), 3.63 (m, 2H), 3.44 (m, 4H), 3.28 (m, 2H), 3.14 (s, 6H), 2.91 (m, 2H), 2.25 (m, 2H), 2.00 (m, 2H), 1.52 (m, 2H), 1.42 (s, 6H), 1.30-1.10 (m, 10H), 0.83 (t, 3H). **HRMS** (m/z): ESI, found $[M+1]^+$ 557.341 (calcd for $C_{32}H_{49}N_2O_4S^+$ 557.341).

4.2. Physical measurements

Fluorescence spectroscopy

Absorption spectra were recorded on a Cary 4 spectrophotometer (Varian) and fluorescence spectra measurements were performed on a spectrofluorometer FluoroMax 3.0 or Fluorolog (Jobin Yvon, Horiba) equipped with a thermostated cuvette holder. The solvents were of spectroscopic grade. Fluorescence emission spectra were systematically recorded at 20°C using the following excitation wavelengths: 400nm for all flavone probes and fluorene probes, and 520nm for all Nile Red probes. For spectroscopic measurements 1μM solutions of dyes were used. All the spectra were corrected from the fluorescence of the corresponding blank solution (neat solvent, cells suspension or lipid vesicles without the probe). The following equation was used for calculation of fluorescence quantum yield (QY):

$$(QY_x) = (QY_r)\frac{I_x A_r}{I_r A_x}\frac{n_x^2}{n_r^2}$$

where QY_x is the quantum yield of the dye; QY_r is the known quantum yield of the reference dye; A_x and A_r are respectively the absorbance of the dye and the reference at an appropriate excitation wavelength; I_x and I_r are their respective fluorescence intensities as measured by integration of the surface under the emission spectrum corrected for the photomultiplier response; n_x and n_r are the refractive indexes of their respective solvents.

We used the following solutions as standards for fluorescence quantum yield calculations:

for 3HF dyes	4'-diethylamino-3-hydroxyflavone in EtOH, QY = 52% (Chou et al., 1993b);
for NR dyes	Nile Red in methanol, QY = 38% (La Deda et al., 2005);
for fluorene dyes	Prodan in EtOH, QY = 71% (Davis and Abelt 2005; Lu et al., 2006).

Fluorescence microscopy

Fluorescence microscopy experiments were performed by using a home-built two-photon laser scanning setup based on an Olympus IX70 inverted microscope with an Olympus 60x1.2NA water immersion objective (Clamme et al., 2003; Azoulay et al., 2003). Two-photon excitation was provided by a titanium-sapphire laser (Tsunami, Spectra Physics), and photons were detected with Avalanche Photodiodes (APD SPCM-AQR-14-FC, Perkin-Elmer) connected to a counter/timer PCI board (PCI6602, National Instrument). Imaging was carried out using two fast galvo mirrors in the descanned fluorescence collection mode. Typical acquisition time was 20 ms with an excitation power around 20 mW at the sample level. Images corresponding to the green and red channels were recorded simultaneously using a dichroic mirror. The images were processed with a homemade program under LabView that generates a ratiometric image by dividing the image of the green channel by that of the red channel. For each pixel a pseudocolor scale was used for coding the ratio while the intensity was defined by the integral intensity recorded for both channels at the corresponding pixel (Klymchenko et al., 2009).

4.3. Preparation of lipid vesicles

Large unilamellar vesicles (LUVs) were obtained by the classical extrusion method (Hope et al., 1985) using a Lipex Biomembranes extruder (Vancouver, Canada). All phospholipids and sterols were from Sigma-Aldrich or Avanti and used without further purification. Properties of vesicles can vary depending on their composition (cationic, anionic, neutral lipid species). However, the same preparation method can be used for all lipid vesicles regardless of their composition. The general steps of the procedure involve: (a) preparation of the lipid films, (b) hydration with agitation and (c) sizing to a homogeneous vesicles.

When preparing liposomes with single or mixed lipid compositions, the lipids must first be dissolved in an organic solvent to ensure their homogeneous distribution. Usually this process is carried out using chloroform or chloroform/methanol mixture. The solvent is then removed by rotary evaporation yielding a thin lipid film on the wall of a round bottom flask. The lipid film is thoroughly dried to remove the residual organic solvent by continuing evaporation with gentle heating (about 35°C) during 30 minutes.

Hydration of the dry lipid film is accomplished simply by adding corresponding buffer to the flask, and the obtained solution is left at the temperature about Tm of corresponding lipid (RT for unsaturated lipids and 55°C for lipids with saturated alkyl chains). Typically, lipid solutions are prepared with the final concentration of 0.2 mM, although higher concentrations may be used. After hydration the solution is vortexed during 2 minutes affording a suspension of multilamellar vesicles with a heterogeneous size distribution.

Once a suspension has been produced, the particles are downsized by extrusion. Lipid extrusion is a technique in which a lipid suspension is forced through a polycarbonate filter with a defined pore size to yield particles having a diameter near the pore size. An extruder (Lipex Biomembranes Inc) with polycarbonate filters of calibrated pores (Nucleopore) is used. Prior to extrusion through the final pore size, the lipid suspension is first downsized by passing through a large pore size (0.2 μm) filter seven times. Then the suspension is passed through the filter with the final pore size (0.1 μm) ten times. This final extrusion through filters with 0.1 μm pores yields large unilamellar vesicles (LUV) with a mean diameter of 110-120 nm. This method ensures a homogeneous size distribution of the final suspension. All preparation steps including hydration, vortexing and the extrusion should be done at a temperature that is higher than the temperature of the gel-liquid crystal transition (Tm) of the lipid. In simple words, heating at 55°C is needed in the case of lipids like DPPC or sphingomyelin, which bear saturated alkyl chains.

Staining. LUVs were labelled by adding aliquots (generally 2μL) of probe stock solution (0.3mM in DMSO) to 1mL of vesicle suspension in buffer. Since all the probes were new molecules, the fluorescence experiments were performed at different incubation times (3, 5, 7 and 30 min) and the optimal conditions were found for each dye. A 20 mM phosphate buffer with pH 7.4 was used in all experiments. Concentrations of the probes and lipids were 1 μM and 200 μM respectively unless indicated.

4.4. Cell preparation

Cell line

For cellular studies we used U87MG human glioblastoma cell line (ATCC). Cells were cultured in Eagle's minimal essential medium (EMEM from LONZA) with 10 % heat-inactivated Fetal bovine serum and 0.6 mg/mL glutamine (Biowhittaker) at 37°C in a humidified 5 % CO_2 atmosphere. Antibiotics were not used because they influence membrane properties. Cell concentration of 5-10×10^4 cells/mL was maintained by removal of a portion of the culture and replacement with fresh medium 2 times per week.

For experiments the cells were counted with a hemacytometer and seeded at a suitable density for spectroscopy and microscopy studies (3×10^5 cells per well in six-well plate and 5×10^5 cells per well in IBIDI LabTek respectively). Culture medium was changed every day and cells were grown during 3 days. Then apoptosis was induced by 18 h incubation of cells with actinomycin D (0.5 μg/ml). For cholesterol extraction, MβCD stock solutions were prepared with DPBS and filtered by a Millipore filter (0.22 μm). The initial cell number was the same as for apoptosis induction. The following MβCD concentrations and incubation times were used: 5mM solution for 2h, 5mM solution for 30 min and 2mM MβCD for 15h. For cholesterol addition, stock solutions of water soluble Cholesterol was prepared with DPBS and filtered by a Millipore filter (0.22 μm).

Samples for fluorescence spectroscopy

After 3 days of growing the sufficient cell number was obtained. They were trypsinized, washed and stained with a fluorescent probe as described below. Firstly, EMEM medium was removed from culture dishes and cells were washed two times with dPBS. Then, trypsin 1x was added to cover the bottom of the culture vessel. Cells were incubated at 37°C for 4 min. Then the cell suspension was diluted by dPBS, transferred to Falcon tube and centrifuged at 1500 RPM for 8 min. Obtained precipitate was decanted to remove traces of trypsin. Cells were mixed with HBSS solution and were gently shaked to remove aggregates. Further, cells were counted and the number of 5×10^5-10^6 cells was transferred into cuvettes (total volume up to 500 μL). To stain the cell suspension with the probe, a freshly prepared solution of probe in HBSS was used. For this purpose, an appropriate aliquot of 0.1 mM probe stock solution in DMSO was added to 500 μL of HBSS. After vortexing it was immediately added to the cell suspension in cuvette (resulting in final solution volume of 1 mL). It should be noted that only a freshly prepared solution of the probe in HBSS should be used (<1min) for cell staining, due to the aggregation of the probe in water. Final probe concentration was 0.1 μM (<0.25 % DMSO). Prior to the measurements, the stained cells were incubated for 7 min at room temperature in the darkness. Finally, blank sample (without probe) and stained samples (with probe) were measured.

Samples for fluorescence microscopy

For microscopy studies, 3×10^5 of cells were started in IBIDI dishes and the medium was changed every day. After 3 days of growing around one million cells in the dish was obteined. For apoptosis and for cholesterol extraction experiments more cells were started (5×10^5), because during washing step some of them were lost. The calculated volume of the effector was added and cells were incubated for a necessary time. After that EMEM medium was removed from culture dishes and attached cells were washed twice by gentle rinsing with HBSS. Further, a freshly prepared solution of probe in HBSS was added to the cells. Final concentration of the probe was 0.3 μM (<0.25% DMSO volume). After incubation for 7 min at room temperature in the darkness the sample was ready for image acquisition.

List of solutions and reagents used for cell work.

1.	DMSO (Fluka)	41639 ultra for molecular biology; stored at + 4°C.
2.	DPBS (Lonza)	Dulbecco's phosphate buffered saline without Ca^{2+} and Mg^{2+}. Was used directly as it was bought; stored at + 4°C.
3.	EMEM (Lonza)	Eagle's minimal essential medium with earle's balanced salt solution without L-glutamine. Before use, into freshly opened bottle of EMEM the Ultraglutamine (5 mL) were added in order to get 1 % solution of Ultraglutamine; stored at + 4°C.
4.	Fetal Bovine Serum (PAN Biotech GmbH)	Before use inactivation was done by heating at 60°C for 40 min; stored at + 4°C.
5.	HBSS (Sigma)	Hanks' balanced salt solution with $NaHCO_3$, without Phenol red, calcium chloride and magnesium sulphate. Was used directly as it was bought; stored at + 4°C.
6.	Trypsin (Lonza)	Usually 1x solution was used, so it was diluted with DPBS to reach 1x concentration (10 mL of Trypsin and 90 mL of DPBS); stored at + 4°C.
7.	Ultraglutamine (Biowhittaker)	Was used directly as it was bought; stored at + 4°C.
8.	Actinomycin D (Sigma)	Yellow powder, it was dissolved in DMSO to get 0.25 mg/mL concentration. For apoptosis induction in cells 0.5 µg/mL was used; stored at -20°C.
9.	Methyl-β-cyclodextrin, MβCD (Aldrich)	White solid, it was dissolved in DPBS to get 0.05 M solution (65mg of MβCD [M=1310 g/mol] in 1 mL of DPBS). Before use sterilisation was done by filtration with Millipore filter (0.22µm). Freshly prepared solution was stored at + 4°C.
10.	Cholesterol water soluble (Aldrich)	White solid, it was dissolved in DPBS to get 0.05 M solution (69mg of Cholesterol [M=1374.5 g/mol] in 1 mL of DPBS). Before use sterilisation was done by filtration with Millipore filter (0.22µm). Freshly prepared solution can be stored at + 4°C.

CHAPTER 5

REFERENCES

5. REFERENCES

1) Akimov, S., E. Hlaponin, P. Bashkirov, I. Boldyrev, I. Mikhalyov, W. Telford and I. Molotkovskaya (2009). Ganglioside GM1 increases line tension at raft boundary in model membranes. Biochemistry (Moscow) Suppl Series A: Membr Cell Biol **3**(2), 216-222.

2) Alberts, B., A. Johnson, J. Lewis, M. Raff, K. Roberts and P. Walter (2002). Molecular Biology of the Cell. New York, Garland Science.

3) Ameer-Beg, S., S. M. Ormson, P. Matousek, M. Towrie, E. T. J. Nibbering, P. Foggi, F. V. R. Neuwahl and R. G. Brown (2001). Ultrafast measurements of excited state intramolecular proton transfer (ESIPT) in room temperature solutions of 3hydroxyflavone and derivatives. J Phys Chem **105**, 3709-3718.

4) Andree, H. A., C. P. Reutelingsperger, R. Hauptmann, H. C. Hemker, W. T. Hermens and G. M. Willems (1990). Binding of vascular anticoagulant alpha (VAC alpha) to planar phospholipid bilayers. J Biol Chem **265**(9), 4923-8.

5) Azoulay, J., J. Clamme, J. Darlix, B. Roques and Y. Mely (2003). Destabilization of the HIV-1 complementary sequence of TAR by the nucleocapsid protein through activation of conformational fluctuations. J Mol Biol **326**(3), 691-700.

6) Bagatolli, L. A. (2006). To see or not to see: Lateral organization of biological membranes and fluorescence microscopy. Biochim Biophys Acta **1758**(10), 1541-1556.

7) Bagatolli, L. (2007). Membranes and fluorescence microscopy in Reviews in Fluorescence C.D. Geddes (ed.), Springer science, 33-51.

8) Balasubramanian, K., E. M. Bevers, G. M. Willems and A. J. Schroit (2001). Binding of annexin V to membrane products of lipid peroxidation. Biochemistry **40**(30), 8672-6.

9) Bartucci, R., R. Guzzi, D. Marsh and L. Sportelli (2003). Intramembrane polarity by electron spin echo spectroscopy of labeled lipids. Biophys J **84**, 1025-30.

10) Becker, R. S., C. Lenoble and A. Zein (1987). Photophysics and photochemistry of the nitro derivatives of salicylidenaniline and 2-(2-hydroxyphenyl)benzothiazole. Chem Phys Lett **91**, 3517-3524.

11) Bedlack, R. S., Jr., M. Wei and L. M. Loew (1992). Localized membrane depolarizations and localized calcium influx during electric field-guided neurite growth. Neuron **9**(3), 393-403.

12) Bernal, J. D. (1933). Liquid crystals and anisotropic melts. A general discussion. Trans Faraday Soc **29**, 1082.

13) Bevers, E. M., P. Comfurius, J. L. van Rijn, H. C. Hemker and R. F. Zwaal (1982). Generation of prothrombin-converting activity and the exposure of phosphatidylserine at the outer surface of platelets. Eur J Biochem **122**(2), 429-36.

14) Bevers, E. M., P. Comfurius and R. F. Zwaal (1983). Changes in membrane phospholipid distribution during platelet activation. Biochim Biophys Acta **736**(1), 57-66.

15) Birks, J. B. (1970). Photophysics of aromatic molecules. New York, Wiley-Interscience.

16) Blankenberg, F. G., P. D. Katsikis, J. F. Tait, R. E. Davis, L. Naumovski, K. Ohtsuki, S. Kopiwoda, M. J. Abrams, M. Darkes, R. C. Robbins, H. T. Maecker and H. W. Strauss (1998). In vivo detection and imaging of phosphatidylserine expression during programmed cell death. PNAS U S A **95**(11), 6349-54.

17) Bondar, O. P. and E. S. Rowe (1999). Preferential interactions of fluorescent probe Prodan with cholesterol. Biophys J **76**(2), 956-962.

18) Bose, S., I. Tuunainen, M. Parry, O. P. Medina, G. Mancini and P. K. Kinnunen (2004). Binding of cationic liposomes to apoptotic cells. Anal Biochem **331**(2), 385-94.

19) Bossy-Wetzel, E. and D. R. Green (2000). Detection of apoptosis by annexin V labeling. Methods Enzymol **322**, 15-8.

20) Briggs, M., I. Bruce, J. Miller, C. Moody, A. Simmonds and E. Swann (1997). Synthesis of functionalised fluorescent dyes and their coupling to amines and amino acids. J Chem Soc Perkin Trans I (7), 1051.

21) Brown, D. A. and J. K. Rose (1992). Sorting of GPI-anchored proteins to glycolipid-enriched membrane subdomains during transport to the apical cell surface. Cell **68**(3), 533-544.

22) Brown, D. A. and E. London (1998). Structure and origin of ordered lipid domains in biological membranes. J Membr Biol **164**, 103-114.

23) Brown, D. A. and E. London (2000). Structure and function of sphingolipid- and cholesterol-rich membrane rafts. J Biol Chem **275**(23), 17223-17224.

24) Bublitz, G. U. and S. G. Boxer (1997). Stark Spectroscopy: Applications in Chemistry, Biology, and Materials Science. Ann Rev Phys Chem. **48**(1), 213.

25) Cairo, C. W., J. A. Key and C. M. Sadek (2010). Fluorescent small-molecule probes of biochemistry at the plasma membrane. Curr Opin Chem Biol **14**(1), 57-63.

26) Callera G. E., Montezano A. C. I., Yogi A., Tostes R. C. A. , and Touyz R. M. (2007). Vascular signaling through cholesterol-rich domains: implications in hypertension. Curr Opin Nephrol Hypertens **16**, 90-104.

27) Catalan, J., P. Perez, J. Laynez and F. G. Blanco (1991). Analysis of the solvent effect on the photophysics properties of 6-propionyl-2-(dimethylamino)naphthalene (PRODAN). J Fluoresc **1**(4), 215.

28) Celli, A. and E. Gratton (2010). Dynamics of lipid domain formation: fluctuation analysis. Biochim Biophys Acta **1798**(7), 1368-1376.

29) Cerezo, F. M., S. C. Rocafort, P. S. Sierra, F. Garcia-Blanco, C. D. Oliva and J. C. Sierra (2001). Photophysical study of the probes acrylodan (1[6-(dimethylamino)naphthalene-2-yl]prop-2-en-1-one), ANS (8-anilino-naphthalene-1-sulfonate) and prodan (1-[6-(dymethylamino)naphthalene-2-yl]propan-1-1) in aqueous mixtures of various alcohols. Helv Chim Acta **84**, 3306-3312.

30) Chapman, D. (1975). Phase-transitions and fluidity characteristics of lipids and cell-membranes. Quart Rev Biophys **8**, 185-235.

31) Chattopadhyay, A. (1990). Chemistry and biology of N-(7-nitrobenz-2-oxa-1,3-diazol-4-yl)-labeled lipids: Fluorescent probes of biological and model membranes. Chem Phys Lipids **53**(1), 1.

32) Cheng, Y. M., S. C. Pu, C. J. Hsu, C. H. Lai and P. T. Chou (2006). Femtosecond dynamics on 2-(2'-hydroxy-4'-diethylaminophenyl)benzothiazole: solvent polarity in the excited-state proton transfer. ChemPhysChem **7**(6), 1372-81.

33) Chong, P. L. (1988). Effects of hydrostatic pressure on the location of Prodan in lipid bilayers and cellular membranes. Biochemistry **27**(1), 399-404.

34) Chou, I.-T., M. L. Martinez and H. Clements (1993). Reversal of excitation behavior of proton-transfer vs. charge-transfer by dielectric pertirbation of electronic manifolds. J Phys Chem **97**, 2618-2622.

35) Chou, P., M. Martinez and J. Clements (1993b). The observation of solvent-dependent proton-transfer charge-transfer lasers from 4'-diethylamino-3-hydroxyflavone. Chem Phys Lett **204**(5-6), 395-399.

36) Chou, P. T., S. C. Pu, Y. M. Cheng, W. S. Yu, Y. C. Yu, F. T. Hung and W. P. Hu (2005). Femtosecond dynamics on excited-state proton/ Charge-transfer reaction in 4'-N,N-diethylamino-3-hydroxyflavone. The role of dipolar vectors in constructing a rational mechanism. J Phys Chem A **109**(17), 3777.

37) Chudakov, D. M., M. V. Matz, S. Lukyanov and K. A. Lukyanov (2010). Fluorescent Proteins and Their Applications in Imaging Living Cells and Tissues. Physiol Rev **90**(3), 1103-1163.

38) Clamme, J., J. Azoulay and Y. Mely (2003). Monitoring of the formation and dissociation of polyethylenimine/DNA complexes by two photon fluorescence correlation spectroscopy. Biophys J **84**(3), 1960-1968.

39) Clarke, R. J. and D. J. Kane (1997). Optical detection of membrane dipole potential: Avoidance of fluidity and dye-induced effects. Biochim Biophys Acta **1323**(2), 223.

40) Cohen, B. E., A. Pralle, X. Yao, G. Swaminath, C. S. Gandhi, Y. N. Jan, B. K. Kobilka, E. Y. Isacoff and L. Y. Jan (2005). A fluorescent probe designed for studying protein conformational change. PNAS U S A **102**(4), 965-70.

41) Coleman, M. L., E. A. Sahai, M. Yeo, M. Bosch, A. Dewar and M. F. Olson (2001). Membrane blebbing during apoptosis results from caspase-mediated activation of ROCK I. Nat Cell Biol **3**(4), 339-345.

42) Connor, J. and A. J. Schroit (1988). Transbilayer movement of phosphatidylserine in erythrocytes: inhibition of transport and preferential labeling of a 31,000-dalton protein by sulfhydryl reactive reagents. Biochemistry **27**(3), 848-51.

43) Connor, J., C. C. Pak and A. J. Schroit (1994). Exposure of phosphatidylserine in the outer leaflet of human red blood cells. Relationship to cell density, cell age, and clearance by mononuclear cells. J Biol Chem **269**(4), 2399-404.

44) Cordy J., Hooper N., and Turner A. (2006). The involvement of lipid rafts in Alzheimer's disease. Mol Membr Biol **23**, 111-122.

45) Coskun, U. and K. Simons (2010). Membrane rafting: From apical sorting to phase segregation. FEBS Lett **584**(9), 1685-1693.

46) Danielli, J. F. and H. Davson (1935). A contribution to the theory of permeability of thin films. J Cell Comp Physiol **5**, 495-508.

47) Davis, B. and C. Abelt (2005). Synthesis and photophysical properties of models for twisted Prodan and dimethylaminonaphthonitrile. J Phys Chem A **109**(7), 1295-1298.

48) Degterev, A. and J. Yuan (2008). Expansion and evolution of cell death programmes. Nat Rev Mol Cell Biol **9**(5), 378-390.

49) Demchenko, A. P. (1986). Ultraviolet Spectroscopy of Proteins. Berlin, Springer-Verlag.

50) Demchenko, A. P., Y. Mely, G. Duportail and A. S. Klymchenko (2009). Monitoring biophysical properties of lipid membranes by environment-sensitive fluorescent probes. Biophys J **96**(9), 3461-70.

51) Demchenko, A. P. (2010). The Concept of lambda-Ratiometry in Fluorescence Sensing and Imaging. J Fluoresc **20**(5), 1099-1128.

52) Devaux, P. F. (1993). Lipid transmembrane asymmetry and flip-flop in biological membranes and in lipid bilayers. Curr Opin Struct Biol **3**(4), 489-494.

53) Diaz, C. and A. J. Schroit (1996). Role of translocases in the generation of phosphatidylserine asymmetry. J Membr Biol **151**(1), 1-9.

54) Diaz, G., M. Melis, B. Batetta, F. Angius and A. Falchi (2008). Hydrophobic characterization of intracellular lipids in situ by Nile Red red/yellow emission ratio. Micron **39**(7), 819-824.

55) Dietrich, C., L. A. Bagatolli, Z. N. Volovyk, N. L. Thompson, M. Levi, K. Jacobson and E. Gratton (2001). Lipid rafts reconstituted in model membranes. Biophys J **80**(3), 1417-28.

56) Diwu, Z., Y. Lu, C. Zhang, D. H. Klaubert and R. P. Haugland (1997). Fluorescent Molecular Probes II. The Synthesis, Spectral Properties and Use of Fluorescent Solvatochromic Dapoxyl^{TM} Dyes. Photochem Photobiol **66**(4), 424.

57) Dombeck, D., M. Blanchard-Desce and W. Webb (2005). Fast optical recording of neuronal membrane potential transients in acute mammalian brain slices by second-harmonic generation microscopy. Biophys J **88**(1), 363A-363A.

58) Dumont, E. A., C. P. Reutelingsperger, J. F. Smits, M. J. Daemen, P. A. Doevendans, H. J. Wellens and L. Hofstra (2001). Real-time imaging of apoptotic cell-membrane changes at the single-cell level in the beating murine heart. Nat Med **7**(12), 1352-5.

59) Durairaj, G. and I. Vijayakumar (1984). Temperature-acclimation and phospholipid phase-transition in hypothalamic membrane phospholipids of garden lizard, calotes-versicolor. Biochim Biophys Acta **770**(1), 7-14.

60) Eggeling, C., L. Brand and C. Seidel (1997). Laser-induced fluorescence of coumarin derivatives in aqueous solution: Photochemical aspects for single molecule detection. Bioimaging **5**(3), 105.

61) Eggeling, C., C. Ringemann, R. Medda, G. Schwarzmann, K. Sandhoff, S. Polyakova, V. N. Belov, B. Hein, C. von Middendorff, A. Schonle and S. W. Hell (2009). Direct observation of the nanoscale dynamics of membrane lipids in a living cell. Nature **457**(7233), 1159-1162.

62) Elmore, S. (2007). Apoptosis: a review of programmed cell death. Toxicol Pathol **35**(4), 495-516.

63) Emoto, K., N. Toyama-Sorimachi, H. Karasuyama, K. Inoue and M. Umeda (1997). Exposure of phosphatidylethanolamine on the surface of apoptotic cells. Exp Cell Res **232**(2), 430-4.

64) Ercelen, S., A. Klymchenko and A. Demchenko (2002a). An ultrasensitive fluorescent probe for hydrophobic range of solvent polarities. Anal Chim Acta **464**, 273-287.

65) Ercelen, S., A. D. Roshal, A. P. Demchenko and A. S. Klymchenko (2002b). Excited-state proton transfer reaction in a new benzofuryl 3-hydroxychromone derivative: the influence of low-polar solvents. Polish J Chem **76**(9), 1287-1299.

66) Erickson, G. F. (1997). Defining apoptosis: players and systems. J Soc Gynecol Investig **4**(5), 219-28.

67) Fadok, V. A., D. R. Voelker, P. A. Campbell, J. J. Cohen, D. L. Bratton and P. M. Henson (1992). Exposure of phosphatidylserine on the surface of apoptotic lymphocytes triggers specific recognition and removal by macrophages. J Immunol **148**(7), 2207-16.

68) Fadok, V. A., D. J. Laszlo, P. W. Noble, L. Weinstein, D. W. Riches and P. M. Henson (1993). Particle digestibility is required for induction of the phosphatidylserine recognition mechanism used by murine macrophages to phagocytose apoptotic cells. J Immunol **151**(8), 4274-85.

69) Fluhler, E., V. G. Burnham and L. M. Loew (1985). Spectra, membrane binding, and potentiometric reponses of new charge shift probes. Biochemistry **24**(21), 5749.

70) Formosinho, S. J. and L. G. Arnaut (1993). Excited-State Proton-Transfer Reactions.2. Intramolecular Reactions. J Photochem Photobiol A **75**(1), 21-48.

71) Freeman M. R., Cinar B., and Lu M. L. (2005). Membrane rafts as potential sites of nongenomic hormonal signaling in prostate cancer. Trends Endocrinol Metabolism **16**, 273-279.

72) Frey, T. (1995). Nucleic acid dyes for detection of apoptosis in live cells. Cytometry **21**(3), 265-74.

73) Frey, T. (1997). Correlated flow cytometric analysis of terminal events in apoptosis reveals the absence of some changes in some model systems. Cytometry **28**(3), 253-63.

74) Frolov, Y., Y. Sapoznikov, S. Barer, N. Pogodayev and N. Tyukavkina (1974). Izv Akad Nauk SSSR **10**, 2364-2367.

75) Fromherz, P., G. Hubener, B. Kuhn and M. Hinner (2008). ANNINE-6plus, a voltage-sensitive dye with good solubility, strong membrane binding and high sensitivity. Eur Biophys J Biophys Lett **37**(4), 509-514.

76) Garcia-Saez, A. J., S. Chiantia and P. Schwille (2007). Effect of line tension on the lateral organization of lipid membranes. J Biol Chem **282**(46), 33537-44.

77) Gidwani, A., D. Holowka and B. Baird (2001). Fluorescence anisotropy measurements of lipid order in plasma membranes and lipid rafts from RBL-2H3 mast cells. Biochemistry **40**(41), 12422-9.

78) Glaser, M. (1993). Lipid domains in biological membranes. Curr Opin Struct Biol **3**(4), 475-481.

79) Golini, C., B. Williams and J. Foresman (1998). Further solvatochromic, thermochromic, and theoretical studies on Nile Red. J Fluoresc **8**(4), 395-404.

80) Gomez-Mouton, C., J. Abad, E. Mira, R. Lacalle, E. Gallardo, S. Jimenez-Baranda, I. Illa, A. Bernad, S. Manes and C. Martinez-A (2001). Segregation of leading-edge and uropod components into specific lipid rafts during T cell polarization. PNAS U S A **98**(17), 9642-9647.

81) Goncalves, M. S. (2009). Fluorescent labeling of biomolecules with organic probes. Chem Rev **109**(1), 190.

82) Gorter, E. and F. Grendel (1925). On bimolecular layers of lipoids on the chromocytes of the blood. J Exp Med **41**, 439-443.

83) Grabowska, A., A. Mordzinski, N. Tamai and K. Yoshihara (1990). Reversible intramolecular proton transfer reactions of electronically exited double benzoxazoles: A direct observation of the effect of the intrinsic barrier. Chem Phys Lett **169**, 450-56.

84) Greenspan, P., E. P. Mayer and S. D. Fowler (1985). Nile red: A selective fluorescent stain for intracellular lipid droplets. J Cell Biol **100**(3), 965.

85) Greenwood, A., S. Tristram-Nagle and J. Nagle (2006). Partial molecular volumes of lipids and cholesterol. Chem Phys Lipids **143**(1-2), 1-10.

86) Grinvald, A., R. Hildesheim, I. C. Farber and L. Anglister (1982). Improved fluorescent probes for the measurement of rapid changes in membrane potential. Biophys J **39**(3), 301-308.

87) Haidekker, M. A. and E. A. Theodorakis (2007). Molecular rotors - Fluorescent biosensors for viscosity and flow. Org Biomol Chem **5**(11), 1669.

88) Hanayama, R., M. Tanaka, K. Miwa, A. Shinohara, A. Iwamatsu and S. Nagata (2002). Identification of a factor that links apoptotic cells to phagocytes. Nature **417**(6885), 182-187.

89) Hancock, J. (2006). Lipid rafts: contentious only from simplistic standpoints. Nat Rev Mol Cell Biol **7**(6), 456.

90) Hanshaw, R. and B. Smith (2005). New reagents for phosphatidylserine recognition and detection of apoptosis. Bioorg Med Chem **13**(17), 5035-5042.

91) Haskard, C. A. and E. C. Y. Li-Chan (1998). Hydrophobicity of Bovine Serum Albumin and Ovalbumin Determined Using Uncharged (PRODAN) and Anionic (ANS-) Fluorescent Probes. J Agricult Food Chem **46**(7), 2671.

92) Hazel, J. and E. Williams (1990). The role of alterations in membrane lipid-composition in enabling physiological adaptation of organisms to their physical-environment. Prog Lipid Res **29**(3), 167-227.

93) Heller, A. and D. L. Williams (1970). Intramolecular proton transfer reactions in exited fluorescent compounds. J Phys Chem **74**, 4473-4480.

94) Herek, J. L., S. Pedersen, L. Banares and A. H. Zewail (1992). Femtosecond real-time probing of reactions. X. Hydrogen atom transfer. J Chem Phys **97**, 9046-9061.

95) Higgins, C. F. (1994). Flip-flop: the transmembrane translocation of lipids. Cell **79**(3), 393-5.

96) Hinterdorfer, P. and Y. F. Dufrene (2006). Detection and localization of single molecular recognition events using atomic force microscopy. Nature Methods **3**(5), 347-355.

97) Holmes-Farley, S. R. and G. M. Whitesides (1986). Fluorescence properties of dansyl groups covalently bonded to the surface of oxidatively functionalized low-density polyethylene film. Langmuir **2**(3), 266.

98) Hope, M., M. Bally, G. Webb and P. Cullis (1985). Production of large unilamellar vesicles by a rapid extrusion procedure – Characterization of size distribution, trapped volume and ability to maintain a membrane-potential. Biochim Biophys Acta **812**(1), 55-65.

99) Hubener, G., A. Lambacher and P. Fromherz (2003). Anellated hemicyanine dyes with large symmetrical solvatochromism of absorption and fluorescence. J Phys Chem B **107**(31), 7896-7902.

100) Huppertz, B., H. G. Frank and P. Kaufmann (1999). The apoptosis cascade--morphological and immunohistochemical methods for its visualization. Anat Embryol (Berl) **200**(1), 1-18.

101) Igarashi, K., K. Asai, M. Kaneda, M. Umeda and K. Inoue (1995). Specific binding of a synthetic peptide derived from an antibody complementarity determining region to phosphatidylserine. J Biochem (Tokyo) **117**(2), 452-7.

102) Inaba, N., N. Sato, M. Ijichi, I. Fukazawa, A. Nito, H. Takamizawa, G. Luben and H. Bohn (1984). The immunocytochemical location of two membrane-associated placental tissue proteins in human and cynomolgus monkey placentae. Tumour Biol **5**(2), 75-85.

103) Itoh, M., K. Tokumura, Y. Tanimoto, Y. Okada, H. Takeuchi, K. Obi and I. Tanaka (1982). Time-resolved and steady-state fluorescence studies of the excited-state proton transfer in 3-hydroxyflavone and 3-hydroxychromone. J Am Chem Soc **104**, 4146-4150.

104) Itoh, M., Y. Tanimoto and K. Tokumura (1983). Transient absorption study of the intramolecular excited-state and ground-state proton transfer in 3-hydroxyflavone and 3-hydroxychromone. J Am Chem Soc **105**(10), 3339-3340.

105) Jacobson, K. and C. Dietrich (1999). Looking at lipid rafts? Trends Cell Biol **9**(3), 87-91.

106) Jacobson, K., O. Mouritsen and R. Anderson (2007). Lipid rafts: at a crossroad between cell biology and physics. Nat Cell Biol **9**(1), 7-14.

107) Jin, L., A. C. Millard, J. P. Wuskell, H. A. Clark and L. M. Loew (2005). Cholesterol-enriched lipid domains can be visualized by di-4-ANEPPDHQ with linear and nonlinear optics. Biophys J **89**(1), L04.

108) Jin, L., A. C. Millard, J. P. Wuskell, X. Dong, D. Wu, H. A. Clark and L. M. Loew (2006). Characterization and application of a new optical probe for membrane lipid domains. Biophys J **90**(7), 2563-75.

109) Kaur, Y. and P. M. Horowitz (2004). Prodan fluorescence mimics the GroEL folding cycle. Protein J **23**(7), 475-81.

110) Kenis, H., H. van Genderen, A. Bennaghmouch, H. A. Rinia, P. Frederik, J. Narula, L. Hofstra and C. P. Reutelingsperger (2004). Cell surface-expressed phosphatidylserine and annexin A5 open a novel portal of cell entry. J Biol Chem **279**(50), 52623-9.

111) Kerr, J. F., A. H. Wyllie and A. R. Currie (1972). Apoptosis: a basic biological phenomenon with wide-ranging implications in tissue kinetics. Br J Cancer **26**(4), 239-57.

112) Kiechle, F. L. and X. Zhang (2002). Apoptosis: biochemical aspects and clinical implications. Clin Chim Acta **326**(1-2), 27-45.

113) Kim, H. M., H. J. Choo, S. Y. Jung, Y. G. Ko, W. H. Park, S. J. Jeon, C. H. Kim, T. Joo and B. R. Cho (2007). A two-photon fluorescent probe for lipid raft imaging: C-laurdan. ChemBioChem **8**(5), 553-9.

114) Kim, H. M., B. H. Jeong, J. Y. Hyon, M. J. An, M. S. Seo, J. H. Hong, K. J. Lee, C. H. Kim, T. H. Joo, S. C. Hong and B. R. Cho (2008). Two-photon fluorescent turn-on probe for lipid rafts in live cell and tissue. J Am Chem Soc **130**(13), 4246-4247.

115) Klymchenko, A., T. Ozturk, V. G. Pivovarenko and A. Demchenko (2002a). Synthesis of furanochromones: a new step in improvement of fluorescence properties. Tetr Lett **43**, 7079-7082.

116) Klymchenko, A., G. Duportail, T. Ozturk, V. G. Pivovarenko, Y. Mely and A. P. Demchenko (2002c). Novel two-band ratiometric fluorescence probes with different location and orientation in phospholipid membranes. Chem Biol **9**(11), 1199-208.

117) Klymchenko, A. and A. P. Demchenko (2003). Multiparametric probing of intermolecular interactions with fluorescent dye exhibiting excited state intramolecular proton transfer. Phys Chem Chem Phys **5**, 461-68.

118) Klymchenko, A., V. G. Pivovarenko and A. P. Demchenko (2003a). Elimination of the Hydrogen Bonding Effect on the Solvatochromism of 3-Hydroxyflavones. J Phys Chem A **107**, 4211-16.

119) Klymchenko, A., V. G. Pivovarenko and A. P. Demchenko (2003b). Perturbation of planarity as the possible mechanism of solvent-dependent variations of fluorescence quantum yield in 2-aryl-3-hydroxychromones. Spectrochim Acta A **59**(4), 787-92.

120) Klymchenko, A., V. Pivovarenko, T. Ozturk and A. Demchenko (2003c). Modulation of the solvent-dependent dual emission in 3-hydroxychromones by substituents. New J Chem **27**(9), 1336-1343.

121) Klymchenko, A., G. Duportail, A. P. Demchenko and Y. Mely (2004a). Bimodal distribution and fluorescence response of environment-sensitive probes in lipid bilayers. Biophys J **86**(5), 2929-41.

122) Klymchenko, A., Y. Mely, A. P. Demchenko and G. Duportail (2004b). Simultaneous probing of hydration and polarity of lipid bilayers with 3-hydroxyflavone fluorescent dyes. Biochim Biophys Acta **1665**(1-2), 6.

123) Klymchenko, A., H. Stoeckel, K. Takeda and Y. Mely (2006). Fluorescent probe based on intramolecular proton transfer for fast ratiometric measurement of cellular transmembrane potential. J Phys Chem B **110**(27), 13624-32.

124) Klymchenko, A., S. Oncul, P. Didier, E. Schaub, L. Bagatolli, G. Duportail and Y. Mely (2009). Visualization of lipid domains in giant unilamellar vesicles using an environment-sensitive membrane probe based on 3-hydroxyflavone. Biochim Biophys Acta **1788**(2), 495-9.

125) Kojima, N. and S. Hakomori (1991). Synergistic effect of two cell recognition systems: glycosphingolipid-glycosphingolipid interaction and integrin receptor interaction with pericellular matrix protein. Glycobiology **1**(6), 623-30.

126) Kooistra, F., J. Knol, F. Kastenberg, L. Popescu, W. Verhees, J. Kroon and J. Hummelen (2007). Increasing the open circuit voltage of bulk-heterojunction solar cells by raising the LUMO level of the acceptor. Org Lett **9**(4), 551-554.

127) Koopman, G., C. P. Reutelingsperger, G. A. Kuijten, R. M. Keehnen, S. T. Pals and M. H. van Oers (1994). Annexin V for flow cytometric detection of phosphatidylserine expression on B cells undergoing apoptosis. Blood **84**(5), 1415-20.

128) Koulov, A. V., K. A. Stucker, C. Lakshmi, J. P. Robinson and B. D. Smith (2003). Detection of apoptotic cells using a synthetic fluorescent sensor for membrane surfaces that contain phosphatidylserine. Cell Death Differ **10**(12), 1357-9.

129) Krasnowska, E. K., E. Gratton and T. Parasassi (1998). Prodan as a membrane surface fluorescence probe: partitioning between water and phospholipid phases. Biophys J **74**(4), 1984-93.

130) Kuhn, B. and P. Fromherz (2003). Anellated hemicyanine dyes in a neuron membrane: Molecular Stark effect and optical voltage recording. J Phys Chem B **107**(31), 7903-7913.

131) Kuhry, J.-G., Fonteneau, P., Duportail, G., Maechling, C., Laustriat, G (1983). TMA-DPH: A suitable fluorescence polarization probe for specific plasma membrane fluidity studies in intact living cells. Cell Biophysics **5**(2), 129-140.

132) Kuhry, J. G., G. Duportail, C. Bronner and G. Laustriat (1985). Plasma membrane fluidity measurements on whole living cells by fluorescence anisotropy of trimethylammoniumdiphenylhexatriene. Biochim Biophys Acta **845**(1), 60-7.

133) Kurad, D., G. Jeschke and D. Marsh (2003). Lipid membrane polarity profiles by high-field EPR. Biophys J **85**(2), 1025-33.

134) Kurzchalia, T. V., E. Hartmann and P. Dupree (1995). Guilty by insolubility--does a protein's detergent insolubility reflect a caveolar location? Trends Cell Biol **5**(5), 187-189.

135) Kuzmin, P., S. Akimov, Y. Chizmadzhev, J. Zimmerberg and F. Cohen (2005). Line tension and interaction energies of membrane rafts calculated from lipid splay and tilt. Biophys J **88**(2), 1120-1133.

136) La Deda, M., M. Ghedini, I. Aiello, T. Pugliese, F. Barigelletti and G. Accorsi (2005). Organometallic emitting dyes: Palladium(II) nile red complexes. J Organomet Chem **690**(4), 857-861.

137) Laemer, F., T. Elsaesser and W. Kaiser (1988). Femtosecond spectroscopy of exited state proton transfer in 2-(2-hydroxyphenyl)benzothiazole. Chem Phys Lett **148**, 119-124.

138) Lakowicz, J. R. (2006). Principles of Fluorescence Spectroscopy. New York, Springer.

139) Langmuir, I. (1917). The constitution and fundamental properties of solids and liquids. II. Liquids. J Am Chem Soc **39**(9), 1848-1906.

140) Lavis, L. D. and R. T. Raines (2008). Bright ideas for chemical biology. ACS Chem Biol **3**(3), 142-55.

141) Laws, W. R. and L. Brand (1979). Analysis of two-state excited-state reactions. The fluorescence decay of 2-naphtol. J Phys Chem **83**(7), 795-802.

142) Legourrierec, D., S. M. Ormson and R. G. Brown (1994). Excited-state intramolecular proton-transfer. 2. ESIPT to Oxygen. Prog React Kinetics **19**(3), 211-275.

143) Lenne, P. F., L. Wawrezinieck, F. Conchonaud, O. Wurtz, A. Boned, X. J. Guo, H. Rigneault, H. T. He and D. Marguet (2006). Dynamic molecular confinement in the plasma membrane by microdomains and the cytoskeleton meshwork. EMBO J **25**(14), 3245-56.

144) Lingwood, D. and K. Simons (2010). Lipid Rafts As a Membrane-Organizing Principle. Science **327**(5961), 46-50.

145) Lippert, E. L. (1975). Laser-spectroscopic studies of reorientation and other relaxation processes in solution. Organic Molecular Photophysics. J. B. Birks. New York, Wiley. **2,** 1-31.

146) Lentz, B. R. (1989). Membrane 'fluidity' as detected by diphenylhexatriene probes. Chem Phys Lipids **50**, 171.

147) Lodish, H., A. Berk, S. L. Zipursky, P. Matsudaira, D. Baltimore and J. Darnell (2004). Molecular Cell Biology. New York, W. H. Freeman Company.

148) Loew, L. M. and L. L. Simpson (1981). Charge-shift probes of membrane potential. A probable electrochromic mechanism for p-aminostyrylpyridinium probes on a hemispherical lipid bilayer. Biophys J **34**(3), 353.

149) Loew, L. M., L. B. Cohen and B. M. Salzberg (1985). Charge-shift probes of membrane potential. Characterization of aminostyrylpyridinium dyes on the squid giant axon. Biophys J **47**(1), 71.

150) Loew, L. M. (1988). Spectroscopic Membrane Probes. Boca Raton, CRC Press.

151) Loew, L. M., L. B. Cohen, J. Dix, E. N. Fluhler, V. Montana, G. Salama and J. Y. Wu (1992). A naphthyl analog of the aminostyryl pyridinium class of potentiometric membrane dyes shows consistent sensitivity in a variety of tissue, cell, and model membrane preparations. J Membr Biol **130**(1), 1-10.

152) London, E. (2005). How principles of domain formation in model membranes may explain ambiguities concerning lipid raft formation in cells. Biochim Biophys Acta **1746**(3), 203-220.

153) Loudet, A. and K. Burgess (2007). BODIPY dyes and their derivatives: syntheses and spectroscopic properties. Chem Rev **107**(11), 4891-932.

154) Loving, G. and B. Imperiali (2008). A versatile amino acid analogue of the solvatochromic fluorophore 4-N,N-dimethylamino-1,8-naphthalimide: a powerful tool for the study of dynamic protein interactions. J Am Chem Soc **130**(41), 13630-8.

155) Lu, Z., S. J. Lord, H. Wang, W. E. Moerner and R. J. Twieg (2006). Long-wavelength analogue of Prodan: synthesis and properties of Anthradan, a fluorophore with a 2,6-donor-acceptor anthracene structure. J Org Chem **71**(26), 9651-7.

156) Malorni, W., T. Garofalo, A. Tinari, V. Manganelli, R. Misasi and M. Sorice (2008). Analyzing lipid raft dynamics during cell apoptosis. Methods Enzymol **442**, 125-40.

157) Marks, D., H. Zhang and M. Glasbeek (1997). Solvent dependence of (sub)picosecond proton transfer in photo-excited [2,2'-bipyridyl]-3,3'-diol. Chem Phys Lett **275**, 370-376.

158) Martin, S. J., G. A. O'Brien, W. K. Nishioka, A. J. McGahon, A. Mahboubi, T. C. Saido and D. R. Green (1995). Proteolysis of fodrin (non-erythroid spectrin) during apoptosis. J Biol Chem **270**(12), 6425-8.

159) Martin, S. J., D. M. Finucane, G. P. Amarante-Mendes, G. A. O'Brien and D. R. Green (1996). Phosphatidylserine externalization during CD95-induced apoptosis of cells and cytoplasts requires ICE/CED-3 protease activity. J Biol Chem **271**(46), 28753-6.

160) Martin-Brown, S. A., Y. Fu, G. Saroja, M. M. Collinson and D. A. Higgins (2005). Single-molecule studies of diffusion by oligomer-bound dyes in organically modified sol-gel-derived silicate films. Anal Chem **77**(2), 486-494.

161) Martinez, M. M., R. D. Reif and D. Pappas (2010). Detection of apoptosis: A review of conventional and novel techniques. Anal Methods **2**, 996-1004.

162) Massey, J. B. (1998). Effect of cholesteryl hemisuccinate on the interfacial properties of phosphatidylcholine bilayers. Biochim Biophys Acta **1415**(1), 193-204.

163) Mataga, N. and T. Kubota (1970). Molecular Interactions and Electronic Spectra. New York, Marcel Dekker.

164) Maxfield, F. and I. Tabas (2005). Role of cholesterol and lipid organization in disease. Nature **438**(7068), 612.

165) M'Baye, G., A. Klymchenko, D. Yushchenko, V. Shvadchak, T. Ozturk, Y. Mely and G. Duportail (2007). Fluorescent dyes undergoing intramolecular proton transfer with improved sensitivity to surface charge in lipid bilayers. Photochem Photobiol Sci **6**(1), 71-76.

166) McElhaney, R. N. (1984). The structure and function of the Acholeplasma Laidlawii plasma membrane. Biochim Biophys Acta **779**, 1-42.

167) McEvoy, L., P. Williamson and R. A. Schlegel (1986). Membrane phospholipid asymmetry as a determinant of erythrocyte recognition by macrophages. PNAS U S A **83**(10), 3311-3315.

168) McMorrow, D. and M. Kasha (1984). Intramolecular excited-state proton transfer in 3-hydroxyflavone. Hydrogen-bonding solvent perturbations. J Phys Chem **88**, 2235-2243.

169) McMorrow, D., T. P. Dzugan and T. J. Aartsma (1984). Excited-state dynamics of the intramolecular proton transfer of 3-hydroxyflavone in the absence of external hydrogen-bonding interactions. Chem Phys Lett **103**(6), 492-496.

170) Meers, P. and T. Mealy (1993). Calcium-dependent annexin V binding to phospholipids: stoichiometry, specificity, and the role of negative charge. Biochemistry **32**(43), 11711-21.

171) Mes, G. F., B. De Jong, H. J. Van Ramesdonk, J. W. Verhoeven, J. M. Warman, M. P. De Haas and L. E. W. Horsman-van Den Dool (1984). Excited-state dipole moment and solvatochromism of highly fluorescent rod-shaped bichromophoric molecules. J Am Chem Soc **106**(22), 6524.

172) Meulmeester, E. and A. G. Jochemsen (2008). p53: a guide to apoptosis. Curr Cancer Drug Targets **8**(2), 87.

173) Miersch, S. and B. Mutus (2007). Membrane lipid domains: Techniques for visualization and characterization. Curr Anal Chem **3**(1), 81-92.

174) Mishra, A., R. K. Behera, P. K. Behera, B. K. Mishra and G. B. Behera (2000). Cyanines during the 1990s: a review. Chem Rev **100**(6), 1973.

175) Miyazawa, A., H. Inoue, T. Yoshioka, T. Horikoshi, K. Yanagisawa, M. Umeda and K. Inoue (1992). Monoclonal antibody analysis of phosphatidylserine and protein kinase C localizations in developing rat cerebellum. J Neurochem **59**(4), 1547-54.

176) Mongrand, S., T. Stanislas, E. M. F. Bayer, J. Lherminier and F. Simon-Plas (2010). Membrane rafts in plant cells. Trends Plant Sci **15**(12), 656-663.

177) Montana, V., D. L. Farkas and L. M. Loew (1989). Dual-wavelength ratiometric fluorescence measurements of membrane potential. Biochemistry **28**(11), 4536-9.

178) Moreau, C., J. C. Sulpice, P. F. Devaux and A. Zachowski (1997). Drug-induced transmembrane lipid scrambling in erythrocytes and in liposomes requires the presence of polyanionic phospholipids. Mol Membr Biol **14**(1), 5-12.

179) Moreno, F., M. Cortijo and J. Gonalez-Jimanez (1999). The fluorescent probe Prodan characterizes the warfarin binding site on human serum albumin. Photochem Photobiol **69**(1), 8.

180) Morrot, G., S. Cribier, P. F. Devaux, D. Geldwerth, J. Davoust, J. F. Bureau, P. Fellmann, P. Herve and B. Frilley (1986). Asymmetric lateral mobility of phospholipids in the human erythrocyte membrane. PNAS U S A **83**(18), 6863-7.

181) Mouritsen, O. G. (1991). Theoretical models of phospholipid phase transitions. Chem Phys Lipids **57**(2-3), 179-194.

182) Mower, D. A., Jr., D. W. Peckham, V. A. Illera, J. K. Fishbaugh, L. L. Stunz and R. F. Ashman (1994). Decreased membrane phospholipid packing and decreased cell size precede DNA cleavage in mature mouse B cell apoptosis. J Immunol **152**(10), 4832-4842.

183) Munro, S. (2003). Lipid rafts: Elusive or illusive? Cell **115**(4), 377-388.

184) Mukherjee, S. and F. Maxfield (2004). Membrane domains. Ann Rev Cell Dev Biol **20**, 839-866.

185) Murakami, Y., H. Takamatsu, J. Taki, M. Tatsumi, A. Noda, R. Ichise, J. F. Tait and S. Nishimura (2004). 18F-labelled annexin V: a PET tracer for apoptosis imaging. Eur J Nucl Med Mol Imaging **31**(4), 469.

186) Murphy S., Hiller N. L., Harrison T., and Lomasney J. (2006). Lipid rafts and malaria parasite infection of erythrocytes. Mol Membr Biol **23**, 81-88.

187) Nagy, K., S. Gokturk and L. Biczok (2003). Effect of microenvironment on the fluorescence of 2-hydroxy-substituted Nile Red dye: A new fluorescent probe for the study of micelles. J Phys Chem A **107**(41), 8784.

188) Nemkovich, N. A., V. G. Pivovarenko, W. Baumann, A. N. Rubinov and A. N. Sobchuk (2005). Dipole moments of 4'-aminoflavonol fluorescent probes in different solvents. J Fluoresc **15**(1), 29-36.

189) Obaid, A. L., L. M. Loew, J. P. Wuskell and B. M. Salzberg (2004). Novel naphthylstyryl-pyridium potentiometric dyes offer advantages for neural network analysis. J Neurosci Methods **134**(2), 179-90.

190) Obaid, A. L., M. E. Nelson, J. Lindstrom and B. M. Salzberg (2005). Optical studies of nicotinic acetylcholine receptor subtypes in the guinea-pig enteric nervous system. J Exp Biol **208**, 2981-3001.

191) Ormson, S. M. and R. G. Brown (1994). Excited-State Intramolecular Proton-Transfer.1. ESIPT To Nitrogen. Prog React Kinetics **19**(1), 45-91.

192) Ormson, S. M., R. G. Brown, F. Vollmer and W. Rettig (1994). Switching between charge- and proton-transfer emission in the excited state of a substituted 3-hydroxyflavone. J Photochem Photobiol A: Chem **81**, 65-72.

193) Otsuki, Y., Z. Li and M. Shibata (2003). Apoptotic detection methods - from morphology to gene. Prog Histochem Cytochem **38**(3), 275-339.

194) Parasassi, T., G. De Stasio, A. d'Ubaldo and E. Gratton (1990). Phase fluctuation in phospholipid membranes revealed by Laurdan fluorescence. Biophys J **57**(6), 1179-86.

195) Parasassi, T., M. Loiero, M. Raimondi, G. Ravagnan and E. Gratton (1993). Absence of lipid gel-phase domains in seven mammalian cell lines and in four primary cell types. Biochim Biophys Acta **1153**(2), 143.

196) Parasassi, T., M. Di Stefano, M. Loiero, G. Ravagnan and E. Gratton (1994). Cholesterol modifies water concentration and dynamics in phospholipid bilayers: a fluorescence study using Laurdan probe. Biophys J **66**, 763-8.

197) Patra, S. K., A. Alonso, J. L. R. Arrondo and F. M. Golni (1999). Liposomes containing sphingomyelin and cholesterol: Detergent solubilisation and infrared spectroscopic studies. J Liposom Res **9**(2), 247-260.

198) Pike, L. J., X. Han, K.-N. Chung and R. W. Gross (2002). Lipid rafts are enriched in arachidonic acid and plasmenylethanolamine and their composition is independent of caveolin-1 expression: a quantitative electrospray ionization/mass spectrometric analysis. Biochemistry **41**, 2075-2088.

199) Pike, L. J. (2006). Rafts defined: a report on the Keystone Symposium on Lipid Rafts and Cell Function. J Lipid Res **47**(7), 1597-8.

200) Pomorski, T., A. Herrmann, B. Zimmermann, A. Zachowski and P. Muller (1995). An improved assay for measuring the transverse redistribution of fluorescent phospholipids in plasma membranes. Chem Phys Lipids **77**(2), 139-46.

201) Quinn, P. (2010). A lipid matrix model of membrane raft structure. Prog Lipid Res **49**(4), 390-406.

202) Ran, S., A. Downes and P. E. Thorpe (2002). Increased exposure of anionic phospholipids on the surface of tumor blood vessels. Cancer Res **62**(21), 6132-40.

203) Reichardt, C. (1994). Solvatochromic dyes as solvent polarity indicators. Chem Rev **94**, 2319-2358.

204) Reutelingsperger, C. P., G. Hornstra and H. C. Hemker (1985). Isolation and partial purification of a novel anticoagulant from arteries of human umbilical cord. Eur J Biochem **151**(3), 625-9.

205) Ribeiro, A. A. and E. A. Dennis (1973). Effect of thermotropic phase transitions of dipalmitoylphosphatidylcholine on the formation of mixed micelles with Triton X-100. Biochim Biophys Acta **332**, 26-35.

206) Robertson, J. D. (1957). New observations on the ultrastructure of the membranes of frog peripheral nerve fibers. J Biophys Biochem Cytol **3**, 1043-1047.

207) Salvesen, G. S. and S. J. Riedl (2008). Caspase mechanisms. Adv Exp Med Biol **615**, 13-23.

208) Samanta, A. and R. W. Fessenden (2000). Excited state dipole moment of Prodan as determined from transient dielectric loss measurements. J Phys Chem A **104**, 8972-8975.

209) Saroja, G., P. Zhang, N. Ernsting and J. Liebscher (2004). Synthesis of alkylated aminofluorenes by palladium-catalyzed substitution at halofluorenes. J Org Chem **69**, 987-990.

210) Saslowsky, D., J. Lawrence, X. Ren, D. Brown, R. Henderson and J. Edwardson (2002). Placental alkaline phosphatase is efficiently targeted to rafts in supported lipid bilayers. J Biol Chem **277**(30), 26966-26970.

211) Schellenberger, E. A., F. Reynolds, R. Weissleder and L. Josephson (2004). Surface-functionalized nanoparticle library yields probes for apoptotic cells. ChemBioChem **5**(3), 275-9.

212) Schlegel, R., M. Stevens, K. Lumleysapanski and P. Williamson (1993). Altered lipid packing identifies apoptotic thymocytes. Immunol Lett **36**(3), 283-288.

213) Schlegel, R. A. and P. Williamson (2001). Phosphatidylserine, a death knell. Cell Death Differ **8**(6), 551.

214) Schroeder, R., E. London and D. Brown (1994). Interactions between saturated acyl chains confer detergent resistance on lipids and glycosylphosphatidylinositol (GPI)-anchored proteins: GPIanchored proteins in cells and liposomes show similar behavior. PNAS USA **91**, 12130-12134.

215) Schroeder, R. J., S. N. Ahmed, Y. Zhu, E. London and D. A. Brown (1998). Cholesterol and sphingolipid enhance the Triton X-100-insolubility of GPI-anchored proteins by promoting the formation of detergent-insoluble ordered membrane domains. J Biol Chem **273**, 1150-1157.

216) Sengupta, P. K. and M. Kasha (1979). Excited state proton-transfer spectroscopy of 3-hytdroxyflavone and quercetin. Chem Phys Lett **68**(2-3), 382-385.

217) Sengupta, P., B. Baird and D. Holowka (2007). Lipid rafts, fluid/fluid phase separation, and their relevance to plasma membrane structure and function. Sem Cell Dev Biol **18**(5), 583-590.

218) Shaner, N. C., G. H. Patterson and M. W. Davidson (2007). Advances in fluorescent protein technology. J Cell Sci **120**, 4247-60.

219) Sharma, P., R. Varma, R. C. Sarasij, Ira, K. Gousset, G. Krishnamoorthy, M. Rao and S. Mayor (2004). Nanoscale organization of multiple GPI-anchored proteins in living cell membranes. Cell **116**(4), 577-589.

220) Shaw, A. (2006). Lipid rafts: now you see them, now you don't. Nature Immunol **7**(11), 1139-1142.

221) Shynkar, V., Y. Mely, G. Duportail, E. Piemont, A. Klymchenko and A. Demchenko (2003). Picosecond time-resolved fluorescence studies are consistent with reversible excited-state intramolecular proton transfer in 4 '-(dialkylaminoe)-3-hydroxyflavones. J Phys Chem A **107**(45), 9522-9529.

222) Shynkar, V. V., A. S. Klymchenko, C. Kunzelmann, G. Duportail, C. D. Muller, A. P. Demchenko, J. M. Freyssinet and Y. Mely (2007). Fluorescent biomembrane probe for ratiometric detection of apoptosis. J Am Chem Soc **129**(7), 2187-93.

223) Simons, K. and E. Ikonen (1997). Functional rafts in cell membranes. Nature **387**(6633), 569.

224) Simons, K. and W. Vaz (2004). Model systems, lipid rafts, and cell membranes. Ann Rev Biophys Biomol Struct **33**, 269-295.

225) Singer, S. J. and G. L. Nicolson (1972). The fluid mosaic model of the structure of cell membranes. Science **175**, 720-731.

226) Sinha, H. K. and S. K. Dogra (1986). Ground and exited state prototropic reaction in 2-(o-hydroxyphenyl)-benzimidazole. JChem Phys **102**, 337-347.

227) Slavik, J. (1982). Anilinonaphthalene Sulfonate as a Probe of Membrane-Composition and Function. Biochim Biophys Acta **694**(1), 1-25.

228) Smith, C., R. Mehta, D. F. Gibson, Z. Levashova, F. G. Blankenberg and J. F. Tait (2010). Characterization of a recombinant form of annexin VI for detection of apoptosis. Bioconjug Chem **21**(8), 1554-1558.

229) Soujanya, T., R. W. Fessenden and A. Samanta (1996). Role of nonfluorescent twisted intramolecular charge transfer state on the photophysical behavior of aminophthalimide dyes. J Phys Chem **100**(9), 3507.

230) Stadelmann, C. and H. Lassmann (2000). Detection of apoptosis in tissue sections. Cell Tissue Res **301**(1), 19.

231) Stekhoven, F. M., J. Tijmes, M. Umeda, K. Inoue and J. J. De Pont (1994). Monoclonal antibody to phosphatidylserine inhibits Na+/K(+)-ATPase activity. Biochim Biophys Acta **1194**(1), 155-65.

232) Stewart, G. T. (1961). Mesomorphic forms of lipid in structure of normal and Atheromatous Tissues. J Pathol Bacteriol **81**, 385-393.

233) Stillwell, W., S. R. Wassall, A. C. Dumaual, W. D. Ehringer, C. W. Browning and L. J. Jenski (1993). Use of merocyanine (MC540) in quantifying lipid domains and packing in phospholipid vesicles and tumor cells. Biochim Biophys Acta **1146**(1), 136-44.

234) Swinney, T. C. and F. D. Kelley (1993). Proton transfer dynamics in substituted 3-hydroxyflavones: Solvent polarization effects. J Chem Phys **99**, 211.

235) Sykora, J., P. Kapusta, V. Fidler and M. Hof (2002). On what time scale does solvent relaxation in phospholipid bilayers happen? Langmuir **18**(3), 571.

236) Sykora, J., P. Jurkiewicz, R. M. Epand, R. Kraayenhof, M. Langner and M. Hof (2005). Influence of the curvature on the water structure in the headgroup region of phospholipid bilayer studied by the solvent relaxation technique. Chem Phys Lipids **135**(2), 213-21.

237) Szabo G., Dolganiuc A., Dai Q., and Pruett S. B. (2007). TLR4, ethanol, and lipid rafts: A new mechanism of ethanol action with implications for other receptor-mediated effects. J Immunol **178**, 1243-1249.

238) Tait, J. F., D. Gibson and K. Fujikawa (1989). Phospholipid binding properties of human placental anticoagulant protein-I, a member of the lipocortin family. J Biol Chem **264**(14), 7944-9.

239) Tait, J. F. (2008). Imaging of apoptosis. J Nucl Med **49**(10), 1573-1576.

240) Takamori, S., M. Holt, K. Stenius, E. Lemke, M. Gronborg, D. Riedel, H. Urlaub, S. Schenck, B. Brugger, P. Ringler, S. Muller, B. Rammner, F. Grater, J. Hub, B. De Groot, G. Mieskes, Y. Moriyama, J. Klingauf, H. Grubmuller, J. Heuser, F. Wieland and R. Jahn (2006). Molecular anatomy of a trafficking organelle. Cell **127**(4), 831-846.

241) Tanaka, K. I. and S. Ohnishi (1976). Heterogeneity in the fluidity of intact erythrocyte membrane and its homogenization upon hemolysis. Biochim Biophys Acta **426**(2), 218-231.

242) Taylor, D. and N. Hooper (2006). The prion protein and lipid rafts. Mol Membr Biol **23**, 89-99.

243) Taylor, R. C., S. P. Cullen and S. J. Martin (2008). Apoptosis: controlled demolition at the cellular level. Nat Rev Mol Cell Biol **9**(3), 231-241.

244) Thompson, T. E. and T. W. Tillack (1985). Organization of glycosphingolipids in bilayers and plasma membranes of mammalian cells. Ann Rev Biophys Biophys Chem **14**, 361-386.

245) Tocanne, J. F., L. Dupou-Cezanne, A. Lopez and J. F. Tournier (1989). Lipid lateral diffusion and membrane organization. FEBS Lett **257**(1), 10-16.

246) Tocanne, J. F., L. Dupou-Cezanne and A. Lopez (1994). Lateral diffusion of lipids in model and natural membranes. Prog Lipid Res **33**(3), 203-237.

247) Tyska, M., R. Nambiar and R. McConnell (2010). Myosin motor function: the ins and outs of actin-based membrane protrusions. Cell Mol Life Sci **67**(8), 1239-1254.

248) Uchida, K., K. Emoto, D. L. Daleke, K. Inoue and M. Umeda (1998). Induction of apoptosis by phosphatidyl serine. J Biochem (Tokyo) **123**(6), 1073-8.

249) Ulrich, G., R. Ziessel and A. Harriman (2008). The chemistry of fluorescent bodipy dyes: Versatility unsurpassed. Angew Chem Int Ed Engl **47**(7), 1184.

250) Valeur, B. (2002). Molecular Fluorescence. Weinheim, Wiley VCH.

251) van Engeland, M., L. J. Nieland, F. C. Ramaekers, B. Schutte and C. P. Reutelingsperger (1998). Annexin V-affinity assay: a review on an apoptosis detection system based on phosphatidylserine exposure. Cytometry **31**(1), 1-9.

252) Varma, R. and S. Mayor (1998). GPI-anchored proteins are organized in submicron domains at the cell surface. Nature **394**(6695), 798-801.

253) Vazquez, M. E., J. B. Blanco and B. Imperiali (2005). Photophysics and biological applications of the environment-sensitive fluorophore 6-N,N-dimethylamino-2,3-naphthalimide. J Am Chem Soc **127**(4), 1300.

254) Veatch, S. L. and S. L. Keller (2005). Seeing spots: complex phase behavior in simple membranes. Biochim Biophys Acta **1746**(3), 172-85.

255) Vereb, G., J. Szollosi, J. Matko, P. Nagy, T. Farkas, L. Vigh, L. Matyus, T. Waldmann and S. Damjanovich (2003). Dynamic, yet structured: The cell membrane three decades after the Singer-Nicolson model. PNAS USA **100**(14), 8053-8058.

256) Watanabe, M., M. Hitomi, K. van der Wee, F. Rothenberg, S. Fisher, R. Zucker, K. Svoboda, E. Goldsmith, K. Heiskanen and A. Nieminen (2002). The pros and cons of apoptosis assays for use in the study of cells, tissues, and organs. Microscopy and Microanalysis **8**(5), 375-391.

257) Weber, G. and E. Daniel (1966). Cooperative effects in binding by bovine serum albumin. II. The binding of 1-anilino-8-naphthalenesulfonate. Polarization of the ligand fluorescence and quenching of the protein fluorescence. Biochemistry **5**, 1900-1907.

258) Weber, G. and F. J. Farris (1979). Synthesis and spectral properties of a hydrophobic fluorescent probe: 6-propionyl-2-(dimethylamino)naphthalene. Biochemistry **18**(14), 3075-8.

259) Weller, A. (1956). Innermolekularer Protonenubergang im angeregten Zustand. Z Elektrochem **60**, 1144.

260) Westover, E., D. Covey, H. Brockman, R. Brown and L. Pike (2003). Cholesterol depletion results in site-specific increases in epidermal growth factor receptor phosphorylation due to membrane level effects - Studies with cholesterol enantiomers. J Biol Chem **278**(51), 51125-51133.

261) Wiener, M. C. and S. H. White (1992). Structure of a fluid dioleoylphosphatidylcholine bilayer determined by joint refinement of x-ray and neutron diffraction data. III Complete structure. Biophys J **61**, 434–447.

262) Williamson, P., J. Bateman, K. Kozarsky, K. Mattocks, N. Hermanowicz, H. R. Choe and R. A. Schlegel (1982). Involvement of spectrin in the maintenance of phase-state asymmetry in the erythrocyte membrane. Cell **30**(3), 725-733.

263) Williamson, P., A. Kulick, A. Zachowski, R. A. Schlegel and P. F. Devaux (1992). Ca^{2+} induces transbilayer redistribution of all major phospholipids in human erythrocytes. Biochemistry **31**(27), 6355.

264) Williamson, P., K. Mattocks and R. A. Schlegel (1983). Merocyanine 540, a fluorescent probe sensitive to lipid packing. Biochim Biophys Acta **732**(2), 387-93.

265) Wolters, S. L., M. F. Corsten, C. P. Reutelingsperger, J. Narula and L. Hofstra (2007). Cardiovascular molecular imaging of apoptosis. Eur J Nucl Med Mol Imaging **34**, S86-98.

266) Woolfe, G. J. and P. J. Thistlethwaite (1981). Direct observation of excited state intramolecular proton transfer kinetics in 3-hydroxyflavone. J Am Chem Soc **103**, 6916-6923.

267) Wu J., W. Liu, J. Ge, H. Zhang and P. Wang (2011). New sensing mechanisms for design of fluorescent chemosensors emerging in recent years. DOI: 10.1039/c0cs00224k.

268) Xie, N., D. Zeng and Y. Chen (2006). 3,4-Bis(5-iodo-2-methylthien-3-yl)-2,5-dihydrothiophene: A Powerful Synthon for the Preparation of Photochromic Dithienylethene Derivatives. Synlett (5), 737-740.

269) Xu, X. and E. London (2000). The effect of sterol structure on membrane lipid domains reveals how cholesterol can induce lipid domain formation. Biochemistry **39**(5), 843-849.

270) Yesylevskyy, S. O., A. S. Klymchenko and A. P. Demchenko (2005). Semi-empirical study of two-color fluorescent dyes based on 3-hydroxychromone. J Mol Struct **755**(1-3), 229.

271) Yu, J. and T. L. Steck (1973). Selective solubilization of proteins and phospholipids from red blood cell membranes by nonionic detergents. J Supramol Struct **1**(3), 220-248.

272) Yamaji-Hasegawa A. and M. Tsujimoto. (2006). Asymmetric distribution of phospholipids in biomembranes. Biol Pharm Bull **29**(8), 1547-1553.

273) Zachowski, A. (1993). Phospholipids in animal eukaryotic membranes: transverse asymmetry and movement. Biochem J **294**, 1-14.

274) Zeng, J. and P. L. Chong (1995). Effect of ethanol-induced lipid interdigitation on the membrane solubility of Prodan, Acdan, and Laurdan. Biophys J **68**(2), 567-73.

275) Zhan, X., C. Risko, F. Amy, C. Chan, W. Zhao, S. Barlow, A. Kahn, J. Bredas and S. Marder (2005). Electron affinities of 1,1-diaryl-2,3,4,5-tetraphenyisiloles: Direct measurements and comparison with experimental and theoretical estimates. J Am Chem Soc **127**(25), 9021-9029.

276) Zwaal, R. F. and A. J. Schroit (1997). Pathophysiologic implications of membrane phospholipid asymmetry in blood cells. Blood **89**(4), 1121-32.

277) Zweifach, A. (2000). FM1-43 reports plasma membrane phospholipid scrambling in T-lymphocytes. Biochem J **349**, 255-60.

6. PUBLICATION LIST

Articles in peer-reviewed journals:

1. Oncul, S., Klymchenko, A., **Kucherak, O.A.**, Demchenko, A.P., Martin, S., Dontenwill, M., Arntz, Y., Didier, P., Duportail, G., Mély, Y. Liquid ordered phase in cell membranes evidenced by a hydration-sensitive probe: Effects of cholesterol depletion and apoptosis. *Biochem.Biophys.Acta* **2010**, 1798, 1436-1443.
2. **Kucherak, O.A.**, Oncul, S., Darwich, Z., Yushchenko, D.A., Arntz, Y., Didier, P., Mély, Y., Klymchenko, A. Switchable Nile Red-based probe for cholesterol and lipid order at the outer leaflet of biomembranes. *J.Am.Chem.Soc.* **2010**, 132, 4907-4916.
3. **Kucherak, O.A.**, Didier, P., Mély, Y., Klymchenko A. Fluorene analogues of Prodan with superior fluorescence brightness and solvatochromism. *J.Phys.Chem.Lett.* **2010**, 1, 616-620.
4. **Kucherak, O.A.**, Richert, L., Mély, Y., Klymchenko, A. Dipolar 3-methoxychromones as bright and highly solvatochromic fluorescent dyes (submitted to Physical Chemistry Chemical Physics).
5. Darwich, Z., **Kucherak, O.A.**, Richert, L., Klymchenko, A., Mély, Y. Improved probes for apoptosis based on 3-hydroxyflavone (in preparation).

Results were presented at the following congresses:

1. **Kucherak O.** Fluorescent probes for apoptosis detection. *Journées de l'Ecole Doctorale*, Université de Strasbourg, 17-18 Décembre 2008 (présentation orale).
2. **Kucherak O.**, Oncul S., Martin S., Dontenwill M., Klymchenko A., Mély Y. Development of new fluorescent membrane probes for apoptosis and raft domains. *Journées Campus d'Illkirch* 2009, Pôle API Illkirch, 16-17 Avril 2009 (poster).
3. **Kucherak O.**, Oncul S., Martin S., Dontenwill M., Arntz Y., Klymchenko A., Mély Y. Cholesterol-rich domains and apoptosis studied by new fluorescent membrane probes. *7th EBSA European Biophysics Congress*, Gênes, Italie, 11-15 July 2009 (poster).
4. **Kucherak O.**, Oncul S., Duportail G., Mély Y., Klymchenko A. Development of new fluorescent membrane probes for apoptosis and raft domains. *11th MAF Conference on Methods and Applications of Fluorescence*, Budapest, Hongrie, 6-9 Septembre 2009 (poster).
5. **Kucherak O.**, Darwich Z., Oncul S., Richert L., Klymchenko A., Mély Y. New fluorescent molecular probes for apoptosis and lipid domains. *Journées Campus d'Illkirch* 2010, Pôle API Illkirch, 3-4 Mai 2010 (poster).

PUBLICATIONS

Spotlight

Riboswitch Switch Hitters

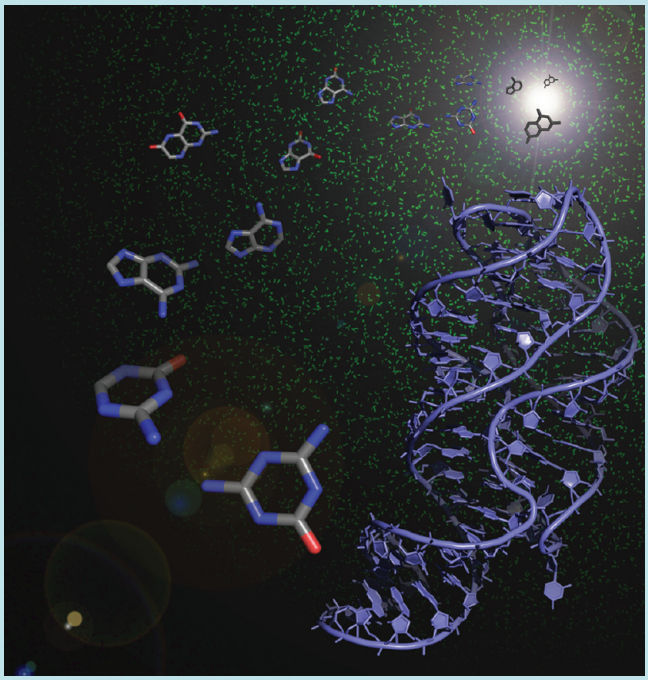

Riboswitches are structured RNA scaffolds that adopt different tertiary structures in the presence or absence of a small molecule effector. These RNA sensors, first discovered in bacteria, detect the levels of a metabolite and regulate genes involved in metabolite biosynthesis or catabolism. Riboswitches can alter the neighboring gene's expression via a variety of mechanisms, affecting either translation or transcription, and thus play critical roles in autoregulating numerous metabolic pathways. Using a riboswitch as an artificial sensor or structural switch would be an attractive tool for biologists, but unfortunately the cognate ligands are often common cellular currency like thiamine pyrophosphate, adenine, or amino acids and would therefore lead to leaky basal expression levels.

Now, Dixon *et al.* (*Proc. Natl. Acad. Sci. U.S.A.* 2010, *17*, 2830−2835) has used one well studied riboswitch to serve as a blueprint in the search for a new RNA switch that no longer responds to the parent ligand but does respond to new ligands not found naturally in cells. The *add* A switch usually senses adenine levels and upregulates expression of the neighboring adenine deaminase gene. The RNA structural arrangement upon binding to adenine was previously solved by X-ray crystallography, and the new study used this information to guide mutations that might alter that specificity. With panels of mutant riboswitches in hand and a battery of almost 80 small molecules, a clever screen in bacteria searched for the RNA/small molecule combinations capable of upregulating a neighboring reporter gene. Mutant *add* A riboswitches that could now respond to synthetic heterocyclic compounds ammeline and azacytosine were chosen for further characterization. Using these RNA switches upstream of GFP allowed for easy screening of additional mutants within bacterial cells. Further refinement of the new M6 riboswitches improved the maximum yield of GFP produced, allowing for a tunable system that gives low, medium, or high expression levels. Finally, to bring the study full circle, the authors solved the X-ray structure of the M6C′′ mutant aptamer domain complexed with azacytosine. They observed how the mutant *add* A-riboswitch has lost selectivity of binding for adenine but gained it for the new ligand. Since the identified ligands are not naturally found inside of cell, these new riboswitches and future ones selected via similar methods could become interesting candidates for engineered switches to control gene expression inside of living cells. **Jason G. Underwood, Ph.D.**

To the Nile for Membrane Characterization

The lipid components of cell membranes are key players in directing membrane structure and function. In particular, strong interactions between cholesterol and the phospholipid sphingomyelin result in a highly packed state in lipid bilayers, called liquid ordered (Lo) phase. Lo phase is distinct from the loosely packed phase formed by cholesterol and other lipids, referred to as liquid disordered (Ld) phase. However, few molecular tools exist that effectively distinguish between Lo and Ld phases *and* selectively target the outer leaflet of cell membranes, which contains the majority of sphingomyelin. Toward gaining a better understanding of the structural and functional relevance of Lo domains in cell membranes, Kucherak *et al.* (*J. Am. Chem. Soc.* 2010, *132*, 4907−4916) developed a fluorescent probe, referred to as NR12S, that is highly selective for the outer leaflet and effectively discriminates between Lo and Ld phases.

Published online April 16, 2010 • 10.1021/cb100086a

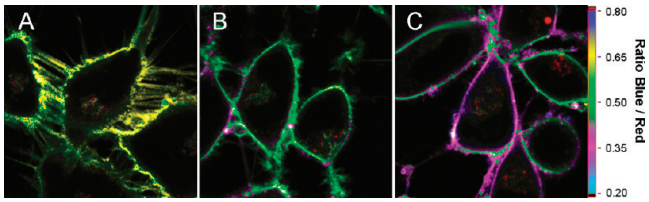

Based on the fluorophore Nile Red, NR12S also contains a long alkyl chain and a zwitterionic group, which presumably enhance its interactions with lipid membranes. Characterization of NR12S demonstrated its high selectivity for the outer leaflet of both model lipid vesicles and live cell membranes. In addition, in contrast to Nile Red itself, NR12S is not internalized, nor does it flip-flop between the inner and outer leaflet. Experiments in model vesicles revealed a significant blue shift in the emission maximum of NR12S in the presence of Lo phase versus Ld phase, illustrating its ability to distinguish the two phases. When examined in live cells, the emission maximum was in between those of Lo and Ld phases, consistent with what is known about composition of plasma membranes. Importantly, the emission color of NR12S was sensitive to increases or decreases in the cholesterol content of the membranes, demonstrating its utility for monitoring cholesterol content as well. These properties make NR12S a valuable tool for investigation of lipid order in model and cell membranes selectively at one leaflet. **Eva J. Gordon, Ph.D.**

Skp-ping to a Cancer Cure

Cellular senescence refers to a process in which cells become unable to divide. Recent evidence has linked cellular senescence to tumor suppression mechanisms, hinting that researchers might be able to hijack the process for the purpose of fighting cancer. Studies have suggested that senescence is dependent on activation of the p19Arf-p53 tumor suppressor pathway, but the frequent mutations in this pathway that are associated with human cancers have confounded the pursuit of senescence as an anticancer strategy. Now, Linet *et al.* (*Nature* 2010, *464*, 374−379) revive senescence in the fight against cancer by discovering the anticancer potential of inhibiting Skp2, a key component of the ubiquitin E3 ligase Skp2-SCF.

Skp2 is overexpressed in many human cancers but is not necessary for survival in mice, making it an intriguing cancer target. Interestingly, it was found that inactivation of the *Skp2* gene in mouse embryonic fibroblasts does not trigger senescence. However, when strong oncogenic signals are present, *Skp2* deficiency triggers a powerful, tumor-suppressive senescence response. Notably, unlike other senescence processes, this response was not associated with DNA damage, nor did it depend on the p19Arf-p53 pathway. Rather, Skp2-triggered senescence was dependent on upregulation of the endoplasmic reticulum stress protein Atf4 and the cyclin-dependent kinase inhibitor proteins p21 and p27. Importantly, inactivation of *Skp2* significantly reduced tumor progression in mouse models of prostate cancer, and investigation into the mechanism of action suggested that in the presence of an oncogenic stimulus inactivation of *Skp2* enhances and prolongs the senescence response. Finally, exposure of prostate cancer cells and mouse models of prostate cancer to a small molecule inhibitor of the Skp2-SCF complex resulted in induction of senescence and slowed tumor growth, respectively. These exciting findings implicate Skp2 and the senescence response as important cancer targets, and point to small molecule inhibitors of Skp2 function as potential cancer drugs. **Eva J. Gordon, Ph.D.**

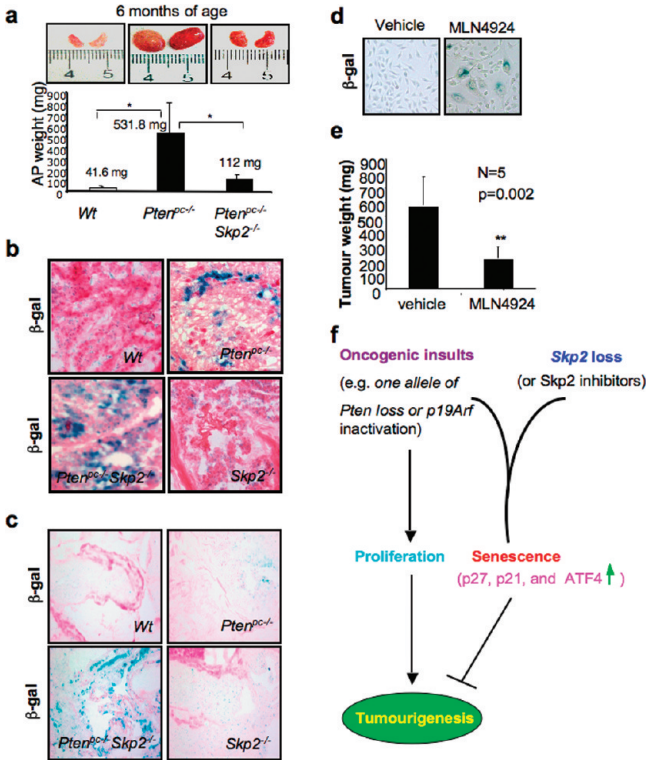

Thalidomide Makes a Molecular Debut

In the 1950s and 60s, many pregnant women battled morning sickness with what they thought was a sedative drug, thalidomide. Sadly, the unseen effects of thalidomide on the fetus would not be fully realized until over 10,000 children were born with birth defects, mostly involving limb formation or size abnormalities. Decades later, the molecular mechanism of the drug's ill effects remained controversial and largely unsolved.

Now, a new study by Ito *et al.* (*Science* 2010 327, 1345−50) has used a powerful combination of biochemistry and developmen-

PUBLICATION 1

LIQUID ORDERED PHASE IN CELL MEMBRANES EVIDENCED BY A HYDRATION-SENSITIVE PROBE: EFFECTS OF CHOLESTEROL DEPLETION AND APOPTOSIS

Biochimica et Biophysica Acta 1798 (2010) 1436–1443

Contents lists available at ScienceDirect

Biochimica et Biophysica Acta

journal homepage: www.elsevier.com/locate/bbamem

Liquid ordered phase in cell membranes evidenced by a hydration-sensitive probe: Effects of cholesterol depletion and apoptosis

Sule Oncul [1], Andrey S. Klymchenko *, Oleksandr A. Kucherak, Alexander P. Demchenko, Sophie Martin, Monique Dontenwill, Youri Arntz, Pascal Didier, Guy Duportail, Yves Mély

Laboratoire de Biophotonique et Pharmacologie, UMR 7213 CNRS, Université de Strasbourg, Faculté de Pharmacie, 74, Route du Rhin, 67401 ILLKIRCH Cedex, France

ARTICLE INFO

Article history:
Received 13 August 2009
Received in revised form 14 December 2009
Accepted 14 January 2010
Available online 25 January 2010

Keywords:
Cell plasma membrane
Lipid bilayers
Liquid ordered phase
Hydration
Fluorescent probes
Cholesterol depletion

ABSTRACT

Herein, using a recently developed hydration-sensitive ratiometric biomembrane probe based on 3-hydroxyflavone (F2N12S) that binds selectively to the outer leaflet of plasma membranes, we compared plasma membranes of living cells and lipid vesicles as model membranes. Through the spectroscopic analysis of the probe response, we characterized the membranes in terms of hydration and polarity (electrostatics). The hydration parameter value in cell membranes was in between the values obtained with liquid ordered (Lo) and liquid disordered (Ld) phases in model membranes, suggesting that cell plasma membranes exhibit a significant fraction of Lo phase in their outer leaflet. Moreover, two-photon fluorescence microscopy experiments show that cell membranes labeled with this probe exhibit a homogeneous lipid distribution, suggesting that the putative domains in Lo phase are distributed all over the membrane and are highly dynamic. Cholesterol depletion affected dramatically the dual emission of the probe suggesting the disappearance of the Lo phase in cell membranes. These conclusions were corroborated with the viscosity sensitive diphenylhexatriene derivative TMA-DPH, showing membrane fluidity in intact cells intermediate between those for Lo and Ld phases in model membranes, as well as a significant increase in fluidity after cholesterol depletion. Moreover, we observed that cell apoptosis results in a similar loss of Lo phase, which could be attributed to a flip of sphingomyelin from the outer to the inner leaflet of the plasma membrane due to apoptosis-driven lipid scrambling. Our data suggest a new methodology for evaluating the Lo phase in membranes of living cells.

1. Introduction

Cellular membranes are not just barriers separating inner and outer cellular volumes but are critical for communication with the outer world by enabling the transfer of many compounds important for cell metabolism and for chemical and electrical signaling. A deeper analysis of the essential role played by lipid bilayers in the integration of membrane proteins has led to the hypothesis of lipid domains or "rafts". The lipid domains have received a large attention [1–9] due to their involvement in many cell functions ranging from regulation of membrane protein activity to membrane trafficking, sorting and signal transduction [10–16]. However, detecting and visualizing lipidic domains is not a simple task, and even their definition is controversial and depends on the experimental methods used for their observation [17,18].

Lipid domains are first identified by their composition: They are enriched in saturated lipids (mainly sphingolipids) and sterols (mainly cholesterol) that form a liquid ordered (Lo) phase. The phase separation between Lo phase and liquid disordered (fluid) phase (Ld) can be observed in model membranes as rafts floating in a sea of loosely-packed domains enriched in unsaturated phospholipids [10,19–22]. Using different techniques (single-particle tracking [23,24], single-molecule microscopy [25], fluorescence correlation spectroscopy [26,27], confocal microscopy [28,29] and spin-label ESR [30]), various amounts of Lo phase (from 10 to 80%) and raft sizes (from 10 to 1000 nm) were reported within cell plasma membranes.

Fluorescence probing is one of the most convenient methods for visualizing and quantifying lipid domains on cell membranes. The probes used for that purpose are either highly selective for domains of a particular phase or partition evenly into Lo and Ld phases providing a different fluorescence response in each phase. Such requirements might help visualizing domains by fluorescence microscopy [17,31,32]. The most common marker is the fluorescently labeled protein Cholera toxin-B (CT-B from bacterium *Vibrio cholerae*), which binds selectively to the ganglioside G_{M1} associated with Lo phase domains in biomembranes [24,33,34]. Because of their exclusion from the Lo phase, most of the molecular membrane probes (lipid-like probes) are not suited for staining Lo phase domains in model systems (or cell membranes) [11]. Remarkable exceptions to this rule are

* Corresponding author. Tel.: +33 368 854255; fax: +33 368 854313.
E-mail address: aklymchenko@pharma.u-strasbg.fr (A.S. Klymchenko).
[1] Present address: Acibadem University, School of Medicine, Department of Biophysics, Fevzi Cakmak Cd. Divan Sk. No:1, 34848, Maltepe, Istanbul, Turkey.

0005-2736/$ – see front matter © 2010 Elsevier B.V. All rights reserved.
doi:10.1016/j.bbamem.2010.01.013

several saturated lipids, fluorescently labeled at their head groups with NBD [19] or Cy5 [25] and GFP-labeled glycosylphosphatidylinositol, [28,35,36]), as well as fluorescent dyes with long alkyl chains, such as LcTMA-DPH [37,38] or diI-C20 [39], or polycyclic probes, such as Terrylene or Naphtopyrene, which show a preferential partitioning for ordered phases in model membranes [40]. However, most of these probes suffer from the dependence of their partition between Lo and Ld phases on the lipid composition of the actual Lo phase domain [41].

Environment-sensitive molecular probes, such as Laurdan [41–43] and its derivatives [44,45] or di-4-ANEPPDHQ [46] constitute improved alternatives for studies of lipid domains in model membranes and cells. These probes distribute in both Ld and Lo phases of membranes and their emission color, intensity, and/or lifetime depend strongly on the local membrane properties (polarity, hydration or fluidity), that in turn are related to the phase state of the membrane. This probe sensitivity to the membrane properties allows a direct visualization of the membrane lateral heterogeneities in model and native biological membranes. Recently, we have shown the application of a novel membrane probe, (N-[[4′-N,N-diethylamino-3-hydroxy-6-flavonyl]-methyl]-N-methyl-N-(3-sulfopropyl)-1-dodecanaminium, inner salt (F2N12S), Fig. 1) for imaging lipid domains in membrane models [47]. This probe belongs to the family of 3-hydroxyflavones (3HFs) and exhibit a dual emission due to its excited-state intramolecular proton transfer (ESIPT) reaction, which is highly sensitive to the environment [48,49]. The ratio of the two emission bands of 3HFs is a valuable analytical signal for probing biological membranes [50] as it is affected by various physicochemical properties of the environment [49], including hydration [51], surface charge [52,53], membrane dipole and transmembrane potentials [54–56]. These dyes show dramatic differences in their fluorescence spectra when membrane vesicles presenting Ld and Lo phases were compared [57]. It was shown that the hydration of the probe is a key parameter to differentiate Lo phase from Ld and gel (L_{β}) phases in large unilamellar vesicles (LUVs) [58]. Using a 3HF probe, the hydration could be quantitatively estimated from the ratio between the hydrated and non-hydrated forms of the probe (Fig. 1) obtained through the band separation analysis of its fluorescence spectrum [51]. The peculiarity of the F2N12S probe is its ability to bind spontaneously to the outer leaflet of the cell plasma membrane without fast transfer to the inner leaflet and internalization into the cell. This makes F2N12S sensitive to the changes in the transmembrane lipid asymmetry taking place during apoptosis [53]. It was shown that cell apoptosis, which results in the loss of the transmembrane asymmetry, modifies strongly the dual emission of the F2N12S probe. However, this spectroscopic response could not be explained by the sole increase in the exposure of PS at the outer leaflet of the cell. Since F2N12S can bind both Ld and Lo phases, showing a different dual emission [47], we hypothesized that the observed response of the probe to apoptosis could also be driven by changes in the phase state (Lo/Ld) of the outer leaflet [47,53].

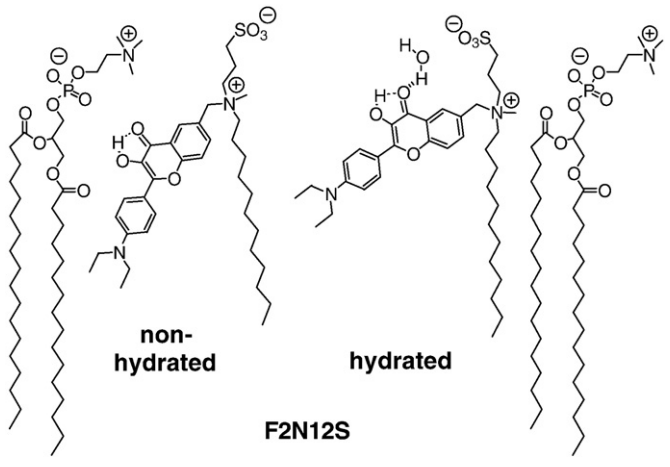

Fig. 1. Probe F2N12S and its two expected forms in lipid bilayers (schematically presented as a monolayer): non-hydrated and hydrated (water-bound).

In the present work, we used F2N12S probe for spectroscopic and microscopic studies of the distribution of Lo/Ld phases in the plasma membranes of living cells (human U87MG glioblastoma). The data were compared to those obtained in lipid vesicles with controlled phase state and surface charge. We did not observe any separation between Lo and Ld phases in intact cells, and the spectroscopic analysis suggested that the Lo phase constitutes an important fraction of the outer leaflet of the plasma membrane. We showed that the fraction of Lo phase could be modulated in a rather broad range by extraction of cholesterol using methyl-β-cyclodextrin (MβCD). Finally, apoptosis was also found to result in a loss of Lo phase of the outer leaflet, probably due to the loss of the transmembrane lipid asymmetry leading to a lower content of sphingomyelin (SM) within this leaflet.

2. Materials and methods

Dioleoylphosphatidylcholine (DOPC), palmitoyloleoylphosphatidylcholine (POPC), dioleoylphosphatidylserine (DOPS), egg yolk phosphatidylcholine (EYPC), bovine brain phosphatidylserine (BBPS) and cholesterol were purchased from Sigma-Aldrich. Bovine brain sphingomyelin (SM) was from Avanti Polar Lipids (Alabaster, USA). N-[[2-[4-Diethylaminophenyl]-3-hydroxychromon-6-yl]-methyl]-N-methyl-N-(3-sulfopropyl)-1-dodecanaminium, inner salt, was synthesized as described [53]. This probe was pure according to thin layer chromatography, ^{1}H-NMR data, absorption and fluorescence spectra in organic solvents. 1-(4-Trimethylammoniumphenyl-6-phenyl-1,3,5-hexatriene p-toluenesulfonate (TMA-DPH) was from Molecular Probes (Invitrogen).

Large unilamellar vesicles (LUVs) were obtained by the classical extrusion method as previously described [58]. Briefly, a suspension of multilamellar vesicles was extruded by using a Lipex Biomembranes extruder (Vancouver, Canada). The size of the filters was first 0.2 μm (7 passages) and thereafter 0.1 μm (10 passages). This protocol leads to monodisperse LUVs with a mean diameter of 0.11 μm as measured with a Malvern Zetamaster 300 (Malvern, UK). LUVs were labeled by adding aliquots (generally 2 μl) of probe stock solutions in dimethyl sulfoxide to 2-ml solutions of vesicles. Since the binding kinetics is very rapid for both probes, the fluorescence experiments were performed a few minutes after addition of the aliquot. A 15 mM phosphate–citrate, pH 7.0 buffer was used in these experiments. Concentrations of the probes and lipids were 2 and 200 μM, respectively.

U87MG human glioblastoma cell line (ATCC) was cultured in Eagle's minimal essential medium (EMEM from LONZA) with 10% heat-inactivated fetal bovine serum (PAN Biotech GmbH) and 0.6 mg/ml glutamine (Biowhittaker) at 37 °C in a humidified 5% CO_2 atmosphere. Cell concentration of $5–10\times10^4$ cells/ml was maintained by removal of a portion of the culture and replacement with fresh medium 3 times per week.

For apoptosis induction by actinomycin D, cells were counted with a hemacytometer and seeded at a suitable density for spectroscopy and microscopy studies (3×10^5 cells per well in six-well plate and 5×10^5 cells per well in IBIDI LabTek, respectively). Culture medium was changed every day and cells were grown during 3 days. Then apoptosis was induced by 18 h incubation of cells with actinomycin D (0.5 μg/ml). For cholesterol extraction, MβCD (Sigma-Aldrich) stock solutions were prepared with DPBS and filtered by a Millipore filter (0.2 μm). The initial cell number was the same as for apoptosis induction. The following MβCD concentrations and incubation times were used: 5 mM MβCD for 2 h, 5 mM MβCD for 30 min and 2 mM MβCD for 15 h.

In fluorescence spectroscopy experiments, cells were detached by trypsinization as described below. Firstly, EMEM medium was removed from culture dishes and cells were washed two times with dPBS. Then, trypsin 10x (LONZA) solution was diluted 10 times by dPBS and added to cover the bottom of the culture vessel. Cells were incubated in a 37 °C incubator for 4 min. The solution of trypsin with cells was then diluted by dPBS, transferred to Falcon tubes and centrifuged at 1500 RPM for 5 min. The washing procedure was repeated one more time with HBSS solution.

To stain the cells in suspension with the F2N12S probe, an appropriate aliquot of its stock solution in DMSO was added to 0.5 ml HBSS buffer and after vortexing the solution was immediately added to 0.5 ml of the cell suspension to obtain a final probe concentration of 0.1 μM (<0.25% DMSO). The cell concentration was 5×10^5–10^6 cells/ml. It should be noted that only a freshly prepared solution of the probe in HBSS should be used (<3 min) for cell staining, due to the slow aggregation of the probe in water. Prior to the measurements, the cell suspension with the probe was incubated for 7 min at room temperature in the dark. For microscopy studies, attached cells were washed twice by gentle rinsing with HBSS. A freshly prepared solution of F2N12S in HBSS was added to the cells to a final concentration of 0.3 μM (<0.25% DMSO volume) and incubated for 7 min in the dark. Staining of cells with TMA-DPH probe was performed using an adapted procedure as previously described [59]. First, 2 μl of 5×10^{-4} M of TMA-DPH stock solution in DMF was added to 1 ml of HBSS buffer. After vigorous vortexing, a 200 μl aliquot of this solution was immediately added to 800 μl of cell suspension and vortexed again. The final probe concentration was 0.2 μM, while the cell concentration was 2×10^5 cells/ml. After 2 min of incubation the samples were ready for fluorescence anisotropy measurements.

Fluorescence spectra of probe F2N12S were recorded on a Jobin-Yvon Fluoromax 3 (Longjumeau, France) spectrofluorometer and corrected by subtracting the spectra of the corresponding blank (unlabeled vesicles or cell suspensions). Excitation wavelength was systematically set at 400 nm. For fluorescence anisotropy measurements with TMA-DPH, a SLM 8000 spectrofluopolarimeter in the T-format was used as previously described [59]. Briefly, the excitation wavelength was set at 350 nm, and the emission was collected through 435 nm interference filters (Schott, Germany). Each sample was measured at least 10 times over 20 s at 20 °C under gentle magnetic stirring. The obtained fluorescence anisotropy values were averaged and corrected for the scattered light as previously described [59], using corresponding unlabeled cell suspensions as blanks. Two-photon fluorescence microscopy experiments were performed on a home-built two-photon laser scanning set-up based on an Olympus IX70 inverted microscope with an Olympus 60× 1.2NA water immersion objective [60,61]. Two-photon excitation was provided by a titanium-sapphire laser (Tsunami, Spectra Physics) and photons were detected with Avalanche Photodiodes (APD SPCM-AQR-14-FC, Perkin Elmer) connected to a counter/timer PCI board (PCI6602, National Instrument). Imaging was carried out using two fast galvo mirrors in the descanned fluorescence collection mode. Typical acquisition time was 5 s with an excitation power around 2.5 mW (830 nm) at the level of the sample. Images corresponding to N* and T* emission bands were recorded simultaneously using a dichroic mirror (Beamsplitter 550 DCXR) and two band-pass filters (Brightline HC 520/20 and HQ 585/40) in front of the APDs [47]. The images were processed with a home-made program under LabView that generates a ratiometric image by dividing the image of the N* band by that of the T* band. For each pixel, a pseudo-color scale is used for coding the ratio, while the intensity is defined by the integral intensity recorded for both channels at the corresponding pixel.

Deconvolution of probe F2N12S fluorescence into three bands (N*, H–N* and T*) was performed using the Siano software kindly provided by Dr. A.O. Doroshenko (Kharkov, Ukraine), as previously described [51,57]. The program is based on an iterative nonlinear least-squares method, where the individual emission bands were approximated by a log-normal function accounting for several parameters: maximal amplitude, I_{max}, spectral maximum position, ν_{max}, and position of half-maximum amplitudes, ν_1 and ν_2, for the blue and red parts of the band, respectively. These parameters determine the shape parameters of the log-normal function, namely full width at the half-maximum, $FWHM=\nu_1-\nu_2$, and band asymmetry, $P=(\nu_1-\nu_{max})/(\nu_{max}-\nu_2)$. An example of deconvolution is presented in Fig. 2B. The resulting fluorescence intensities of the separated N*, H–N* and T* bands (I_{N^*}, I_{H-N^*} and I_{T^*}) were used for calculation of the hydration parameter, which was expressed as the ratio of the peak emission intensity of the hydrated (H–N*) form to the summed intensities of the non-hydrated (N* and T*) forms. Taking into account that the FWHM for the T* band is ca 2.5-fold narrower than for the N* and H–N* bands, the hydration was estimated as $I_{H-N^*}/(I_{N^*}+0.4\times I_{T^*})$. The "polarity" parameter was expressed as I_{N^*}/I_{T^*} ratio [51,57].

3. Results and discussion

Being bound to U87MG glioblastoma cells, probe F2N12S shows a dual emission (Fig. 2), similar to that previously reported in other cellular systems [47,53]. Remarkably, the emission spectrum of F2N12S in U87MG glioblastoma cells shows a much larger band separation than in model vesicles made of unsaturated phospholipids DOPC, POPC or EYPC (Fig. 2, Table 1), so that the short-wavelength emission band is significantly blue-shifted in the former. In vesicles composed of DOPC, POPC or EYPC with cholesterol (phospholipid/chol, 2/1, mol/mol), the short-wavelength band of F2N12S is somewhat blue-shifted and decreased in relative intensity in respect with the corresponding vesicles in the absence of cholesterol (Fig. 2,

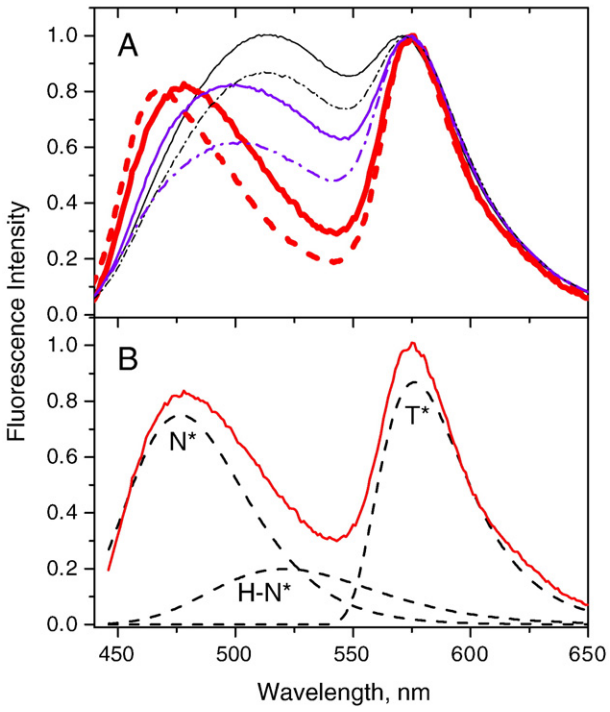

Fig. 2. Fluorescence spectra of probe F2N12S in suspensions of cells and LUVs. (A) Fluorescence spectra in non-treated U87MG cells (thick solid red curve) and in LUVs of different lipid composition: DOPC (solid black curve), POPC (dash-dotted black curve), DOPC/Chol, (solid blue curve), POPC/Chol (dash-dotted blue curve) and SM/Chol (thick dashed red curve). Concentrations of lipids and probe were 200 μM, and 2 μM, respectively. Excitation wavelength was 400 nm. (B) Fluorescence spectrum of F2N12S in non-treated U87MG cells (solid curve) and the three separated bands (dashed curves) obtained by deconvolution of this spectrum.

Table 1
Spectroscopic data and estimated values of polarity and hydration obtained with probe F2N12S in model membranes and living cells.[a]

Sample	λ_{SW}, nm	I_{SW}/I_{LW}	Hydration	Polarity
DOPC	512	1.00	0.61	1.63
POPC	512	0.87	0.56	1.18
EYPC	512	0.91	0.56	1.27
BBPS	504	1.27	0.36	2.25
DOPS	505	1.41	0.38	3.24
DOPC/Chol	499	0.82	0.39	1.20
POPC/Chol	501	0.61	0.37	0.77
EYPC/Chol	497	0.73	0.32	0.98
BBPS/Chol	492	0.94	0.23	1.33
DOPS/Chol	496	1.21	0.26	2.06
SM/Chol	470	0.70	0.01	0.88
SM/DOPC/Chol	494	0.84	0.32	1.22
Intact cells	478	0.83	0.18	0.86
Cells-MβCD	497	1.18	0.58	1.07
Apoptotic cells	489	1.38	0.34	1.47

[a] λ_{SW} — position of the maximum of the short-wavelength band, I_{SW}/I_{LW} —intensity ratio of the short- to the long-wavelength bands at their maxima. Hydration and polarity were estimated from the deconvolution of the corresponding spectra into three bands, as shown in Fig. 2B. SM/DOPC/Chol corresponds to 1/1/1 molar ratio of the lipids. Cells-MβCD corresponds to the extraction of cholesterol with 5 mM MβCD for 2 h. The spectroscopic values are an average of several independent measurements: commonly two for lipid vesicles and three for cells. The estimated errors: λ_{SW} ±2 nm for vesicles and ±3 nm for cells; I_{SW}/I_{LW} ±2% for vesicles and ±3% for cells; hydration ±5% for vesicles and ±7% for cells; Polarity ±3% for vesicles and ±5% for cells.

Table 1), but the spectra are still largely differed from that in cells. Thus, comparison of the spectra suggests that lipid membranes of unsaturated phospholipids with or without cholesterol, presenting a liquid disordered (Ld) phase [19–22] cannot model cell plasma membranes. In contrast, the spectrum in U87MG cells is close to that obtained with vesicles composed of SM and cholesterol (SM/Chol 2/1 mol/mol), a composition which corresponds to the liquid ordered (Lo) phase [62].

To quantitatively analyze the spectral data for describing the physicochemical properties of lipid membranes, we used the band-decomposition methodology previously developed for probe F2N8, a close analogue of F2N12S [51]. This method decomposes the fluorescence spectrum of the probe into three bands corresponding to normal (N*), H-bonded normal (H–N*) and tautomer (T*) forms of the dye (Fig. 2B). The obtained separated bands allow a simultaneous estimation of the two independent "hydration" and "polarity" parameters [50,51]. For F2N12S probe, the polarity estimated through the N*/T* ratio of the H-nonbonded forms of the probe (Fig. 1) correlates well with the surface charge of the vesicles. Indeed, the polarity parameter strongly increases in anionic lipid vesicles (DOPS and BBPS) as compared to the corresponding neutral vesicles (DOPC, POPC and EYPC) (Table 1), in line with previous data obtained for probes of the same family [50,63]. Cholesterol also decreases this parameter for all unsaturated lipids studied (Table 1), but does not mask the effect of surface charge. In contrast to the polarity parameter, the hydration parameter, deduced from the relative contribution of the H-bonded (hydrated) (Fig. 1), is critically dependent on the lipid phase. Indeed, in Lo phase vesicles (SM/Chol), this parameter is much lower than in all studied Ld phase vesicles (Table 1), confirming that the Lo phase is strongly dehydrated [57]. Noticeably, a significant decrease of the hydration parameter value in the Ld phase is also observed in the presence of cholesterol, in line with the well-known dehydration effect of cholesterol in membranes [64] (Table 1).

In U87MG cells, the hydration parameter is much lower than in any Ld phase vesicles studied, but higher than in Lo phase vesicles. Moreover, the polarity parameter measured in cell membranes corresponds well to that in lipid vesicles composed of neutral lipids and cholesterol (Table 1). According to previous studies [53], F2N12S binds spontaneously to the outer leaflet of the cell membranes, with no detectable flip-flop to the inner leaflet within the measurement time (<1 h). Therefore, the intermediate hydration values measured with probe F2N12S suggest that, in the outer leaflet of cell membranes, the probe redistributes between Ld and Lo phases. The significant fraction of Lo phase in the outer leaflet of the plasma membranes thus deduced is in line with previous fluorescence [29,65] and spin-label ESR [30] data. This conclusion is also consistent with the high content of SM and cholesterol of this leaflet in normal eukaryotic cells [12,66]. Moreover, the observed relatively low polarity value is fully in accordance with the low content of negatively charged lipids in the outer leaflet [66].

However, the low hydration of cell membranes as compared to model membranes in Ld phase could also be due to interaction of the probe with other components, like membrane proteins. To further determine if the probe reports specifically to the presence of Lo phase in cell membranes, the cholesterol content, a key component of the Lo phase in biomembranes, was modulated [3,19] by extraction with MβCD [67]. This extraction results in an increase of the relative intensity of the short-wavelength emission band accompanied by its red shift (Fig. 3A, Table 1), so that the resulting spectrum resembles that obtained in LUVs in Ld phase (i.e. composed of DOPC, EYPC and POPC). The value of the hydration parameter increases dramatically after cholesterol extraction and becomes very close to that obtained in LUVs of Ld phase, while only minor changes are observed with the N*/T* polarity parameter. These data suggest that cholesterol extraction decreases the fraction of Lo phase in favor of Ld phase in the outer leaflet of the cell plasma membrane, in agreement with recent data obtained using another environment-sensitive membrane probe di-4-ANEPPDHQ [46]. In this respect, the influence of membrane proteins on the probe response is likely marginal, since MβCD cannot extract proteins from biomembranes [67].

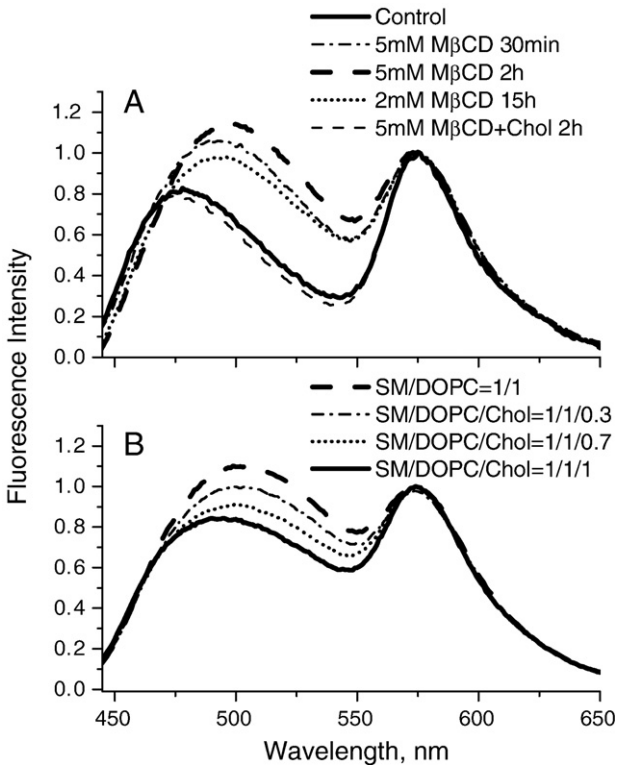

Fig. 3. Monitoring variation in cholesterol content in cell membranes and membrane models. (A) Cholesterol extraction and enrichment in U87MG cells using MβCD monitored by recording the fluorescence spectra of F2N12S probe. (B) Variation of cholesterol content in lipid vesicles containing SM/DOPC mixture (molar ratio is indicated).

Interestingly, the response of the probe depends on the conditions of the cholesterol extraction. A 30 min extraction with 5 mM of MβCD was sufficient to induce strong spectroscopic changes for F2N12S. Longer incubation period (2 h) induced slightly larger spectroscopic effects (Fig. 3). Significantly smaller spectroscopic effects were observed with 2 mM MβCD for 15 h incubation, indicating that short treatment of cells with high concentrations of MβCD are more appropriate for efficient cholesterol extraction. Our data are in accordance with the literature showing that a high concentration of MβCD (10 mM) for 30 min leads to efficient cholesterol depletion from cell membranes [67]. In contrast, treatment of cells for 2 h with MβCD–Cholesterol complex to enrich the cholesterol content in cell membranes [67] led only to a marginal spectroscopic response of the probe in the opposite direction. This small effect suggests that the plasma membrane is almost saturated with cholesterol so that the fraction of the Lo phase cannot be significantly increased by cholesterol addition.

To provide a closer model of cell plasma membranes at different levels of cholesterol extraction, we used LUVs composed of SM/DOPC mixtures with different amounts of cholesterol. Interestingly, a decrease in the cholesterol content in LUVs provided similar changes in the fluorescence spectra as cholesterol extraction in cells, with an increase in the intensity of the short-wavelength band and its concomitant red shift (Fig. 3B). However, the spectrum in the ternary mixture SM/DOPC/Chol (1/1/1) still does not perfectly match the spectrum in intact cells (Fig. 3A and B). Indeed, the value of the hydration parameter in the ternary lipid mixture is significantly larger than in intact cells or in homogeneous Lo phase of lipid membranes (Table 1), being close to that in the Ld phase (DOPC/Chol). This indicates that, in model membranes, the dye partitions preferentially in the Ld phase, in line with our previous data [47]. In contrast, in cell membranes, the spectrum of the probe and the hydration value are intermediate between those observed in Lo and Ld phases. This indicates that the cell membranes either present a homogeneous phase, intermediate between Lo and Ld phases or, unlike model vesicles, the probe binds well to both Ld and Lo phases.

To further investigate the phase behavior of cell membranes, we used the well-established probe TMA-DPH, which describes the fluidity of lipid membranes through fluorescence anisotropy measurements [59]. In lipid vesicles in the Lo phase (SM/Chol), TMA-DPH presents high values of anisotropy [57], while in vesicles in the Ld phase (DOPC, POPC and POPC/Chol) it shows much lower values (Fig. 4), due to the higher fluidity of the latter phase. Remarkably, the anisotropy values of TMA-DPH in intact cells are relatively high (Fig. 4), in line with a significant fraction of Lo phase in the cell membranes, as suggested by the F2N12S data. The high anisotropy values of TMA-DPH in intact U87MG cells are also in accordance with those measured in L929 mouse fibroblasts [59] or by a DPH-labeled lipid in RBL-2H3 mast cells [65]. On cholesterol extraction, we observed a significant decrease in the fluorescence anisotropy value. The effect depends on the incubation time of cells with MβCD, so that after 2 h of incubation, the effect is nearly twice that observed after 30 min. This time-dependent cholesterol depletion effect correlates well with the spectroscopic data obtained with F2N12S probe in the same conditions. Thus, both probes suggest that the fraction of Lo phase in the cell membrane depends on the time of cholesterol extraction.

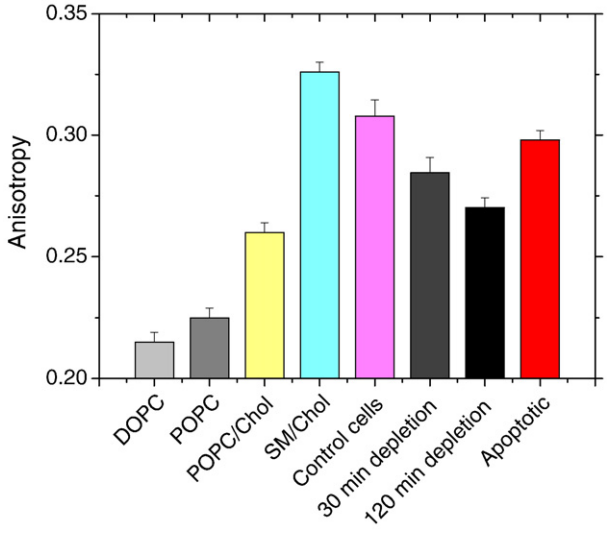

Fig. 4. Fluorescence anisotropy of TMA-DPH in lipid vesicles and U87MG cells. Model vesicles composed of DOPC, POPC and POPC/Chol represent model membranes in Ld phase, while SM/Chol composition represents Lo phase. The presented values for intact cells, cells incubated with 5 mM MβCD for 30 and 120 min and apoptotic cells are an average of four independent measurements.

We then attempted to visualize the distribution of Lo/Ld phases in cell membranes using two-photon fluorescence microscopy with a linearly polarized infra-red femtosecond laser source. Fluorescence ratiometric imaging was performed by recording two images simultaneously at 520 and 580 nm, and building their intensity ratio with a home-made program. The ratiometric images of cells labeled with F2N12S probe show a remarkable homogeneity, as it can be seen from the pseudo-color distribution (Fig. 5A). Moreover, the value (*ca* 0.18) of the intensity ratio of 520/580 nm channels is close to the value (*ca* 0.28) estimated from the fluorescence spectra of intact cells. This homogeneous low value of the ratio suggests that the Lo phase distributes all over the outer leaflet of the cell plasma membrane and thus constitutes a large fraction of this leaflet. The absence of heterogeneity in the images of the cell membranes further suggests that the separation between Lo and Ld phases cannot be detected probably due the limited spatial and temporal resolution of the optical microscope. Indeed, the putative separate domains are likely too small and dynamic [17,26,27] to be visualized by taking into account the diffraction-limited (~300 nm) resolution and the observation time in the range of seconds. In contrast, in lipid vesicles mimicking the lipid composition of the biomembrane outer leaflet (DOPC/SM/Chol), the separated lipid domains could be easily observed due to their large size and slow dynamics [19,41,47].

After cholesterol extraction (2 mM MβCD for 15 h), we observed a modification in the emission pseudo-color at the cell membranes, revealing an increase in the 520/580 nm intensity ratio (Fig. 5). This ratio increase is in full agreement with that observed in the fluorescence spectra of cell suspensions (Fig. 3), suggesting that F2N12S can be used to monitor the depletion of cholesterol through the decrease in the fraction of the Lo phase within the cell plasma membrane. Moreover, the ratiometric images of MβCD-treated cells are also rather homogeneous, so that no phase separation can be observed. After cholesterol extraction with high concentration of MβCD (5 mM), we also observe changes in the pseudo-color corresponding to an increase in the 520/580 nm intensity ratio (Fig. 5), in line with the spectroscopic data (Fig. 3). Noticeably, the membranes of cells treated with the high concentration of MβCD for a short incubation time (30 min) appear very smooth, unlike the native cells or cells treated with the lower concentration of MβCD for a long period of time (12 h). Moreover, the pseudo-color at high concentration of MβCD varies within the cell contour. The color variations correlate with the direction of the polarization of the excitation laser light, so that the lower values of the 520/580 nm intensity ratio correspond to the membrane regions perpendicular to the light polarization axis. The effect of light polarization was previously reported for F2N12S probe in giant vesicles and was connected with two different orientations of the probe in the lipid membrane [47]. Indeed, when the light polarization axis is perpendicular to the bilayer plane, the probe molecules oriented perpendicularly to the bilayer (as shown in Fig. 1) are photo-selected. These photo-selected probes

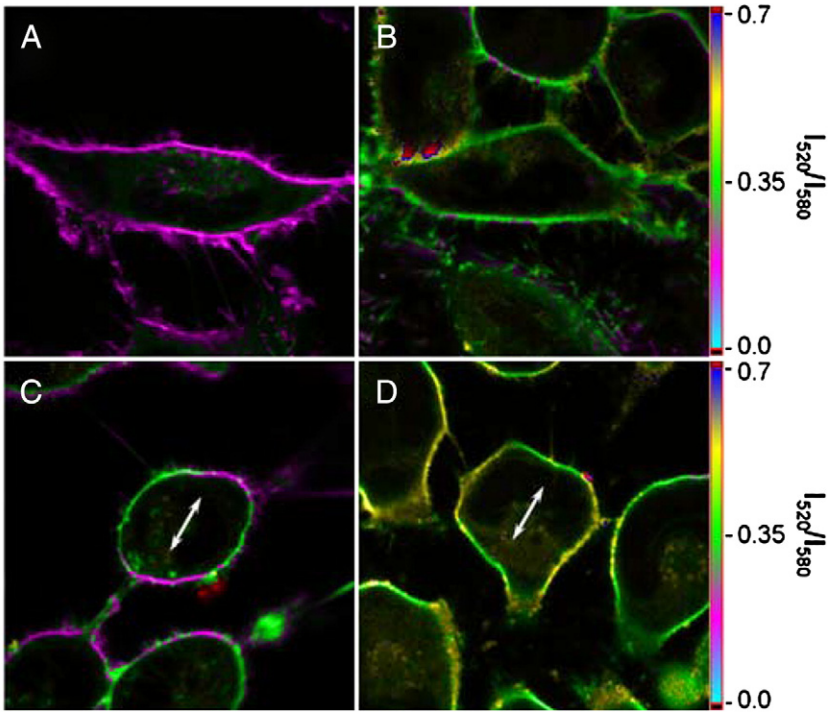

Fig. 5. Fluorescence ratiometric images of U87MG cells stained with F2N12S probe at different levels of cholesterol extraction. Intact cells (A). Cells after cholesterol extraction with 2 mM MβCD for 15 h (B) and with 5 mM MβCD for 30 min (C) and with 5 mM MβCD for 2 h (D). Arrows show the direction of the excitation light polarization.

correspond to the non-hydrated species exhibiting low 520/580 nm intensity ratio. These light polarization effects were observed with giant vesicles in Lo phase but not in pure fluid phase [47], indicating that even after cholesterol extraction, fractions of Lo phase are still present in cell membranes. The absence of polarization effects in native cells is likely related to the great variety of invaginations and extensions (due to endocytosis and influence of the cytoskeleton) in their membranes. Therefore, the membrane of normal cells does not present any preferential direction with respect to the light polarization, unlike the smooth membrane exhibited by cells treated with a high concentration of MβCD.

The cholesterol extraction experiments on cells and their comparison with lipid vesicles of different composition helped us to better understand the changes within the cell plasma membrane during apoptosis. We have previously reported that F2N12S probe shows a strong response to apoptosis, due to the loss of transmembrane lipid asymmetry [53]. From Fig. 6A, it further appears that the spectroscopic response of F2N12S to apoptosis is similar to that observed during cholesterol extraction. In addition, the value of hydration increases strongly during apoptosis and becomes similar to that observed in cells with extracted cholesterol and in model vesicles in Ld phase (EYPC and DOPC), suggesting a loss of Lo phase at the outer membrane leaflet of apoptotic cells. To confirm the changes in the phase state of cell membranes on apoptosis, we compared the fluorescence anisotropy values of TMA-DPH in intact and apoptotic cells. However, we observed only a minor decrease in anisotropy after apoptosis, which was much smaller than the effect of cholesterol extraction (Fig. 4). Though the observed changes are in agreement with the expected decrease in the fraction of Lo phase on apoptosis, TMA-DPH probably redistributes rather rapidly from the outer to the inner membrane leaflet, which minimizes its response to the apoptotic loss of the transmembrane asymmetry. Unlike F2N12S, TMA-DPH is a cationic molecule with no long hydrophobic chains, which may explain its relatively fast flip-flop towards the inner membrane leaflet. A similar rapid intracellular internalization, mainly driven by the transmembrane electric potential has also been observed with a number of other cationic fluorophores, such as octadecyl rhodamine [68], cyanine derivatives [69] and an analogue of F2N12S, probe F2N8 [53].

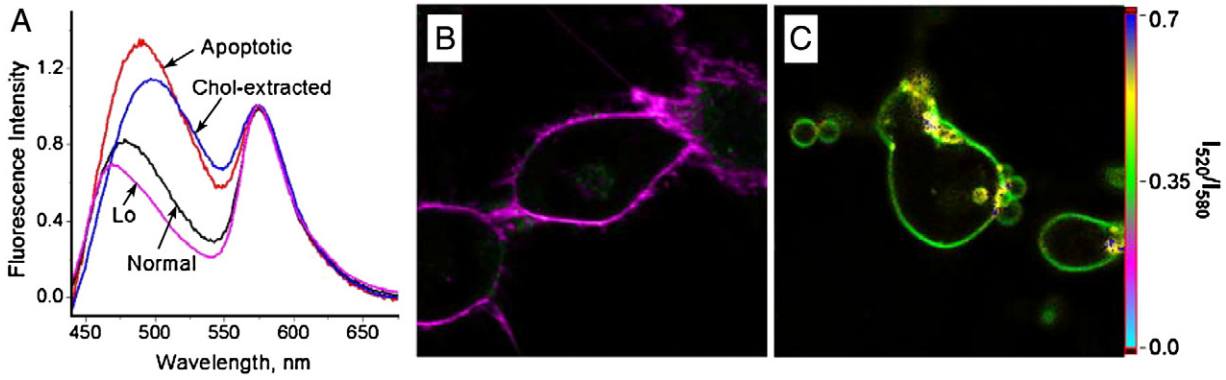

Fig. 6. Monitoring apoptosis with F2N12S probe. Fluorescence spectra of F2N12S probe in non apoptotic and apoptotic cells, compared to the spectra of the probe in LUVs of Lo phase and to that in cells after cholesterol extraction (A). Fluorescence ratiometric images of intact (B) and apoptotic (C) cells stained with F2N12S.

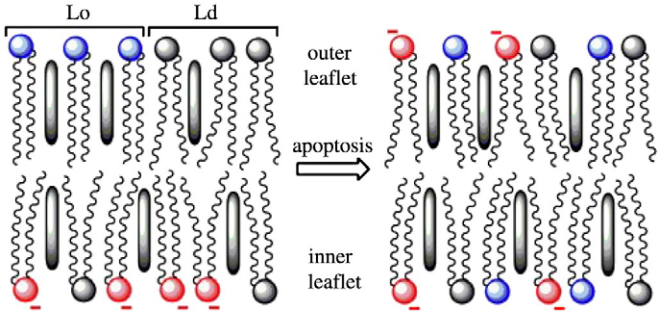

Fig. 7. Simplified model of the loss of transmembrane asymmetry during apoptosis. This loss of asymmetry results both in an increase of the negative surface charge and a decrease in the fraction of the Lo phase at the outer leaflet of the cell membrane. Balls represent the head groups of neutral phospholipids (black), anionic phospholipids (red) and sphingolipids (blue). The black bars represent cholesterol. The regions representing Lo and Ld phases are marked.

Furthermore, the much larger polarity value observed with apoptotic cells compared to intact and cholesterol depleted cells (Table 1) is in line with an increase in the negative surface charge of their outer membrane leaflet. The observed increase in the negative surface charge and the decrease of the Lo phase fraction in the external membrane leaflet during apoptosis suggest the following events at the cell membrane (Fig. 7). First, as it is well-established, the loss of transmembrane lipid asymmetry during apoptosis results in the appearance at the cell surface of anionic lipids (mainly PS), contributing to an increase in the negative charge at the surface [66]. In parallel, apoptosis results also in a transfer of SM from the outer leaflet, where it is abundant, to the inner leaflet, thus explaining the loss of Lo phase (Fig. 7). This conclusion is in line with a previous report showing that the executive step of apoptosis resulting in PS exposure is accompanied with the transfer of SM from the outer to the inner leaflet, a process preceding the formation of ceramides [70]. Thus, the loss of Lo phase on apoptosis is different from that occurring on cholesterol extraction, since the former is mainly due to the decrease in the SM fraction in the outer leaflet.

The loss of the Lo phase during apoptosis as well as after cholesterol extraction is associated with dramatic changes in the cellular morphology, so that the membrane becomes smoother and the cell attachment ability to the surface is strongly decreased (Figs. 5C, D and 6C). Such morphological alterations were already reported after cholesterol depletion [71,72] and are at least in part due to the disorganization of the actin network [73] and the alteration of the function of adhesion proteins (such as integrins) [74,75] leading consequently to the disappearance of cell adhesion structures. Similar morphological features were also observed during apoptosis. In line with previous reports [76–79], we also observe smoother membranes as well as intensive membrane blebbing in apoptotic cells (Fig. 5B). This blebbing process has been connected with the formation of ceramide from SM within the inner leaflet [78].

4. Conclusion

In the present work, we have studied cell membranes of U87MG cells using a membrane probe sensitive to both the surface charge and the bilayer phase. We observed that the outer leaflet of cell membranes contains a significant fraction of Lo phase, probably due to its high content in sphingomyelin. After extraction of cholesterol with MβCD, a dramatic loss of Lo phase was observed in cell membranes. The spectroscopic changes of the probe emission after cholesterol extraction are similar to those following apoptosis. Thus, our data suggest that the loss of transmembrane lipid asymmetry of the plasma membrane during apoptosis might lead, in addition to the increase of the negative surface charge due to PS exposure, to a loss of the Lo phase within the outer leaflet due to the transfer of sphingolipids to the inner leaflet. Our data suggest a new methodology for studying the Lo phase in membranes of living cells.

Acknowledgements

This work was supported by a Conectus Alsace grant and by the ARCUS program between France, Ukraine and Russia.

References

[1] K. Simons, E. Ikonen, Functional rafts in cell membranes, Nature 387 (1997) 569–572.
[2] D.A. Brown, E. London, Structure and origin of ordered lipid domains in biological membranes, J. Membr. Biol. 164 (1998) 103–114.
[3] K. Simons, E. Ikonen, How cells handle cholesterol, Science 290 (2000) 1721–1726.
[4] M. Edidin, The state of lipid rafts: from model membranes to cells, Annu. Rev. Biophys. Biomol. Struct. 32 (2003) 257–283.
[5] S. Munro, Lipid rafts: elusive or illusive? Cell 115 (2003) 377–388.
[6] E. London, How principles of domain formation in model membranes may explain ambiguities concerning lipid raft formation in cells, Biochim. Biophys. Acta 1746 (2005) 203–220.
[7] L.J. Pike, Growth factor receptors, lipid rafts and caveolae: an evolving story, Biochim. Biophys. Acta 1746 (2005) 260–273.
[8] E. Kiyokawa, T. Baba, N. Otsuka, A. Makino, S. Ohno, T. Kobayashi, Spatial and functional heterogeneity of sphingolipid-rich membrane domains, J. Biol. Chem. 280 (2005) 24072–24084.
[9] J.F. Hancock, Lipid rafts: contentious only from simplistic standpoints, Nat. Rev. Mol. Cell Biol. 7 (2006) 456–462.
[10] D.A. Brown, J.K. Rose, Sorting of GPI-anchored proteins to glycolipid-enriched membrane subdomains during transport to the apical cell surface, Cell 68 (1992) 533–544.
[11] G. van Meer, K. Simons, Lipid polarity and sorting in epithelial cells, J. Cell. Biochem. 36 (1988) 51–58.
[12] K. Simons, D. Toomre, Lipid rafts and signal transduction, Nat. Rev. Mol. Cell Biol. 1 (2000) 31–39.
[13] D.A. Brown, E. London, Functions of lipid rafts in biological membranes, Annu. Rev. Cell Dev. Biol. 14 (1998) 111–136.
[14] K.A. Field, D. Holowka, B. Baird, Compartmentalized activation of the high affinity immunoglobulin E receptor within membrane domains, J. Biol. Chem. 272 (1997) 4276–4280.
[15] M.F. Hanzal-Bayer, J.F. Hancock, Lipid rafts and membrane traffic, FEBS Lett. 581 (2007) 2098–2104.
[16] T. Tian, A. Harding, K. Inder, S. Plowman, R.G. Parton, J.F. Hancock, Plasma membrane nanoswitches generate high-fidelity Ras signal transduction, Nat. Cell Biol. 9 (2007) 875–877.
[17] P.H.M. Lommerse, H.P. Spaink, T. Schmidt, In vivo plasma membrane organization: results of biophysical approaches, Biochim. Biophys. Acta 1664 (2004) 119–131.
[18] L.J. Pike, Rafts defined: a report on the Keystone symposium on lipid rafts and cell function, J. Lipid Res. 47 (2006) 1597–1598.
[19] C. Dietrich, L.A. Bagatolli, Z.N. Volovyk, N.L. Thompson, M. Levi, K. Jacobson, E. Gratton, Lipid rafts reconstituted in model membranes, Biophys. J. 80 (2001) 1417–1428.
[20] S.L. Veatch, S.L. Keller, Organization in lipid membranes containing cholesterol, Phys. Rev. Lett. 89 (2002) 268101.
[21] S.L. Veatch, S.L. Keller, Separation of liquid phases in giant vesicles of ternary mixtures of phospholipids and cholesterol, Biophys. J. 85 (2003) 3074–3083.
[22] T. Baumgart, S.T. Hess, W.W. Webb, Imaging coexisting fluid domains in biomembrane models coupling curvature and line tension, Nature 425 (2003) 821–824.
[23] A. Pralle, P. Keller, E.L. Florin, K. Simons, J.K. Horber, Sphingolipid-cholesterol rafts diffuse as small entities in the plasma membrane of mammalian cells, J. Cell Biol. 148 (2000) 997–1008.
[24] C. Dietrich, B. Yang, T. Fujiwara, A. Kusumi, K. Jacobson, Relationship of lipid rafts to transient confinement zones detected by single particle tracking, Biophys. J. 82 (2002) 274–284.
[25] G.J. Schultz, G. Kada, V.P. Pastushenko, H. Schindler, Properties of lipid microdomains in a muscle cell membrane visualized by single molecule microscopy, EMBO J. 19 (2000) 892–901.
[26] P.F. Lenne, L. Wawrezinieck, F. Conchonaud, O. Wurtz, A. Boned, X.J. Guo, H. Rigneault, H.T. He, D. Marguet, Dynamic molecular confinement in the plasma membrane by microdomains and the cytoskeleton meshwork, EMBO J. 25 (2006) 3245–3256.
[27] L. Wawrezinieck, H. Rigneault, D. Marguet, P.F. Lenne, Fluorescence correlation spectroscopy diffusion laws to probe the submicron cell membrane organization, Biophys. J. 89 (2005) 4029–4042.
[28] P. Sharma, R. Varma, R.C. Sarasij, Ira K. Gousset, G. Krishnamoorthy, M. Rao, S. Mayor, Nanoscale organization of multiple GPI-anchored proteins in living cell membranes, Cell 116 (2004) 577–589.
[29] M. Hao, S. Mukherjee, F.R. Maxfield, Cholesterol depletion induces large scale domain segregation in living cell membranes, Proc. Natl. Acad. Sci. U. S. A. 98 (2001) 13072–13077.

[30] M.J. Swamy, L. Ciani, M. Ge, A.K. Smith, D. Holowka, B. Baird, J.H. Freed, Coexisting domains in the plasma membranes of live cells characterized by spin-label ESR spectroscopy, Biophys. J. 90 (2006) 4452–4465.
[31] D.M. Owen, M.A.A. Neil, P.M.W. French, A.I. Magee, Optical techniques for imaging membrane lipid microdomains in living cells, Semin. Cell Dev. Biol. 18 (2007) 591–598.
[32] B.C. Lagerholm, G.E. Weinreb, K. Jacobson, N.L. Thompson, Detecting microdomains in intact cell membranes, Annu. Rev. Phys. Chem. 56 (2005) 309–336.
[33] P.W. Janes, S.C. Ley, A.I. Magee, Aggregation of lipid rafts accompanies signaling via the T cell antigen receptor, J. Cell. Biol. 147 (1999) 447–461.
[34] A.K. Kenworthy, N. Petranova, M. Edidin, High-resolution FRET microscopy of cholera toxin B-subunit and GPI-anchored proteins in cell plasma membranes, Mol. Biol. Cell 11 (2000) 1645–1655.
[35] M. Vrljic, S.Y. Nishimura, S. Brasselet, W.E. Moerner, H.M. McConnell, Translational diffusion of individual class II MHC membrane proteins in cells, Biophys. J. 83 (2002) 2681–2692.
[36] A.K. Kenworthy, B.J. Nichols, C.L. Remmert, G.M. Hendrix, M. Kumar, J. Zimmerberg, J. Lippincott-Schwartz, Dynamics of putative raft-associated proteins at the cell surface, J. Cell Biol. 165 (2004) 735–746.
[37] C.K. Haluska, A.P. Schröder, P. Didier, D. Heissler, G. Duportail, Y. Mély, C.M. Marques, Combining fluorescence lifetime and polarization microscopy to discriminate phase separated domains in giant unilamellar vesicles, Biophys. J. 95 (2008) 5737–5747.
[38] X. Xu, R. Bittman, G. Duportail, D. Heissler, C. Vilchéze, E. London, Effect of the structure of natural sterols and sphingolipids on the formation of ordered sphingolipid/sterol domains (rafts). Comparison of cholesterol to plant, fungal, and disease-associated sterols and comparison of sphingomyelin, cerebrosides, and ceramide, J. Biol. Chem. 276 (2001) 33540–33546.
[39] J. Korlach, P. Schwille, W.W. Webb, G.W. Feigenson, Characterization of lipid bilayer phases by confocal microscopy and fluorescence correlation spectroscopy, Proc. Natl. Acad. Sci. U. S. A. 96 (1999) 8461–8466.
[40] T. Baumgart, G. Hunt, E.R. Farkas, W.W. Webb, G.W. Feigenson, Fluorescence probe partitioning between Lo/Ld phases in lipid membranes, Biochim. Biophys. Acta 1768 (2007) 2182–2194.
[41] L.A. Bagatolli, To see or not to see: lateral organization of biological membranes and fluorescence microscopy, Biochim. Biophys. Acta 1758 (2006) 1541–1556.
[42] T. Parasassi, E. Gratton, W.M. Yu, P. Wilson, M. Levi, Two-photon fluorescence microscopy of Laurdan generalized polarization domains in model and natural membranes, Biophys. J. 72 (1997) 2413–2429.
[43] K. Gaus, E. Gratton, E.P.W. Kable, A.S. Jones, I. Gelissen, L. Kritharides, W. Jessup, Visualizing lipid structure and raft domains in living cells with two-photon microscopy, Proc. Natl. Acad. Sci. U. S. A. 100 (2003) 15554–15559.
[44] H.M. Kim, H.-J. Choo, S.-Y. Jung, Y.-G. Ko, W.-H. Park, S.-J. Jeon, C.H. Kim, T. Joo, B.R. Cho, A two-photon probe for lipid raft imaging: C-Laurdan, ChemBioChem 8 (2007) 553–559.
[45] H.M. Kim, B.H. Jeong, J.-Y. Hyon, M.J. An, M.S. Seo, J.H. Hong, K.J. Lee, C.H. Kim, T. Joo, S.-C. Hong, B.R. Cho, Two-photon fluorescent turn-on probe for lipid rafts in live cell and tissue, J. Am. Chem. Soc. 130 (2008) 4246–4247.
[46] L. Jin, A.C. Millard, J.P. Wuskell, X. Dong, D. Wu, H.A. Clark, L.M. Loew, Characterization and application of a new optical probe for membrane lipid domains, Biophys. J. 90 (2006) 2563–2575.
[47] A.S. Klymchenko, S. Oncul, P. Didier, E. Schaub, L. Bagatolli, G. Duportail, Y. Mély, Visualization of lipid domains in giant unilamellar vesicles using an environment-sensitive membrane probe based on 3-hydroxyflavone, Biochim. Biophys. Acta 1788 (2009) 495–499.
[48] P.-T. Chou, M.L. Martinez, J.-H. Clements, Reversal of excitation behavior of proton-transfer vs. charge-transfer by dielectric perturbation of electronic manifolds, J. Phys. Chem. 97 (1993) 2618–2622.
[49] A.S. Klymchenko, A.P. Demchenko, Multiparametric probing of intermolecular interactions with fluorescent dye exhibiting excited state intramolecular proton transfer, Phys. Chem. Chem. Phys. 5 (2003) 461–468.
[50] A.P. Demchenko, Y. Mély, G. Duportail, A.S. Klymchenko, Monitoring biophysical properties of lipid membranes by environment-sensitive fluorescent probes, Biophys. J. 96 (2009) 3461–3470.
[51] A.S. Klymchenko, Y. Mély, A.P. Demchenko, G. Duportail, Simultaneous probing of hydration and polarity of lipid bilayers with 3-hydroxyflavone fluorescent dyes, Biochim. Biophys. Acta 1665 (2004) 6–19.
[52] A.S. Klymchenko, G. Duportail, T. Oztürk, V.G. Pivovarenko, Y. Mély, A.P. Demchenko, Novel two-band ratiometric fluorescence probes with different location and orientation in phospholipid membranes, Chem. Biol. 9 (2002) 1199–1208.
[53] V.V. Shynkar, A.S. Klymchenko, C. Kunzelmann, G. Duportail, C.D. Muller, A.P. Demchenko, J.-M. Freyssinet, Y. Mély, Fluorescent biomembrane probe for ratiometric detection of apoptosis, J. Am. Chem. Soc. 129 (2007) 2187–2193.
[54] A.S. Klymchenko, G. Duportail, Y. Mély, A.P. Demchenko, Ultrasensitive two-color fluorescence probes for dipole potential in phospholipids membranes, Proc. Natl. Acad. Sci. U. S. A. 100 (2003) 11219–11224.
[55] V.V. Shynkar, A.S. Klymchenko, G. Duportail, A.P. Demchenko, Y. Mély, Two-color fluorescent probes for imaging dipole potential of cell plasma membranes, Biochim. Biophys. Acta 1712 (2005) 128–136.
[56] A.S. Klymchenko, H. Stoeckel, K. Takeda, Y. Mély, Fluorescent probe based on intramolecular proton transfer for fast ratiometric measurement of cellular transmembrane potential, J. Phys. Chem. B 110 (2006) 13624–13632.
[57] G. M'Baye, Y. Mély, G. Duportail, A.S. Klymchenko, Liquid ordered and gel phases of lipid bilayers: fluorescent probes reveal close fluidity but different hydration, Biophys. J. 95 (2008) 1217–1225.
[58] M.J. Hope, M.B. Bally, G. Webb, P.R. Cullis, Production of large unilamellar vesicles by a rapid extrusion procedure. Characterization of size distribution, trapped volume and ability to maintain a membrane potential, Biochim. Biophys. Acta 812 (1985) 55–65.
[59] J.-G. Kuhry, G. Duportail, C. Bronner, G. Laustriat, Plasma membrane fluidity measurements on whole living cells by fluorescence anisotropy of trimethylammoniumdiphenylhexatriene, Biochim. Biophys. Acta 845 (1985) 60–67.
[60] J. Azoulay, J.-P. Clamme, J.-L. Darlix, B.P. Roques, Y. Mély, Destabilization of the HIV-1 complementary sequence of TAR by the nucleocapsid protein through activation of conformational fluctuations, J. Mol. Biol. 326 (2003) 691–700.
[61] J.-P. Clamme, J. Azoulay, Y. Mély, Monitoring of the formation and dissociation of polyethylenimine/DNA complexes by two photon fluorescence correlation spectroscopy, Biophys. J. 84 (2003) 1960–1968.
[62] M.B. Sankaram, T.E. Thompson, Interaction of cholesterol with various glycerophospholipids and sphingomyelin, Biochemistry 29 (1990) 10670–10675.
[63] A.S. Klymchenko, G. Duportail, A.P. Demchenko, Y. Mély, Bimodal distribution and fluorescence response of environment-sensitive probes in lipid bilayers, Biophys. J. 86 (2004) 2929–2941.
[64] T. Parasassi, M. Di Stefano, M. Loiero, G. Ravagnan, E. Gratton, Cholesterol modifies water concentration and dynamics in phospholipid bilayers: a fluorescence study using Laurdan probe, Biophys. J. 66 (1994) 763–768.
[65] A. Gidwani, D. Holowka, D. Baird, Fluorescence anisotropy measurements of lipid order in plasma membranes and lipid rafts from RBL-2H3 mast cells, Biochemistry 40 (2001) 12422–12429.
[66] R.F. Zwaal, A.J. Schroit, Pathophysiologic implications of membrane phospholipid asymmetry in blood cells, Blood 89 (1997) 1121–1132.
[67] R. Zidovetzki, I. Levitan, Use of cyclodextrins to manipulate plasma membrane cholesterol content: evidence, misconceptions and control strategies, Biochim. Biophys. Acta 1768 (2007) 1311–1324.
[68] J.M. Leenhouts, B. De Kruijff, Membrane potential-driven translocation of a lipid-conjugated rhodamine, Biochim. Biophys. Acta 1237 (1995) 121–126.
[69] P.J. Sims, A.S. Waggoner, C.-H. Wang, J.F. Hoffman, Studies on the mechanism by which cyanine dyes measure membrane potential in red blood cells and phosphatidylcholine vesicles, Biochemistry 13 (1974) 3315–3330.
[70] A.D. Tepper, P. Ruurs, T. Wiedmer, P.J. Sims, J. Borst, W.J. van Blitterswijk, Sphingomyelin hydrolysis to ceramide during the execution phase of apoptosis results from phospholipid scrambling and alters cell-surface morphology, J. Cell Biol. 150 (2000) 155–164.
[71] S. Martin, D.C. Phillips, K. Szekely-Szucs, L. Elghazi, F. Desmots, J.A. Houghton, Cyclooxygenase-2 inhibition sensitizes human colon carcinoma cells to TRAIL-induced apoptosis through clustering of DR5 and concentrating death-inducing signaling complex components into ceramide-enriched caveolae, Cancer Res. 65 (2005) 11447–11458.
[72] O.G. Ramprasad, G. Srinivas, K.S. Rao, P. Joshi, J.P. Thiery, S. Dufour, G. Pande, Changes in cholesterol levels in the plasma membrane modulate cell signaling and regulate cell adhesion and migration on fibronectin, Cell Motil. Cytoskelet. 64 (2007) 199–216.
[73] S.K. Patra, Dissecting lipid raft facilitated cell signaling pathways in cancer, Biochim. Biophys. Acta 1785 (2008) 182–206.
[74] B. Leitinger, N. Hogg, The involvement of lipid rafts in the regulation of integrin function, J. Cell Sci. 115 (2002) 963–972.
[75] G. Pande, The role of membrane lipids in regulation of integrin functions, Curr. Opin. Cell Biol. 12 (2000) 569–574.
[76] S. Martin, G. Giannone, R. Andriantsitohaina, M.C. Martinez, Delphinidin, an active compound of red wine, inhibits endothelial cell apoptosis via nitric oxide pathway and regulation of calcium homeostasis, Br. J. Pharmacol. 139 (2003) 1095–1102.
[77] G. Kroemer, L. Galluzzi, P. Vandenabeele, J. Abrams, E.S. Alnemri, E.H. Baehrecke, M.V. Blagosklonny, W.S. El-Deiry, P. Golstein, D.R. Green, M. Hengartner, R.A. Knight, S. Kumar, S.A. Lipton, W. Malorni, G. Nunez, M.E. Peter, J. Tschopp, J. Yuan, M. Piacentini, B. Zhivotovsky, G. Melino, Classification of cell death: recommendations of the Nomenclature Committee on Cell Death 2009, Cell Death Differ. 16 (2009) 3–11.
[78] J. Zhang, T.A. Driscoll, Y.A. Hannun, L.M. Obeid, Regulation of membrane release in apoptosis, Biochem. J. 334 (1998) 479–485.
[79] J.C. Mills, N.L. Stone, J. Erhardt, R.N. Pittman, Apoptotic membrane blebbing is regulated by myosin light chain phosphorylation, J. Cell Biol. 140 (1998) 627–636.

PUBLICATION 2

SWITCHABLE NILE RED-BASED PROBE FOR CHOLESTEROL AND LIPID ORDER AT THE OUTER LEAFLET OF BIOMEMBRANES

J|A|C|S ARTICLES

Published on Web 03/12/2010

Switchable Nile Red-Based Probe for Cholesterol and Lipid Order at the Outer Leaflet of Biomembranes

Oleksandr A. Kucherak, Sule Oncul,† Zeinab Darwich, Dmytro A. Yushchenko, Youri Arntz, Pascal Didier, Yves Mély, and Andrey S. Klymchenko*

Laboratoire de Biophotonique et Pharmacologie, UMR 7213 CNRS, Université de Strasbourg, Faculté de Pharmacie, 74, Route du Rhin, 67401 Illkirch Cedex, France

Received January 14, 2010; E-mail: andrey.klymchenko@unistra.fr

Abstract: Cholesterol and sphingomyelin form together a highly ordered membrane phase, which is believed to play important biological functions in plasma membranes of mammalian cells. Since sphingomyelin is present mainly at the outer leaflet of cell membranes, monitoring its lipid order requires molecular probes capable to bind specifically at this leaflet and exhibit negligibly slow flip-flop. In the present work, such a probe was developed by modifying the solvatochromic fluorescent dye Nile Red with an amphiphilic anchor group. To evaluate the flip-flop of the obtained probe (NR12S), we developed a methodology of reversible redox switching of its fluorescence at one leaflet using sodium dithionite. This method shows that NR12S, in contrast to parent Nile Red, binds exclusively the outer membrane leaflet of model lipid vesicles and living cells with negligible flip-flop in the time scale of hours. Moreover, the emission maximum of NR12S in model vesicles exhibits a significant blue shift in liquid ordered phase (sphingomyelin-cholesterol) as compared to liquid disordered phase (unsaturated phospholipids). As a consequence, these two phases could be clearly distinguished in NR12S-stained giant vesicles by fluorescence microscopy imaging of intensity ratio between the blue and red parts of the probe emission spectrum. Being added to living cells, NR12S binds predominantly, if not exclusively, their plasma membranes and shows an emission spectrum intermediate between those in liquid ordered and disordered phases of model membranes. Importantly, the emission color of NR12S correlates well with the cholesterol content in cell membranes, which allows monitoring the cholesterol depletion process with methyl-β-cyclodextrin by fluorescence spectroscopy and microscopy. The attractive photophysical and switching properties of NR12S, together with its selective outer leaflet staining and sensitivity to cholesterol and lipid order, make it a new powerful tool for studying model and cell membranes.

Introduction

The structure and function of cell plasma membranes is largely controlled by their lipid composition and particularly by cholesterol, which represents up to 40% of the lipids in plasma membranes.[1] Cholesterol interacts strongly with phospholipids in membranes and, notably, with sphingomyelin (SM), another major lipid component of cell membranes.[2−4] Cholesterol and SM form a highly packed state, called liquid ordered (Lo) phase, in lipid bilayers. This phase is clearly separated in model membranes from the loosely packed liquid disordered (Ld) phase formed by unsaturated lipids and cholesterol.[5] The presence of Lo domains (or rafts) in cell plasma membranes was hypothesized from the discovery of detergent-insoluble membrane fractions enriched with SM, saturated phospholipids, and cholesterol.[6] This hypothesis stimulated intensive research and debates,[1−7] since their evidence was mainly provided from indirect techniques,[8] while their direct visualization remains a challenge. Estimation of the fraction of Lo phase in cell

† Present address: Acibadem University, School of Medicine, Department of Biophysics, Fevzi Cakmak Cd. Divan Sk. No. 1, 34848 Maltepe, Istanbul, Turkey.

(1) (a) Yeagle, P. L. *Biochim. Biophys. Acta* **1985**, *822*, 267–287. (b) Simons, K.; Ikonen, E. *Nature* **1997**, *387*, 569–572. (c) Simons, K.; Ikonen, E. *Science* **2000**, *290*, 1721–1726. (d) Brown, D. A.; London, E. *J. Membr. Biol.* **1998**, *164*, 103–114. (e) Brown, D. A.; London, E. *J. Biol. Chem.* **2000**, *275*, 17221–17224. (f) Ohvo-Rekila, H.; Ramstedt, B.; Leppimaki, P.; Peter Slotte, J. *Prog. Lipid Res.* **2002**, *41*, 66–97. (g) Maxfield, F. R.; Tabas, I. *Nature* **2005**, *438*, 612–621.

(2) (a) Lange, Y.; Ye, J.; Rigney, M.; Steck, T. *J. Biol. Chem.* **2000**, *275*, 17468–17475. (b) Lange, Y.; Swaisgood, M. H.; Ramos, B. V.; Steck, T. L. *J. Biol. Chem.* **1989**, *264*, 3786–3793.

(3) (a) Radhakrishnan, A.; McConnell, H. M. *J. Am. Chem. Soc.* **1999**, *121*, 486–487. (b) McConnell, H. M.; Radhakrishnan, A. *Biochim. Biophys. Acta* **2003**, *1610*, 159–173.

(4) Sankaram, M. B.; Thompson, T. E. *Biochemistry* **1990**, *29*, 10670–10675.

(5) (a) Dietrich, C.; Bagatolli, L. A.; Volovyk, Z. N.; Thompson, N. L.; Levi, M.; Jacobson, K.; Gratton, E. *Biophys. J.* **2001**, *80*, 1417–1428. (b) Veatch, S. L.; Keller, S. L. *Phys. Rev. Lett.* **2002**, *89*, 268101. (c) Veatch, S. L.; Keller, S. L. *Biophys. J.* **2003**, *85*, 3074–3083. (d) Baumgart, T.; Hess, S. T.; Webb, W. W. *Nature* **2003**, *425*, 821–824. (e) Ahmed, S. N.; Brown, D. A.; London, E. *Biochemistry* **1997**, *36*, 10944–10953. (f) De Almeida, R. F. M.; Fedorov, A.; Prieto, M. *Biophys. J.* **2003**, *85*, 2406–2416.

(6) (a) Brown, D. A.; Rose, J. K. *Cell* **1992**, *68*, 533–544. (b) Schroeder, R.; London, E.; Brown, D. *Proc. Natl. Acad. Sci. U.S.A.* **1994**, *91*, 12130–12134. (c) London, E.; Brown, D. A. *Biochim. Biophys. Acta* **2000**, *1508*, 182–195.

(7) (a) Simons, K.; Toomre, D. *Nat. Rev. Mol. Cell Biol.* **2000**, *1*, 31–39. (b) Brown, D. A.; London, E. *Annu. Rev. Cell Dev. Biol.* **1998**, *14*, 111–136. (c) Field, K. A.; Holowka, D.; Baird, B. *J. Biol. Chem.* **1997**, *272*, 4276–4280. (d) Hanzal-Bayer, M. F.; Hancock, J. F. *FEBS Lett.* **2007**, *581*, 2098–2104. (e) Tian, T.; Harding, A.; Inder, K.; Plowman, S.; Parton, R. G.; Hancock, J. F. *Nat. Cell Biol.* **2007**, *9*, 875–877.

membranes ranges from 10% to 80%, depending on the method used for its quantification. The difficulties to characterize Lo phase in cell membranes are first connected with their complex lipid composition, the presence of membrane proteins and cytoskeleton.[9] The second complication raises from the asymmetric distribution of lipids between the two leaflets. Indeed, while the outer leaflet contains a large amount of SM (up to 40%), its fraction in the inner leaflet is marginal.[10] Therefore, correct evaluation of Lo phase requires high specificity to this phase as well as high selectivity to the outer membrane leaflet.

To characterize the cholesterol content in membranes, the most classical method is to directly measure the lipid composition by isolation of cell plasma membrane fractions.[2] However, it is an invasive method, which does not allow real-time in situ measurements and may lead to artifacts because cholesterol can migrate between different cellular compartments[1] during the membrane isolation. More recent approaches are based on the extraction of radiolabeled cholesterol by cyclodextrin[11] and cholesterol-oxidation by microelectrode,[12] which allow real-time kinetics measurements of cholesterol in cells. However, these methods cannot address the spatial distribution of Lo and Ld phases in lipid membranes.

Fluorescent probes are probably the most attractive tool to study Lo/Ld phase separation and lipid compositions in model and cell membranes. Two classes of probes are mainly used. The first class corresponds to probes that stain selectively the Lo phase in model vesicles. This class includes the fluorescently labeled cholera toxin B-subunit (CT-B),[8a,13] saturated phospholipids labeled with NBD[5a] or Cy5[14] and GFP-labeled glycosylphosphatidylinositol (GPI),[15] as well as fluorescent dyes with long alkyl chains, such as LcTMA-DPH,[16] diI-C20, or polycyclic probes such as Terrylene or Naphtopyrene.[17] Though these probes are useful for imaging the phase separation in model and cell membranes, they cannot provide information about the actual composition of the separated phases. The second class corresponds to environment-sensitive probes, such as Laurdan[18] and its derivatives,[19] di-4-ANEPPDHQ[20] and 3-hydroxyflavone derivatives.[21] These probes distribute in both Ld and Lo phases, and their emission color or intensity depends strongly on the local polarity/hydration or fluidity, which in turn is related to the lipid composition and the actual phase state of the membrane.[18] Thus, these probes provide a unique possibility to study the membrane phases in connection to their lipid composition. However, only a small number of these probes is really applicable to membranes of living cells,[19,20,22] because most of them internalize rapidly inside the cell. Moreover, the flip-flop of these probes is not clearly addressed in literature, since the flip-flop studies are mainly based on indirect measurements,[20,22] so that it is difficult to evaluate precisely the distribution of the probes between the two leaflets. Therefore, it still remains a challenge to develop an environment-sensitive fluorescent probe that stains exclusively the outer leaflet of cell membranes. In the present work, we selected Nile Red[23] (Chart 1) as an environment-sensitive fluorophore for designing this fluorescent probe. Nile Red shows a number of attractive features, such as high fluorescence quantum yield, suitable excitation wavelength for application with common lasers and satisfactory photostability.[24] This dye found a variety of applications to characterize hydrophobic domains of proteins, dendrimers, micelles and model lipid membranes.[25] However, it cannot be used for studying cell plasma membranes, because it internalizes readily inside the cell and binds specifically to lipid droplets,[23] which are the most apolar cell compartments. Recently, we showed that a selective localization of a hydrophobic fluorophore at the plasma membrane can be achieved

(8) (a) Dietrich, C.; Yang, B.; Fujiwara, T.; Kusumi, A.; Jacobson, K. *Biophys. J.* **2002**, *82*, 274–284. (b) Pralle, A.; Keller, P.; Florin, E. L.; Simons, K.; Horber, J. K. *J. Cell. Biol.* **2000**, *148*, 997–1008. (c) Schultz, G. J.; Kada, G.; Pastushenko, V. P.; Schindler, H. *EMBO J.* **2000**, *19*, 892–901. (d) Lenne, P. F.; Wawrezinieck, L.; Conchonaud, F.; Wurtz, O.; Boned, A.; Guo, X. J.; Rigneault, H.; He, H. T.; Marguet, D. *EMBO J.* **2006**, *25*, 3245–3256. (e) Wawrezinieck, L.; Rigneault, H.; Marguet, D.; Lenne, P. F. *Biophys. J.* **2005**, *89*, 4029–4042. (f) Swamy, M. J.; Ciani, L.; Ge, M.; Smith, A. K.; Holowka, D.; Baird, B.; Freed, J. H. *Biophys. J.* **2006**, *90*, 4452–4465.

(9) Kusumi, A.; Sako, Y. *Curr. Opin. Cell Biol.* **1996**, *8*, 566–574.

(10) (a) Van Meer, G. *Annu. Rev. Cell Biol.* **1989**, *5*, 247–275. (b) Zwaal, R. F.; Schroit, A. J. *Blood* **1997**, *89*, 1121–1132.

(11) (a) Haynes, M. P.; Phillips, M. C.; Rothblat, G. H. *Biochemistry* **2000**, *39*, 4508–4517. (b) Lange, Y.; Ye, J.; Steck, T. L. *Proc. Natl. Acad. Sci. U.S.A.* **2004**, *101*, 11664–11667.

(12) Jiang, D.; Devadoss, A.; Palencsár, M. S.; Fang, D.; White, N. M.; Kelley, T. J.; Smith, J. D.; Burgess, J. D. *J. Am. Chem. Soc.* **2007**, *129*, 11352–11353.

(13) (a) Janes, P. W.; Ley, S. C.; Magee, A. I. *J. Cell. Biol.* **1999**, *147*, 447–461. (b) Kenworthy, A. K.; Petranova, N.; Edidin, M. *Mol. Biol. Cell* **2000**, *11*, 1645–1655.

(14) Schultz, G. J.; Kada, G.; Pastushenko, V. P.; Schindler, H. *EMBO J.* **2000**, *19*, 892–901.

(15) (a) Sharma, P.; Varma, R.; Sarasij, R. C.; Ira; Gousset, K.; Krishnamoorthy, G.; Rao, M.; Mayor, S. *Cell* **2004**, *116*, 577–589. (b) Vrljic, M.; Nishimura, S. Y.; Brasselet, S.; Moerner, W. E.; McConnell, H. M. *Biophys. J.* **2002**, *83*, 2681–2692. (c) Kenworthy, A. K.; Nichols, B. J.; Remmert, C. L.; Hendrix, G. M.; Kumar, M.; Zimmerberg, J.; Lippincott-Schwartz, J. *J. Cell. Biol.* **2004**, *165*, 735–46.

(16) (a) Haluska, C. K.; Schröder, A. P.; Didier, P.; Heissler, D.; Duportail, G.; Mély, Y.; Marques, C. M. *Biophys. J.* **2008**, *95*, 5737–5747. (b) Xu, X.; Bittman, R.; Duportail, G.; Heissler, D.; Vilchéze, C.; London, E. *J. Biol. Chem.* **2001**, *276*, 33540–33546.

(17) (a) Korlach, J.; Schwille, P.; Webb, W. W.; Feigenson, G. W. *Proc. Natl. Acad. Sci. U.S.A.* **1999**, *96*, 8461–8466. (b) Baumgart, T.; Hunt, G.; Farkas, E. R.; Webb, W. W.; Feigenson, G. W. *Biochim. Biophys. Acta* **2007**, *1768*, 2182–2194.

(18) (a) Bagatolli, L. A. *Biochim. Biophys. Acta* **2006**, *1758*, 1541–1556. (b) Parasassi, T.; Gratton, E.; Yu, W. M.; Wilson, P.; Levi, M. *Biophys. J.* **1997**, *72*, 2413–2429. (c) Gaus, K.; Gratton, E.; Kable, E. P. W.; Jones, A. S.; Gelissen, I.; Kritharides, L.; Jessup, W. *Proc. Natl. Acad. Sci. U.S.A.* **2003**, *100*, 15554–15559.

(19) (a) Kim, H. M.; Choo, H.-J.; Jung, S.-Y.; Ko, Y.-G.; Park, W.-H.; Jeon, S.-J.; Kim, C. H.; Joo, T.; Cho, B. R. *ChemBioChem* **2007**, *8*, 553–559. (b) Kim, H. M.; Jeong, B. H.; Hyon, J.-Y.; An, M. J.; Seo, M. S.; Hong, J. H.; Lee, K. J.; Kim, C. H.; Joo, T.; Hong, S.-C.; Cho, B. R. *J. Am. Chem. Soc.* **2008**, *130*, 4246–4247.

(20) (a) Jin, L.; Millard, A. C.; Wuskell, J. P.; Clark, H. A.; Loew, L. M. *Biophys. J.* **2005**, *89*, L4–L6. (b) Jin, L.; Millard, A. C.; Wuskell, J. P.; Dong, X.; Wu, D.; Clark, H. A.; Loew, L. M. *Biophys. J.* **2006**, *90*, 2563–2575.

(21) (a) Klymchenko, A. S.; Oncul, S.; Didier, P.; Schaub, E.; Bagatolli, L.; Duportail, G.; Mély, Y. *Biochim. Biophys. Acta* **2009**, *1788*, 495–499. (b) M'Baye, G.; Mély, Y.; Duportail, G.; Klymchenko, A. S. *Biophys. J.* **2008**, *95*, 1217–25. (c) Klymchenko, A. S.; Mély, Y.; Demchenko, A. P.; Duportail, G. *Biochim. Biophys. Acta* **2004**, *1665*, 6–19.

(22) Shynkar, V. V.; Klymchenko, A. S.; Kunzelmann, C.; Duportail, G.; Muller, C. D.; Demchenko, A. P.; Freyssinet, J.-M.; Mély, Y. *J. Am. Chem. Soc.* **2007**, *129*, 2187–2193.

(23) (a) Greenspan, P.; Mayer, E. P.; Fowler, S. D. *J. Cell. Biol.* **1985**, *100*, 965–973. (b) Diaz, G.; Melis, M.; Batetta, B.; Angius, F.; Falchi, A. *Micron* **2008**, *39*, 819–824.

(24) Greenspan, P.; Fowler, S. D. *J. Lipid Res.* **1985**, *26*, 781–789.

(25) (a) Lampe, J. N.; Fernandez, C.; Nath, A.; Atkins, W. M. *Biochemistry* **2008**, *47*, 509–516. (b) Gillies, E. R.; Jonsson, T. B.; Freíchet, Jean M. J. *J. Am. Chem. Soc.* **2004**, *126*, 11936–11943. (c) Maiti, N. C.; Krishna, M. M. G.; Britto, P. J.; Periasamy, N. *J. Phys. Chem. B* **1997**, *101*, 11051–11060. (d) Freeman, D. M.; Kroe, R. R.; Ruffles, R.; Robson, J.; Coleman, J. R.; Grygon, C. A. *Biophys. J.* **2001**, *80*, 2375. (e) Gao, F.; Mei, E.; Lim, M.; Hochstrasser, R. M. *J. Am. Chem. Soc.* **2006**, *128*, 4814–4822. (f) Nath, A.; Koo, P. K.; Rhoades, E.; Atkins, W. M. *J. Am. Chem. Soc.* **2008**, *130*, 15746–15747. (g) Chen, G.; Guan, Z. *J. Am. Chem. Soc.* **2004**, *126*, 2662–2663. (h) Mukherjee, S.; Raghuraman, H.; Chattopadhyay, A. *Biochim. Biophys. Acta* **2007**, *1768*, 59–66.

Chart 1. Probes Nile Red and NR12S and Their Hypothetic Localization with Respect to Lipids (Blue) in Membranes; Anchor Part of the NR12S Probe Is in Red

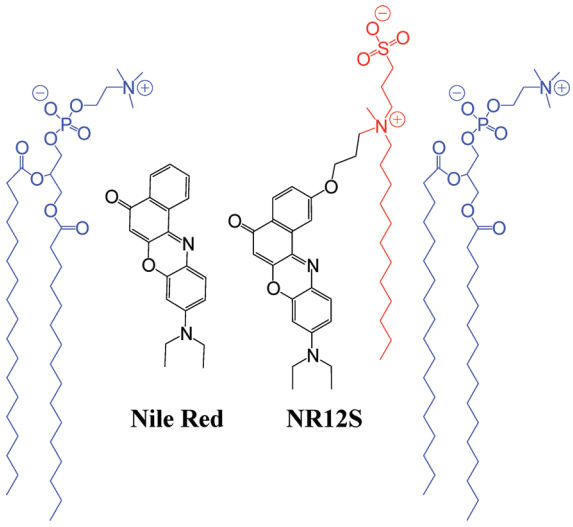

by conjugating it with a zwitterionic group and a long hydrophobic chain.[22] Though the obtained probe was hypothesized to bind to the outer biomembrane leaflet without further fast flip-flop, we could not provide a direct evidence for this.

In the present work, using the same design, we developed a new Nile Red based probe for cell plasma membranes. Moreover, using a unique switching property of Nile Red fluorophore that was not reported before, we showed that, unlike the parent Nile Red, the novel probe stains exclusively the outer leaflet of lipid vesicles and cells. Furthermore, the probe was found to exhibit strongly different emission in Lo and Ld phases, and in living cells, its emission color varies with the cholesterol content. Thus, this probe constitutes a new tool for quantification of cholesterol-rich Lo phase in cell plasma membranes.

Materials and Methods

All chemicals and solvents for synthesis were from Sigma-Aldrich. Synthesis of NR12S is described in Supporting Information.

Lipid Vesicles. Dioleoylphosphatidylcholine (DOPC), dioleoylphosphatidylserine (DOPS), and cholesterol were purchased from Sigma-Aldrich. Bovine brain sphingomyelin (SM) was from Avanti Polar Lipids (Alabaster, AL). Large unilamellar vesicles (LUVs) were obtained by the extrusion method as previously described.[26] Briefly, a suspension of multilamellar vesicles was extruded by using a Lipex Biomembranes extruder (Vancouver, Canada). The size of the filters was first 0.2 μm (7 passages) and thereafter 0.1 μm (10 passages). This generates monodisperse LUVs with a mean diameter of 0.11 μm as measured with a Malvern Zetamaster 300 (Malvern, U.K.). LUVs were labeled by adding aliquots (generally 2 μL) of probe stock solutions in dimethyl sulfoxide to 1-mL solutions of vesicles. Since the probe binding kinetics is very rapid, the fluorescence experiments were performed a few minutes after addition of the aliquot. A 20 mM phosphate buffer, pH 7.4, was used in these experiments. Concentrations of the probes and lipids were generally 1 and 200 μM, respectively.

Giant unilamellar vesicles (GUVs) were generated by electroformation in a home-built liquid cell (University of Odense, Denmark), using previously described procedures.[27] A 0.1 mM solution of lipids in chloroform was deposited on the platinum wires of the chamber, and the solvent was evaporated under vacuum for 30 min. The chamber, thermostatted at 55 °C, was filled with a 300 mM sucrose solution, and a 2-V, 10-Hz alternating electric current was applied to this capacitor-like configuration for ca. 2 h. Then, a 50 μL aliquot of the obtained stock solution of GUVs in sucrose (cooled down to room temperature) was added to 200 μL of 300 mM glucose solution to give the final suspension of GUVs used in microscopy experiments. The staining of GUVs was performed by addition of an aliquot of the probe stock solution in DMSO to obtain a 0.1 μM final probe concentration (final DMSO volume <0.25%).

Reversible Bleaching of Nile Red and NR12S with Sodium Dithionite and Flip-Flop Studies. A 1 M stock solution of sodium dithionite in 1 M Tris was used for the experiments. To 1 mL of 5 μM solution of Nile Red or NR12S in a 1:1 (v/v) ethanol/water mixture in a quartz cuvette was added an aliquot of the stock solution of dithionite to a final concentration 2 mM. Then, approximately 25 mL of air was applied to this solution through a syringe for approximately 20 s. The procedure of dithionite and air treatment was repeated several times. During all steps of this cyclic treatment, the absorbance at 590 nm (Nile Red) was measured as a function of time. For the flip-flop studies, DOPC LUVs were labeled with probes Nile Red and NR12S by two different methods. In method 1, the probe was mixed with lipids in chloroform, and the vesicles were prepared from this mixture as described above. This method ensured symmetric distribution of the probe between both leaflets. In method 2, the probe was added to 0.5 mL of buffer and then mixed with 0.5 mL of suspension of nonlabeled vesicles and incubated at room temperature for 5 min, which allowed initial staining of the outer membrane leaflet. The final probe concentration for both methods was 1 μM. To study the flip-flop kinetics, the fraction (%) of NR12S probe flipped from the outer to the inner leaflet in LUVs was evaluated as a function of time at 20 and 37 °C. The suspension of LUVs was stained with a probe by method 2. After a given incubation time (at 20 or 37 °C), the fluorescence intensities at 610 nm before (I_0) and 3 min after addition of 10 mM sodium dithionite (I_{DT}) were measured. The fraction of flipped probe for a given incubation time was expressed as $I_{DT}/I_0 \times 100\%$.

Cell Lines, Culture Conditions, and Treatment. The U87MG human glioblastoma cell line (ATCC) was cultured in Eagle's minimal essential medium (EMEM from LONZA) with 10% heat-inactivated fetal bovine serum (PAN Biotech GmbH) and 0.6 mg/mL glutamine (Biowhittaker) at 37 °C in a humidified 5% CO_2 atmosphere. Cell concentration of $5-10 \times 10^4$ cells/mL was maintained by removal of a portion of the culture and replacement with fresh medium 3 times per week. Cholesterol depletion and enrichment of cell membranes was performed using methyl-β-cyclodextrin (MβCD) and MβCD−cholesterol complex (Sigma-Aldrich), respectively, according to described procedures.[28] Briefly, stock solutions of MβCD and MβCD−cholesterol complex in Dulbecco's phosphate-buffered saline (DPBS) were prepared at a suitable concentration, filtered by Millipore filter (0.2 μm), and added to the cells to a final concentration of 5 mM. The treated cells were kept in the incubator at 37 °C for 30 min or 2 h.

In fluorescence spectroscopy experiments, cells were detached by trypsinization. EMEM medium was first removed from the culture dish, and cells were washed two times with DPBS. Trypsin 10x (LONZA) solution was diluted 10 times by DPBS and incubated with the cells at 37 °C for 4 min. The solution of trypsinized cells was then diluted by DPBS, transferred to Falcon tubes and centrifuged at 1500 rpm for 5 min. The washing procedure was repeated one more time with HBSS solution. To stain the cell suspension with the NR12S probe, an appropriate aliquot of its stock

(26) Hope, M. J.; Bally, M. B.; Webb, G.; Cullis, P. R. *Biochim. Biophys. Acta* **1985**, *812*, 55–65.

(27) (a) Angelova, M. I.; Dimitrov, D. S. *Faraday Discuss.* **1986**, *81*, 303–311. (b) Fidorra, M.; Duelund, L.; Leidy, C.; Simonsen, A. C.; Bagatolli, L. A. *Biophys. J.* **2006**, *90*, 4437–4451. (c) Kahya, N.; Scherfeld, D.; Bacia, K.; Poolman, B.; Schwille, P. *J. Biol. Chem.* **2003**, *278*, 28109–28115.

(28) Zidovetzki, R.; Levitan, I. *Biochim. Biophys. Acta* **2007**, *1768*, 1311–1324.

solution in DMSO was added to 0.5 mL of HBSS buffer, and after vortexing the solution was immediately added to 0.5 mL of the cell suspension to obtain a final probe concentration of 0.1 μM (<0.25% DMSO) and a cell concentration of $5 \times 10^5-10^6$ cells/mL. It should be noted that only freshly prepared solutions of the probe in HBSS should be used (<1 min) for cell staining, because of the slow aggregation of the probe in water. Before measurements, the cell suspension with probe was incubated for 7 min at room temperature in the dark. For the microscopy studies, attached cells were washed two times by gentle rinsing with HBSS. A freshly prepared solution of NR12S or Nile Red in HBSS was then added to the cells to a final concentration of 0.3 μM (<0.25% DMSO volume) and incubated for 7 min in the dark at room temperature.

Fluorescence Spectroscopy and Microscopy. Absorption spectra were recorded on a Cary 4 spectrophotometer (Varian) and fluorescence spectra on a FluoroMax 3.0 (Jobin Yvon, Horiba) spectrofluorometer. Fluorescence emission spectra were systematically recorded at 520 nm excitation wavelength at room temperature, unless indicated. All the spectra were corrected from the fluorescence of the corresponding blank (suspension of cells or lipid vesicles without the probe). Fluorescence quantum yields (QY) were measured using solution of Nile Red in methanol as a reference (QY = 38%).[29] Fluorescence microscopy experiments were performed by using a home-built two-photon laser scanning setup based on an Olympus IX70 inverted microscope with an Olympus 60x 1.2NA water immersion objective.[30] Two-photon excitation was provided by a titanium-sapphire laser (Tsunami, Spectra Physics), and photons were detected with Avalanche Photodiodes (APD SPCM-AQR-14-FC, Perkin-Elmer) connected to a counter/timer PCI board (PCI6602, National Instrument). Imaging was carried out using two fast galvo mirrors in the descanned fluorescence collection mode. Typical acquisition time was 5 s with an excitation power around 2.5 mW (λ = 830 nm) at the sample level. Images corresponding to the blue and red channels were recorded simultaneously using a dichroic mirror (Beamsplitter 585 DCXR) and two APDs. The images were processed with a homemade program under LabView that generates a ratiometric image by dividing the image of the blue channel by that of the red channel. For each pixel, a pseudocolor scale is used for coding the ratio, while the intensity is defined by the integral intensity recorded for both channels at the corresponding pixel.[21a]

Results and Discussion

Design and Synthesis. The design of the new probe NR12S (Chart 1) is based on the conjugation of the Nile Red fluorophore with an anchor group, which was recently proposed for localizing 3-hydroxychromone dyes at the outer leaflet of the cell plasma membrane.[22] This anchor group is composed of a long alkyl chain and a zwitterionic group, allowing strong interactions with the lipid membranes and thus their specific staining.

To functionalize Nile Red, we prepared 2-hydroxy-substituted Nile Red from 5-(diethylamino)-2-nitrosophenol and naphthalene-1,6-diol according to an available procedure.[31] The obtained 2-hydroxy-Nile Red was alkylated with 1-bromo-3-chloropropane. The product was further reacted with dodecylmethylamine, and the obtained tertiary amine was then quaternized by 1,3-propane sultone affording the final probe NR12S (see Supporting Information).

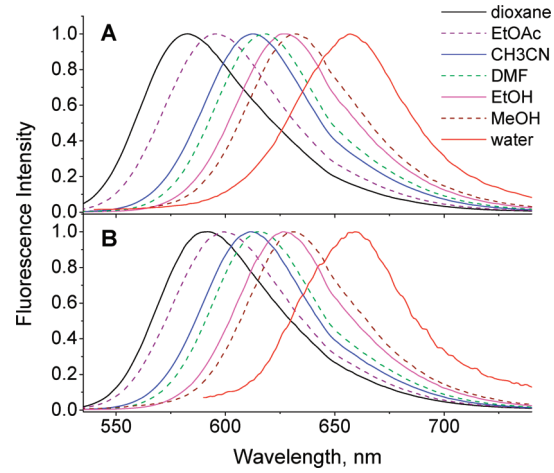

Figure 1. Normalized fluorescence spectra of Nile Red (A) and NR12S (B) in different solvents.

Table 1. Spectroscopic Properties of Studied Dyes in Organic Solvents[a]

		dye					
		Nile Red			NR12S		
solvent	$E_T(30)$	λ_{abs}, nm	λ_{fluor}, nm	QY, %	λ_{abs}, nm	λ_{fluo}, nm	QY, %
dioxane	36.0	520	583	91	526	592	74
EtOAc	38.1	525	595	87	527	599	84
THF	37.4	530	595	90	530	597	81
CH_2Cl_2	40.7	541	601	88	542	602	80
DMF	43.2	544	618	63	544	615	69
DMSO	45.1	554	629	46	554	627	55
CH_3CN	45.6	536	612	82	536	612	81
EtOH	51.9	550	626	52	550	626	52
MeOH	55.4	553	632	38[b]	555	631	40
buffer	63.1	591	657	5.0	521	657	0.2

[a] λ_{abs} and λ_{fluor}, are absorption and emission maxima, respectively. Buffer refers to a 20 mM phosphate buffer (pH 7.4). [b] The QY value is from ref 29.

Characterization in Solvents. The spectroscopic properties of NR12S were studied in comparison to the parent Nile Red in different organic solvents. The absorption and fluorescence spectra of the two dyes were highly similar (Figure 1), especially in solvents of medium polarity. Moreover, both dyes show a similar strong red shift of their emission on increase in solvent polarity. However, differences in the emission spectra were observed in less polar solvents (dioxane and ethyl acetate), which could be connected with the effect of the proximal polar charged group.[32]

Similarly to the parent Nile Red, NR12S shows high fluorescence QY in most organic solvents (Table 1). Remarkably, in aqueous buffer NR12S is almost nonfluorescent (QY = 0.2%), whereas Nile Red is significantly fluorescent (QY = 5.0%). This could be explained by the detergent-like structure of NR12S, so that in water it may form oligomers or micelles, where its fluorophore is probably self-quenched. The existence of NR12S oligomers in water is also supported by the strongly blue-shifted absorption maximum in water as compared to that in organic solvents (Table 1). A similar quenching in water was observed for 3-hydroxyflavone derivatives bearing an amphiphilic group analogous to NR12S.[22,32b]

(29) Deda, M. L.; Ghedini, M.; Aiello, I.; Pugliese, T.; Barigelletti, F.; Accorsi, G. *J. Organomet. Chem.* **2005**, *690*, 857–861.
(30) (a) Clamme, J.-P.; Azoulay, J.; Mély, Y. *Biophys. J.* **2003**, *84*, 1960–1968. (b) Azoulay, J.; Clamme, J.-P.; Darlix, J.-L.; Roques, B. P.; Mely, Y. *J. Mol. Biol.* **2003**, *326*, 691–700.
(31) (a) Martin-Brown, S. A.; Fu, Y.; Saroja, G.; Collinson, M. M.; Higgins, D. A. *Anal. Chem.* **2005**, *77*, 486–494. (b) Briggs, M. S. J.; Bruce, I.; Miller, J. N.; Moody, C. J.; Simmonds, A. C.; Swann, E. *J. Chem. Soc. Perkin Trans. 1* **1997**, 1051–1058.
(32) (a) Klymchenko, A. S.; Demchenko, A. P. *J. Am. Chem. Soc.* **2002**, *124*, 12372–12379. (b) Klymchenko, A. S.; Duportail, G.; Ozturk, T.; Pivovarenko, V. G.; Mély, Y.; Demchenko, A. P. *Chem. Biol.* **2002**, *9*, 1199–1208.

Table 2. Spectroscopic Properties of Nile Red and NR12S in Lipid Vesicles[a]

		dye					
		Nile Red			NR12S		
composition	phase state	λ_{abs}, nm	λ_{fluo}, nm	QY, %	λ_{abs}, nm	λ_{fluo}, nm	QY, %
DOPC	Ld	549	628	42	530	608	48
DOPC/CL	Ld	550	624	48	527	605	47
DPPC	Lβ	550	608	34	527	599	8
DPPC/CL	Lo	552	595	60	521	556	32
DPPC/CL (60)	Ld		603	72		601	57
SM	Lβ	543	617	40	528	596	18
SM/CL	Lo	530	586	45	521	572	30
SM/CL (60)	Ld		612	53		593	45
DOPS	Ld	553	628	41	532	606	50

[a] λ_{abs} and λ_{fluor} are absorption and emission maxima, respectively. All spectra were recorded at 20 °C, except those marked "(60)", which were recorded at 60 °C. In lipid mixtures, the cholesterol/lipid ratio was 1:2, mol/mol. Ld, Lo, and Lβ correspond to liquid disordered, liquid ordered, and solid gel phases.

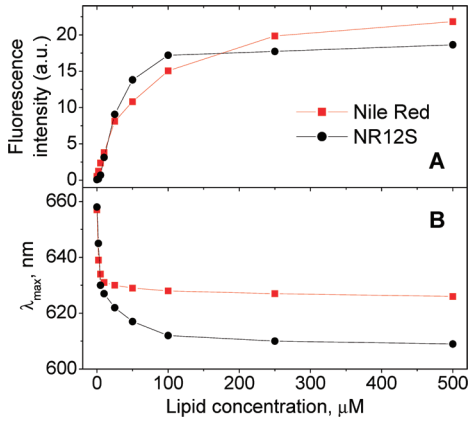

Figure 2. Fluorescence of Nile Red and NR12S probes at different concentrations of DOPC LUVs. Integral intensity (A) and position of the maximum (B) vs DOPC concentration (phosphate buffer 20 mM, pH 7.4). Probe concentration was 0.5 μM.

Binding to Lipid Vesicles. Binding of the NR12S probe to DOPC lipid vesicles results in an about 200-fold increase of its fluorescence intensity, as can be seen from the quantum yields in aqueous buffer and in lipid vesicles (Tables 1 and 2). With the parent Nile Red, this increase is much less pronounced (only ca. 8-fold) due to its relatively high quantum yield in aqueous buffer. Therefore, NR12S dye is advantageous as a membrane probe, since unlike Nile Red its background fluorescence from the buffer can be neglected. The high fluorescence quantum yield of NR12S in lipid vesicles indicates that the probe oligomerization in water is likely reversible, so that an efficient membrane staining is achieved without additional solubilization techniques (with detergents or cyclodextrins). Moreover, titrations (Figure 2A) show that on increase in the lipid concentration, the fluorescence intensity of NR12S grows steeply and saturates at a probe/lipid ratio of 1:200, while for Nile Red this increase is less steep and saturation is reached only at a probe/lipid ratio 1:1000. These results suggest that NR12S binds more strongly to lipid membranes than Nile Red as a result of its amphiphilic anchor group. In addition, the position of the emission maximum of NR12S in DOPC LUVs at low probe/lipid ratio ($\leq$1:200) is significantly blue-shifted (17 nm) with respect to Nile Red (Figure 2B), indicating a deeper embedding of the fluorophore in the bilayer. However, at high probe/lipid ratios ($\geq$1:10), the emission maximum of NR12S becomes

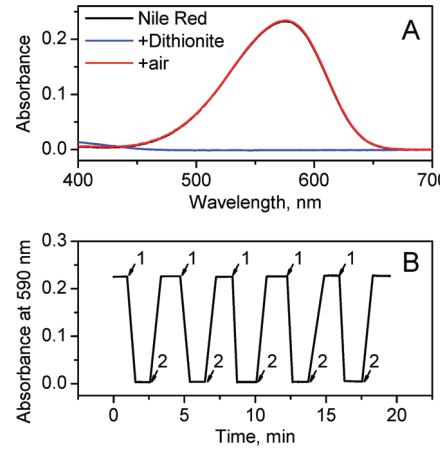

Figure 3. On/off redox switching of Nile Red by dithionite/air treatment. (A) Absorption spectra of Nile Red in ethanol/water mixture (1:1, v/v) before treatment, after addition of 2 mM dithionite, and after further bubbling of air for 20 s. Extended spectral data are presented in Supporting Information. (B) Absorbance at 590 nm of Nile Red solution (ethanol/water) on repetitive treatment with 2 mM dithionite (1) and air bubbling (2). Inclined lines in (B) are used only for convenient presentation (connecting the experimental data points) and do not represent the transition kinetics between the low and high values of absorbance.

nearly the same as that of Nile Red, suggesting that the excess of NR12S probe binds nonspecifically to DOPC lipid bilayers and exhibits a shallower fluorophore insertion, similar to that of Nile Red.

Flip-Flop Studies Using Nile Red Reversible Bleaching with Dithionite. One important issue in application of biomembrane probes is to evaluate their ability to stain selectively the outer membrane leaflet without fast flip-flop redistributing the dye between both leaflets. This problem was previously addressed for lipids modified with the NBD[33] fluorophore or spin-labels[34] using reducing agents, sodium dithionite and ascorbate, respectively, which inactivate the labels selectively in the outer leaflet of lipid vesicles. Though Nile Red is a chemically stable dye, it contains a quinoid fragment, which is a potential target for reduction. Moreover, the Nile Red analogues Nile Blue and resorufin can be reversibly reduced by different agents,[35] including dithionite. We checked the ability of Nile Red to be reduced by sodium dithionite in water/ethanol (1:1, v/v) solution. Addition of 2 mM dithionite leads to a complete disappearance of the absorption band of Nile Red (Figure 3A). Remarkably, after bubbling of air through this sample, the absorption band is fully recovered. This indicates that bleaching of Nile Red by dithionite is a fully reversible reduction process, so that this fluorophore can be switched off and on in a well-controlled manner. Furthermore, our data show that the reduction−oxidation cycle can be repeated many times without noticeable loss of the fluorophore (Figure 3B). The same results were obtained with the NR12S dye (see Supporting Information).

(33) McIntyret, J. C.; Sleight, R. G. *Biochemistry* **1991**, *30*, 11819–11827.
(34) (a) Seigneuret, M.; Devaux, P. F. *Proc. Natl. Acad. Sci. U.S.A.* **1984**, *81*, 3751–3755. (b) Kornberg, R. D.; McConnell, H. M. *Biochemistry* **1971**, *10*, 1111–1120.
(35) (a) Lemmon, T. L.; Westall, J. C.; Ingle, J. D., Jr. *Anal. Chem.* **1996**, *68*, 947–953. (b) Gorodetsky, A. A.; Ebrahim, A.; Barton, J. K. *J. Am. Chem. Soc.* **2008**, *130*, 2924–2925. (c) Cincotta, L.; Foley, J. W.; Cincotta, A. H. *Cancer Res.* **1993**, *53*, 2571–2580. (d) Erb, R. E.; Ehlers, M. H. *J. Dairy Sci.* **1950**, *33*, 853–864. (e) Zhou, M.; Diwu, Z.; Panchuk-Voloshina, N.; Haugland, R. P. *Anal. Biochem.* **1997**, *253*, 162–168. (f) Talbot, J. D.; Barrett, J. N.; Barrett, E. F.; David, G. *J. Neurochem.* **2008**, *105*, 807–819.

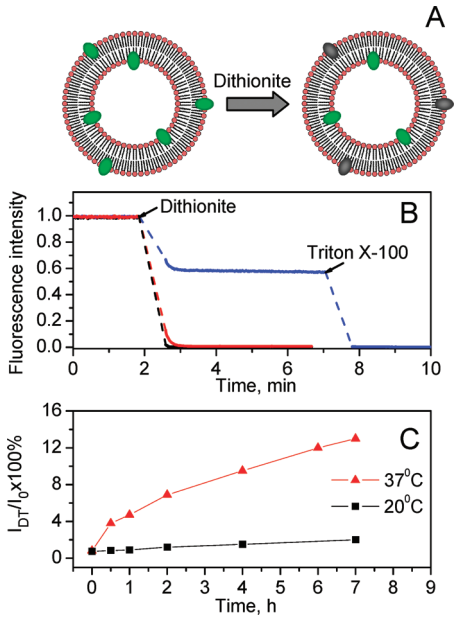

Figure 4. Flip-flop studies of probes Nile Red and NR12S in DOPC LUVs using the dithionite bleaching method. (A) Schematic presentation of the selective bleaching of the probes at the outer leaflet of LUV by dithionite. (B) Evolution of the probe fluorescence intensity after addition of 10 mM dithionite and 1% (vol) of Triton X-100. Dyes were added to lipids either before LUV preparation to achieve staining of both leaflets (Nile Red = black line, NR12S = blue line) or after LUV preparation to stain the outer leaflet (NR12S = red line). (C) Fraction (%) of NR12S probe flipped from the outer to the inner leaflet in LUVs as a function of time at 20 and 37 °C. The suspension of LUVs was stained with the probe by method 2. After a given incubation time (at 20 or 37 °C), the fluorescence intensities at 600 nm before (I_0) and 3 min after addition of 10 mM sodium dithionite (I_{DT}) were measured. The fraction of flipped probe for a given incubation time was expressed as $I_{DT}/I_0 \times 100\%$. The probes concentration for both methods was 1 μM.

Since sodium dithionite is unable to penetrate the lipid bilayers, it can bleach the Nile Red fluorophore exclusively on the external leaflet (Figure 4A) and thus allows evaluation of the probe flip-flop, as it was done previously with NBD-labeled lipids.[33] For this purpose, we stained the lipid membranes in two different ways. In method 1, the probe was mixed with lipids first and then the vesicles were prepared, which ensured its symmetric distribution between both leaflets. In method 2, the probe was added to the vesicles from the external bulk solution to target the outer membrane leaflet. When the parent Nile Red probe was distributed in both leaflets (method 1), the addition of 10 mM dithionite resulted in complete bleaching (Figure 4B). An identical result was observed when the dye was added to vesicles from the bulk water (method 2, data not shown). Thus, Nile Red undergoes probably a very fast flip-flop, so that addition of dithionite can rapidly bleach the dye located initially on both leaflets. In contrast, when dithionite was added to vesicles stained with NR12S symmetrically on both leaflets (method 1), the fluorescence intensity drops rapidly until approximately 50% of the initial value (Figure 4B) and then remains relatively stable. Further addition of Triton X-100, which disrupts the lipid vesicles, leads to complete disappearance of fluorescence. This result is fully in line with that previously reported for NBD-lipids,[33] indicating that selective bleaching of NR12S fluorophore at the outer leaflet was achieved (Figure 4A), while the other 50% of the probe at the inner leaflet remained intact. The stabilization of the fluorescence intensity at ca. 50% of its initial value suggests that NR12S does not flip

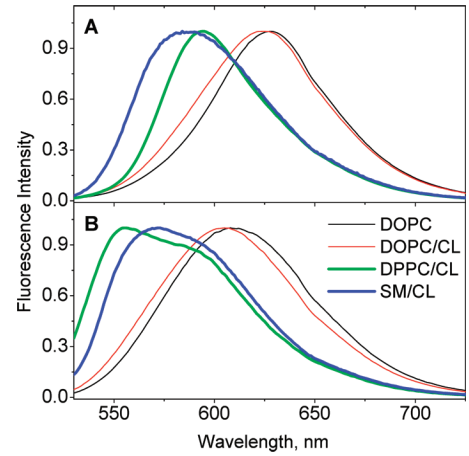

Figure 5. Normalized fluorescence spectra of Nile Red (A) and NR12S (B) in LUVs of different lipid compositions. Probe and lipid concentrations were 1 and 200 μM, respectively.

to the outer leaflet within the experimental time. Importantly, when the staining was performed by addition of the probe to blank vesicles (method 2), the treatment with sodium dithionite resulted in rapid and complete bleaching (Figure 4B). The absence of residual fluorescence in this case clearly shows that NR12S stains exclusively the outer leaflet of vesicles and remains there at least within the incubation time (7 min, rt). We also incubated vesicles with the NR12S probe initially bound to the outer leaflet for longer time periods at 20 and 37 °C. Remarkably, at room temperature the residual fluorescence after dithionite treatment was still negligible even after 2 h of incubation and became significant (2%) only after 7 h of incubation (Figure 4C). Thus, at room temperature, the flip-flop process for NR12S is extremely slow. At 37 °C, the flip-flop was faster, though after 4 h only 9% of the probe migrated to the inner leaflet (Figure 4C).

Thus, according to our data, Nile Red redistributes between the two leaflets on the time scale of seconds or faster, whereas NR12S shows only marginal flip-flop for hours at room temperature. This dramatically decreased flip-flop dynamics of NR12S is evidently due to the anchor group containing a zwitterion and a long alkyl chain, which interact strongly with lipids, preventing the probe flip-flop. This is one of the first reports where a spontaneous binding of a nonlipidic membrane fluorescent probe to the outer leaflet is demonstrated by a chemical method. Previously, outer leaflet staining was suggested for styrylpyridinium and 3-hydroxyflavone dyes from their sensitivity to the transmembrane electric potential and lipid asymmetry, or detection of second harmonic generation signal in cell membranes.[20,22] It should be also noted that, similarly to our data in water/ethanol mixtures, the bleached NR12S probe in lipid vesicles can be further switched "on" by air bubbling. However, the fluorescence recovery in this case takes more time (data not shown).

Sensitivity to Lipid Composition in Model Membranes. Nile Red, being an environment-sensitive probe, shows a dependence of its spectrum on the lipid composition and the phase state in lipid bilayers (Figure 5). Since spectroscopic differences between the Lo and Ld phases are an important requirement for the development of probes for lipid domains,[18–21] the new probe NR12S was compared to Nile Red in these two phases. Similar to Nile Red, the new probe shows a significantly blue-shifted emission maximum in Lo phase vesicles composed of sphingomyelin and cholesterol (SM/CL) or DPPC and cholesterol

(DPPC/CL), compared to Ld phase vesicles composed of DOPC or DOPC/CL (Figure 5). These results are in line with other environment-sensitive probes such as Prodan, Laurdan,[18] di-4-ANEPPDHQ,[20] and 3-hydroxyflavone derivatives[21] showing a less polar and less hydrated environment in the Lo phase. Importantly, in DPPC and SM vesicles presenting gel phase (Lβ), the probes show intermediate positions of their emission maxima (Table 2). Thus, for both probes the emission maximum shifts to the blue in the following sequence of membrane phases: Ld → Lβ → Lo, in line with recent data[20,21b] suggesting that the environment of these probes is the most dehydrated in the Lo phase.

An outstanding feature of the present dyes is that within the Ld phase, the position of their emission maximum is poorly sensitive to the presence of cholesterol (DOPC/CL vs DOPC, Figure 5, Table 2) Therefore, these dyes can clearly distinguish between cholesterol-rich Ld (DOPC/CL) and Lo (SM/CL or DPPC/CL) phases. In contrast, Prodan, Laurdan, 3-hydroxyflavone-based and di-4-ANEPPDHQ probes show a significant dependence of their spectra on the cholesterol content in the Ld phase,[18,20,36] so that the spectral differences between cholesterol-rich Ld and Lo phases are less pronounced for these probes. Moreover, unlike 3-hydroxyflavone-based probes, Nile Red and NR12S are insensitive to the surface charge (DOPS vs DOPC) (Table 2). Thus, in contrast to the other mentioned probes, Nile Red and NR12S show a characteristic blue-shifted emission only in cholesterol-rich Lo phase.

The fluorescence quantum yield of the probes also depends on the phase state of the lipid membranes, especially in the case of probe NR12S. Indeed, the highest quantum yields are observed with the Ld phase, and the lowest ones are associated with the Lβ phase. Because of its highly dense packing, the Lβ phase is likely characterized by a relatively low number of binding sites for the probe, leading to a less efficient probe binding (so that a significant fraction of the probe is in bulk solution), which decreases the apparent fluorescence quantum yield of the probe. In contrast, the loosely packed Ld phase presents a much larger number of binding sites, thus explaining a more efficient probe binding accompanied by a higher fluorescence intensity. The Lo phase presents an intermediate case. The weaker dependence of the fluorescence quantum yield of Nile Red on the phase state is probably due to its smaller size and less specific binding to lipid bilayers as compared to NR12S, which ensures a sufficient number of binding sites independently of the membrane phase. Noticeably, in contrast to data in organic solvents, the emission of NR12S in all studied lipid vesicles is systematically blue-shifted with respect to Nile Red (Tables 1 and 2). This indicates that the fluorophore of NR12S is more deeply embedded in the bilayer than Nile Red, in line with our conclusions on a more specific binding of NR12S to lipid membranes.

To further characterize the sensitivity of the dyes to the Lo phase, the effect of temperature was investigated. In SM/CL vesicles at 60 °C, both NR12S and Nile Red show significantly red-shifted spectra compared to those at 20 °C (Table 2), confirming the strong sensitivity of the probes to the Lo → Ld transition. This transition also increases the fluorescence quantum yield of the NR12S probe, likely due to the increase in the number of the probe binding sites.

Thus, the experiments in model membranes show that the new probe similarly to the parent Nile Red is highly sensitive to the phase state of lipid bilayers and distinguishes Lo from Ld phases by the color of its emission.

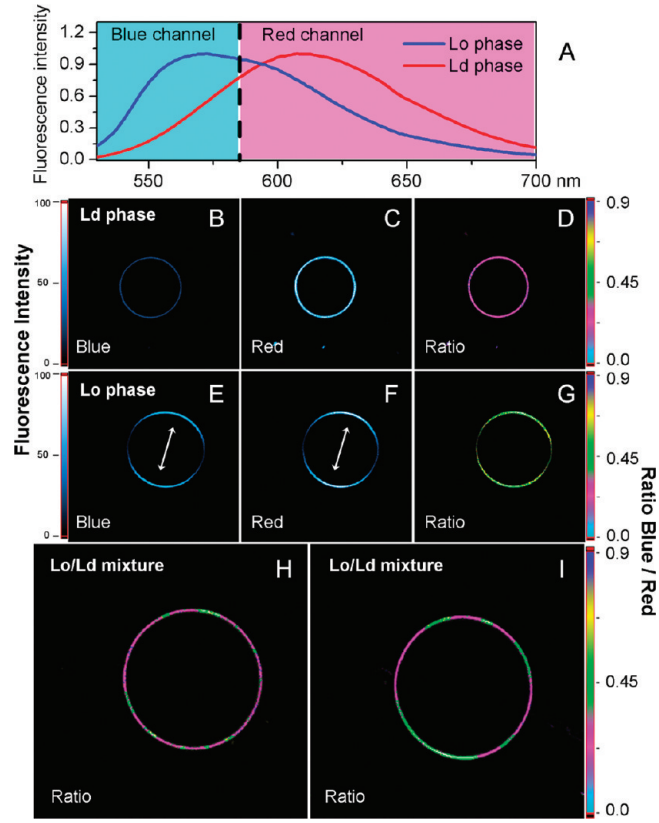

Figure 6. Fluorescence microscopy imaging of Lo and Ld phases in GUVs using NR12S. (A) Normalized fluorescence spectra of NR12S in Ld (DOPC) and Lo (SM/Chol) phases of LUVs. The cyan and magenta regions separated at 585 nm represent the detection range for the blue and red channels of the microscope. GUVs were composed of DOPC (Ld phase: B, C, D), SM/Chol, 2/1 (Lo phase: E, F, G), and DOPC/SM/Chol, 1/1/0.7 (mixed Lo/Ld phases: H,I). Intensity images at the blue (<585 nm, B and E) and the red (>585 nm, C and F) channels. In the ratiometric images (D, G, H, and I), the color of each pixel represents the value of the intensity ratio I_{blue}/I_{red}, while the pixel intensity corresponds to the total intensity at both channels. Two-photon excitation wavelength was at 830 nm. Arrows indicate the orientation of the light polarization. Sizes of the images were 70 μm × 70 μm. Probe concentration was 1 μM.

Imaging Cholesterol-Rich Phases in Giant Vesicles. Because of their relatively large size (5−100 μm), giant vesicles (GUVs) are an excellent biomembrane model for fluorescence microscopy studies.[27] We thus performed two-photon fluorescence imaging of GUVs using NR12S, in order to evaluate its capability to visualize Ld and Lo phases. We first measured the two-photon absorption cross-section of Nile Red and NR12S at 830 nm using Rhodamine B as a standard as described previously (see Supporting Information).[37] The observed values 32 and 30 GM (10^{-50} cm^4 × s × photon^{-1}) for Nile Red and NR12S, respectively, are sufficiently large for their application in two-photon microscopy.[37] Since the position of the emission maximum of NR12S changes in response to the phase state, ratiometric imaging[18,20] can be performed by splitting its emission into blue and red regions (Figure 6A). For the Ld phase (DOPC), the area under the NR12S emission spectrum in the blue region (<585 nm) is much smaller as compared to the red

(36) Massey, J. B. *Biochim. Biophys. Acta* **1998**, *1415*, 193–204.

(37) (a) Xu, C.; Webb, W. W. *J. Opt. Soc. Am. B* **1996**, *13*, 481–491. (b) Albota, M. A.; Xu, C.; Webb, W. W. *Appl. Opt.* **1998**, *37*, 7352–7356.

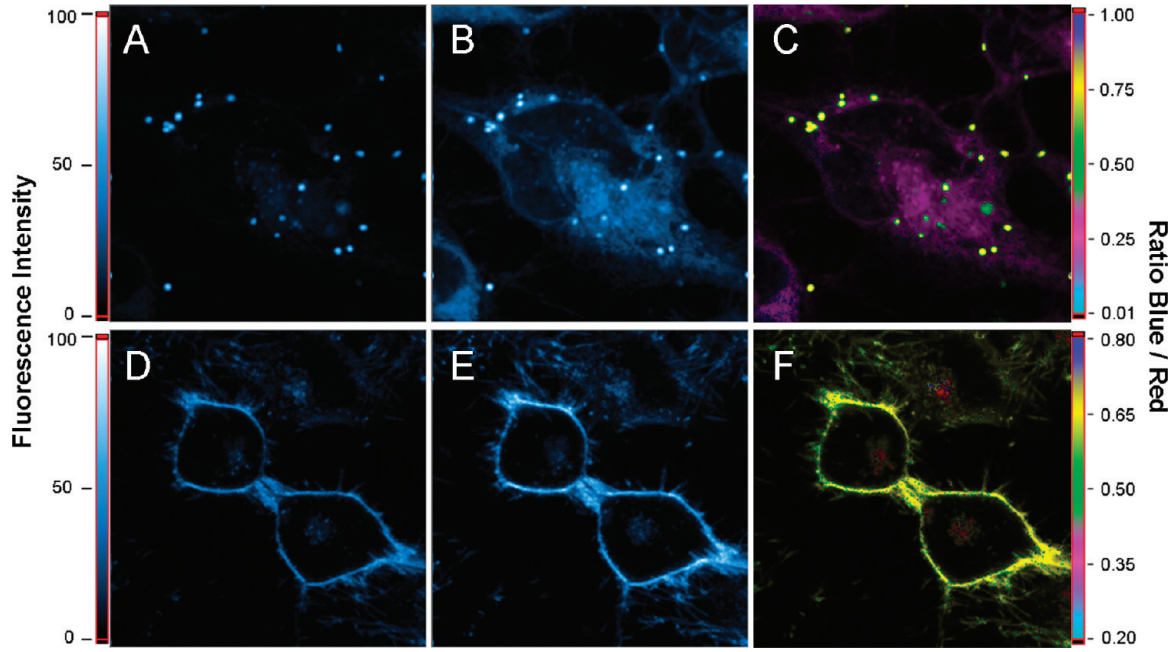

Figure 7. Fluorescence intensity (A, B, D, E) and ratiometric (C, F) images of cells stained with Nile Red (A−C) and NR12S (D−F). Intensity images at the short-wavelength "blue" (<585 nm, A and D) and the long-wavelength "red" (>585 nm, B and E) channels are presented. In the ratiometric images, the color of the pixel represents the value of the intensity ratio of the blue channel to that of the red channel, while the pixel intensity corresponds to the total number of photons collected at both channels. Two-photon excitation wavelength was at 830 nm. Sizes of the images were 70 μm × 70 μm. Probe concentration was 0.3 μM.

region (>585 nm), so that the estimated ratio of the integral intensities I_{blue}/I_{red} is ca. 0.23. In contrast, for Lo phase (SM/Chol), these areas are similar, and the corresponding I_{blue}/I_{red} value is ca. 0.88. This 4-fold difference in the ratio should be easily detectable by a fluorescence microscope having blue (<585 nm) and red (>585 nm) detection channels. In line with these expectations, the fluorescence images of the equatorial section of GUVs composed of DOPC (Ld phase) show that the intensity at the blue channel is much lower than at the red channel (Figure 6B and C), while for SM/Chol GUVs (Lo phase) these intensities are comparable (Figure 6E and F). In the ratiometric images, the GUV membranes in Ld phase appear predominantly in pink pseudocolor corresponding to a ratio around 0.20−0.25 (Figure 6D), which matches perfectly the predicted ratio from the fluorescence spectra. For Lo phase, GUV membranes appear in green-yellow pseudocolor corresponding to a ratio around 0.62−0.67 (Figure 6G), which also matches well the expected ratio.

Importantly, the ratiometric images of GUVs composed of DOPC/SM/Chol (1/1/0.7 molar ratios) present clear separated domains with two different pseudocolors (Figure 6H and I). These pseudocolors correspond well to those observed in pure Ld and Lo phases, which allows unambiguous assignment of the pink domains (low I_{blue}/I_{red} ratio) to Ld phase and the green domains (high I_{blue}/I_{red} ratio) to Lo phase. Importantly, the high fluorescence intensity from both Lo and Ld phases in the ternary mixture suggests that NR12S partitions evenly between them, though it is difficult to estimate the exact partition ratio. Since most fluorescent dyes preferentially bind Ld phase in ternary mixtures,[17] the even distribution of NR12S between Lo and Ld phases is an important advantage for their simultaneous visualization. Only few environment-sensitive dyes show this ability: Prodan derivatives, styrylpyrydinium dyes and, to lesser extent, 3-hydroxyflavone derivatives.[18–21]

Noticeably, while the fluorescence intensity of NR12S is homogeneously distributed all over the DOPC GUV membrane (Figure 6B and C), it depends on the orientation of the bilayer plane with respect to the polarization plane of the excitation light in SM/Chol GUVs (Figure 6E and F). In line with already reported data for other environment-sensitive and rod-shaped probes,[18,19,21a] the fluorescence intensity of NR12S in Lo phase is the highest when the light polarization is parallel to the probe fluorophore exhibiting preferentially vertical orientation due to the constrained lipid packing. In contrast, the loosely packed Ld phase of DOPC membrane imposes no preferential orientation for the fluorophore, so that efficient probe excitation can always be achieved.

Cellular Studies. Two-photon fluorescence imaging of living cells stained with the probes shows that Nile Red exhibits mainly intracellular fluorescence (Figure 7A−C), which according to the literature corresponds to a staining of lipid droplets.[23] Remarkably, the fluorescence ratio (blue/red channels) from the intracellular droplets is much larger than from other parts of the cell, in line with their highly apolar nature. In contrast, the new probe NR12S stains exclusively the cell plasma membrane, as it can be seen from the typical membrane staining profile and the rather uniform fluorescence intensity ratio within the image (Figure 7D−F). Thus, the conjugation of the Nile Red fluorophore with the detergent-like anchor group allows localizing the fluorophore on the cell membrane. Moreover, addition of 10 mM dithionite results in >90% bleaching of NR12S bound to the cells (see Supporting Information), showing a specific binding to the outer leaflet of the plasma membrane with almost no internalization into the cell.

The new probe showing high binding specificity together with high sensitivity to the membrane phase appears thus as an attractive tool for studying the lipid phases at the outer leaflet of living cells. The fluorescence maximum of NR12S in intact

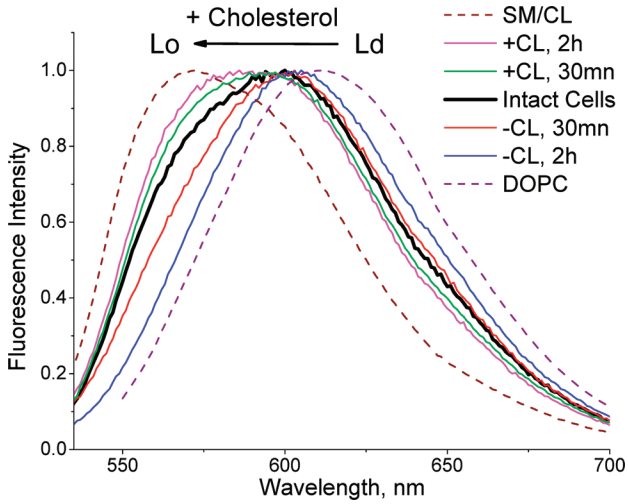

Figure 8. Normalized fluorescence spectra of 0.1 μM NR12S in cells at different levels of cholesterol depletion/enrichment and in model membranes presenting Lo (SM/CL) and Ld (DOPC) phases.

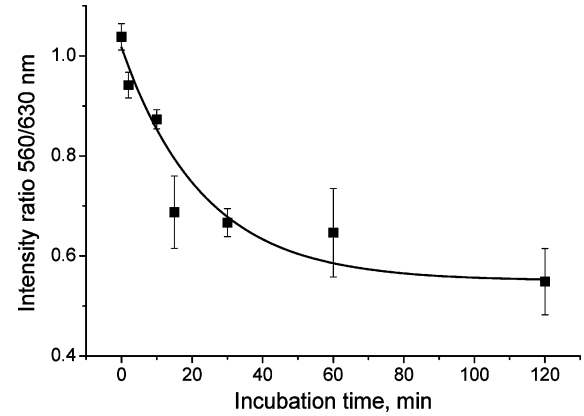

Figure 9. Monitoring the kinetics of cholesterol extraction from astrocytoma cells using NR12S probe. Ratio of the emission intensities at 560 and 630 nm of NR12S in cells treated with 5 mM MβCD for different times. The curve represents a single exponential fit to the experimental data. Each data point is the average of three measurements.

cells is intermediate to those with the Lo and Ld phases of model membranes (Figure 8), in line with the high content in plasma membranes of unsaturated lipids, sphingomyelin and cholesterol favoring both phases.[1,10] Other reports also suggested a significant fraction of Lo phase in the cell plasma membranes.[38] Importantly, the emission maximum of NR12S is stable for 30 min, confirming that flip-flop and internalization of the probe are relatively slow. Since cholesterol is a key component of the Lo phase, we modified its content in cell membranes, using methyl-β-cyclodextrin (MβCD).[11,28] On cholesterol depletion, the NR12S probe shows a red shift (Figure 8), so that the obtained spectrum is close to that with the Ld phase vesicles (DOPC, Figure 8). As NR12S is rather insensitive to cholesterol variation within Ld phase (see above), it likely reports on the disappearance of the Lo phase after cholesterol depletion. It should be noted that the present data do not provide a proof for the presence of separated Lo phase domains in cell membranes. Indeed, cell membranes can present a special phase, having features of both Lo and Ld phases, which can be converted into Ld phase after cholesterol depletion. Importantly, the red shift value depends on the incubation time of the cells with MβCD, suggesting an application of NR12S for a quantitative description of cholesterol depletion.

In order to monitor the kinetics of cholesterol depletion, we took the intensity ratio at the blue and red sides of the NR12S spectra, namely, 560 and 630 nm, where the variations of the relative intensities are maximal (Figure 8). Incubation with 5 mM MβCD results in a relatively rapid decrease in the intensity ratio 560/630 nm within the first 15 min, followed by slower changes at longer incubation times (Figure 9). Fitting the data to a single exponential decay provided a cholesterol depletion time constant of 23 $\pm$ 6 min, in excellent agreement with the half-time of 21 $\pm$ 6 min obtained previously from extraction of ^{3}H-labeled cholesterol with 2-hydroxypropyl-β-cyclodextrin.[11a] Other reports on model[39] and cellular membranes[11b,28] also suggest a similar time scale of cholesterol depletion, though the rate of the process depends strongly on the initial cholesterol content. The correspondence of our data with the literature shows that our method using NR12S can quantify cholesterol in cell membranes and describe its depletion kinetics.

In contrast to its depletion, cholesterol enrichment in living cells using MβCD−cholesterol complex shifts the NR12S emission to the blue, so that the obtained spectrum becomes closer to that of model vesicles presenting a homogeneous Lo phase (SM/CL, Figure 8). The spectroscopic effect increases with the time of incubation with the MβCD−cholesterol complex. Thus, the new probe can monitor in a rather broad range the cholesterol content and the fraction of cholesterol-rich Lo phase in cell membranes.

To visualize cells at different concentrations of cholesterol, we performed fluorescence ratiometric imaging before and after treatment with MβCD. After cholesterol depletion, there is a clear change in the pseudocolor of the cells, indicating a decrease in the intensity ratio recorded at the blue (<585 nm) and the red (>585 nm) parts of the probe emission spectrum (Figure 10). This decrease is in agreement with the red shift of the fluorescence spectra in cell suspensions (Figure 8). It can be also noticed that after cholesterol depletion, the cells differ one from another by their blue/red intensity ratio (Figure 10C), suggesting that the efficiency of cholesterol extraction varies from cell to cell. Moreover, after cholesterol extraction the cell membranes appear smoother, so that the numerous extensions of cell membranes are no more observed (Figure 10). These changes in morphology can be attributed to the disruption of the native cytoskeleton, which is highly cholesterol-dependent.[40] It can also be noted that neither intact cells nor cells treated with MβCD show membrane heterogeneity, which one would expect from separated Lo/Ld phase domains in the microscopic scale. Thus, though our data suggests the presence of

(38) (a) Hao, M.; Mukherjee, S.; Maxfield, F. R. *Proc. Natl. Acad. Sci. U.S.A.* **2001**, *98*, 13072–13077. (b) Gidwani, A.; Holowka, D.; Baird, D. *Biochemistry* **2001**, *40*, 12422–12429. (c) Swamy, M. J.; Ciani, L.; Ge, M.; Smith, A. K.; Holowka, D.; Baird, B.; Freed, J. H. *Biophys. J.* **2006**, *90*, 4452–4465. (d) Oncul, S.; Klymchenko, A. S.; Kucherak, O. A.; DemchenkoA. P.; Martin, S.; Dontenwill, M.; Arntz, Y.; Didier, P.; Duportail, G.; Mély, Y. *Biochim. Biophys. Acta* **2010**, in press, doi: 10.1016/j.bbamem.2010.01.013.

(39) Radhakrishnan, A.; McConnell, H. M. *Biochemistry* **2000**, *39*, 8119–8124.

(40) (a) Martin, S.; Phillips, D. C.; Szekely-Szucs, K.; Elghazi, L.; Desmots, F.; Houghton, J. A. *Cancer Res.* **2005**, *65*, 11447–11458. (b) Ramprasad, O. G.; Srinivas, G.; Rao, K. S.; Joshi, P.; Thiery, J. P.; Dufour, S.; Pande, G. *Cell Motil. Cytoskeleton* **2007**, *64*, 199–216. (c) Patra, S. K. *Biochim. Biophys. Acta* **2008**, *1785*, 182–206.

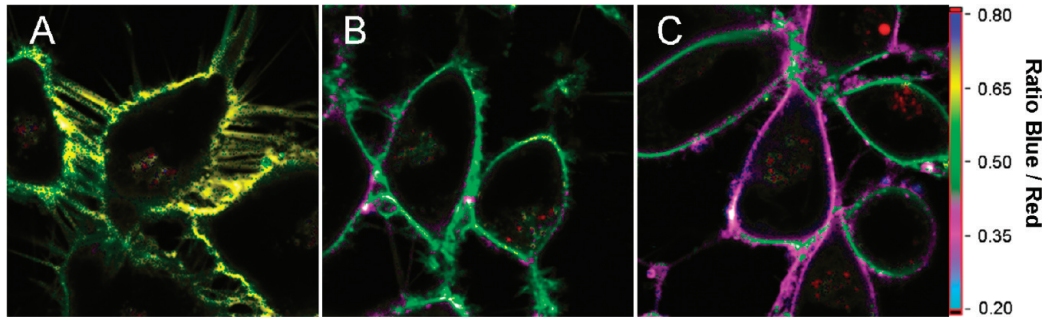

Figure 10. Fluorescence ratiometric images of cells stained with NR12S at different levels of cholesterol depletion. Intact cells (A) and cells after incubation with 5 mM MβCD for 30 min (B) and 2 h (C). The color of each pixel represents the value of the intensity ratio of the blue to the red channel, while the pixel intensity corresponds to the total number of photons collected at both channels. Two-photon excitation wavelength was at 830 nm. Sizes of the images were 50 $\times$ 50 μm. Probe concentration was 0.3 μM.

cholesterol-rich Lo phase in cell membranes, we cannot visualize separated domains with optical microscopy. The hypothetic Lo phase domains, if they exist, are probably too small and dynamic to be detected in our fluorescence images, due to the limited spatial and temporal resolution of the imaging technique.[41]

Conclusions

A probe based on Nile Red has been synthesized for studying cholesterol and lipid order in biomembranes. Unlike the parent Nile Red, the new probe binds spontaneously to the outer leaflet of model and cell plasma membranes with very slow flip-flop and internalization. Spectroscopy studies of LUVs and fluorescence imaging of GUVs further show that the probe can distinguish by its emission color between liquid ordered and disordered phases. Using cholesterol depletion/enrichment with methyl-β-cyclodextrin, we showed that the emission color of this probe correlates well with the cholesterol content in cell membranes. The key advantages of the new probe compared to existing membranes probes arise from its Nile Red fluorophore: superior brightness, red-shifted absorption and emission, high photostability and on/off switching capability. These properties make the new probe a powerful tool for monitoring cholesterol and lipid order selectively at the outer leaflet of cell membranes.

Acknowledgment. This work was supported by Conectus Alsace and ANR blanc grants.

Supporting Information Available: Synthesis of NR12S, additional data on bleaching by dithionite, and two-photon absorption cross section results. This material is available free of charge via the Internet at http://pubs.acs.org.

JA100351W

(41) (a) Lenne, P. F.; Wawrezinieck, L.; Conchonaud, F.; Wurtz, O.; Boned, A.; Guo, X. J.; Rigneault, H.; He, H. T.; Marguet, D. *EMBO J.* **2006**, *25*, 3245–3256. (b) Wawrezinieck, L.; Rigneault, H.; Marguet, D.; Lenne, P. F. *Biophys. J.* **2005**, *89*, 4029–4042. (c) Veatch, S. L.; Cicuta, P.; Sengupta, P.; Honerkamp-Smith, A.; Holowka, D.; Baird, B. *ACS Chem. Biol.* **2008**, *3*, 287–293.

Supporting information

Switchable Nile Red-based probe for cholesterol and lipid order at the outer leaflet of biomembranes

Oleksandr A. Kucherak, Sule Oncul, Zeinab Darwich, Dmytro A. Yushchenko, Youri Arntz, Pascal Didier, Yves Mély, Andrey S. Klymchenko

Experiential details

Probe synthesis.

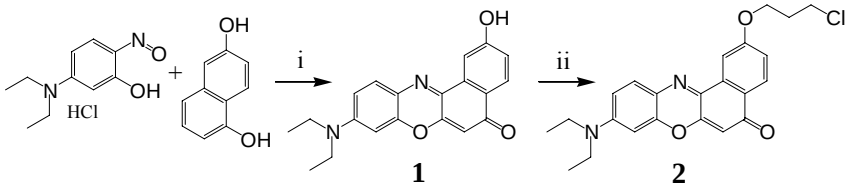

i) DMF, reflux 4h (28%); ii) DMF, K_2CO_3, 1-bromo-3-chloropropane, 70°C, 3h (96%); iii) 2-butanone, K_2CO_3, KI, dodecylmethylamine, reflux, 48h (95%); iv) CH3CN, 1,3-propansulton, 80°C, 48h (33%)

Scheme S1. Synthesis of NR12S probe.

9-(Diethylamino)-2-(3-chloropropoxy)-5*H*-benzo[*a*]phenoxazin-5-one (2). 9-(Diethylamino)-2-hydroxy-5*H*-benzo[*a*]phenoxazin-5-one **1**[1] (500mg, 1.5mmol) was dissolved in dry dimethyl formamide (DMF) and cooled to 5°C. Then potassium carbonate (1.035g, 7.5mmol) and 1-bromo-3-chloropropane (1.6mL, ρ=1.47g/mL, 15.0mmol) were added to this solution. The reaction mixture was stirred at 70°C for 3h. Then the solvent was evaporated and the residue was treated with water. The precipitate was filtered off and washed with water and heptane to give the desired product as a dark-violet solid (600mg, yield 96%). ^{1}H NMR (300MHz, $CDCl_3$): 8.22 (1H, d, 4-H), 8.06 (1H, d, 1-H), 7.60 (1H, d, 11-H), 7.16 (1H, dd, 3-H), 6.66 (1H, dd, 10-H), 6.46 (1H, d, 8-H), 6.30 (1H, s, 6-H), 4.33 (2H, t, OCH_2), 3.80 (2H, t, CH_2Cl), 3.46 (4H, q, CH_2), 2.32 (2H, m, OCH_2CH_2), 1.26 (6H, t, CH_3). LC-MS (ESI) calcd for C23H23ClN2O3 + H^+: 411.1; found $[M+1]^+$: 411.1.

9-(Diethylamino)-2-[3-(dodecylmethylamino)propoxy]-5*H*-benzo[*a*]phenoxazin-5-one (3). The Nile Red derivative **2** (150mg, 0.365mmol) was mixed with dodecylmethylamine (0.366mL, ρ=0.795g/mL, 1.460mmol) in butanone-2 in the presence of K_2CO_3 (126mg, 0.913mmol) and KI (60mg, 0.183mmol). The reaction mixture was refluxed for 48h. The solvent was evaporated under reduced pressure and the residue was purified by column chromatography (eluent CH_2Cl_2:MeOH= 95:5) to give the title compound as a dark-violet solid (200mg, yield 95%). ^{1}H NMR (300MHz,

$CDCl_3$): δ 8.20 (1H, d, 4-H), 8.03 (1H, d, 1-H), 7.60 (1H, d, 11-H), 7.13 (1H, dd, 3-H), 6.66 (1H, dd, 10-H), 6.45 (1H, d, 8-H), 6.29 (1H, s, 6-H), 4.27 (2H, t, OCH_2), 3.47 (4H, q, CH_2), 2.99 (2H, m, CH_2), 2.76 (2H, m, CH_2), 2.57 (3H, s, NCH_3), 2.32 (2H, m, CH_2), 1.71 (2H, m, CH_2), 1.40-1.20 (24H, m, CH_2, CH_3), 0.86 (3H, t, CH_3). LC-MS (ESI) calcd for C36H51N3O3 + H^+: 574.4; found $[M+1]^+$: 574.4.

***N*-[3-[[9-(diethylamino)-5-oxo-5*H*-benzo[*a*]phenoxazin-2-yl]oxy]propyl]-*N*-methyl-*N*-(3-sulfopropyl)-1-dodecanaminium.** The amine derivative **3** (50mg, 0.087mmol) was dissolved in 7mL of dry acetonitrile under inert atmosphere. Then 1,3-propansulton (8.4μL, ρ=1.392g/mL, 0.096mmol) was added to the solution. The reaction mixture was stirred at 80°C for 48h. After cooling, the solvent was evaporated under reduced pressure and the residue was purified by column chromatography (eluent CH_2Cl_2:MeOH=85:15) to obtain the final product as a dark violet solid (10mg, yield 33%). ^{1}H NMR (200MHz, $CDCl_3$): δ 8.03 (1H, d, 4-H), 7.69 (1H, d, 1-H), 7.35 (1H, d, 11-H), 7.06 (1H, dd, 3-H), 6.45 (1H, dd, 10-H), 6.20 (1H, d, 8-H), 6.01 (1H, s, 6-H), 4.20-4.15 (2H, m, OCH_2), 3.80-3.50 (4H, m, CH_2), 3.45-3.15 (7H, m, CH_2, NCH_3), 3.10-2.95 (2H, m, CH_2), 2.80-2.65 (2H, m, CH_2), 2.30-2.15 (4H, m, CH_2), 1.85-1.60 (2H, m, CH_2), 1.40-1.25-1.10 (24H, m, CH_2, CH_3), 0.80 (3H, t, CH_3). LC-MS (ESI) calcd for C39H57N3O6S + H^+: 696.4; found $[M+1]^+$: 696.4.

Two-photon absorption cross-section measurements.
Two-photon absorption cross section measurements were performed using Rhodamine B calibration standard according to the method of Webb et al.[2] Two-photon excitation was provided by a mode-locked titanium-sapphire laser (Tsunami, Spectra Physics) with a pulse duration of 200 fs. The laser was focused by an achromatic lens (f = 2 cm) in a cuvette containing the dye (30-100 μM in an appropriate solvent) and the spectra were recorded with a fibered spectrometer (Avantes) by collecting the fluorescence emission at 90° with a 20X Olympus objective. Rhodamine B in methanol was used as reference.[2] The quadratic dependence of the fluorescence intensity with respect to the laser power was checked for all the dyes to avoid saturation artefact.

Results

Bleaching of Nile Red and NR12S in ethanol/water mixture.

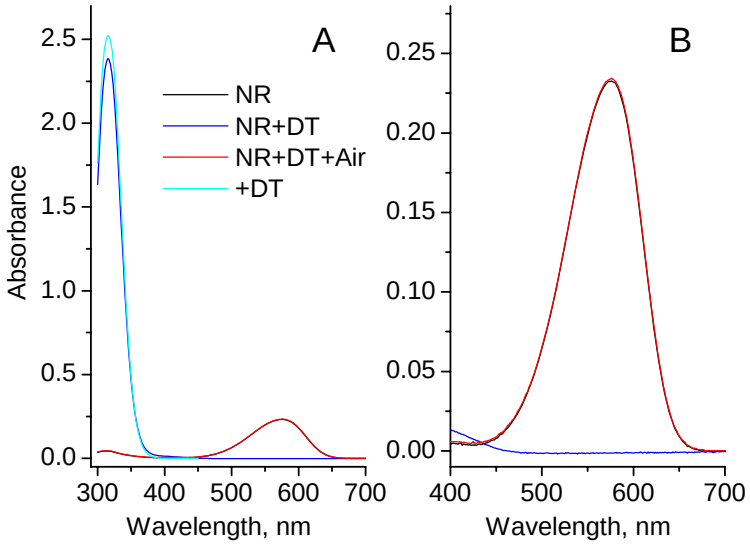

Fig. S1. Absorption spectra of Nile Red (NR) in ethanol/water mixture (1/1, v/v) before treatment (black), after addition of 2 mM dithionite (blue) and after further bubbling of air for 20 seconds (red). Absorption spectrum of 2 mM dithionite (cyan) in ethanol/water mixture is also shown. The whole spectrum is shown in panel A, while the zoomed region is shown in panel B.

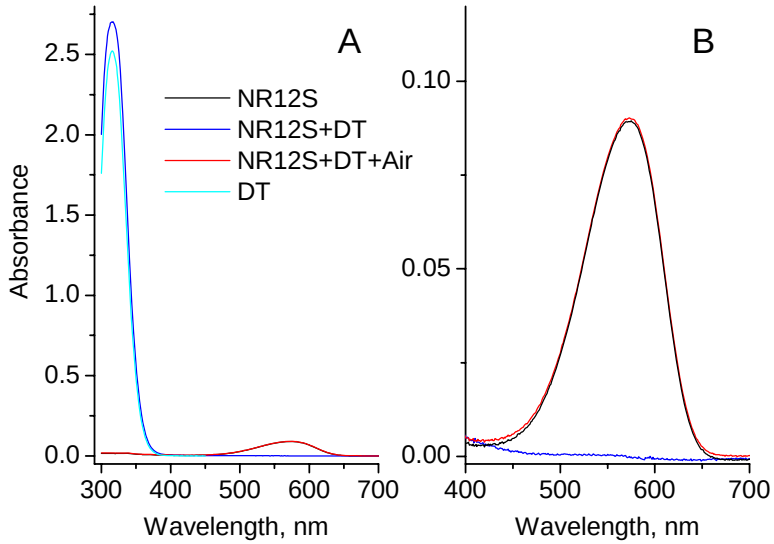

Fig. S2. Absorption spectra of NR12S in ethanol/water mixture (1/1, v/v) before treatment (black), after addition of 2 mM dithionite (blue) and after further bubbling of air for 20 seconds (red). Absorption spectrum of 2 mM dithionite (cyan) in ethanol/water mixture is also shown. The whole spectrum is shown in panel A, while the zoomed region is shown in panel B.

Bleaching of NR12S bound to living cells.

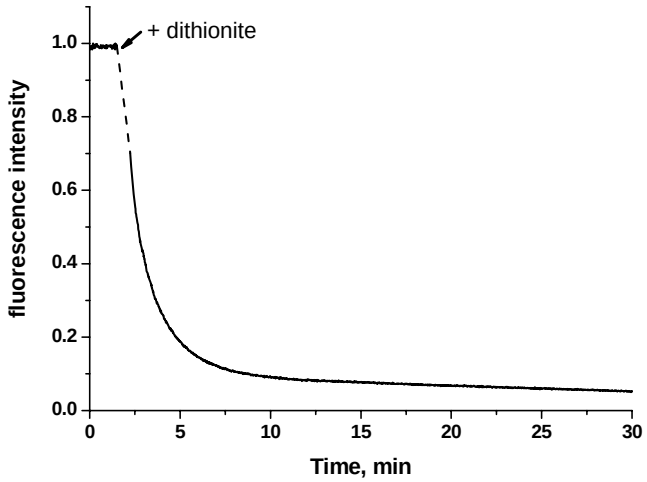

Fig. S3. Time dependence of fluorescence intensity at 600 nm of NR12S in astrocytoma cells after addition of 10 mM sodium dithionite.

Two-photon absorption cross section measurements.

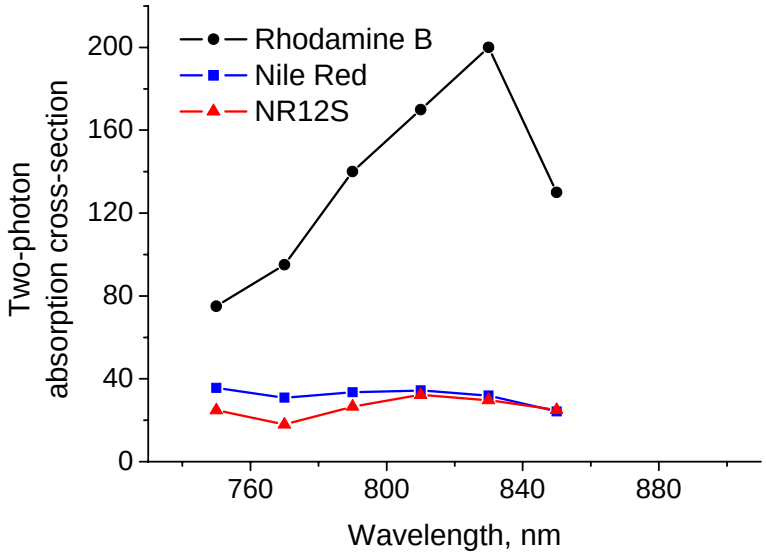

Fig. S4. Two-photon absorption cross section (GM, 10^{-50} $cm^4 \times s \times photon^{-1}$) of **NR12S** (red triangle), **Nile Red** (blue square), and reference Rhodamine B (black circle), as a function of wavelength. Data on rhodamine B are from Ref 2a. The error is ±25%.

References

1. (a) Martin-Brown, S. A.; Fu, Y.; Saroja, G.; Collinson, M. M.; Higgins, D. A. *Anal Chem.* **2005**, *77*, 486-494. (b) Briggs, M. S. J.; Bruce, I.; Miller, J. N.; Moody, C. J.; Simmonds, A. C.; Swann, E. *J. Chem. Soc. Perkin Trans. 1* **1997**, 1051-1058.

2. (a) Xu, C.; Webb, W. W. *J. Opt. Soc. Am. B* **1996**, *13*, 481-491. (b) Albota, M. A.; Xu, C.; Webb, W. W. *Applied Optics* **1998**, *37*, 7352-7356.

PUBLICATION 3

FLUORENE ANALOGUES OF PRODAN WITH SUPERIOR FLUORESCENCE BRIGHTNESS AND SOLVATOCHROMISM

THE JOURNAL OF PHYSICAL CHEMISTRY Letters

pubs.acs.org/JPCL

Fluorene Analogues of Prodan with Superior Fluorescence Brightness and Solvatochromism

Oleksandr A. Kucherak, Pascal Didier, Yves Mély, and Andrey S. Klymchenko*

Laboratoire de Biophotonique et Pharmacologie, UMR 7213 CNRS, Faculté de Pharmacie, Université de Strasbourg, 74 Route du Rhin, 67401 ILLKIRCH Cedex, France

ABSTRACT In a search for environmentally sensitive (solvatochromic) dyes with superior properties, we extended the electronic conjugation of one of the best solvatochromic dyes, Prodan, by substituting its naphthalene core with fluorene. The newly synthesized fluorene derivatives bearing strong electron-donor (dialkylamino) and -acceptor (carbonyl) groups at the 2 and 7 positions showed red-shifted absorption (close to 400 nm), twice as large of a absorption coefficient (43 000 M^{-1} cm^{-1}), and a manifold larger two-photon absorption cross section (~400 GM) compared to Prodan. Studies in solvents revealed much stronger fluorescence solvatochromism of the new dyes, which is connected with their twice as large transition dipole moment (14.0 D). Similarly to Prodan, they exhibit high fluorescence quantum yields, while their photostability is largely improved. Thus, substitution of the naphthalene core in Prodan with fluorene resulted in new fluorophores with superior spectroscopic and solvatochromic properties. We expect them to find a variety of applications as environmentally sensitive probes and labels in biology.

SECTION Kinetics, Spectroscopy

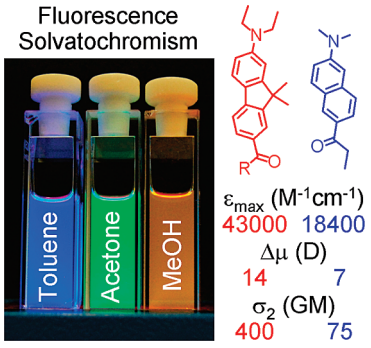

Fluorescent dyes found a variety of applications as probes and labels in biology.[1] Of special interest are the environmentally sensitive (solvatochromic) fluorescent dyes[2−13] that exhibit strong changes in their dipole moment upon electronic excitation[14] and thus show red shifts in their emission maximum upon an increase in their solvent polarity.[15,16] Typical examples are dansyl derivatives,[17] Prodan,[18] Nile Red,[19,20] Fluoroprobe,[21] dimethylaminophthalimide (DMAP),[11−13] 3-hydroxychromones,[22,23] and so forth. Due to their sensitivity to the local environment, these dyes found a number of applications for monitoring protein[2−5,11−13] and DNA[6,7] interactions and probing biophysical properties of biomembranes.[8−10] However, none of these dyes meet simultaneously all of the desired spectroscopic requirements for biological applications, absorption in the visible (>400 nm), high absorption coefficient (>30 000 M^{-1} cm^{-1}), high fluorescence quantum yield (>50%) and photostability, as well as strong solvatochromism. For instance, dansyl derivatives,[17] DMAP, and its analogues[11−13] show a low absorption coefficient, while Nile Red exhibits relatively weak solvatochromism.[19,20] The most solvatochromic dye described to date, Fluoroprobe, exhibits poor absorption properties and low fluorescence quantum yield in polar solvents.[21] 3-Hydroxyflavone derivatives, showing strong two-color solvatochromism,[22,23] suffer from poor photostability.[24] Among the best solvatochromic dyes reported so far are Prodan[18] and dapoxyl[25] derivatives, for which most of the mentioned criteria are fulfilled. Prodan, which is composed of a naphthalene aromatic core substituted at the 2 and 6 positions with donor and acceptor groups (Chart 1), and its derivatives are probably among the most popular environmentally sensitive dyes for biological applications, particularly for probing the local environment of lipid membranes, proteins, and DNA.[2−10] However, Prodan fluorophore absorbs in the UV range, which limits its applications in biology. A recently developed extended analogue of Prodan, Anthradan, showed significantly red-shifted absorption (around 460 nm) and emission, but its low absorption coefficient (12,000 M^{-1} cm^{-1}) is a severe drawback.[26] All of these examples clearly show a strong need for improved solvent-sensitive fluorescent dyes.

In the present work, we substituted the naphthalene aromatic core of Prodan with fluorene, which presents longer electronic conjugation together with rigid conjugated structure. Though fluorene was extensively used as a building block for the development of dyes with good two-photon absorption properties,[27−32] the structural analogues of Prodan, bearing electron-donor dialkylamino and -acceptor carbonyl groups at the 2 and 7 positions, were not described. Therefore, we have synthesized two fluorene derivatives, **FR0** (7-diethylamino-9,9-dimethyl-9H-fluorene-2-carbaldehyde) and **FR8** (1-(7-diethylamino-9,9-dimethyl-9H-fluoren-2-yl)-nonan-1-one). Our spectroscopic studies show that compared to Prodan, the new dyes exhibit a 2-fold larger solvatochromism and absorption coefficient, a manifold larger two-photon absorption

Received Date: December 7, 2009
Accepted Date: January 4, 2010
Published on Web Date: January 12, 2010

DOI: 10.1021/jz9003685 | *J. Phys. Chem. Lett.* **2010**, *1*, 616–620

Chart 1. Structures of New Dyes and Prodan

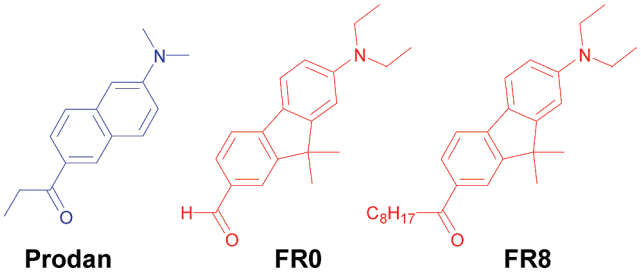

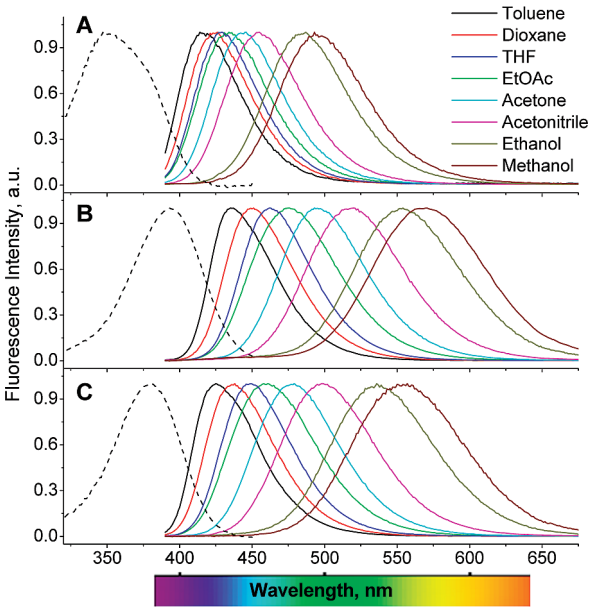

Figure 1. Absorption (dash) and fluorescence (solid) spectra of Prodan (A), **FR0** (B), and **FR8** (C) in organic solvents of different polarity. Absorption spectra were recorded in toluene. The excitation wavelength was 380 nm.

cross section, red-shifted absorption and emission, and higher photostability. These superior properties make these dyes a very attractive replacement of Prodan for applications in biology.

Dyes **FR0** and **FR8** were synthesized in five and seven steps, respectively, starting from 2-bromofluorene (see Supporting Information (SI)). Absorption and fluorescence spectra of the new dyes were recorded in different organic solvents and compared to those of the reference compound Prodan. Both **FR0** and **FR8** showed a significantly red-shifted absorption maximum, close to 400 nm (Figure 1, Table 1). At 405 nm in ethanol, **FR0** and **FR8** exhibited 92 and 68% of their maximal absorbance, respectively (only 23% for Prodan), so that the new dyes were fully compatible with the common 405 nm diode laser. Moreover, in ethanol, their absorption coefficient of 43 000 M^{-1} cm^{-1} at the maximum is twice as large as that of Prodan (18 400 M^{-1} cm^{-1}).[18] The red shift and the increase in the absorption coefficient are probably due to the larger electronic conjugation and polarizability of the fluorene core in **FR0** and **FR8** compared to that in naphthalene in Prodan. Noticeably, the absorption spectrum

Table 1. Spectroscopic Properties of New Dyes in Comparison to Prodan in Representative Solvents[a]

		λ_{max} (abs), nm			λ_{max} (fluo), nm			QY, %		
solvent	$E_T(30)$	**Pro**	**FR0**	**FR8**	**Pro**	**FR0**	**FR8**	**Pro**	**FR0**	**FR8**
toluene[b]	33.9	347	395	383	416	434	425	56	98	83
1,4-dioxane[b]	36.0	346	390	378	422	445	435	75	98	98
THF	37.4	348	393	378	430	462	449	78	85	90
dichloromethane	40.7	355	399	384	440	497	479	98	75	85
DMF	43.2	350	399	385	452	512	490	92	64	75
acetonitrile	45.6	350	394	380	455	518	498	80	56	66
ethanol	51.9	362	395	383	485	554	536	71	33	47
methanol	55.4	362	396	384	496	570	555	51	19	35

[a] The extended table with all of the studied solvents is presented in SI. $E_T(30)$ is the polarity index from ref 14. **Pro** is Prodan. QY is the fluorescence quantum yield, and the excitation wavelength was 380 nm. [b] The excitation wavelength was 360 nm.

of **FR0** is slightly red-shifted with respect to **FR8**, probably because the formyl group is a slightly stronger acceptor group than the acyl group. The weaker electron-acceptor ability for the acyl group is expected because its alkyl group is a stronger electron donor than the hydrogen of the formyl group (for instance, the Hammett constants (σ_p) for ethyl and hydrogen are −0.13 and 0, respectively).[33] The position of the absorption maximum for both dyes varied poorly in different solvents, while for Prodan, it shifted slightly to the red in more polar solvents (Table 1). This difference in solvatochromism could be explained by a smaller ground-state dipole moment of **FR0** and **FR8** compared to that of Prodan.[15,16]

The **FR0** and **FR8** dyes exhibit fluorescence quantum yields (QY) in the range of 70−90% for most of the solvents studied, which are comparable to those of Prodan (Table 1). Taking into account the differences in the absorption coefficients, the new dyes are at least twice as bright as Prodan. The QY of **FR0** and **FR8** decreases gradually with solvent polarity (Table 1), which is a common property of dyes exhibiting large charge separation in their excited state.[11−13,17,21,25] Nevertheless, the QY values for the new dyes in polar alcohols remain sufficiently high for their applications in polar protic media.

The emission maximum of the new dyes is also significantly red-shifted with respect to that of Prodan, especially in polar solvents (Figure 1, Table 1). Moreover, their emission maximum varies strongly with solvent polarity; for example, from apolar hexane to polar methanol, it shifts to the red by 175 (7770 cm^{-1}) and 168 nm (7820 cm^{-1}) for **FR0** and **FR8**, respectively. For the same solvents, Prodan shows a much smaller shift (107 nm, 5550 cm^{-1}). To describe quantitatively this solvent dependence, we studied the correlation of the band position versus the polarity index $E_T(30)$ of aprotic solvents. For all three studied dyes, a linear correlation with $E_T(30)$ is observed (Figure 2), but the new dyes exhibit a much steeper slope than Prodan, indicating a larger fluorescence solvatochromism. It is important to note that the full width at half-maximum (in cm^{-1}) of the emission band is similar for all

DOI: 10.1021/jz9003685 | J. Phys. Chem. Lett. 2010, 1, 616–620

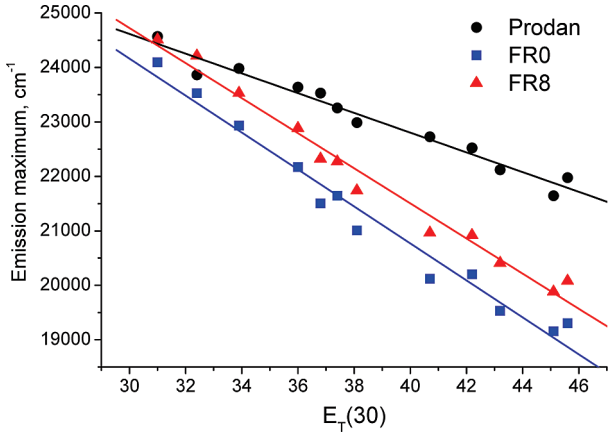

Figure 2. Position of the emission maxima of **FR0** (blue square), **FR8** (red triangle), and Prodan (black circle) versus the polarity $E_T(30)$ in aprotic solvents. The slopes of the linear fits (solid lines) are 340, 320, and 180 cm^{-1}, respectively, and r^2 values (goodness of fit) are 0.970, 0.978, and 0.963, respectively.

three dyes and shows only a small increase with solvent polarity; for example, in apolar dioxane and polar methanol, the corresponding bandwidth values are 2790 and 2830 cm^{-1} for Prodan, 2650 and 2790 cm^{-1} for **FR0**, and 2760 and 2940 cm^{-1} for **FR8**. These results suggest that the emission of all three dyes originates from the same S_1-S_0 electronic transition in solvents of different polarity. Therefore, the observed larger solvatochromism of **FR0** and **FR8** could be connected with their larger transition dipole moment.

Using the correlation of the dye's Stokes shift versus the orientation polarizability function (see SI) and Lippert equation,[1,15,16] we estimated the transition dipole moment of **FR0** and **FR8** to be 14.0 D. This is exactly twice the corresponding value for Prodan (7.0 D) measured in the present study. The obtained transition dipole moment for Prodan is in line with the previously reported experimental[34,35] and theoretical[36] data. Remarkably, the obtained transition dipole moment for **FR0** and **FR8** is also much larger than that for Anthradan, which is characterized by a similar length of the electronic conjugation as **FR0** and **FR8**.[26] This indicates that the fluorene system presents a unique electronic configuration, allowing strong charge transfer between the donor and acceptor groups at positions 2 and 7. Recently, 2,7-subsituted fluorene derivatives bearing dialkylamino and sulfonate groups were described.[37,38] However, compared to **FR0** and **FR8**, these derivatives showed significantly blue-shifted absorption and emission as well as much weaker dependence of their emission maximum with solvent polarity. These strong spectroscopic differences could be connected with the weaker electron-acceptor ability of the sulfonate group compared to that of the carbonyl group in **FR0** and **FR8**. It should be noted that the observed solvatochromism of **FR0** and **FR8** is among the largest known so far. The other dyes, showing comparable solvatochromism, are relatively large donor–acceptor systems, such as fluoroprobe,[21] dapoxyl,[25] and conjugated fluorene derivatives.[30] The key advantage of the present dyes in this respect is their relatively small size.

Table 2. Photostability of **FR0** and **FR8** in Comparison to Prodan[a]

	Prodan		FR0		FR8	
solvent	τ_p, min	R, %	τ_p, min	R, %	τ_p, min	R, %
toluene	25	10	240	76	70	44
DMF	50	36	850	92	440	87
triacetin	80	44	1100	94	560	88
ethanol	90	49	> 4000[b]	99	360	85

[a] τ_p is the time constant of photodegradation (min); R is the remaining fluorescence intensity (%) after 60 min of illumination at 360 nm. [b] Photodegradation was almost not detectable.

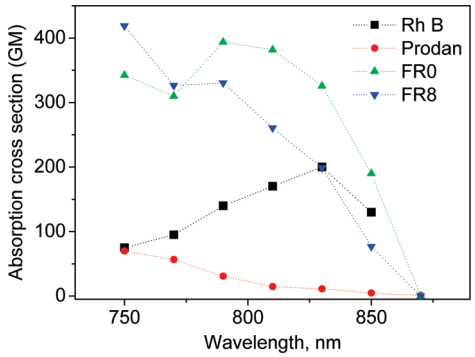

Figure 3. Two-photon absorption cross section (GM, 10^{-50} cm^4 s $photon^{-1}$) of **FR0** (green triangle), **FR8** (blue triangle), Prodan (red circle), and reference rhodamine B, as a function of the wavelength. Data on rhodamine B are from ref 42. The error is ±25%.

To evaluate the photostability of our dyes, their photodegradation curves in different solvents were compared with that of Prodan (see SI). These curves were fitted by a single-exponential function to estimate the time constant of photodegradation (Table 2). **FR0** and **FR8** dyes were found to be far more photostable than Prodan in all studied solvents, showing a large remaining fluorescence intensity after 60 min of illumination (Table 2). Surprisingly, **FR0** showed a higher photostability than **FR8**, suggesting that the 7-acyl group can participate in the photodegradation due to, for instance, slow Norrish type I and type II reactions.[39–41]

Finally, taking into account that fluorene was largely explored as a building block for the design of dyes for two-photon (TP) excitation techniques,[27–32] we studied the TP absorption cross section of **FR0** and **FR8**. TP excitation spectra in ethanol were recorded for Prodan, **FR0**, and **FR8**, and relative values of the TP absorption cross section at different wavelengths were evaluated (Figure 3) using rhodamine B standard as described previously.[42,43] We studied a spectral range (750–850 nm) which covers the optimal wavelengths for the TP excitation of Prodan and its homologue Laurdan (750–780 nm).[10,44] In the studied spectral range, the maximal values of the TP absorption cross section for **FR0** and **FR8** are about 5-fold larger than that for Prodan (Figure 3). The maximal TP absorption cross section value of 75 GM obtained presently for Prodan in ethanol is close to that reported in the literature for its homologue Laurdan.[10] The difference in the TP absorption cross section between the new

DOI: 10.1021/jz9003685 | J. Phys. Chem. Lett. 2010, 1, 616–620

dyes and Prodan is even more dramatic at the longer wavelength (Figure 3), where Prodan does not show significant TP absorption. It should be noted that the TP excitation spectrum of **FR0** is considerably shifted to the longer wavelengths compared to **FR8** and Prodan, which is in line with the one-photon absorption data (Table 1). The observed significant improvement in the TP absorption cross section compared to that of Prodan is evidently connected with the fluorene ring, which is known to be a key unit in the design of the efficient two-photon fluorophores.[27−32] The high TP absorption cross section of the new dyes makes them attractive for applications in two-photon excitation spectroscopy and microscopy.[45−48]

In conclusion, we synthesized fluorescent dyes based on fluorene, showing superior spectroscopic properties compared to their close structural analogue Prodan. The substitution of the naphthalene conjugated core (in Prodan) with the fluorene (in **FR0** and **FR8**) resulted in a 2-fold increased solvatochromism and absorption coefficient, a manifold larger two-photon absorption cross section, red-shifted absorption and emission, and larger photostability. These remarkable properties make the new dyes very attractive for applications as environmentally sensitive fluorescent probes and labels in biology.

SUPPORTING INFORMATION AVAILABLE Detailed experimental section, synthesis, and fluorescent properties of the dyes. This material is available free of charge via the Internet at http://pubs.acs.org.

AUTHOR INFORMATION

Corresponding Author:

*To whom correspondence should be addressed. Fax: +33 368 854313. Tel: +33 368 854255. E-mail: aklymchenko@unistra.fr.

ACKNOWLEDGMENT This work was supported by ANR and Conectus grants.

REFERENCES

(1) Lakowicz, J. R. *Principles of Fluorescence Spectroscopy*, 3rd ed.; Springer-Verlag: New York, 2006.
(2) Cohen, B. E.; McAnaney, T. B.; Park, E. S.; Jan, Y. N.; Boxer, S. G.; Jan, L. Y. Probing Protein Electrostatics with a Synthetic Fluorescent Amino Acid. *Science* **2002,** *296*, 1700–1703.
(3) Nitz, M.; Mezo, A. R.; Ali, M. H.; Imperiali, B. Enantioselective Synthesis and Application of the Highly Fluorescent and Environment-Sensitive Amino Acid 6-(2-Dimethylaminonaphthoyl) Alanine (DANA). *Chem. Commun.* **2002,** 1912–1913.
(4) Vazquez, M. E.; Rothman, D. M.; Imperiali, B. A New Environment-Sensitive Fluorescent Amino Acid for Fmoc-Based Solid Phase Peptide Synthesis. *Org. Biomol. Chem.* **2004,** *2*, 1965–1966.
(5) Cohen, B. E.; Pralle, A.; Yao, X.; Swaminath, G.; Gandhi, C. S.; Jan, Y. N.; Kobilka, B. K.; Isacoff, E. Y.; Jan, L. Y. A Fluorescent Probe Designed for Studying Protein Conformational Change. *Proc. Natl. Acad. Sci. U.S.A.* **2005,** *102*, 965–970.
(6) Kimura, T.; Kawai, K.; Majima, T. Probing the Microenvironments in the Grooves of Z-DNA using dan-Modified Oligonucleotides. *Chem. Commun.* **2006,** 1542–1544.
(7) Tainaka, K.; Tanaka, K.; Ikeda, S.; Nishiza, K.-I.; Unzai, T.; Fujiwara, Y.; Saito, I.; Okamoto, A. PRODAN-Conjugated DNA: Synthesis and Photochemical Properties. *J. Am. Chem. Soc.* **2007,** *129*, 4776–4784.
(8) Bagatolli, L. A. To See or Not to See: Lateral Organization of Biological Membranes and Fluorescence Microscopy. *Biochim. Biophys. Acta* **2006,** *1758*, 1541–1556.
(9) Demchenko, A. P.; Mély, Y.; Duportail, G.; Klymchenko, A. S. Monitoring Biophysical Properties of Lipid Membranes by Environment-Sensitive Fluorescent Probes. *Biophys. J.* **2009,** *96*, 3461–3470.
(10) Kim, H. M.; Choo, H. J.; Jung, S. Y.; Ko, Y. G.; Park, W. H.; Jeon, S. J.; Kim, C. H.; Joo, T.; Cho, B. R. A Two-Photon Fluorescent Probe for Lipid Raft Imaging: C-Laurdan. *ChemBioChem* **2007,** *26*, 553–559.
(11) Soujanya, T.; Fessenden, R. W.; Samanta, A. Role of Nonfluorescent Twisted Intramolecular Charge Transfer State on the Photophysical Behavior of Aminophthalimide Dyes. *J. Phys. Chem.* **1996,** *100*, 3507–3512.
(12) Vázquez, M. E.; Blanco, J. B.; Imperiali, B. Photophysics and Biological Applications of the Environment-Sensitive Fluorophore 6-*N*,*N*-Dimethylamino-2,3-naphthalimide. *J. Am. Chem. Soc.* **2005,** *127*, 1300–1306.
(13) Loving, G.; Imperiali, B. A Versatile Amino Acid Analogue of the Solvatochromic Fluorophore 4-*N*,*N*-Dimethylamino-1,8-naphthalimide: A Powerful Tool for the Study of Dynamic Protein Interactions. *J. Am. Chem. Soc.* **2008,** *130*, 13630–13638.
(14) Reichardt, C. Solvatochromic Dyes as Solvent Polarity Indicators. *Chem. Rev.* **1994,** *94*, 2319–2358.
(15) Lippert E. L. *Organic Molecular Photophysics*; Wiley-Interscience: New York, 1975.
(16) Mataga, N.; Kubota, T. *Molecular Interactions and Electronic Spectra*; M. Dekker, New York, 1970.
(17) Holmes-Farley, S. R.; Whitesides, G. M. Fluorescence Properties of Dansyl Groups Covalently Bonded to the Surface of Oxidatively Functionalized Low-Density Polyethylene Film. *Langmuir* **1986,** *2*, 266–281.
(18) Weber, G.; Farris, F. J. Synthesis and Spectral Properties of a Hydrophobic Fluorescent Probe: 6-Propionyl-2-(dimethylamino)-naphthalene. *Biochemistry* **1979,** *18*, 3075–3078.
(19) Greenspan, P.; Mayer, E. P.; Fowler, S. D. Nile Red: A Selective Fluorescent Stain for Intracellular Lipid Droplets. *J. Cell Biol.* **1985,** *100*, 965–973.
(20) Greenspan, P.; Fowler, S. D. Spectrofluorometric Studies of the Lipid Probe, Nile Red. *J. Lipid Res.* **1985,** *26*, 781–789.
(21) Mes, G. F.; De Jong, B.; Van Ramesdonk, H. J.; Verhoeven, J. W.; Warman, J. M.; De Haas, M. P.; Horsman-Van den Dool, L. E. W. Excited-State Dipole Moment and Solvatochromism of Highly Fluorescent Rod-Shaped Bichromophoric Molecules. *J. Am. Chem. Soc.* **1984,** *106*, 6524–6528.
(22) Klymchenko, A. S.; Pivovarenko, V. G.; Ozturk, T.; Demchenko, A. P. Modulation of the Solvent- Dependent Dual Emission in 3-Hydroxychromones by Substituents. *New J. Chem.* **2003,** *27*, 1336–1343.
(23) Klymchenko, A. S.; Demchenko, A. P. Multiparametric Probing of Intermolecular Interactions with Fluorescent Dye Exhibiting Excited State Intramolecular Proton Transfer. *Phys. Chem. Chem. Phys.* **2003,** *5*, 461–468.
(24) Chou, P.-T.; Martinez, M. L. Photooxygenation of 3-Hydroxyflavone and Molecular Design of the Radiation-Hard Scintillator Based on the Excited State Proton Transfer. *Radiat. Phys. Chem.* **1993,** *41*, 373–378.
(25) Diwu, Z.; Lu, Y.; Zhang, C.; Klaubert, D. H.; Haugland, R. P. Fluorescent Molecular Probes 2. The Synthesis, Spectral

DOI: 10.1021/jz9003685 | *J. Phys. Chem. Lett.* **2010,** *1*, 616–620

Properties and Use of Fluorescent Solvatochromic Dapoxyl Dyes. *Photochem. Photobiol.* **1997,** *66*, 424–431.
(26) Lu, Z.; Lord, S. J.; Wang, H.; Moerner, W. E.; Twieg, R. J. Long-Wavelength Analogue of PRODAN: Synthesis and Properties of Anthradan, a Fluorophore with a 2,6-Donor−Acceptor Anthracene Structure. *J. Org. Chem.* **2006,** *71*, 9651–9657.
(27) Belfield, K. D.; Schafer, K. J.; Mourad, W.; Reinhardt, B. A. Synthesis of New Two-Photon Absorbing Fluorene Derivatives via Cu-Mediated Ullmann Condensations. *J. Org. Chem.* **2000,** *65*, 4475–4481.
(28) Kannan, R.; He, G. S.; Yuan, L.; Xu, F.; Prasad, P. N.; Dombroskie, A. G.; Reinhardt, B. A.; Baur, J. W.; Vaia, R. A.; Tan, L.-S. Diphenylaminofluorene-Based Two-Photon-Absorbing Chromophores with Various π-Electron Acceptors. *Chem. Mater.* **2001,** *13*, 1896–1904.
(29) Mongin, O.; Porrès, L.; Katan, C.; Pons, T.; Mertz, J.; Blanchard-Desce, M. Synthesis and Two-Photon Absorption of Highly Soluble Three-Branched Fluorenylene-Vinylene Derivatives. *Tetrahedron Lett.* **2003,** *44*, 8121–8125.
(30) Droumaguet, C. L.; Mongin, O.; Werts, M. H. V.; Blanchard-Desce, M. Towards Smart Multiphoton Fluorophores: Strongly Solvatochromic Probes for Two-Photon Sensing of Micropolarity. *Chem. Commun.* **2005,** 2802–2804.
(31) Belfield, K. D.; Bondar, M. V.; Hernandez, F. E.; Przhonska, O. V.; Yao, S. Two-Photon Absorption Cross Section Determination for Fluorene Derivatives: Analysis of the Methodology and Elucidation of the Origin of the Absorption Processes. *J. Phys. Chem. B* **2007,** *111*, 12723–12729.
(32) Nguyen, K. A.; Rogers, J. E.; Slagle, J. E.; Day, P. N.; Kannan, R.; Tan, L.-S.; Fleitz, P. A.; Pachter, R. Effects of Conjugation in Length and Dimension on Spectroscopic Properties of Fluorene-Based Chromophores from Experiment and Theory. *J. Phys. Chem. A* **2006,** *110*, 13172–13182.
(33) Carey, F. A.; Sundberg, R. J. *Advanced Organic Chemistry, Part A*, 4th ed.; Kluwer Academic/Plenum Publishers: New York, 2000.
(34) Catalan, J.; Perez, P.; Laynez, J.; Blanco, F. G. Analysis of the Solvent Effect on the Photophysics Properties of 6-Propionyl-2-(dimethylamino) Naphthalene (PRODAN). *J. Fluoresc.* **1991,** *1*, 215–223.
(35) Samanta, A.; Fessenden, R. W. Excited State Dipole Moment of PRODAN as Determined from Transient Dielectric Loss Measurements. *J. Phys. Chem. A* **2000,** *104*, 8972–8975.
(36) Mennucci, B.; Caricato, M.; Ingrosso, F.; Cappelli, C.; Cammi, R.; Tomasi, J.; Scalmani, G.; Frisch, M. J. How the Environment Controls Absorption and Fluorescence Spectra of PRODAN: A Quantum-Mechanical Study in Homogeneous and Heterogeneous Media. *J. Phys. Chem. B* **2008,** *112*, 414–423.
(37) Park, K. K.; Park, J. W.; Hamilton, A. D. Solvent and pH Effects on the Fluorescence of 7-(Dimethylamino)-2-fluorenesulfonate. *J. Fluoresc.* **2007,** *17*, 361–369.
(38) Park, K. K.; Park, J. W.; Hamilton, A. D. Novel 7-(Dimethylamino)fluorene-Based Fluorescent Probes and Their Binding to Human Serum Albumin. *Org. Biomol. Chem.* **2009,** *7*, 4225–4232.
(39) Norrish, R. G. W. Part II. Free Radicals of Short Life: Chemical Aspects. A. General and Inorganic. The Primary Photochemical Production of Some Free Radicals. *Trans. Faraday Soc.* **1934,** *30*, 103–113.
(40) Norrish, R. G. W. On the Principle of Primary Recombination in Relation to the Velocity of Thermal Reactions in Solution. *Trans. Faraday Soc.* **1937,** *33*, 1521–1527.
(41) Laue, T.; Plagens, A. *Named Organic Reactions*, 2nd ed.; John Wiley & Sons: New York, 2005.
(42) Xu, C.; Webb, W. W. Measurement of Two-Photon Excitation Cross Sections of Molecular Fluorophores with Data from 690 to 1050 nm. *J. Opt. Soc. Am. B* **1996,** *13*, 481–491.
(43) Albota, M. A.; Xu, C.; Webb, W. W. Two-Photon Fluorescence Excitation Cross Sections of Biomolecular Probes from 690 to 960 nm. *Appl. Opt.* **1998,** *37*, 7352–7356.
(44) Bagatolli, L. A.; Gratton, E. Two Photon Fluorescence Microscopy of Coexisting Lipid Domains in Giant Unilamellar Vesicles of Binary Phospholipid Mixtures. *Biophys. J.* **2000,** *78*, 290–305.
(45) Denk, W.; Strickler, J. H.; Webb, W. W. Two-Photon Laser Scanning Fluorescence Microscopy. *Science* **1990,** *248*, 73–76.
(46) Xu, C.; Zipfel, W.; Shear, J. B.; Williams, R. M.; Webb, W. W. Multiphoton Fluorescence Excitation: New Spectral Windows for Biological Nonlinear Microscopy. *Proc. Natl. Acad. Sci. U.S.A.* **1996,** *93*, 10763–10768.
(47) Konig, K. Multiphoton Microscopy in Life Science. *J. Microscopy* **2000,** *200*, 83–104.
(48) Clamme, J.-P.; Krishnamoorthy, G.; Mély, Y. Intracellular Dynamics of the Gene Delivery Vehicle Polyethylenimine during Transfection: Investigation by Two-Photon Fluorescence Correlation Spectroscopy. *Biochim. Biophys. Acta* **2003,** *1617*, 52–61.

DOI: 10.1021/jz9003685 | *J. Phys. Chem. Lett.* **2010,** *1*, 616–620

Supporting information

Fluorene analogues of Prodan with superior fluorescence brightness and solvatochromism

Oleksandr A. Kucherak, Pascal Didier, Yves Mely, Andrey S. Klymchenko

Laboratoire de Biophotonique et Pharmacologie, UMR 7213 CNRS, Université de Strasbourg, Faculté de Pharmacie, 74, Route du Rhin, 67401 ILLKIRCH Cedex, France

Materials and methods

All the solvents and chemicals were purchased from Aldrich. The solvents were of spectroscopic grade. Absorption and fluorescence spectra were recorded on Cary 4 spectrophotometer (Varian) and FluoroLog spectrofluorometer (Jobin Yvon, Horiba), respectively. Fluorescence quantum yields were determined by taking Prodan in ethanol (quantum yield, QY = 71 %)[1,2] as a reference. The quantum yield values were corrected for the solvent refractive index. For spectroscopic measurements, 1 μM solutions of dyes were used. All the spectra are corrected from the background (spectrum of neat solvent).

In photodegradation assays, a 0.33 μM solution of a given dye in a quartz micro-cuvette (50 μM volume) was illuminated by a 360 nm light of Xenon lamp of a FluoroLog spectrofluorometer (slits were open to 8 nm). During the time of illumination (5000 seconds), the fluorescence at the maximum was recorded as a function of time. The fluorescence photodegradation curves were fitted to a single exponential decay function: $I = y_0+\exp(-t/\tau_d)$, where $y_0 = 0$ (final intensity after total photobleaching), τ_d is the degradation constant, I is the measured fluorescence intensity, and t is the time of experiment.

Two-photon absorption cross section measurements were performed using Rhodamine B calibration standard according to the method of Webb et al.[3,4] Two-photon excitation was provided by a mode-locked titanium-sapphire laser (Tsunami, Spectra Physics) with a pulse duration of 200 fs. The laser was focused by an achromatic lens (f = 2 cm) in a cuvette containing the dye (30-100 μM in an appropriate solvent) and the spectra were recorded with a fibered spectrometer (Avantes) by collecting the fluorescence emission at 90° with a 20X Olympus objective. Rhodamine B in methanol was used as

reference.[4] The quadratic dependence of the fluorescence intensity with respect to the laser power was checked for all the dyes to avoid saturation artefact.

Synthesis of fluorescent dyes FR0 and FR8.

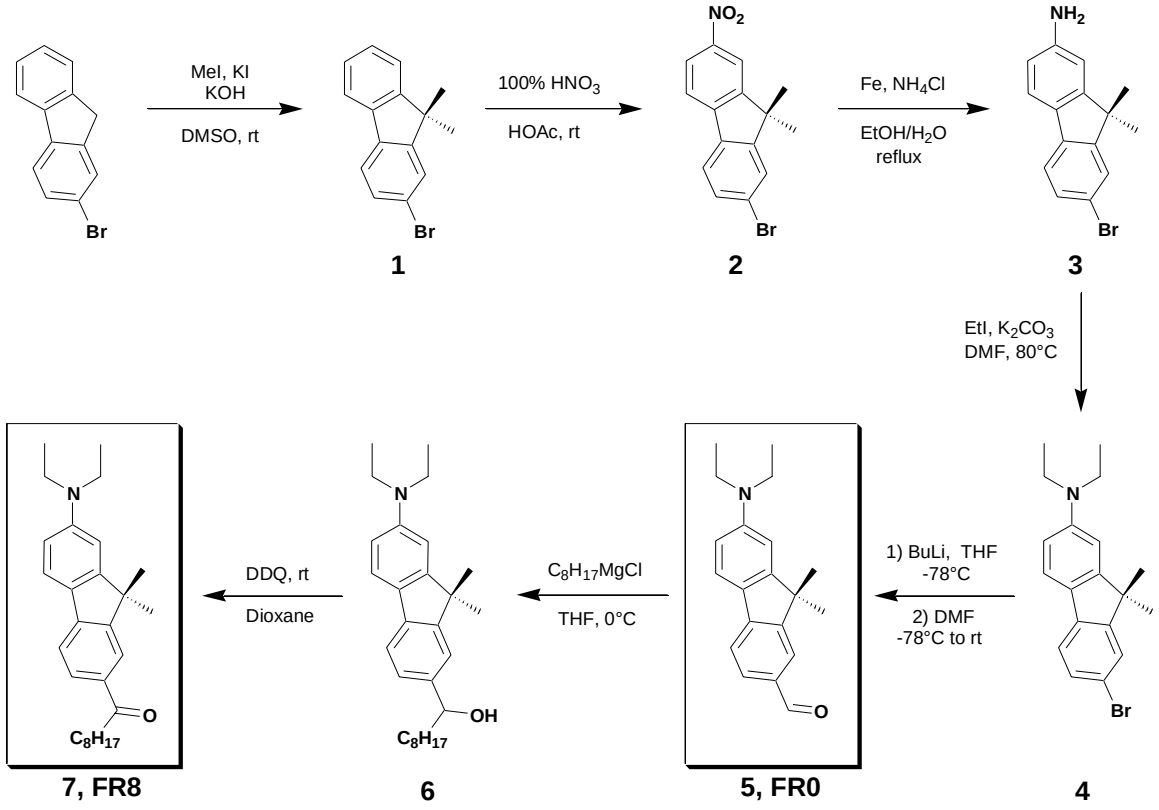

Scheme S1. Synthesis of dyes **FR0** and **FR8.**

2-Bromo-9,9-dimethylfluorene (1). 2-Bromofluorene (160.0mmol, 39.2g) was dissolved in 300 mL of DMSO at 60°C. Potassium iodide (16.0mmol, 2.7g) and iodomethane (360.0mmol, 51.1g) were then added; finally, powdered potassium hydroxide (640.0mmol, 36.0g) was slowly added. The mixture was stirred at room temperature overnight. Then the mixture was poured into 2000 mL of water, and a light yellow precipitate was formed. The solid was filtered, washed with water, and dried under vacuum. The light yellow solid was purified by crystallization from methanol to give product **1** (40.3g, 92%) as white crystals. NMR is in good correspondence with literature data.[5,6] ^{1}H NMR (300 MHz, $CDCl_3$): δ 7.72-7.65 (m, 1H), 7.60-7.54 (m, 2H), 7.48-7.39 (m, 2H), 7.37-7.30 (m, 2H), 1.47 (s, 6H). MS: *(m/z)* Found $[M]^+$ = 271.9 (calcd for C15H13Br = 272.02).

2-Bromo-9,9-dimethyl-7-nitrofluorene (2). 2-Bromo-9,9-dimethylfluorene **1** (5g, 18.3mmol) was dissolved in 100mL of glacial acetic acid. To the formed solution, 15mL of fuming nitric acid were added dropwise (~10 min) at 0°C upon vigorous stirring. After addition was completed, reaction mixture was further stirred at RT. In 30min, yellow-green residue appeared. Reaction was monitored by TLC, solvent EtOAc/Heptane = 1/9. After appearance of the spot of dinitroproduct (~100 min, Rf ≈25%), the mixture was poured into 600mL of water. Formed residue was filtered off, washed with water and recrystallized from 200mL acetonitrile to give compound **2** (4.2g, 72%) as slightly-green needle crystals. NMR is in good correspondence with literature data.[7] ^{1}H NMR (400 MHz, $CDCl_3$): δ 8.27-8.23 (m, 2H), 7.78 (dd, 1H), 7.65 (d, 1H), 7.62 (d, 1H), 7.53 (dd, 1H), 1.53 (s, 6H). MS: *(m/z)* Found $[M+1]^+$ = 318.0 (calcd for C15H12BrNO2 = 317.01).

7-Bromo-9,9-dimethylfluorenyl-2-amine (3). A mixture of nitrofluorene **2** (2g, 6.23mmol), iron powder (1g, 18.7 mmol, 3eq), and NH_4Cl (740mg, 12.46 mmol, 2eq) was refluxed in aqueous ethanol (90mL of alcohol and 25mL of water) at 85°C for 2h under inert atmosphere. Reaction was monitored by TLC, solvent EtOAc/Heptane = 9/1. After complete transformation of initial compound, the reaction mixture was treated with 50mL of aqueous saturated sodium bicarbonate and filtered through paper filter. Transparent solution was concentrated in vacuum in order to remove organic solvent. Formed residue was filtered off to yield compound **3** (1.72g, 95%) as transparent plates. The crude product was used directly in the next step. ^{1}H NMR (200 MHz, $CDCl_3$): δ 7.47 (s, 1H), 7.45 (d, 1H), 7.42-7.38 (m, 2H), 6.72 (d, 1H), 6.64 (dd, 1H), 3.70 (br s, 2H), 1.42 (s, 6H). MS: *(m/z)* Found $[M+1]^+$ = 287.9 (calcd for C15H14BrN = 287.03).

(**7-Bromo-9,9-dimethylfluorenyl)-2-diethylamine (4).** To the solution of aminofluorene **3** (1g, 3.5mmol) in DMF, iodethane (1.365g, 8.75mmol, 2.5eq) and K_2CO_3 (1.45g, 10.5mmol, 3eq) were subsequently added. The resulting mixture was heated at 80°C for 5h. After cooling, it was poured into water, neutralized with 10% aqueous HCl and extracted with chloroform (2 times). Organic layer was dried with Na_2SO_4 and evaporated in vacuum. Residue was purified by column chromatography (eluent CH_2Cl_2/Heptane = 1/9) to obtain product **4** (0.9g, 75%) as a light-yellow powder. ^{1}H NMR (200 MHz, $CDCl_3$): δ 7.55-7.30 (m, 4H), 6.70-6.60 (m, 2H), 3.41 (q, 4H), 1.44 (s, 6H), 1.20 (t, 6H). MS: *(m/z)* Found $[M+1]^+$ = 344.1 (calcd for C19H22BrN = 343.09).

7-Diethylamino-9,9-dimethylfluorene-2-carbaldehyde (5, FR0). (7-Bromo-9,9-dimethylfluorenyl)-2-diethylamine **4** (500mg, 1.45mmol) was dissolved in dry THF. To the resulted clear yellow solution, BuLi (640μL of 2.5M solution in Hexane, 1.1eq) was added dropwise at -78°C under inert atmosphere. Reaction mixture was stirred for 1h, and yellow precipitate was formed. Then DMF (160mg, 2.18mmol, 1.5eq) was added dropwise and the formed solution was stirred for additional 2h at -78°C. Reaction mixture was allowed to heat to room temperature for 1h, quenched with 1M aqueous HCl and extracted with EtOAc (2 times). Organic layer was dried with Na_2SO_4 and evaporated in vacuum. Residue was purified by column chromatography (eluent EtOAc/Heptane = 1/9) to produce compound **5** (256mg, 60%) as a yellow powder. M.p. 106-107°C. ^{1}H NMR (400 MHz, $CDCl_3$): δ 9.96 (s, 1H), 7.86 (d, 1H), 7.76 (dd, 1H), 7.62 (d, 1H), 7.60 (dd, 1H), 6.72-6.64 (m, 2H), 3.45 (q, 4H), 1.48 (s, 6H), 1.22 (t, 6H). ^{13}C NMR (400 MHz, $CDCl_3$): δ 12.59, 27.24, 44.72, 46.62, 105.14, 110.95, 118.12, 122.37, 122.46, 125.27, 131.21, 133.48, 146.90, 149.05, 153.23, 157.35, 191.97. Pure according to LCMS. High resolution mass spectrometry, HRMS ESI: *(m/z)* Found $[M+1]^+$ = 294.186 (calcd for $C20H24NO^+$ = 294.186).

1-(7-Diethylamino-9,9-dimethylfluorenyl-2)-nonanol-1 (6).

Carbaldehyde **5** (50mg, 0.170mmol) was dissolved in 5mL of dry THF. To the resulted yellow solution, octyl magnesium chloride (94μL of 2M solution in THF, 1.1eq) was added dropwise at 0°C under inert atmosphere. Then, reaction mixture was stirred for 1h at RT. To decompose excess of Grignard reagent, one drop of water was added. Formed solution was concentrated in vacuum, treated with water and extracted with EtOAc (2 times). Organic layer was dried with Na_2SO_4 and evaporated in vacuum. Residue was purified by column chromatography (eluent CH_2Cl_2/Heptane = 1/1) to obtain **6** (48mg, 70%) as a slightly-green oil. ^{1}H NMR (300 MHz, $CDCl_3$): δ 7.54 (d, 1H), 7.50 (d, 1H), 7,34 (d, 1H), 7.22 (dd, 1H), 6.73 (d, 1H), 6.66 (dd, 1H), 4.70 (t, 1H), 3.43 (q, 4H), 1.85-1.75 (m, 2H), 1.47 (s, 6H), 1.45-1.24 (m, 12H), 1.22 (t, 6H), 0.88 (t, 3H). MS: *(m/z)* Found $[M+1]^+$ = 408.3 (calcd for C28H41NO = 407.32).

1-(7-Diethylamino-9,9-dimethylfluorenyl-2)-nonanon-1 (7, FR8). Previously obtained compound **6** (20mg, 0.049mmol) was dissolved in 1mL of dioxane. Resulted solution was added dropwise to the solution of DDQ (17mg, 0.074mmol, 1.5eq) in 1 mL dioxane. Initially, the solution turned red, and in 1h a precipitate was formed. It was filtered off, and clear yellow solution was evaporated in vacuum. Residue was purified by preparative TLC (eluent EtOAc/Heptane = 1/9) to give of the desired product **7** (2mg, 10%) as a yellow powder. ^{1}H NMR (300 MHz, $CDCl_3$): δ 7.96 (d, 1H), 7.89 (dd, 1H), 7,58 (d,

1H), 7.55 (dd, 1H), 6.71-6.63 (m, 2H), 3.44 (q, 4H), 2.97 (t, 2H), 1.81-1.69 (m, 2H), 1.47 (s, 6H), 1.34-1.24 (m, 10H), 1.22 (t, 6H), 0.87 (t, 3H). Pure according to LCMS. HRMS ESI: *(m/z)* Found $[M+1]^+$ = 406.311 (calcd for $C28H40NO^+$ = 406.311).

Spectroscopic properties of FR0, FR8 and Prodan.

Table S1 Spectroscopic properties of new dyes in comparison to Prodan.[a]

#	Solvent	Abs max, nm			Fluo max, nm			QY, %		
		Pro	FR0	FR8	Pro	FR0	FR8	Pro	FR0	FR8
1	hexane[b]	340	387	378	389	395	387	2.0	11	4.0
2	1,4-dioxane[b]	346	390	378	422	445	435	75	98	98
3	Toluene[b]	347	395	383	416	434	425	56	98	83
4	PhCl	353	400	386	425	465	448	84	83	90
5	EtOAc	347	390	377	435	476	460	76	76	82
6	Triacetin	351	394	381	435	477	460	96	80	88
7	THF	348	393	378	430	462	449	78	85	90
8	CH2Cl2	355	399	384	440	497	479	98	75	85
9	acetone	350	393	379	444	495	478	80	68	77
10	Ethanol	362	395	383	485	554	536	71	33	47
11	Methanol	362	396	384	496	570	555	51	19	35
12	acetonitrile	350	394	380	455	518	498	80	56	66
13	DMF	350	399	385	452	512	490	92	64	75
14	DMSO	357	403	387	462	522	503	91	61	70
15	Water	358	397	376	521	608	472	12	2.6	6.7

[a] QY is fluorescence quantum yield; excitation wavelength was 380nm; [b]excitation wavelength was 360 nm.

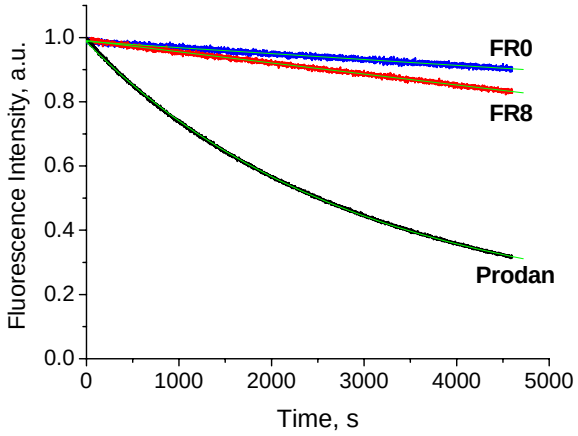

Figure S1. Typical photodegradation decay curves as a function of time for **FR0**, **FR8** and Prodan in DMF. The curves in green correspond to a single exponential decay fit. Photodegradation was performed at 360 nm with the xenon lamp in the spectrofluorometer.

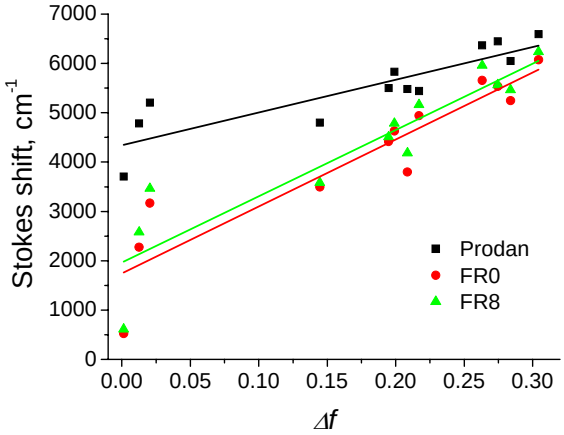

Figure S2. Stokes shift vs. orientation polarizability function (Δf) for **FR0**, **FR8** and Prodan. Only aprotic solvents were used. Results of linear fit for **FR0**: $\Delta\nu = 1745+13565\Delta f$, $r^2 = 0.844$; for **FR8**: $\Delta\nu = 1963+13440\Delta f$, $r^2 = 0.825$; for Prodan: $\Delta\nu = 4342+6634\Delta f$, $r^2 = 0.740$, where r^2 is goodness of fit.

Using a plot of Stokes shift vs. orientation polarizability function (Δf) (Fig. S2) and the Lippert equation, we estimated the transition dipole moment for all three dyes. For **FR0** and **FR8**, the cavity radius was assumed based on their chemical structure, namely 5.15Å. The obtained transition dipole moments ($\Delta\mu$) were 14.0±0.5 D, 14.0±0.5 D, 7.0±0.5 D for **FR0**, **FR8** and Prodan, respectively. The estimated $\Delta\mu$ for Prodan is in good accordance with literature.[8]

References

1. Davis, B. N.; Abelt, C. J. Synthesis and Photophysical Properties of Models for Twisted PRODAN and Dimethylaminonaphthonitrile. *J. Phys. Chem. A* **2005**, *109*, 1295-1298.
2. Lu, Z.; Lord, S. J.; Wang, H.; Moerner, W. E.; Twieg, R. J. Long-Wavelength Analogue of PRODAN: Synthesis and Properties of Anthradan, a Fluorophore with a 2,6-Donor−Acceptor Anthracene Structure. *J. Org. Chem.* **2006**, *71*, 9651-9657.
3. Xu, C.; Webb, W. W. Measurement of two-photon excitation cross sections of molecular fluorophores with data from 690 to 1050 nm. *J. Opt. Soc. Am. B* **1996**, *13*, 481-491.
4. Albota, M. A.; Xu, C.; Webb, W. W. Two-photon fluorescence excitation cross sections of biomolecular probes from 690 to 960 nm. *Applied Optics* **1998**, *37*, 7352-7356.
5. Zhan, X.; Risko, C.; Amy, F.; Chan, C.; Zhao, W.; Barlow, S.; Kahn, A.; Brédas, J.-L.; Marder, S. R. Electron Affinities of 1,1-Diaryl-2,3,4,5-tetraphenylsiloles: Direct Measurements and Comparison with Experimental and Theoretical Estimates. *J. Am. Chem. Soc.* **2005**, *127*, 9021-9029.
6. Xie, N.; Zeng, D. X.; Chen, Y. 3,4-Bis(5-iodo-2-methylthien-3-yl)-2,5-dihydrothiophene: A Powerful Synthon- for the Preparation of Photochromic Dithienylethene Derivatives. *Synlett* **2006**, 737-740.
7. Saroja, G.; Pingzhu, Z.; Ernsting, N. P.; Liebscher, J. Synthesis of Alkylated Aminofluorenes by Palladium-Catalyzed Substitution at Halofluorenes. *J. Org. Chem.* **2004,** *69*, 987-990.
8. Catalan, J.; Perez, P.; Laynez, J.; Blanco, F. G. Analysis of the solvent effect on the photophysics properties of 6-propionyl-2-(dimethylamino) naphthalene (PRODAN). *J. Fluorescence* **1991**, *1*, 215-223.

PUBLICATION 4

DIPOLAR 3-METHOXYCHROMONES AS BRIGHT AND HIGHLY SOLVATOCHROMIC FLUORESCENT DYES

Manuscript

Dipolar 3-methoxychromones as bright and highly solvatochromic fluorescent dyes

Oleksandr A. Kucherak, Ludovic Richert, Yves Mély and Andrey S. Klymchenko*

[a]Laboratoire de Biophotonique et Pharmacologie, UMR 7213 CNRS, Université de Strasbourg, Faculté de Pharmacie, 74, Route du Rhin, 67401 ILLKIRCH Cedex, France

*Corresponding author: Tel: +33 368854255. Fax: +33 368854313. E-mail:

aklymchenko@unistra.fr

Abstract

Herein, three environment-sensitive (solvatochromic) fluorescent dyes presenting a strong electron acceptor 3-methoxychromone unit and varied electron donor 2-aryl were developed. All three dyes showed remarkable polarity-dependent shifts of the emission maximum, which increase with extension of the dye conjugation. For the 3-methoxychromone bearing a 7-(diethylamino)-9,9-dimethylfluoren-2-yl donor group the difference between the excited and the ground state dipole moments reached 20D, which is among the largest reported for neutral dipolar fluorophores. Moreover, the new dyes are characterized by significant two-photon absorption cross-section (up to 450 GM) and large fluorescence quantum yield. In comparison to the parent 3-hydroxychromone derivatives, the new dyes present significantly improved photostability, which confirms that photodegradation of 3-hydroxychromones occurs from a product of the excited-state intramolecular proton transfer (phototautomer). This new class of fluorescent dyes may serve as attractive building blocks for future molecular sensors utilizing environment-sensitive fluorophores.

Introduction

Despite the large number of fluorescent probes already developed,[1-3] the search for new fluorophores and in particular, environment-sensitive dipolar fluorophores, which change their emission properties in response to changes in their local environment, raised strong interest in recent years.[4-6] Due to their sensitivity to the environment, these dyes are able to monitor the properties of lipid membranes[7] as well as interactions of proteins with their partners, such as other proteins, DNA and biomembranes.[8-10] They are also of interest for studying conformational changes of biomolecules.[11] Despite their large range of applications, this class of fluorescent dyes is largely under-developed compared to the classical non-solvatochromic dyes. The major problem is that most of these dyes do not meet simultaneously all the spectroscopic requirements for biological applications: absorption in the visible (> 400 nm), high absorption coefficient (≥ 30,000 $cm^{-1}\times M^{-1}$), high fluorescence quantum yield (> 50 %) and photostability as well as strong solvatochromism.

For instance, dansyl derivatives,[12] DMAP and its analogues[13-15] show low absorption coefficients, while Nile Red exhibits relatively weak solvatochromism.[16] The most solvatochromic dye described to date, Fluoroprobe, exhibits poor absorption properties and low fluorescence quantum yield in polar solvents.[17] Among the best solvatochromic dyes reported so far are Prodan[18] and dapoxyl[19] derivatives, though they appear borderline with respect to the mentioned spectroscopic requirements. Recently developed anthracene and fluorene analogues of Prodan,[20, 21] appear promising, since they overcome the UV-absorption drawback of Prodan. Dicyanomethylenedihydrofuran fluorophores, characterized by red-shifted absorption and good solvatochromism, appear also as advanced environment-sensitive dyes.[5, 22, 23] 3-Hydroxychromone (3HC) derivatives, show exceptional two-color solvatochromism,[24, 25] due to an Excited-State Intramolecular Proton Transfer (ESIPT), but suffer from poor photostability.[26] This class of dyes found variety of applications for probing biomembranes and protein interactions as well as for cellular imaging,[7, 10, 27-29] so that we were particularly interested to design photostable fluorescent dyes based on these chromophores. It has been shown that the nature of photodegradation of 3HCs is photo-oxidation [26] and/or re-arrangement [30] in the tautomer state (T*) of the dye, which is a product of the ESIPT reaction. Therefore, in the present work we substituted the 3-hydroxyl group in 3HCs with methyl, in order to prevent the molecules from ESIPT transformation. To obtain solvatochromic dyes, we selected dipolar 3HC derivatives (for instance **1a** in Fig. 1), presenting significant solvatochromism of the normal excited state [24, 25, 31]. 3-Methoxychromones (3MC) **1-3** were synthesized presenting different conjugation lengths. Among them, only a homologue of **1** has already been reported [32], though its solvatochromism and photostability were not evaluated. The obtained compounds showed strong absorption in the visible range, high fluorescence quantum yields and much higher photostability compared to their 3HC analogues. The single emission band

of these dyes showed strong solvatochromism, which increased significantly with the length of the 3MC fluorophore. The new dyes constitute prospective building blocks for construction of environment-sensitive probes and labels in biological applications.

Materials and Methods

All chemicals were from Sigma-Aldrich, Alfa Aesar or TCI Europe. For synthesis, solvents were of reagent or ACS grade, while for spectroscopy they were of spectroscopic grade.

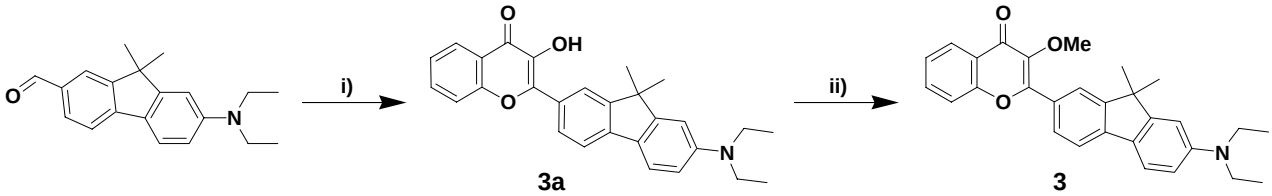

i) 2-hydroxy acetophenone, MeONa, DMF, then MeONa, H_2O_2, EtOH, reflux, 32%; ii) MeI, K_2CO_3, MeOH, r.t., 77%.

Scheme 1. Synthesis of 3-methoxychromone **3**.

Synthesis of 3-methoxychromone dyes 1, 2 and 3.

2-(7-Diethylamino-9,9-dimethyl-9H-fluoren-2-yl)-3-hydroxychromone (3a) (adapted from [33]). 2-hydroxyacetophenone (31mg, 0.23mmol) was mixed with 7-diethylamino-9,9-dimethylfluorene-2-carbaldehyde[21] (65mg, 0.22mmol) and sodium methoxide (50mg, 0.88mmol) in 3mL of DMF. Reaction mixture was stirred overnight at RT. Then it was diluted with 10mL of ethanol and more sodium methoxide (145mg, 2.64mmol) and 30% aqueous H_2O_2 (230µL, 2.20mmol) were added. Resulted solution was refluxed for 2-3 min, cooled and poured into 100mL of water. After neutralizing with 10% HCl, the formed precipitate was filtered off and purified by preparative TLC (eluent CH_2Cl_2/Heptane = 1/1) to produce the desired chromone **3a** as a yellow powder. Yield 30mg (32%). **^{1}H NMR** ($CDCl_3$, 300MHz): δ ppm 8.30-8.20(m, 3H), 7.75-7.55(m, 4H), 7.40(t, 1H), 6.80-6.65(m,2H), 3.45(q, 4H), 1.55(s, 6H), 1.24(t, 6H). **LCMS** (m/z): ESI calcd for $C_{28}H_{28}NO_3^+$ 426.2; found $[M+1]^+$ 426.2.

General procedure for preparation of 3-methoxychromones. A 3-hydroxychromone was mixed with an excess of methyl iodide (20eq) and potassium carbonate (2eq) in methanol. If necessary, some DMF was added to complete dissolution. Reaction mixture was stirred for 24h at RT. Organic solvent was removed under vacuum, and the residue was purified by preparative TLC (eluent CH_2Cl_2/MeOH = 98/2, 2nd fraction) to give the corresponding 3-methoxychromone.

4'-(Diethylamino)-3-methoxyflavone (1). Synthesized from 15 mg of 4'-(diethylamino)-3-hydroxyflavone (**1a**) [31]. Yellow solid, yield 8mg (50%). **^{1}H NMR** ($CDCl_3$, 400MHz): δ ppm 8.25(dd, 1H), 8.09(d, 2H), 7.62(m, 1H), 7.49(d, 1H), 7.35(t, 1H), 6.80-6.70(br s, 2H), 3.89(s, 3H), 3.45(q, 4H), 1.23(t, 6H). **HRMS** (m/z): ESI calcd for $C_{20}H_{22}NO_3^+$ 324.16; found $[M+1]^+$ 324.16.

2-(6-diethylaminobenzo[*b*]furan-2-yl)-3-methoxychromone (2). Synthesized from 10 mg of corresponding 3-hydroxychromone **2a**[25]. Orange solid, yield 6mg (58%). **^{1}H NMR** ($CDCl_3$, 400MHz): δ ppm 8.25(dd, 1H), 7.70-7.58(m, 3H), 7.47(d, 1H), 7.38(t, 1H), 6.83(s, 1H), 6.76(d, 1H), 4.07(s, 3H), 3.45(q, 4H), 1.23(t, 6H). **HRMS** (m/z): ESI calcd for $C_{22}H_{22}NO_4^+$ 364.15; found $[M+1]^+$ 364.15.

2-(7-Diethylamino-9,9-dimethyl-9H-fluoren-2-yl)-3-methoxychromone (3). Synthesized from 15 mg of corresponding 3-hydroxychromone **3a**. Yellow-orange solid, yield 12mg (77%). **^{1}H NMR** ($CDCl_3$, 400MHz): δ ppm 8.28(dd, 1H), 8.13(s, 1H), 8.07(dd, 1H), 7.70-7.55(m, 4H), 7.39(m, 1H), 6.73(d, 1H), 6.69(dd, 1H), 3.91(s, 3H), 3.45(q, 4H), 1.53(s, 6H), 1.23(t, 6H). **^{13}C NMR** ($CDCl_3$, 100MHz): δ 12.63, 27.40, 44.71, 46.84, 59.92, 105.37, 110.82, 117.93, 118.12, 121.82, 122.37, 124.29, 124.46, 125.77, 125.91, 126.89, 127.78, 133.15, 141.07, 143.02, 148.58, 152.70, 155.23, 156.60, 156.68, 174.95. **HRMS** (m/z): ESI calcd for $C_{29}H_{30}NO_3^+$ 440.22; found $[M+1]^+$ 440.22.

All solvents and chemicals were purchased from Aldrich. The solvents were of spectroscopic grade. Absorption and fluorescence spectra were recorded on Cary 4 spectrophotometer (Varian) and FluoroLog spectrofluorometer (Jobin Yvon, Horiba), respectively. For spectroscopic measurements, ~ 1 μM solutions of dyes were used. All the spectra are corrected from the background (spectra of neat solvents were subtracted). Fluorescence quantum yields were determined by taking 4'-(dimethylamino)-3-methoxyflavone in ethanol (quantum yield, QY = 29 %) [32] as a reference. The quantum yield values were corrected for the solvent refractive index.

In the photostability assays, a 0.33 μM solution of a given dye in a quartz micro-cuvette (50 μL volume) was illuminated by the Xenon lamp of a FluoroLog spectrofluorometer (excitation slits were opened to 8 nm). The excitation wavelength was a 400 nm for dyes **1** and **1a**, 430 nm for dyes **2** and **3** and 360 nm for Prodan. During the time of illumination (5000 seconds), the fluorescence intensity maximum was recorded as a function of time. The resulting fluorescence photodegradation curve was fitted to a single exponential decay function $I = I_0\exp(-t/\tau_d)$, where I is the measured fluorescence intensity, I_0 is the fluorescence intensity at t = 0, t is the illumination time , and τ_d is the photodegradation time constant.

Two-photon absorption cross section measurements were performed using Rhodamine B in methanol as a calibration standard according to the method of Webb et al.[34, 35] Two-photon excitation was provided by a mode-locked titanium-sapphire laser (Tsunami, Spectra Physics). The laser was focused by an achromatic lens (f = 2 cm) in a cuvette containing the dye (100 μM in DMF) and the spectra were recorded with a fibered spectrometer (Avantes) by collecting the fluorescence emission at 90° with a 20X Olympus objective. The quadratic dependence of the

fluorescence intensity with respect to the laser power was checked for all the dyes to avoid a saturation artifact.

Results and discussion

The new dyes **1-3** (Fig.1) were readily synthesized from the corresponding 3-hydroxy-chromones. Methylation of the 3-hydroxy group was performed under basic conditions using methyl iodide as a methylation agent. While **1** and **2** were synthesized from already described 3HCs,[25, 31] dye **3** was prepared in several steps starting from 9,9-dimethyl-7-(diethylamino)-2-formylfluorene[21]. The obtained fluorescent dyes consist of a donor, an acceptor and a π-conjugated system. All three dyes are based on the electron withdrawing 3-methoxychromone core, while the donor part is represented by a diethylamino group. Compared to compound **1**, the electronic conjugation is extended for compound **2** by a benzofuran ring and for compound **3** by a fluorene ring.

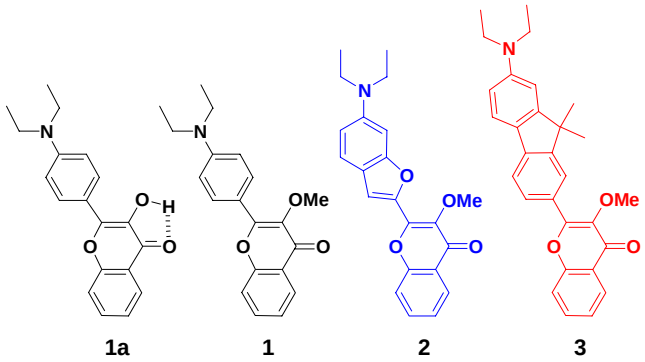

Figure 1. Structure of 3-methoxychromones **1-3** and a 3-hydroxyflavone **1a**.

At first, the absorption properties of the new compounds were characterized in different organic solvents. A weak positive solvatochromism was observed, as the absorption maxima in polar solvents were red shifted as compared to those in apolar solvents (Table 1 and Table S1 in SI). This suggests that the electronic excitation increases the dipole moment of the molecule and that the directions of the ground- and excited-state dipoles are similar. Remarkably, **1** and **2** showed a slightly blue shifted absorption as compared to their 3HC analogues.[25] We speculate that in 3HC derivatives, the intramolecular H-bond between the 3-hydroxyl and 4-carbonyl groups decreases the energy of electronic transition, explaining the red shifted absorption for 3HCs. Moreover, the absorption maximum for 3MFs shifts to the red in the following order: **1→3→2**. Compared to **1**, the absorption maxima of **2** and **3** were shifted by 50 and 20 nm, respectively. (Table 1 and Fig. S1 in SI). The red-shift of **3** with respect to **1** is obviously connected with the extension of the electronic conjugation, while the red-shifted absorption of **2** with respect to **3** is probably connected with the stronger electron donating properties of the π-abundant benzofurane heterocycle.

Absorption coefficients at the long-wavelength absorption maxima in ethanol were found to be 29000, 29000 and 31000 $M^{-1}cm^{-1}$ for compounds **1**, **2** and **3,** respectively. These values are close to those reported for parent 3HCs [25].

Table 1. Spectroscopic properties of dyes **1-3** in different solvents.[a]

Solvent	$E_T(30)$	dye **1**			dye **2**			dye **3**		
		λ_{Abs} nm	λ_{Fluo} nm	QY %	λ_{Abs} nm	λ_{Fluo} nm	QY %	λ_{Abs} nm	λ_{Fluo} nm	QY %
Hexane[b]	31.0	371	412	11.9	404	443	74.6	393	433	73.0
Toluene[b]	33.9	384	438	42.4	435	485	68.0	404	480	73.0
Dioxane[b]	36.0	383	446	54.3	430	500	71.4	401	500	67.1
$CHCl_3$[b]	39.1	394	462	68.0	443	526	56.0	414	540	50.0
CH_2Cl_2	40.7	393	471	63.0	440	539	45.5	412	562	34.8
DMF	43.2	394	485	59.3	440	560	37.2	413	595	22.4
DMSO	45.1	398	494	65.0	445	572	33.3	418	608	18.0
Acetonitrile	45.6	389	486	59.5	433	560	31.5	406	598	18.1
1-Octanol	48.1	400	492	62.6	446	566	33.8	420	594	16.8
1-Butanol	49.7	400	501	53.8	446	579	21.4	420	612	6.6
Ethanol	51.9	400	508	33.3	445	587	7.8	418	623	2.0
Methanol	55.4	402	520	4.7	445	597	1.4	417	632	0.3
Water	63.1	413	539	0.1	447	616	0.2	410	562	2.0

[a] QY is the fluorescence quantum yield. Excitation wavelength was 420 or [b]380 nm. For complete table with all solvents studied, see supporting information. $E_T(30)$ is polarity index from Ref.[36]

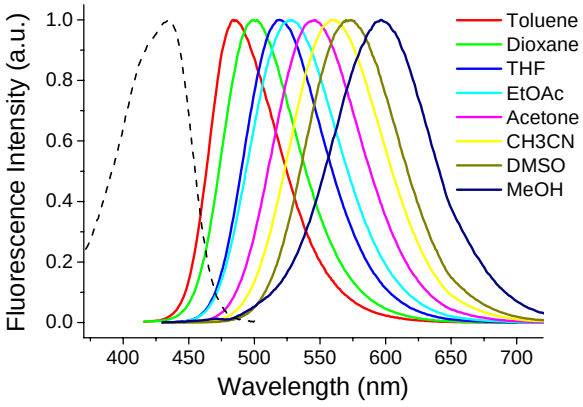

Figure 2. Spectroscopic properties of dye **2**. Absorption spectrum in toluene (dashed line) and emission spectra (solid lines) in selected organic solvents.

Next, fluorescence of compounds **1-3** was studied in solvents of different polarities. In contrast to the parent 3HC analogues, 3MC derivatives show a single emission band in all solvents studied, since they are unable to undergo ESIPT reaction due to the methylation of the 3-hydroxy group. For all three dyes, the emission spectra shifted dramatically to longer wavelengths as the solvent polarity was increased (for **2** see Fig. 2). Moreover, we found a perfect correlation between the position of the emission maximum and the empirical polarity parameter $E_T(30)$[36] for all three dyes (Fig. 3), which indicates that they can be used as fluorescence indicators of solvent polarity.

Since all new dyes bear electron donor and acceptor groups, a charge transfer (CT) occurs probably in the excited state from the electron-donor to the electron acceptor group through the conjugation core. The CT process is thought to strongly increase the dipole moment in the excited state, explaining the positive fluorescence solvatochromism in these compounds. When the spectra are presented in a wavenumber scale (see Fig. S2 in SI), one can notice that the emission peaks exhibit the same full width at half-maximum (about 2500 cm^{-1}) in all solvents. This value is close to that of PRODAN,[21] suggesting that the emission of these dyes occurs from the same S1-S0 electronic transition in all solvents.

The solvent-dependent red-shift of the emission maximum grows in the following order: **1→2→3**. While for **1** the emission band shifts by 3970 cm^{-1} from hexane to methanol, the corresponding shifts were 5090 and 6650 cm^{-1} for **2** and **3**, respectively. Moreover, the slope of the curves of the emission maximum versus $E_T(30)$ increased in the same order **1→2→3**, confirming the increase in solvent sensitivity. These differences in solvent sensitivity correlate perfectly with the length of the π-conjugated system of the dyes and the differences in the electron polarizability which likely increase the dipole moment difference in the following order **1→2→3.**

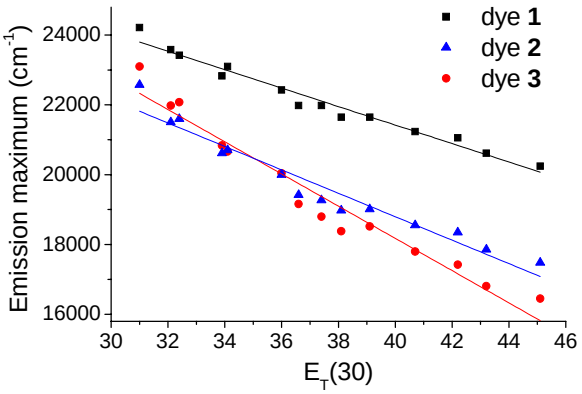

Figure 3. Dependence of the emission maxima of compounds **1-3** on the $E_T(30)$ parameter in aprotic solvents. Linear fit resulted in slopes of 264 (r^2=0.969), 336 (r^2=0.941) and 462 cm^{-1} (r^2=0.953) for compounds **1**, **2** and **3**, respectively; r^2 value represents the goodness of fit.

To further validate this conclusion, we studied the dependence of the Stokes shifts on the Lippert polarizability function (see Fig. S3 in SI), which allows estimating the difference between the ground and excited state dipole moments (Δμ) of the dyes.[37, 38] The dipole moment differences were found to be 8.4 D, 13.1 D and 20.0 D for compounds **1**, **2** and **3**, respectively. Remarkably, the 20 D value for compound 3 is very high for a neutral molecule, being comparable with the Δμ value obtained for anionic dyes, such as 1,8-ANS.[39] This value is much larger than that measured for common solvatochromic dyes, such as Nile Red (6.8D) [40] and PRODAN (7D),[41] or the parent fluorene aldehyde derivative FR8 (13D) [21]. Among the neutral compounds, this large value of Δμ could be compared to that of Fluoroprobe (25D),[17] a dye exhibiting a "through-space" CT, and to

very long conjugated fluorene derivatives.[42] It should be also added that the Δμ value observed for **1** matches closely the value reported for the parent 3HC analogue **1a** (9D),[43-45] indicating that methylation of the 3-hydroxyl group did not change the nature of CT in the chromone dye.

Fluorescence quantum yields of dyes **1-3** were relatively high, especially in organic solvents of medium and low polarity. Compared to the reported 3HC analogues,[24, 25] the quantum yields of **1** and **2** are generally higher in most solvents, except in alcohols. For compounds **2** and **3,**, a clear decrease in the QY was observed with increase in the polarity index $E_T(30)$ (Fig. 4). A very similar phenomenon was observed for dapoxyl [19] and fluorene [21] dyes. Thus, the effect of solvent polarity appears as a rather general phenomenon where highly dipolar fluorophores are quenched by polar solvents. Noticeably, the decrease in QY with polarity is faster for **3** than for **2**, indicating that stronger dipolar moments favor the quenching by polar solvents. In contrast, for the least dipolar dye **1** this correlation is more complex as QY is highest for solvents of medium polarity. Finally, all three dyes show very low quantum yield in highly polar solvents such as methanol and water, which appears as a useful property in a variety of applications. For instance, upon binding to apolar biologic targets, such as lipid membranes, these dyes will "turn on" their fluorescence,[27, 46] so that the detected signal will originate only from the bound species, and not from the free probe in the buffer. Moreover, changes in the quantum yield will also be useful for monitoring ligand-protein binding when binding of the labeled ligand will lead to a strong fluorescence increase as a consequence of the drop in polarity of the probe environment.[8, 15]

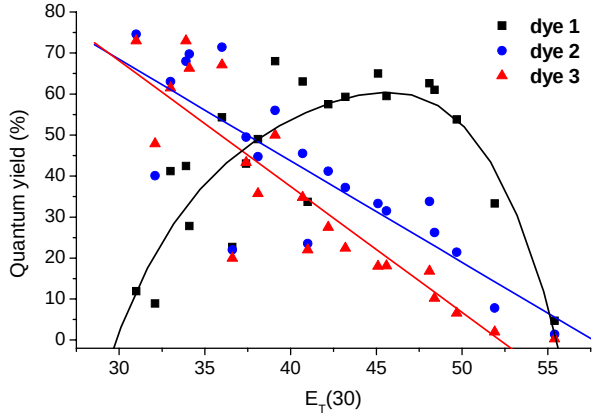

Figure 4. Fluorescence quantum yield of dyes **1-3** vs. polarity index $E_T(30)$ of organic solvents. Straight lines (red and blue) present linear fits, while black curve is used for guiding eye.

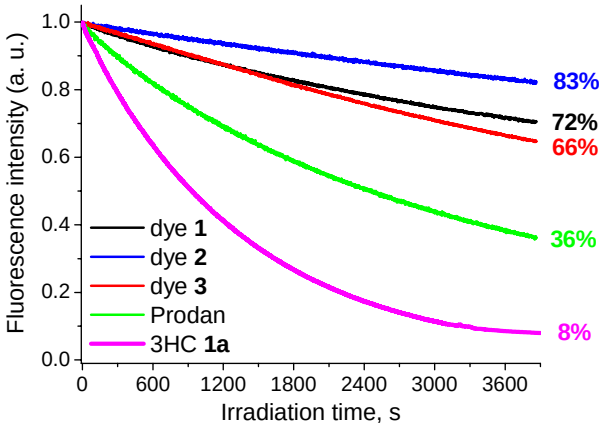

Figure 5. Photodegradation of dyes **1-3** in DMF in comparison to that of Prodan and 3HF analogue **1a**. The fluorescence intensity of the dyes was recorded as a function of the irradiation time. Numbers (%) correspond to residual fluorescence intensity after 1h of irradiation. Concentration of the dyes was 1μM. Excitation wavelength was 400 nm for **1** and **1a**, 430 nm for **2** and **3** and 360 nm for Prodan.

Modern fluorescence detection and imaging techniques, and particularly single molecule fluorescence micrsocpy[47] impose more severe requirements to dye photostability. However, the parent 3HC derivatives are not photostable, due to photodegradation of their tautomer (T*) excited state.[26, 30] The photostability of the dyes was characterized by recording the time-dependent fluorescence of dye solutions illuminated by the xenon lamp of the spectrofluorometer. As expected, the photodegradation of 3HC **1a** in DMF appears rather rapid, showing only 8 % of residual fluorescence after 1 h of irradiation. Methylation of the 3-hydroxyl group improved remarkably the photostability, as 66 to 83% of the initial fluorescence of compounds **1-3** was still present after 1h illumination (Fig. 5, Table S2 in SI). Thus, preventing the ESIPT transformation into the T* state improves dramatically the photostability. The new compounds are also more photostable than the common environment-sensitive dye Prodan, since their residual fluorescence after 1h of irradiation is twice of that of Prodan. Finally, the photodegradation time constants of **1-3** obtained by fitting the photodegradation curves to a mono exponential decay function were found to be significantly higher in ethanol than in DMF, this effect being especially pronounced for compounds **2** and **3**.

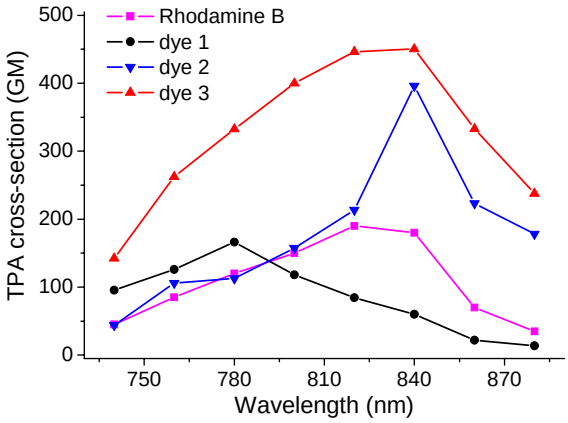

Figure 6. Two-photon absorption cross-section (GM, 10^{-50} cm^4 s $photon^{-1}$) of compounds **1-3** (in DMF) and reference Rhodamine B (in MeOH) as a function of the excitation wavelength. Error is ± 25%. Data on rhodamine B are from Ref. [34].

Taking into account that the absorption maximum of the new dyes is close to 400 nm, the new dyes are attractive for two-photon (TP) excitation[48-50] with femtosecond infrared laser (around 800 nm) as an excitation source. TP excitation spectra were recorded for dyes **1-3** in ethanol and their TP absorption cross-section values were evaluated at different wavelengths (Fig. 3), using Rhodamine B as a standard.[34, 35] In the 750-850 nm spectral range, the maximal values of TP absorption cross-section increase in the following order **1→2→3** (Fig. 6), which correlates well with the increase in the dye conjugation. It can be also seen that the TP absorption maximum of dyes **2** and **3** is shifted to the red as compared to **1**, in line with their red-shifted absorption in one-photon spectroscopy (Table 1). Interestingly, the maximal value of TP absorption cross-section of dye **1** (160 GM at 780 nm) is comparable to that of Rhodamine B (210 GM at 840 nm), while for dye **3**, the corresponding value is more than 2-fold larger (450 GM at 840nm). The high TP absorption cross-section of the new dyes makes them attractive for applications in TP spectroscopy and microscopy. [48, 49]

Conclusions

A new class of fluorescent solvatochromic (environment-sensitive) dyes, 3-methoxychromones, is introduced. They exhibit attractive spectroscopic properties, e.g. high absorption coefficient and two-photon absorption cross-section as well as high fluorescence quantum yields and photostability. Their solvatochromism increases with the fluorophore length, providing extremely large spectral shifts due to the large dipole moment difference (up to 20 D). Taking into account that the chemistry and applications of the parent 3HCs are well-explored,[7, 10, 25, 27, 28] we expect 3-methoxychromones, presenting higher brightness and photostability, to find numerous applications as fluorescence probes and labels in biology.

Acknowledgments

This work was supported by the Agence Nationale de la Recherche (ANR blanc 07-BLAN-0287), Conectus Alsace grant and the ARCUS program between France, Ukraine and Russia.

Supporting Information Available. Details on the fluorescence properties of the dyes are available, free of charge via the Internet at http:www.

References

1 B. N. G. Giepmans, S. R. Adams, M. H. Ellisman, and R. Y. Tsien, *Science*, 2006, **312**, 217.

2 L. D. Lavis and R. T. Raines, *ACS Chem. Biol.*, 2008, **3**, 142.

3 J. Zhang, R. E. Campbell, A. Y. Ting, and R. Y. Tsien, *Nat. Rev. Mol. Cell Biol.*, 2002, **3**, 906.

4 P. Yan, A. Xie, M. Wei, and L. M. Loew, *J. Org. Chem.*, 2008, **73**, 6587.

5 Z. Lu, N. Liu, S. J. Lord, S. D. Bunge, W. E. Moerner, and R. J. Twieg, *Chem. Mater.*, 2009, **21**, 797.

6 E. Font-Sanchis, R. E. Galian, F. J. Cespedes-Guirao, A. Sastre-Santos, L. R. Domingo, F. Fernandez-Lazaro, and J. Perez-Prieto, *Phys. Chem. Chem. Phys.*, 2010, **12**, 7768.

7 A. P. Demchenko, Y. Mely, G. Duportail, and A. S. Klymchenko, *Biophys. J.*, 2009, **96**, 3461.

8 G. S. Loving, M. Sainlos, and B. Imperiali, *Trends Biotechnol.*, 2010, **28**, 73.

9 V. Y. Postupalenko, V. V. Shvadchak, G. Duportail, V. G. Pivovarenko, A. S. Klymchenko, and Y. Mely, *Biochim. Biophys. Acta*, 2010, **1808**, 424.

10 V. V. Shvadchak, A. S. Klymchenko, H. De Rocquigny, and Y. Mely, *Nucl. Acids Res.*, 2009, **37**.

11 B. E. Cohen, A. Pralle, X. Yao, G. Swaminath, C. S. Gandhi, Y. N. Jan, B. K. Kobilka, E. Y. Isacoff, and L. Y. Jan, *Proc. Natnl. Acad. Sci. USA*, 2005, **102**, 965.

12 S. R. Holmes-Farley and G. M. Whitesides, *Langmuir*, 1986, **2**, 266.

13 T. Soujanya, R. W. Fessenden, and A. Samanta, *J. Phys. Chem.*, 1996, **100**, 3507.

14 M. E. Vazquez, J. B. Blanco, and B. Imperiali, *J. Am. Chem. Soc.*, 2005, **127**, 1300.

15 G. Loving and B. Imperiali, *J. Am. Chem. Soc.*, 2008, **130**, 13630.

16 P. Greenspan and S. D. Fowler, *J. Lipid Res.*, 1985, **26**, 781.

17 G. F. Mes, B. De Jong, H. J. Van Ramesdonk, J. W. Verhoeven, J. M. Warman, M. P. De Haas, and L. E. W. Horsman-van Den Dool, *J. Am. Chem. Soc.*, 1984, **106**, 6524.

18 G. Weber and F. J. Farris, *Biochemistry*, 1979, **18**, 3075.

19 Z. Diwu, Y. Lu, C. Zhang, D. H. Klaubert, and R. P. Haugland, *Photochem. Photobiol.*, 1997, **66**, 424.

20 Z. Lu, S. J. Lord, H. Wang, W. E. Moerner, and R. J. Twieg, *J. Org. Chem.*, 2006, **71**, 9651.

21 O. A. Kucherak, P. Didier, Y. Mely, and A. S. Klymchenko, *J. Phys. Chem. Lett.*, 2010, **1**, 616.

22 S. J. Lord, Z. Lu, H. Wang, K. A. Willets, P. J. Schuck, H. L. D. Lee, S. Y. Nishimura, R. J. Twieg, and W. E. Moerner, *J. Phys. Chem. A*, 2007, **111**, 8934.

23 Z. Lu, N. Liu, S. J. Lord, S. D. Bunge, W. E. Moerner, and R. J. Twieg, *Chemistry of Materials*, 2009, **21**, 797.

24 A. S. Klymchenko and A. P. Demchenko, *Phys. Chem. Chem. Phys.*, 2003, **5**, 461.

25 A. S. Klymchenko, V. G. Pivovarenko, T. Ozturk, and A. P. Demchenko, *New J. Chem.*, 2003, **27**, 1336.

26 P. T. Chou and M. L. Martinez, *Radiation Phys. Chem.*, 1993, **41**, 373.

27 V. V. Shynkar, A. S. Klymchenko, C. Kunzelmann, G. Duportail, C. D. Muller, A. P. Demchenko, J. M. Freyssinet, and Y. Mely, *J. Am. Chem. Soc.*, 2007, **129**, 2187.

28 O. M. Zamotaiev, V. Y. Postupalenko, V. V. Shvadchak, V. G. Pivovarenko, A. S. Klymchenko, and Y. Mely, *Bioconj. Chem.*, 2011, **DOI: 10.1021/bc100434d**.

29 C. Dyrager, A. Friberg, K. Dahlén, M. Fridén-Saxin, K. Börjesson, L. M. Wilhelmsson, M. Smedh, M. Grøtli, and K. Luthman, *Chem. Eur. J.*, 2009, **15**, 9417.

30 S. Tommasini, M. L. Calabra, P. Donato, D. Raneri, G. Guglielmo, P. Ficarra, and R. Ficarra, *J. Pharm. Biomed. Anal.*, 2004, **35**, 389.

31 P. T. Chou, M. L. Martinez, and J. H. Clements, *J. Phys. Chem.*, 1993, **97**, 2618.

32 S. M. Ormson, R. G. Brown, F. Vollmer, and W. Rettig, *J. Photochem. Photobiol. A*, 1994, **81**, 65.

33 A. S. Klymchenko, T. Ozturk, and A. P. Demchenko, *Tet. Lett.*, 2002, **43**, 7079.

34 C. Xu and W. W. Webb, *J. Opt. Soc. Am. B*, 1996, **13**, 481.

35 M. A. Albota, C. Xu, and W. W. Webb, *Appl. Optics*, 1998, **37**, 7352.

36 C. Reichardt, *Chem. Rev.*, 1994, **94**, 2319.

37 E. L. Lippert, 'Organic molecular photophysics', Wiley-Interscience, 1975.

38 N. Mataga and T. Kubota, 'Molecular interactions and electronic spectra', M. Dekker, 1970.

39 J. R. Lakowicz, 'Principles of Fluorescence Spectroscopy', Springer-Verlag, 2006.

40 A. K. Dutta, K. Kamada, and K. Ohta, *J. Photochem. Photobiol. A*, 1996, **93**, 57.

41 J. Catalan, P. Perez, J. Laynez, and F. G. Blanco, *J. Fluorescence*, 1991, **1**, 215.

42 C. Le Droumaguet, O. Mongin, M. H. V. Werts, and M. Blanchard-Desce, *Chem. Comm.*, 2005, 2802.

43 N. A. Nemkovich, W. Baumann, and V. G. Pivovarenko, *J. Photochem. Photobiol. A*, 2002, **153**, 19.

44 P. T. Chou, S. C. Pu, Y. M. Cheng, W. S. Yu, Y. C. Yu, F. T. Hung, and W. P. Hu, *J. Phys. Chem. A*, 2005, **109**, 3777.

45 S. O. Yesylevskyy, A. S. Klymchenko, and A. P. Demchenko, *J. Mol. Struct.*, 2005, **755**, 229.

46 O. A. Kucherak, S. Oncul, Z. Darwich, D. A. Yushchenko, Y. Arntz, P. Didier, Y. Mely, and A. S. Klymchenko, *J. Am. Chem. Soc.*, 2010, **132**, 4907.

47 S. Weiss, *Science*, 1999, **283**, 1676.

48 W. Denk, J. H. Strickler, and W. W. Webb, *Science*, 1990, **248**, 73.

49 C. Xu, W. Zipfel, J. B. Shear, R. M. Williams, and W. W. Webb, *Proc. Natnl. Acad. Sci. USA*, 1996, **93**, 10763.

50 M. Johnsen, M. J. Paterson, J. Arnbjerg, O. Christiansen, C. B. Nielsen, M. Jorgensen, and P. R. Ogilby, *Phys. Chem. Chem. Phys.*, 2008, **10**, 1177.

Supporting information

Dipolar 3-methoxychromones as bright and highly solvatochromic fluorescent dyes

Oleksandr A. Kucherak, Ludovic Richert, Yves Mély and Andrey S. Klymchenko

Laboratoire de Biophotonique et Pharmacologie, UMR 7213 CNRS, Université de Strasbourg, Faculté de Pharmacie, 74, Route du Rhin, 67401 ILLKIRCH Cedex, France

Spectroscopic characterization of compounds 1-3

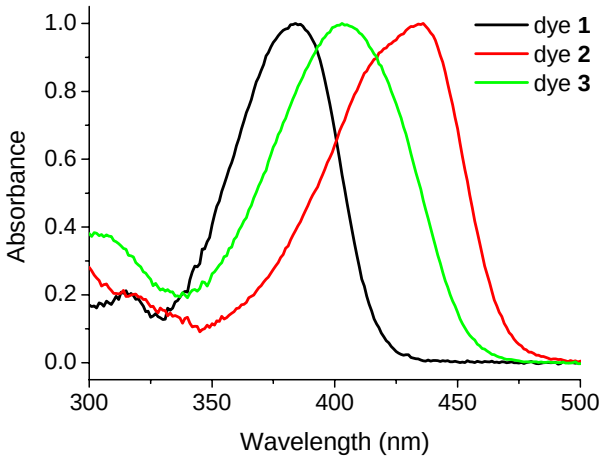

Figure S1. Absorption spectra of compounds **1-3** in toluene.

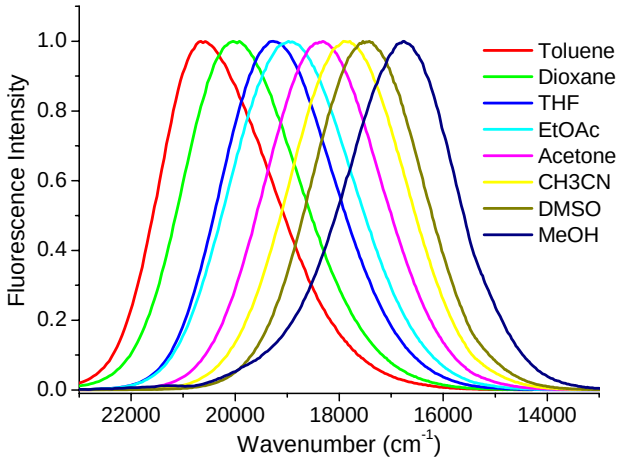

Figure S2. Fluorescence spectra of dye **2**, presented in a wavenumber scale.

Table S1. Spectroscopic properties of compounds **1-3** in various solvents[a].

#	Solvent	Dye 1			Dye 2			Dye 3		
		λ_{Abs} nm	λ_{Fluo} nm	QY %	λ_{Abs} nm	λ_{Fluo} nm	QY %	λ_{Abs} nm	λ_{Fluo} nm	QY %
1	Hexane[b]	371	412	11,9	404	443	74.6	393	433	73.0
2	Tetrachloromethane[b]	382	427	3.8	436	464	19.0	403	452	8.0
3	Toluene[b]	384	438	42.4	435	485	68.0	404	480	73.0
4	Dioxane[b]	383	446	54.3	430	500	71.4	401	500	67.1
5	Triethylamine[b]	376	424	8.9	427	465	40.1	396	455	47.9
6	Di-*n*-bytyl ether[b]	381	445	41.2	428	496	63.0	400	493	61.5
7	Diisopropyl ether [b]	378	433	27.8	425	483	69.7	397	484	66.3
8	Bromobenzene[b]	393	455	22.7	443	515	22.0	416	522	20.0
9	Chloroform[b]	394	462	68.0	443	526	56.0	414	540	50.0
10	*Tert*-pentanol	392	472	33.7	439	539	23.5	412	554	22.0
11	Ethyl acetate[b]	384	462	49.0	429	527	44.7	403	544	35.7
12	THF[b]	386	455	43.0	433	519	49.5	407	532	43.3
13	Dichloromethane	393	471	63.0	440	539	45.5	412	562	34.8
14	1-Octanol	400	492	62.6	446	566	33.8	420	594	16.8
15	1-Butanol	400	501	53.8	446	579	21.4	420	612	6.6
16	DMSO	398	494	65.0	445	572	33.3	418	608	18.0
17	DMF	394	485	59.3	440	560	37.2	413	595	22.4
18	2-Propanol	398	496	61.0	443	573	26.2	416	606	10.2
19	Acetone	388	475	57.5	432	545	41.2	405	574	27.5
20	Ethanol	400	508	33.3	445	587	7.8	418	623	2.0
21	Acetonitrile	389	486	59.5	433	560	31.5	406	598	18.1
22	Methanol	402	520	4.7	445	597	1.4	417	632	0.3
23	Water	413	539	0.1	447	616	0.2	410	562	2.0

[a] QY is fluorescence quantum yield; excitation wavelength was 420 nm.
[b] excitation wavelength was 380 nm.

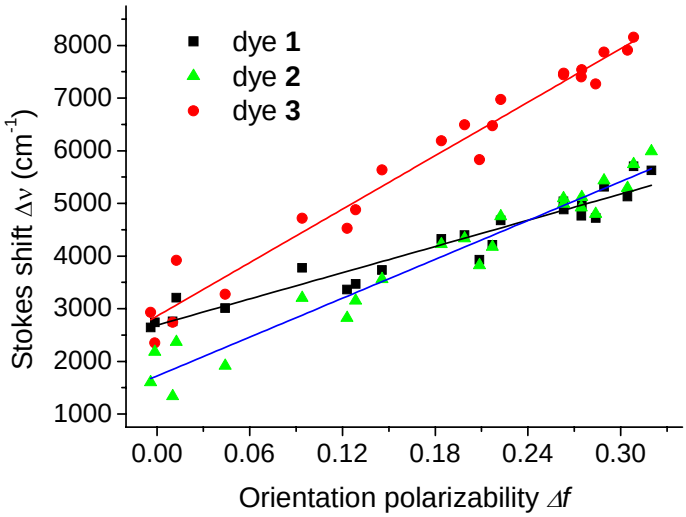

Figure S3. Dependence of the Stokes shifts ($\Delta\nu$) of dyes **1-3** as a function of the Lippert parameter (Δf). Results of the linear fits are: dye **1** $\Delta\nu$ = 2688+8300*Δf, r^2 = 0.927, dye **2** $\Delta\nu$ = 1721+12310*Δf, r^2 = 0.950, dye **3** $\Delta\nu$ = 2859+16935*Δf, r^2 = 0.967, where the r^2 value represents goodness of fit.

Plotting the Stokes shift $\Delta\nu$ versus the Lippert parameter Δf (Fig. S3) and using the Lippert-Mataga equation,[1,2] we estimated the dipole moment difference $\Delta\mu$ to be equal to 8.4±0.5 D (a=4.4Å), 13.1±0.5 D (a=5.2Å) and 20.0±0.5 D (a=6.2Å) for compounds **1, 2** and **3,** respectively. The cavity radius (a) was determined from their chemical structure (through the distance between donating Nitrogen atom and accepting Oxygen) using a chemical modeling software.

Table S2. Photostability of compounds **1-3** in different solvents[a].

Solvent	**Dye 1**		**Dye 2**		**Dye 3**	
	τ_d, min	**R, %**	**τ_d, min**	**R, %**	**τ_d, min**	**R, %**
EtOH	215	75	2445	97	>10000	99
DMF	185	72	335	83	145	66

[a] τ_d is the time constant of photodegradation; R is residual fluorescence intensity after 60 min of irradiation.

Table S3. Physical parameters of solvents used in calculations.

№	Solvent	Refractive index[a] $n_{20°C}$	Dielectric constant ε [a]	Δf [b]	$E_T(30)$ [c]
1	Hexane	1.3749	1.88	-0.0014	31.0
2	CCl_4	1.4601	2.23	0.0102	32.4
3	Toluene	1.4961	2.37	0.0126	33.9
4	Dioxane	1.4224	2.21	0.0205	36.0
5	Et_3N	1.4010	2.38	0.0441	32.1
6	n-Bu_2O	1.3992	3.05	0.0939	33.0
7	iPr_2O	1.3679	3.38	0.1230	34.1
8	PhBr	1.5597	5.40	0.1286	36.6
9	$CHCl_3$	1.4459	4.71	0.1456	39.1
10	*Tert*-pentanol	1.4050	5.80	0.1841	41.0
11	EtOAc	1.3723	5.99	0.1991	38.1
12	THF	1.4050	7.43	0.2086	37.4
13	CH_2Cl_2	1.4242	8.93	0.2171	40.7
14	1-Octanol	1.4295	9.86	0.2225	48.1
15	1-Butanol	1.3993	17.3	0.2630	49.7
16	DMSO	1.4790	46.8	0.2632	45.1
17	DMF	1.4305	37.2	0.2746	43.2
18	2-Propanol	1.3776	19.3	0.2749	48.4
19	Acetone	1.3588	20.5	0.2839	42.2
20	EtOH	1.3611	24.9	0.2893	51.9
21	CH_3CN	1.3442	35.7	0.3044	45.6
22	MeOH	1.3288	32.6	0.3084	55.4
23	Water	1.3328	78.4	0.3200	63.1

[a] refractive index and dielectric constant are from Ref. 3.
[b] Δf is Lippert orientation polarizability function, $\Delta f = (\varepsilon-1)/(2\varepsilon+1) - (n^2-1)/(2n^2+1)$, where ε is dielectric constant, n is refractive index.
[c] E_T30 values are from Ref. 4.

References

1. E. L. Lippert, 'Organic molecular photophysics', Wiley-Interscience, 1975.

2. N. Mataga and T. Kubota, 'Molecular interactions and electronic spectra', M. Dekker, 1970.

3. J.-L. M. Abboud, R. Notatio. *Pure Appl. Chem.* 1999, **71**, 645.

4. C. Reichardt, *Chem. Rev.*, 1994, **94**, 2319.

RESUME DE LA THESE EN FRANÇAIS

NOUVELLES SONDES FLUORESCENTES MEMBRANAIRES POUR ETUDIER L'APOPTOSE ET L'ORDRE LIPIDIQUE

Résumé de la thèse en Français

INTRODUCTION. La fluorescence est un phénomène photophysique qui appartient à la luminescence, qui correspond à l'émission de la lumière par des atomes et des molécules dans un état électronique excité.

Quelques types de luminescence moléculaire peuvent être considérés comme dépendants de la nature de l'état excité. Si l'émission a lieu à partir d'un état excité singlet, le processus s'appelle fluorescence (10^8-10^9 s^{-1}). La fluorescence a lieu avec un nombre limité de molécules (généralement les hydrocarbures polyaromatiques ou hétérocycliques) dites fluorophores ou sondes fluorescentes (Fig. 1). A l'exception de 3 étapes de processus de fluorescence (excitation, relaxation non-radiative et émission de fluorescence), l'influence du solvant peut modifier l'émission d'un fluorophore. Cet effet du solvant déplace l'émission vers de bas niveaux d'énergie permettant une stabilisation de l'état excité par les molécules du solvant.

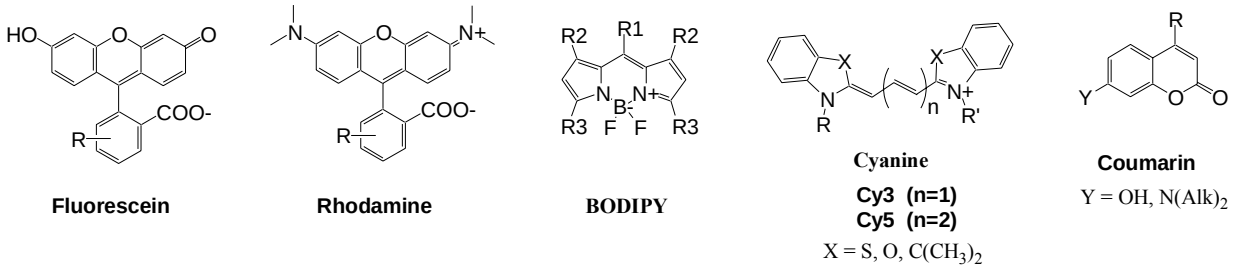

Figure 1. Les molécules fluorescentes synthétiques les plus communes.

Généralement, le fluorophore montre un transfert de charge photoinduit (PCT), et le dipôle du solvant réoriente autour de la molécule excitée, ce qui diminue l'énergie de l'état excité, induisant le processus de relaxation du solvant. Cet effet devient plus grand en augmentant la polarité du solvant, résultant par l'émission à basses énergies (ou longueurs d'ondes plus grandes). Le déplacement de la bande d'émission en réponse aux changements de la polarité de solvant est dit *solvatochromisme de fluorescence*.

Les fluorophores ayant une transition de dipôle élevée à partir de l'état fondamental vers l'état excité, montrent un grand solvatochromisme de fluorescence. Ils sont dits des sondes solvatochromiques ou des probes environnement-sensitive (Fig. 2a-b). Des molécules apolaires comme les hydrocarbones aromatiques non substitués ou les molécules symétriques comme fluorescéine, rhodamine et les cyanines sont moins sensibles à l'environnement.

A noter que des interactions solvant-fluorophore spécifiques, comme les liaisons hydrogènes, produisent de grands changements dans les pics d'émission. Ainsi, le

solvatochromisme de fluorescence reflète généralement des interactions universelles et spécifiques qui s'établissent entre la molécule émettrice et son microenvironnement.

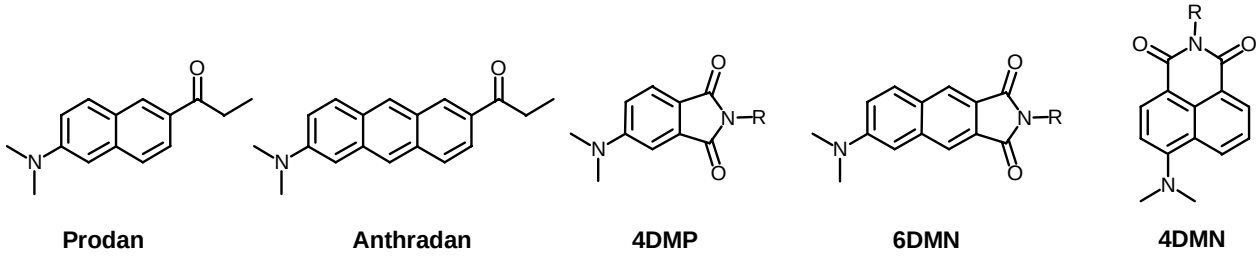

Figure 2a. Prodan, son analogue Anthradan, phthalimide et naphthymide dérivée.

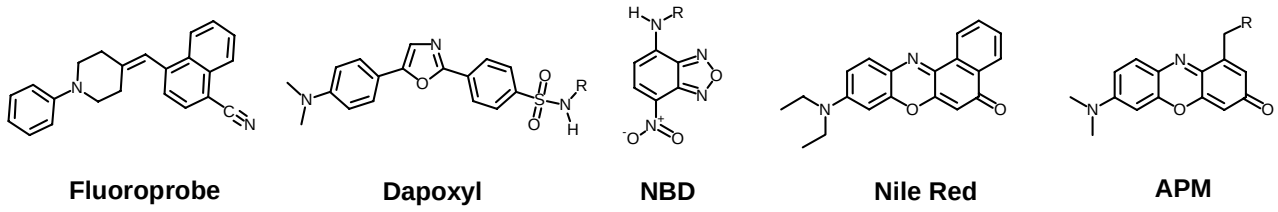

Figure 2b. Sondes solvatochromiques fluorescentes avancées

ACTUALITE. Les sondes fluorescentes sont d'une importance majeure en imagerie cellulaire, pour suivre les processus biologiques tant au niveau cellulaire que moléculaire. Malgré les progrès réalisés, l'étude de l'organisation lipidique des biomembranes à l'aide de sondes fluorescentes reste problématique. Un intérêt grandissant se porte vers la conception de sondes membranaires construites à partir de colorants fluorescents sensibles à l'environnement, permettant ainsi de suivre les modifications de leur microenvironnement par la variation de leur spectre d'émission.

Bien qu'une grande variété des probes est disponible pour visualiser les membranes biologiques, juste une petite partie peut être utilisée pour des mesures quantitatives des paramètres liés aux membranes. Le manque des outils simples est l'obstacle majeur pour des investigations membranaires supplémentaires. Le but de ce travail était de développer de nouvelles sondes membranaires fluorescentes permettant une visualisation effective et une mesure analytique de l'organisation lipidique dans les systèmes modèles et les cellules vivantes.

RESULTATS. Notre laboratoire est fortement impliqué dans le développement de sondes membranaires de la famille des 3-hydroxychromones. Ces fluorophores sont caractérisés par un spectre d'émission à deux couleurs, suite à un transfert de proton intramoléculaire à l'état excité (ESIPT) fortement dépendant de l'environnement. Ainsi, notre laboratoire a introduit la première

sonde membranaire fluorescente à émission duale (F2N12S) capable de détecter l'apoptose (mort cellulaire programmée) par le suivi de la modification de la composition lipidique membranaire [Brevet WO2007057782]. Cette sonde moléculaire, qui s'insère spontanément dans le feuillet externe de la membrane plasmique cellulaire, détecte la perte de l'asymétrie membranaire consécutive à l'apoptose.

Le but du présent travail a consisté à poursuivre le développement d'outils moléculaires fluorescents de cette famille pour étudier les propriétés physicochimiques des membranes biologiques (phase lipidique, charge de surface, polarité, hydratation, etc..) et corréler ces propriétés au phénomène d'apoptose et à l'ordre lipidique des membranes. Plus précisément, ce travail a été focalisé sur la conception de nouvelles sondes fluorescentes pour détecter l'apoptose de performances supérieures à la sonde initiale F2N12S. Dans ce but, nous nous sommes fixés les tâches suivantes: **(I)** élucider le mécanisme de la réponse de F2N12S à l'apoptose; **(II)** déterminer la structure optimale basée soit sur la 3-hydroxychromone, soit sur d'autres fluorophores sensibles à l'environnement, et (**III**) développer de nouveaux fluorophores originaux pour des sondes membranaires.

En premier lieu, nous avons entrepris des études systématiques sur la réponse de F2N12S dans différents types de membranes modèles et cellulaires. Nous avons mis en évidence que le degré d'hydratation et l'état de phase sont des facteurs importants de la réponse de la sonde à l'apoptose. Ainsi, nous avons montré que l'apoptose augmente le degré d'hydratation du feuillet externe de la membrane plasmique cellulaire, ce qui suggère la disparition de la phase liquide ordonnée (riche en sphingomyéline et cholestérol) de ce feuillet. Ce point a été confirmé par l'extraction du cholestérol du feuillet externe à l'aide de la méthyl-ß-cyclodextrine, induisant des changements similaires à ceux induit par l'apoptose, du spectre de fluorescence et des images ratiométriques de fluorescence (Publication 1). Ces résultats nous ont indiqué une nouvelle direction à suivre pour la conception de sondes sensibles à l'apoptose, par l'utilisation de fluorophores répondant au degré d'hydratation et à l'état de phase de la membrane.

Dans un deuxième temps, nous avons synthétisé plusieurs sondes originales de la famille des 3-hydroxyflavones (Fig. 3). Ainsi, nous avons synthétisé des sondes se positionnant soit parallèlement, soit perpendiculairement à la surface membranaire. Selon les études spectroscopiques menées sur des vésicules lipidiques, les colorants se localisant en surface ne présentent pratiquement aucune sensibilité à l'état de phase lipidique, alors que leur sensibilité à la charge de surface est trois fois supérieure à celle observée avec F2N12S (Fig. 4). En outre, des études sur cellules ne révèlent aucune réponse à l'apoptose pour ce type de sondes, suggérant que F2N12S répond à l'apoptose principalement suite au changement d'état de phase de la membrane.

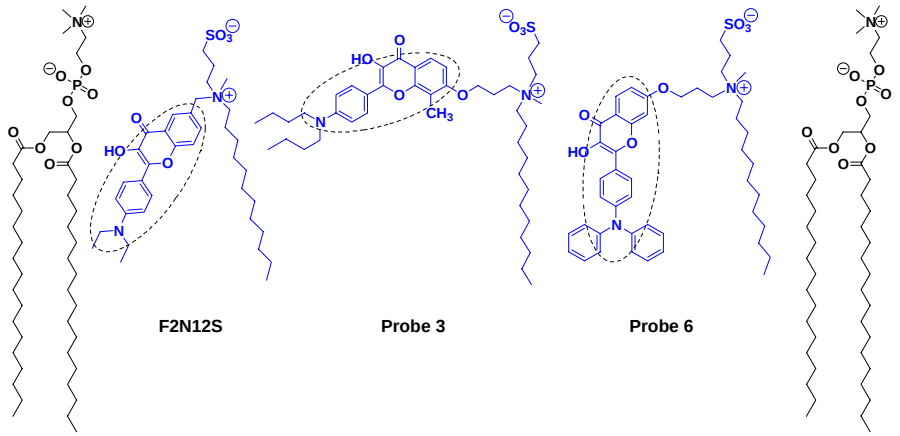

Figure 3. Localisation hypothétique des sondes 3HF dans les lipides membranaires (un seul feuillet est montré). Les lignes pointillées montrent la position du fluorophore (incliné, horizontal et vertical).

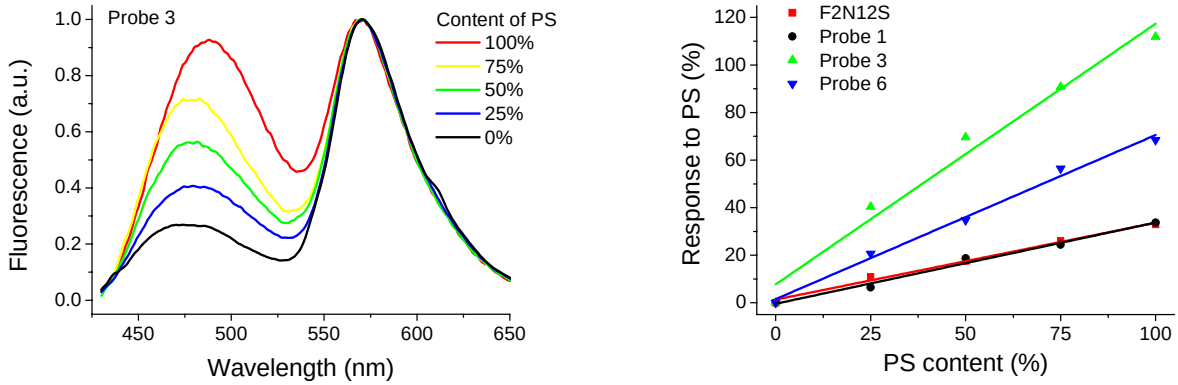

Figure 4. Réponse de quelques sondes 3HF à la composition en DOPS des vésicules DOPC. La concentration en sonde était 1 µM, concentration lipidique 200 µM dans du tampon phosphate 20mM, pH 7.4. La réponse était calculée à la base de N*/T* valeur selon $2(a-b)/(a+b)\times 100\%$.

A l'inverse, les sondes adoptant une orientation verticale au sein de la bicouche, tout en voyant leur sensibilité à la charge de surface négative préservée, démontrent une sensibilité à l'état de phase significativement améliorée (Tableau 1). Des études sur cellules menées avec ces sondes à orientation verticale montrent une réponse à l'extraction du cholestérol et à l'apoptose deux fois supérieure à celle de F2N12S (Fig. 5-6). En outre, l'un des dérivés synthétisés (Probe **10**) présente une brillance trois fois supérieure comparée à F2N12S. Ces nouveaux dérivés apparaissent donc comme des sondes fluorescentes prometteuses pour la détection de l'apoptose et l'étude de l'ordre lipidique.

Tableau 1. Propriétés spectroscopiques des sondes 3HF verticales dans les modèles membranaies. [a)]

	Probe 7 F4O7NS		Probe 8 F6O7NS		Probe 9 F4O6NS		Probe 10 F6O6NS		Probe 11 [b)] F8O6NS	
T* band, nm	571		571		561		561		561	
Lipid vesicle	**N* band, nm**	**N*/T***	**N* band, nm**	**N*/T***	**N* band, nm**	**N*/T***	**N* band, nm**	**N*/T***	**N* band, nm**	**N*/T***
DOPS (Ld)	488	0.78	479	0.85	487	1.75	489	1.55	-	-
DOPC (Ld)	500	0.51	491	0.43	485	1.05	492	1.00	484	1.05
DOPC-Chol (2:1) (Ld)	496	0.32	482	0.27	477	0.78	479	0.72	475	0.76
DOPC-Chol-Sm (1:1:1) (Ld+Lo)	493	0.34	484	0.29	477	0.83	480	0.75	476	0.84
Sm-Chol (2:1) (Lo)	480	0.25	482	0.31	470	0.67	463	0.56	462	0.72

[a)]Concentration de sonde était 1 µM, concentration lipidique 200 µM dans du tampon phosphate 10mM, pH 7.0. Le temps d'incubation était 5 min à 20°C. [b)] Le temps d'incubation était 30 min à 20°C

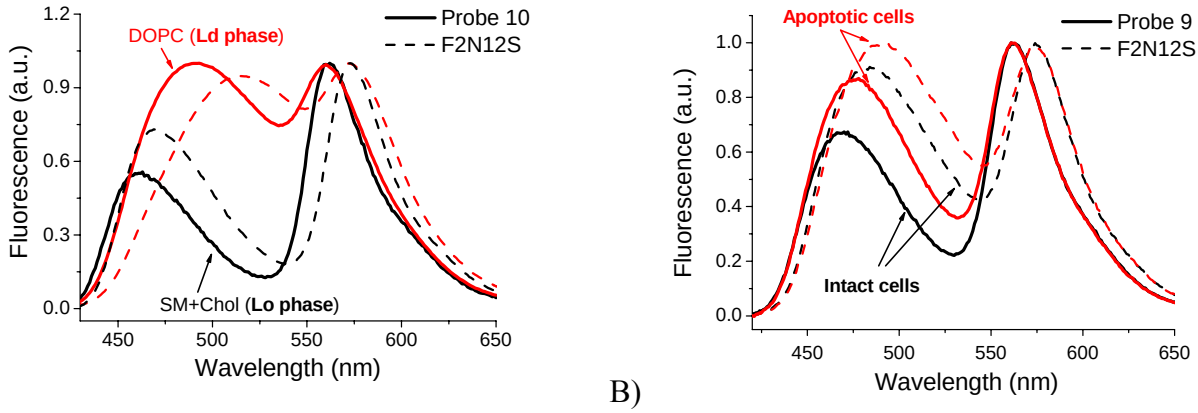

A) B)

Figure 5. Comparaison des propriétés d'émission des sondes 3HF verticales (ligne continue) et F2N12S parental (ligne pointillée) dans des modèles (A) et membranes cellulaires(B).

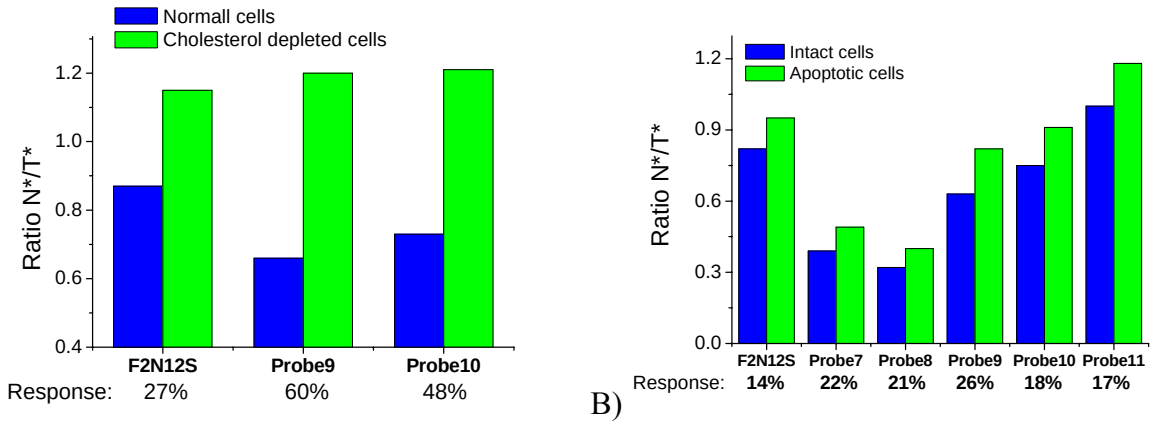

A) B)

Figure 6. Sensibilité des sondes 3HF verticales à la composition en cholestérol dans la membrane plasmique et leur réponse à l'apoptose. Le cholestérol était extrait avec 5 mM methyl-β-cyclodextrin pour 2 h à 37°C. La concentration de sonde était 0.1 µM. Le temps d'incubation 7 min à 20°C.

Puisque la réponse de ces sondes à l'apoptose apparaît liée aux modifications d'ordre lipidique de la membrane, nous avons décidé de remplacer le fluorophore 3-hydroxychromone par un colorant plus classique, le Rouge Nil, connu pour sa sensibilité à l'environnement et ses propriétés de fluorescence très favorables (rendement quantique élevé, spectre déplacé vers le rouge). Pour la sonde NR12S ainsi obtenue (Fig. 7), nous avons mis au point une méthode permettant d'évaluer son flip-flop entre les deux feuillets (Publication 2). Cette méthode est fondée sur une inhibition de fluorescence réversible, de type redox, induite au niveau du seul feuillet externe par le dithionite de sodium. Cette méthode montre que la sonde NR12S, contrairement au Rouge Nil, se lie exclusivement au feuillet externe d'une vésicule lipidique ou d'une membrane plasmique cellulaire, le flip-flop restant négligeable sur plusieurs heures. Par ailleurs, le maximum d'émission de NR12S incorporé dans des vésicules lipidiques montre un déplacement hypsochrome (*blue-shift*) significatif pour des vésicules en phase liquide-ordonnée (sphingomyéline-cholestérol) en comparaison avec des vésicules en phase liquide désordonnée (phospholipides insaturés). Ces deux phases ont donc pu être clairement différenciées par microscopie de fluorescence en imagerie ratiométrique sur des vésicules géantes marquées au NR12S (Fig. 7).

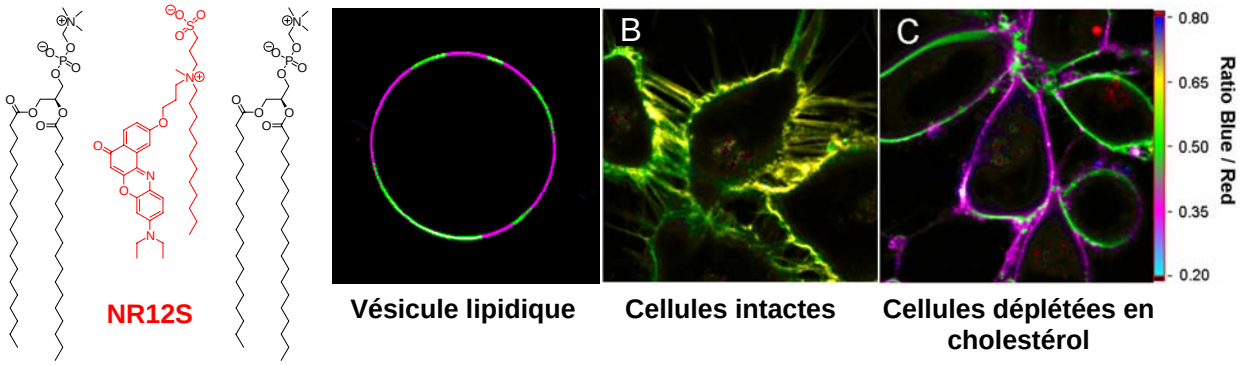

Figure 7. Structure et application de la sonde NR12S en imagerie ratiométique de vésicules géantes (A) et de cellules vivantes (B et C).

Lors du marquage de cellules vivantes, cette sonde se lie préférentiellement, sinon exclusivement, à la membrane plasmique et présente un spectre d'émission intermédiaire entre ceux observés pour des vésicules modèles en phase liquide ordonnée et liquide désordonnée. Il est important de remarquer que la "couleur" du spectre d'émission NR12S apparait corrélée avec le contenu en cholestérol des membranes étudiées, ce qui permet de suivre par fluorescence (en spectroscopie ou en microscopie) le processus de déplétion en cholestérol induit par la méthyl-β-cyclodextrine. En outre, NR12S montre lors de l'apoptose un déplacement de son spectre de fluorescence similaire à celui observé lors de la déplétion en cholestérol. Ces résultats obtenus avec NR12S confirment ceux obtenus avec F2N12S, suggérant que l'apoptose peut résulter en une perte de la phase liquide ordonnée du feuillet externe de la membrane plasmique cellulaire (Fig. 8-10).

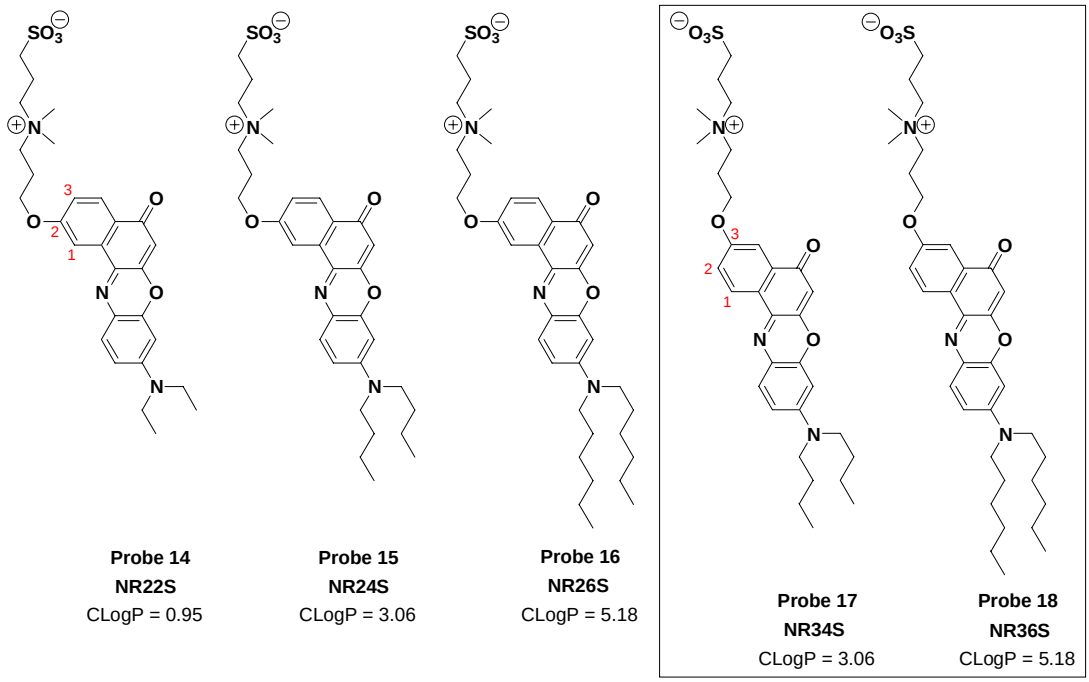

Figure 8. Structures chimiques des sondes NR verticales.

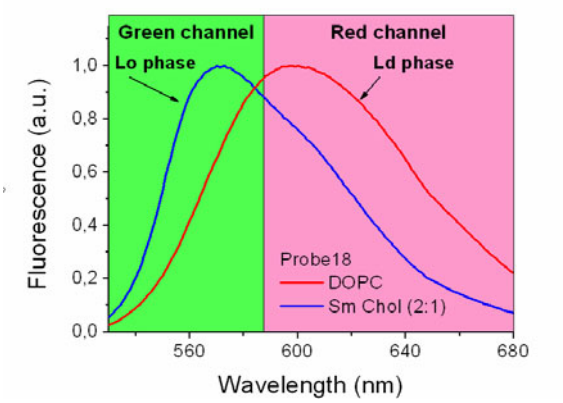

Probe	Ratio Green/Red		Response, %
	Lo phase	Ld phase	
NR12S	0.91	0.26	111
Probe **15**	0.54	0.23	80
Probe **16**	0.82	0.30	93
Probe **17**	0.98	0.28	111
Probe **18**	0.88	0.32	93

Figure 9. Approche ratiométrique pour l'imagerie multicouleur avec les sondes NR verticales et leurs sensibilités à l'ordre lipidique. Les canaux correspondent aux régions spectrales 530-585 nm (vert) et 585-700 nm (rouge). La réponse était calculée selon *2(a-b)/(a+b)×100%* à la base de la valeur Vert/Rouge.

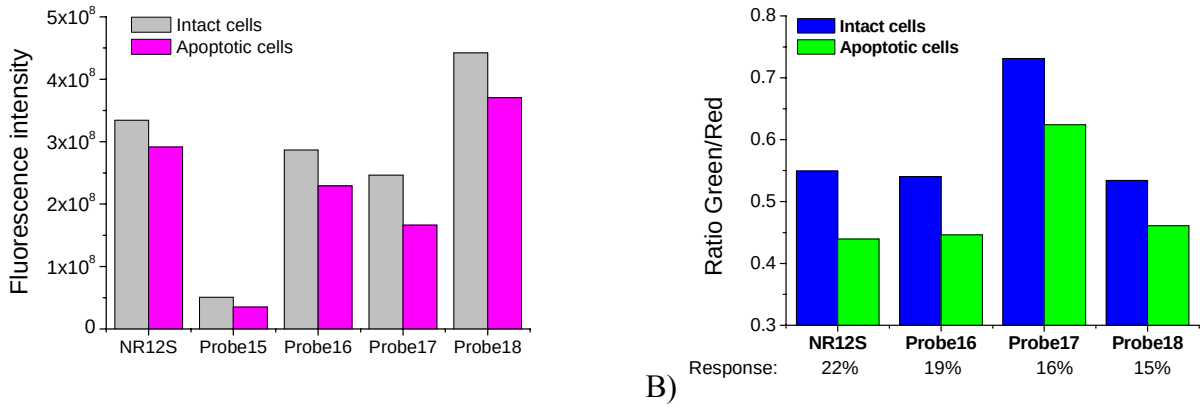

Figure 10. Intensités d'émission des sondes NR verticales dans membranes plasmiques (A) et leur réponse à l'apoptose (B).

En dernier lieu, notre recherche a porté sur le développement de fluorophores de sensibilité accrue à l'environnement. Dans ce but, nous avons considéré deux types de molécules. Les premières, basées sur un résidu fluorène avec de forts groupements électro-donneur et électro-accepteur, respectivement en positions 2 et 7, peuvent être considérées comme des analogues plus conjugués que la meilleure des sondes solvatochromiques actuelles, le Prodan (Fig. 11).

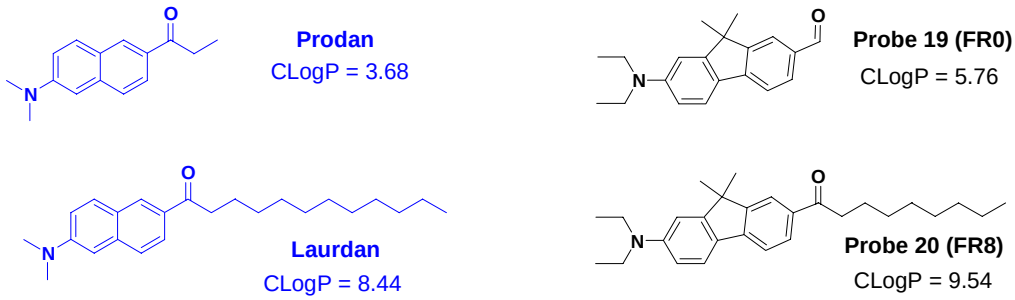

Figure 11. Les sondes **19** et **20** : sondes fluorescentes membranaires.

Ces sondes à base de fluorène montrent un déplacement bathochrome de leur spectre d'absorption (~ 400 nm), un coefficient d'absorption moléculaire presque doublé (43,000 $M^{-1}\times cm^{-1}$), et une section efficace en absorption biphotonique fortement augmentée (*ca* 400 GM) en comparaison avec le Prodan (Publication 3). De plus, une étude sur une gamme de solvants démontre un bien meilleur solvatochromisme de ces sondes, en accord avec leur important moment dipolaire (14 D). Ces sondes présentent en outre un rendement quantique élevé, ainsi qu'une photo-stabilité nettement supérieure à celle du Prodan. Ainsi, en substituant le noyau naphthalène du Prodan par un fluorène, nous avons obtenu de nouvelles sondes fluorescentes présentant d'excellentes propriétés spectroscopiques et solvatochromiques, pour lesquelles nous devrions trouver de nombreuses applications comme sondes sensibles à l'environnement.

La seconde classe de molécules est basée sur le résidu 3-methoxychromone (Fig. 12). Ces colorants sont caractérisés par des valeurs élevées du coefficient d'extinction molaire (30000 $M^{-1}\times cm^{-1}$), de la section efficace en absorption biphotonique (jusqu'à 450 GM) et du rendement quantique de fluorescence. Comparés aux dérivés de la 3-hydroxychromone, leur photostabilité est considérablement améliorée, confirmant par la même que la photodégradation des 3-hydroxychromones résulte d'une voie associée à la réaction ESIPT. Ces sondes démontrent un remarquable solvatochromisme de fluorescence, qui augmente avec le degré de leur conjugaison électronique. Ainsi, pour une 3-methoxychromone portant un groupe électro-donneur 2-fluorényl, la différence de moment dipolaire atteint 20D (Publication 4).

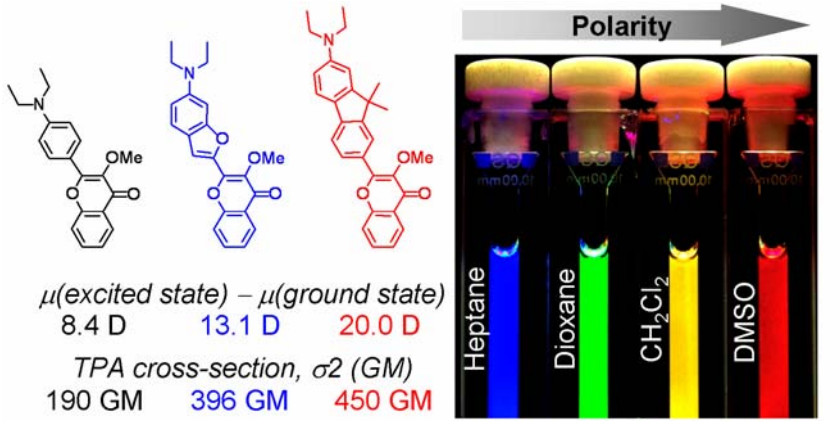

Figure 12. Solvatochromisme de fluorescence des 3-methoxychromones.

CONCLUSIONS. Nous avons synthétisé une large gamme de sondes fluorescentes membranaires, dont nous avons optimisé les propriétés par rapport aux sondes existantes. Nous avons utilisé ces sondes pour étudier par spectroscopie et imagerie de fluorescence, les caractéristiques biophysiques des vésicules lipidiques modèles et des membranes plasmiques cellulaires. Nous avons pu ainsi corréler la réponse de ces sondes avec leur localisation et leur orientation dans la membrane. Ceci nous a permis de déterminer qu'un senseur « idéal » des propriétés physico-chimiques d'une membrane devait comprendre une longue chaîne alkyle, un groupe zwitterionique et un résidu fluorescent. Les études cellulaires menées avec ces nouvelles sondes ont clairement démontré une corrélation entre l'apoptose et l'organisation lipidique de la membrane plasmique. Ainsi, nous avons prouvé que durant le processus d'apoptose, le feuillet externe évoluait vers une phase désordonnée.

PERSPECTIVES. On expecte que les molecules synthétisées serviront pour de nombreuses applications dans le futur. La 1ère perspective est de faire des mesures quantitatives de l'apoptose par cytométrie de flux. Les sondes présentées peuvent être utilisées pour l'étude des ondulations membranaires dont l'origine est l'interaction actine myosine. C'est connu que ces interactions renforcent la membrane plasmique, et font partie de l'endocytose, exocytose et la libération des vésicules extracellulaires et la régulation de la tension entre membrane et cytosquelette. Les nouvelles sondes peuvent être utilisées dans l'étude des changements membranaires durant l'adaptation physiologique. Pour l'instant, quelques cellules animales n'ont pas la thermorégulation physiologique et doivent contrôler les propriétés membranaires en variant la composition membranaire.

En plus de l'apoptose, le traffic membranaire et la variation de la composition membranaire, des autres événements liés à la membrane peuvent être explorés avec nos probes (signal de traduction) et la connexion entre ces événements et les propriétés membranaires physiques peut être établie. Finalement, une application intéressante de ces sondes est de développer une approche pour l'imagerie in vivo des membranes cellulaires directement sur des animaux en utilisant la tomographie fluorescente.

La théorie proposée de conception des sondes membranaires peut être intéressante pour le développement de nouveaux senseurs pour les différentes propriétés physiques membranaires. Ainsi, la classe des fluorophores nouvellement décrite, basée en fluorène et 3-methoxychromone, les 2 présentent des propriétés spectroscopiques améliorées, peuvent être transformées en sondes membranaires avancées.

Généralement, ce travail doit stimuler la recherche sur les membranes biologiques et le développement de nouveaux outils moléculaires fluorescents pour l'imagerie membranaire.

APPENDIX

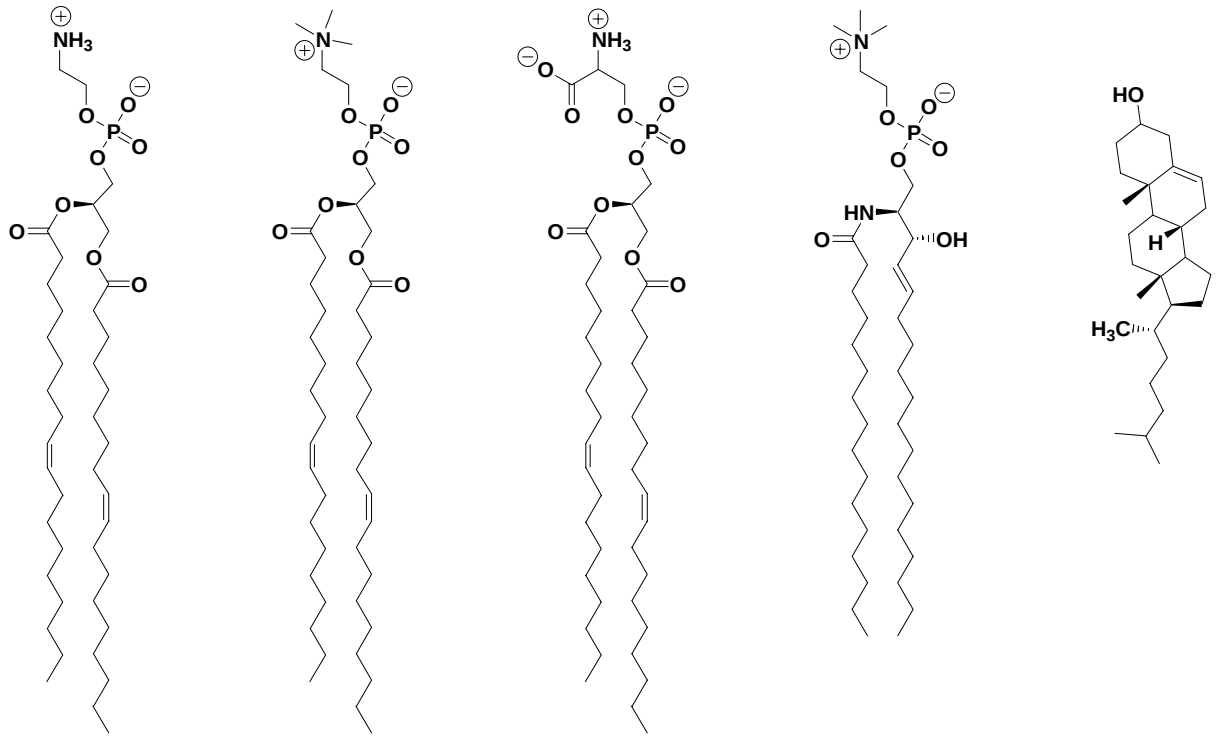

DOPE (0) CLogP = 9.78 | **DOPC (0)** CLogP = 5.15 | **DOPS (-1)** CLogP = 6.25 | **SM (0)** CLogP = 2.20 | **Chol (0)** CLogP = 9.52

Figure 7.1. Chemical structures of common membrame lipids and sterols, their charge and ClogP values (calculated using the software ChemDraw Ultra 6.0, Cambridgesoft Corporation).

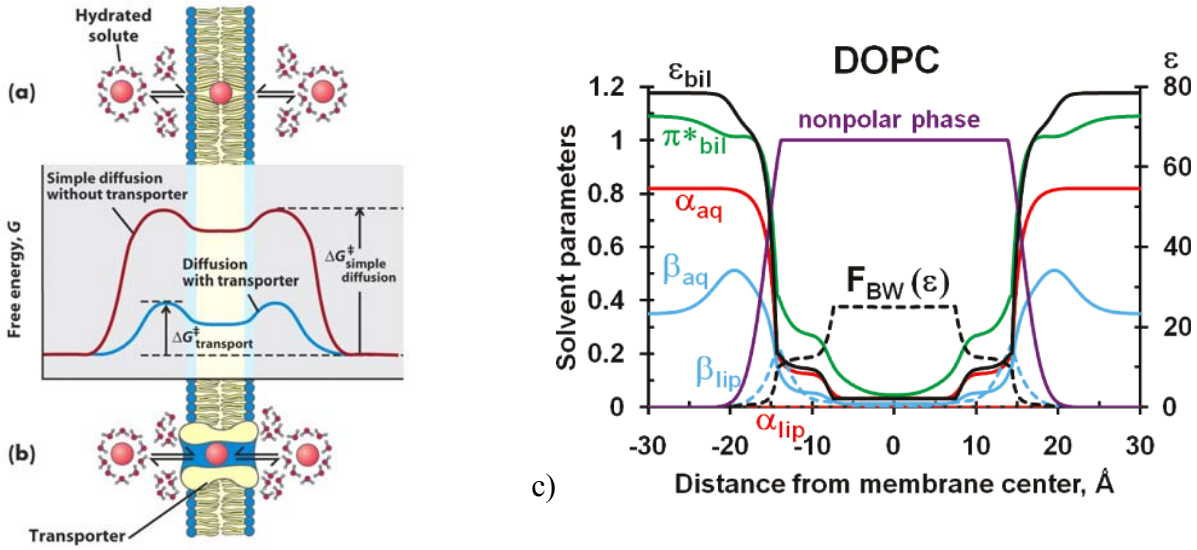

Figure 7.2. (a,b) Changes of free energy (ΔG) upon transmembrane diffusion (from Lehninger, Principles of Biochemistry, 3rd ed., 2000). (c) Profiles of hydrogen bonding donor (α_{aq} and α_{lip}) and acceptor (β_{aq} and β_{lip}) capacities, solvatochromic dipolarity parameter (π^*_{lip}), dielectric constant (ε_{bil}), Block-Walker dielectric function, $F_{BW}(\varepsilon)$, and volume fraction of nonpolar phase ($CH+CH_2+CH_3+CG$) calculated for DOPC bilayer (from Mosberg et al., J. Chem. Inf. Model. 2011)

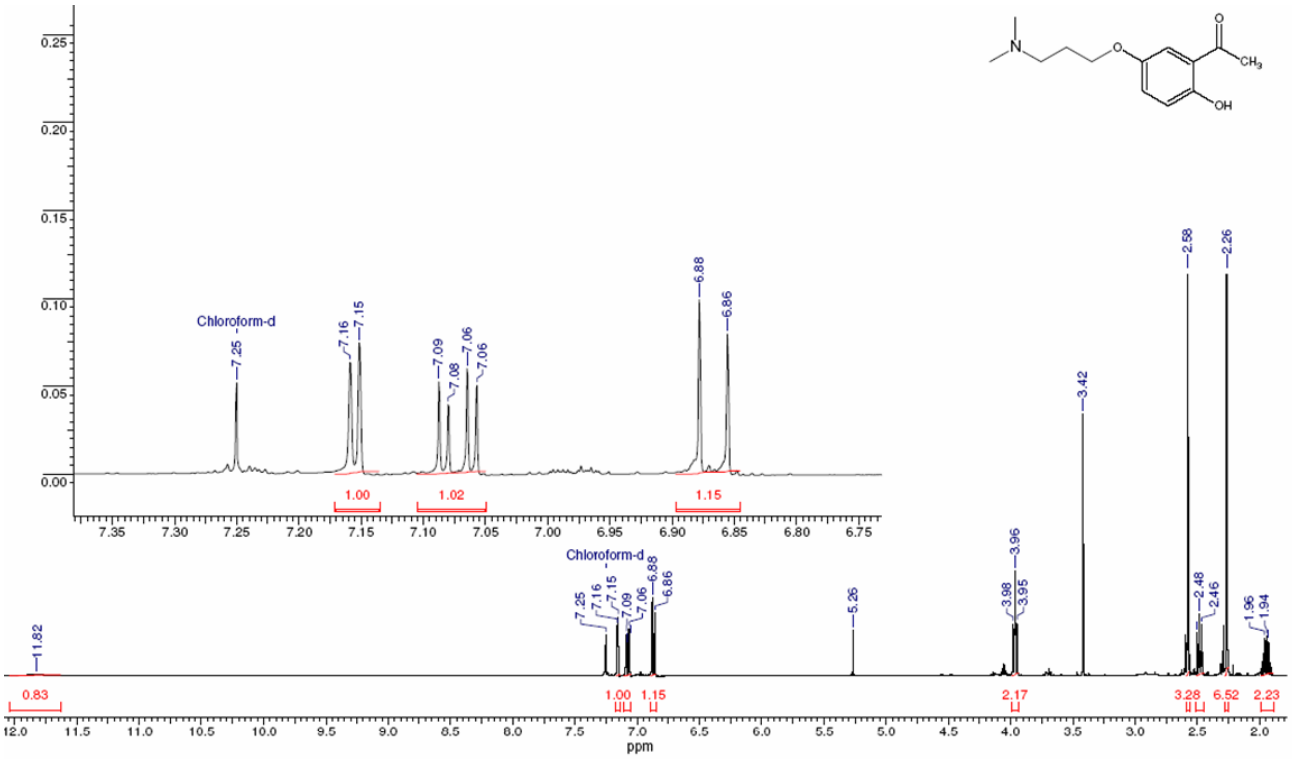

Figure 7.3. ^{1}H NMR spectrum of compound **3**.

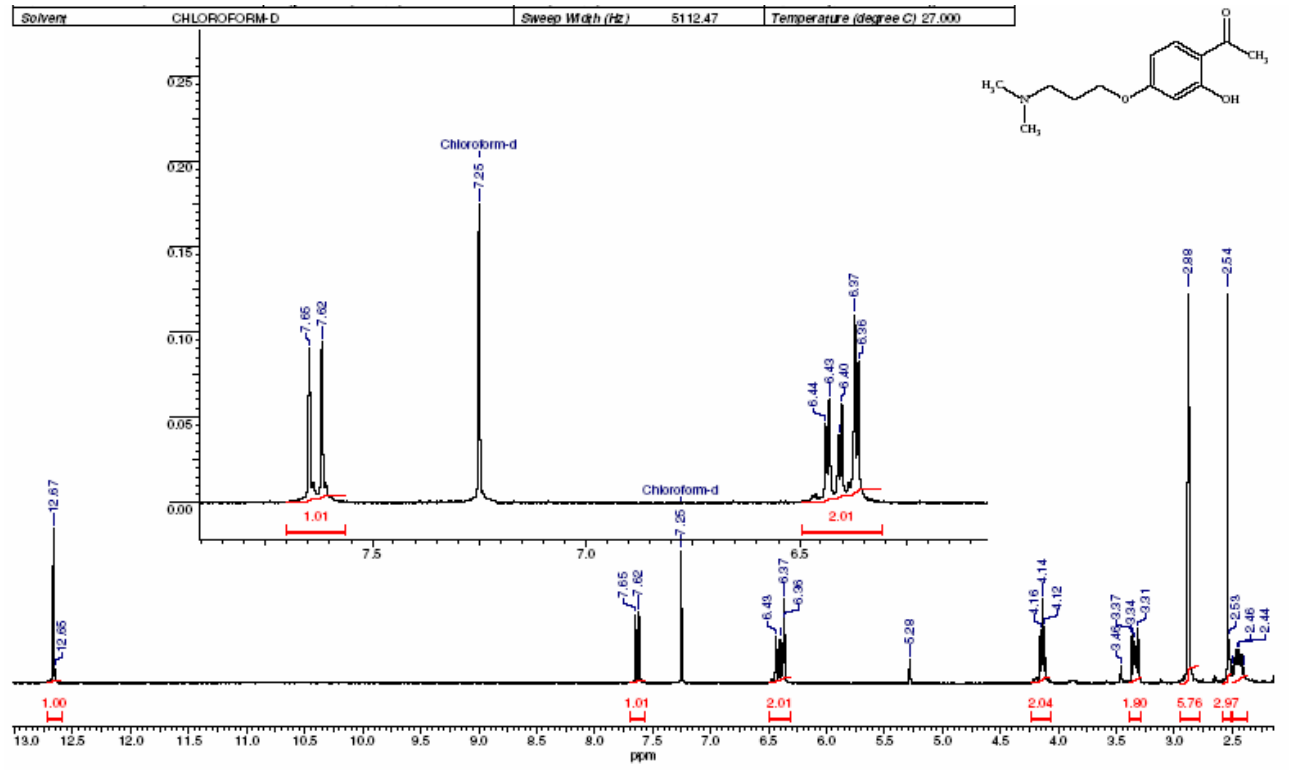

Figure 7.4. ^{1}H NMR spectrum of compound **6**.

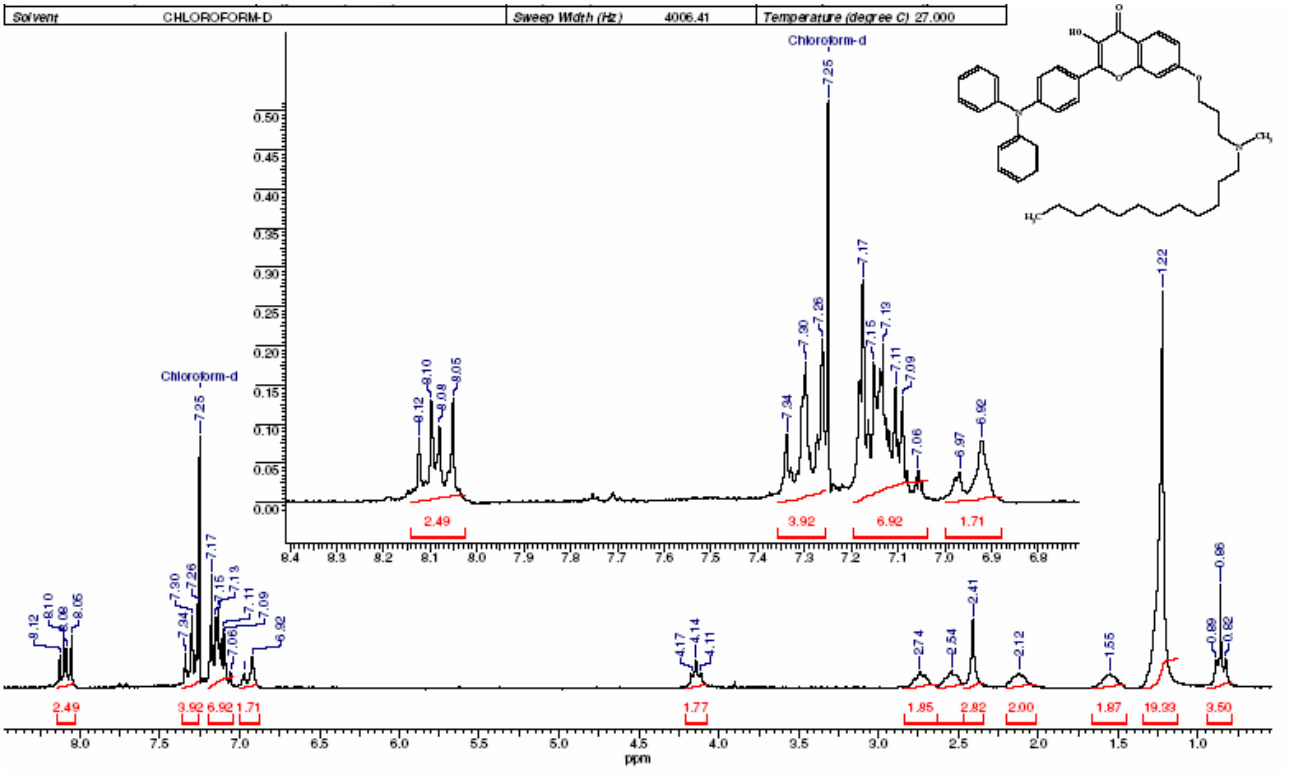

Figure 7.5. ^{1}H NMR spectrum of compound **13b**.

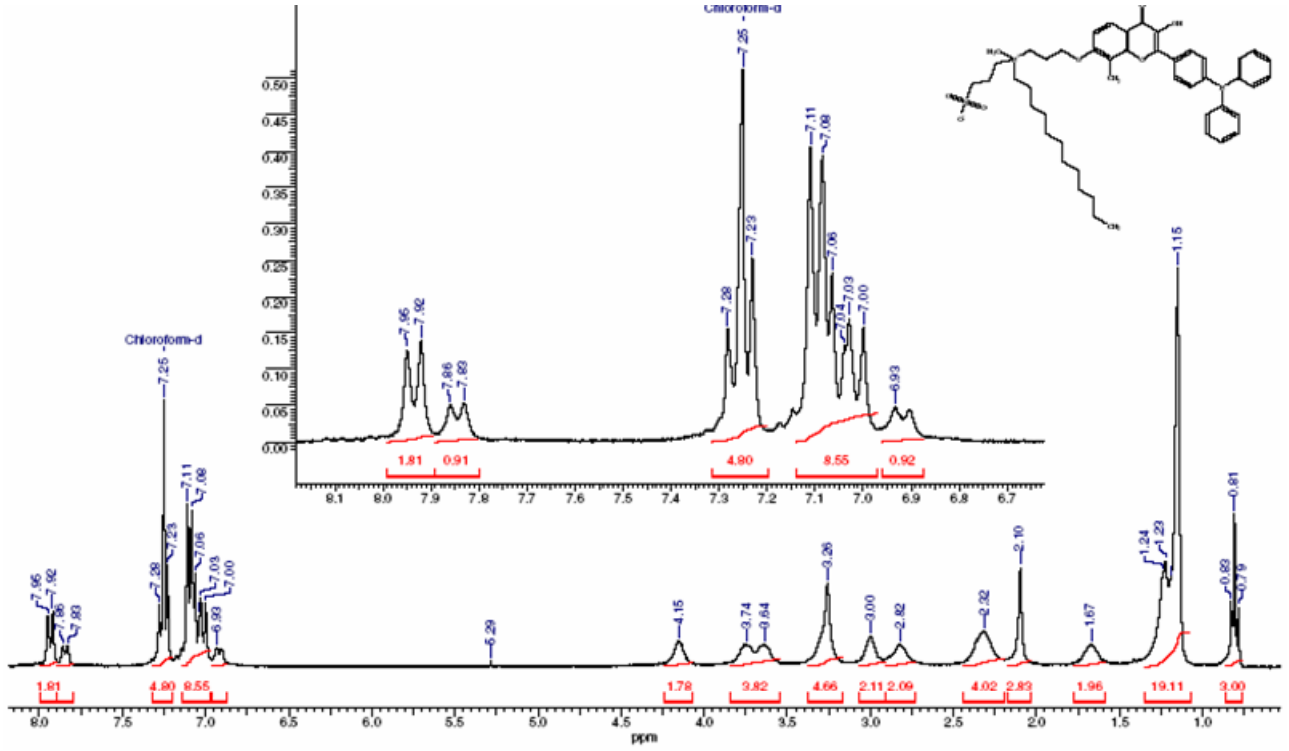

Figure 7.6. ^{1}H NMR spectrum of compound **14a** (Probe **5**).

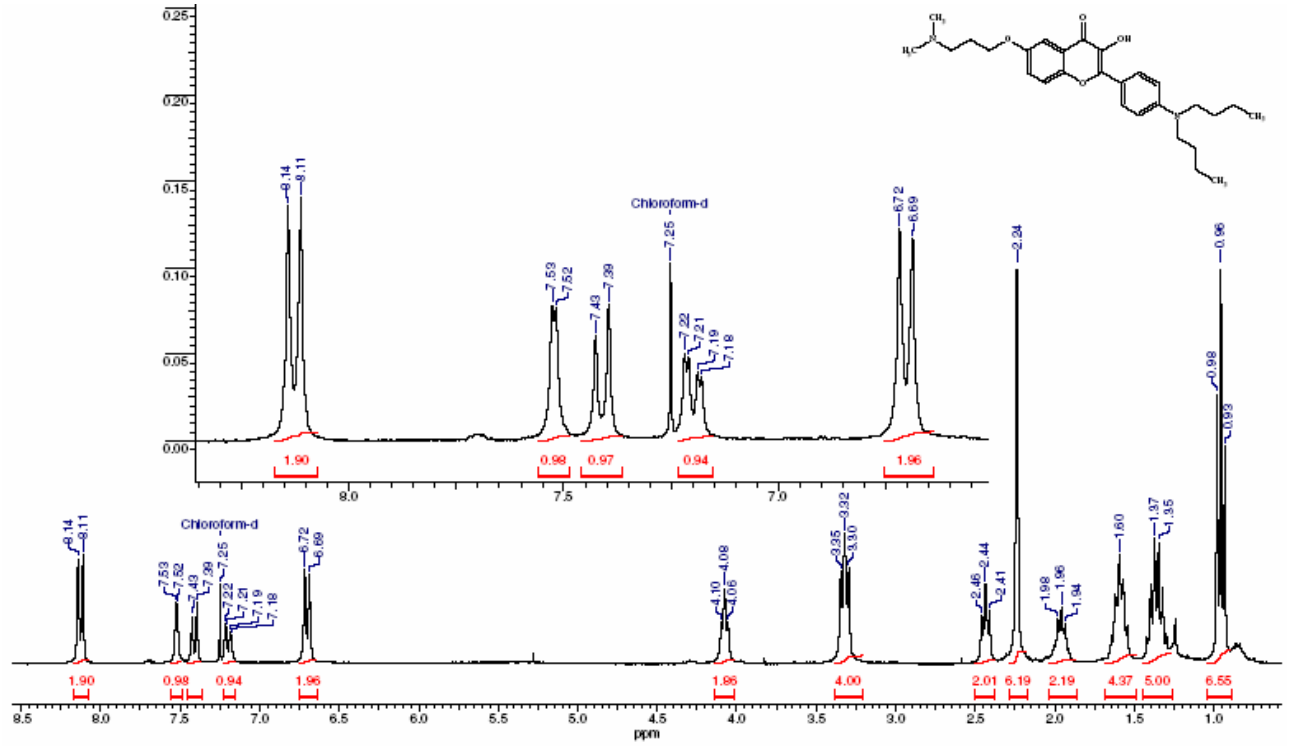

Figure 7.7. ^{1}H NMR spectrum of compound **17a**.

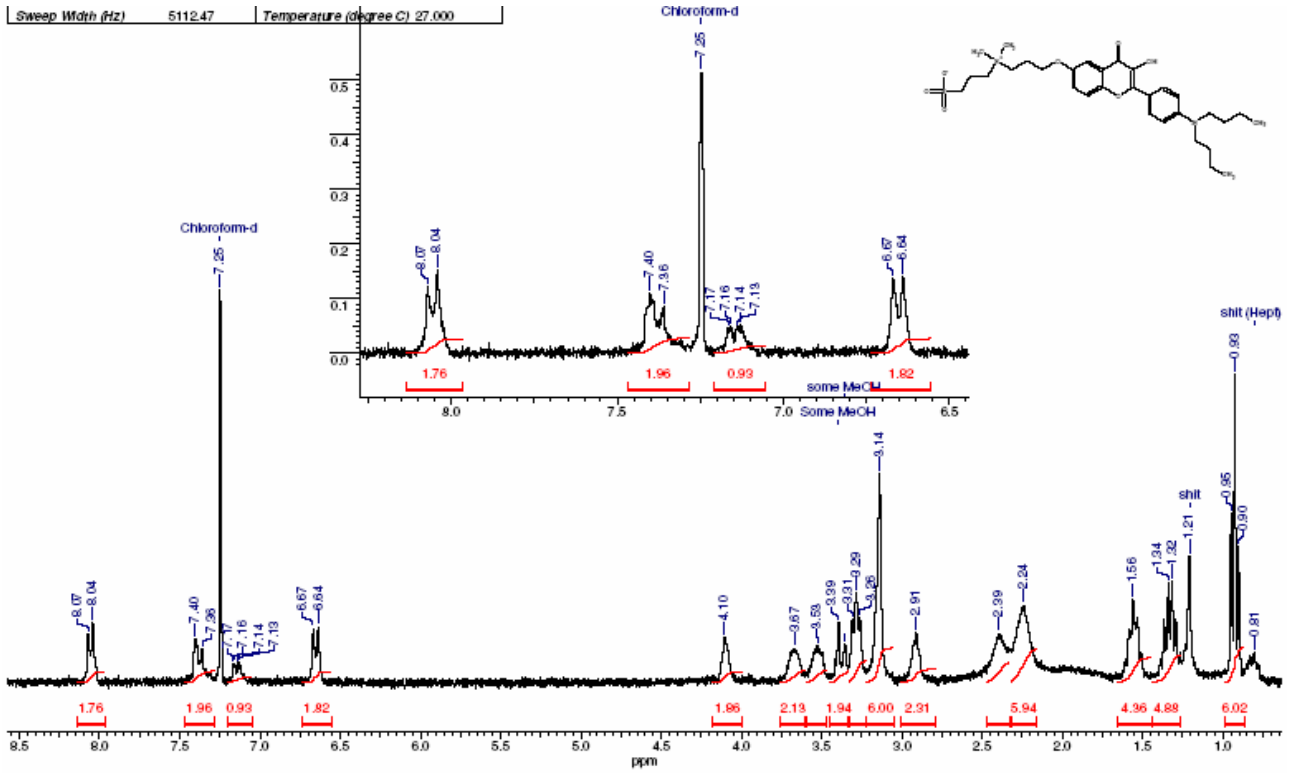

Figure 7.8. ^{1}H NMR spectrum of compound **18a** (Probe **9**).

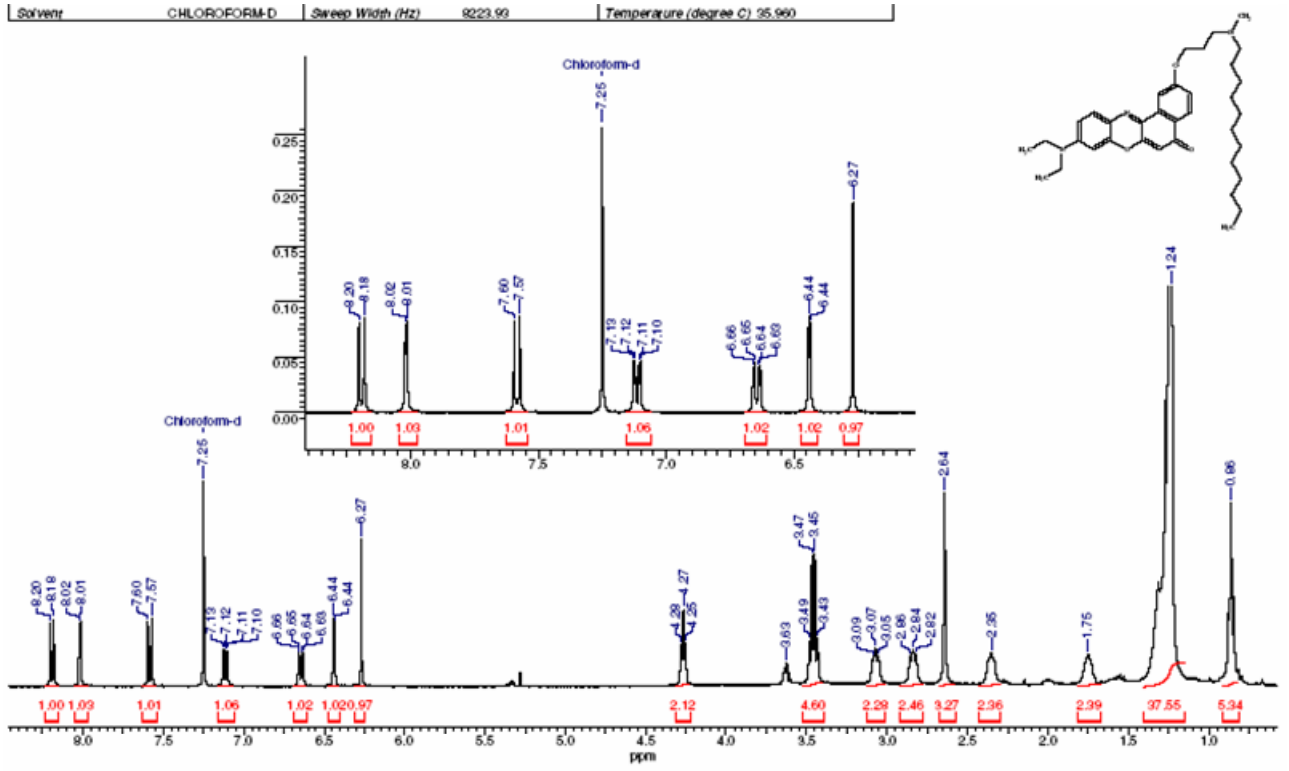

Figure 7.9. ^{1}H NMR spectrum of compound **20a**.

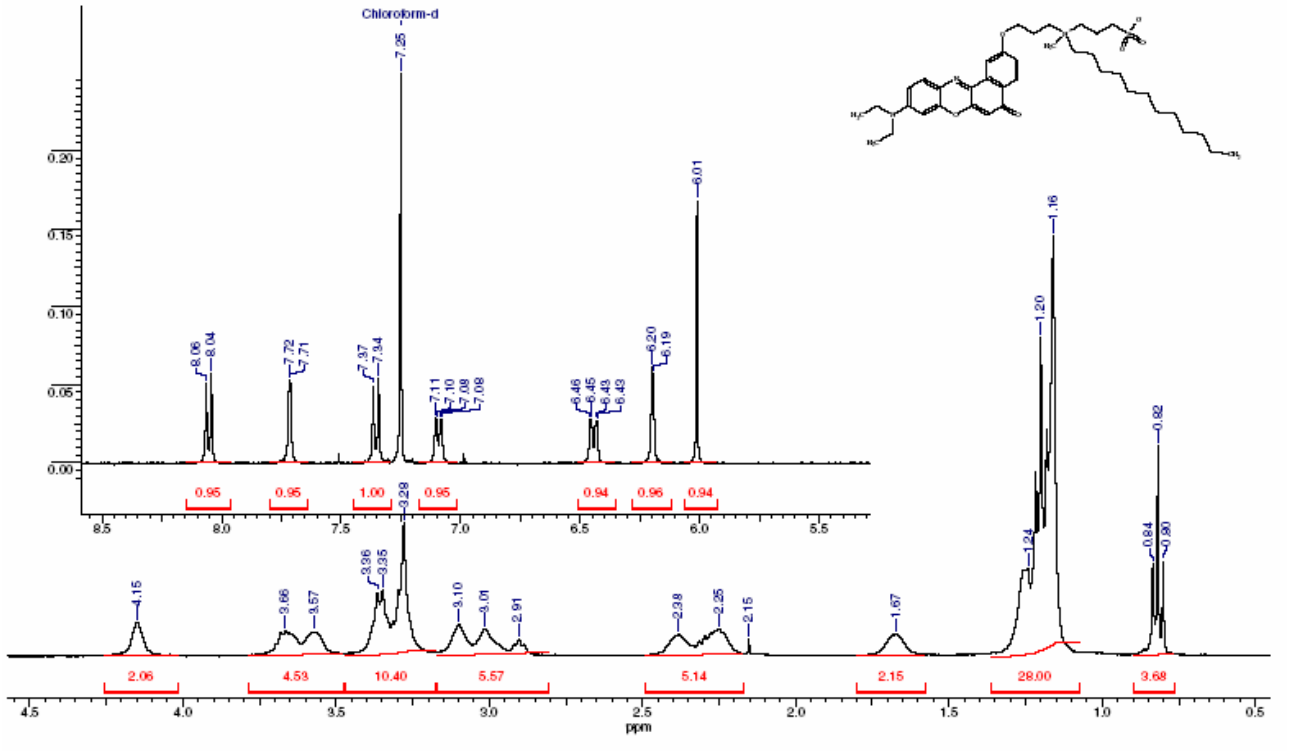

Figure 7.10. ^{1}H NMR spectrum of compound **21** (Probe **12**, NR12S).

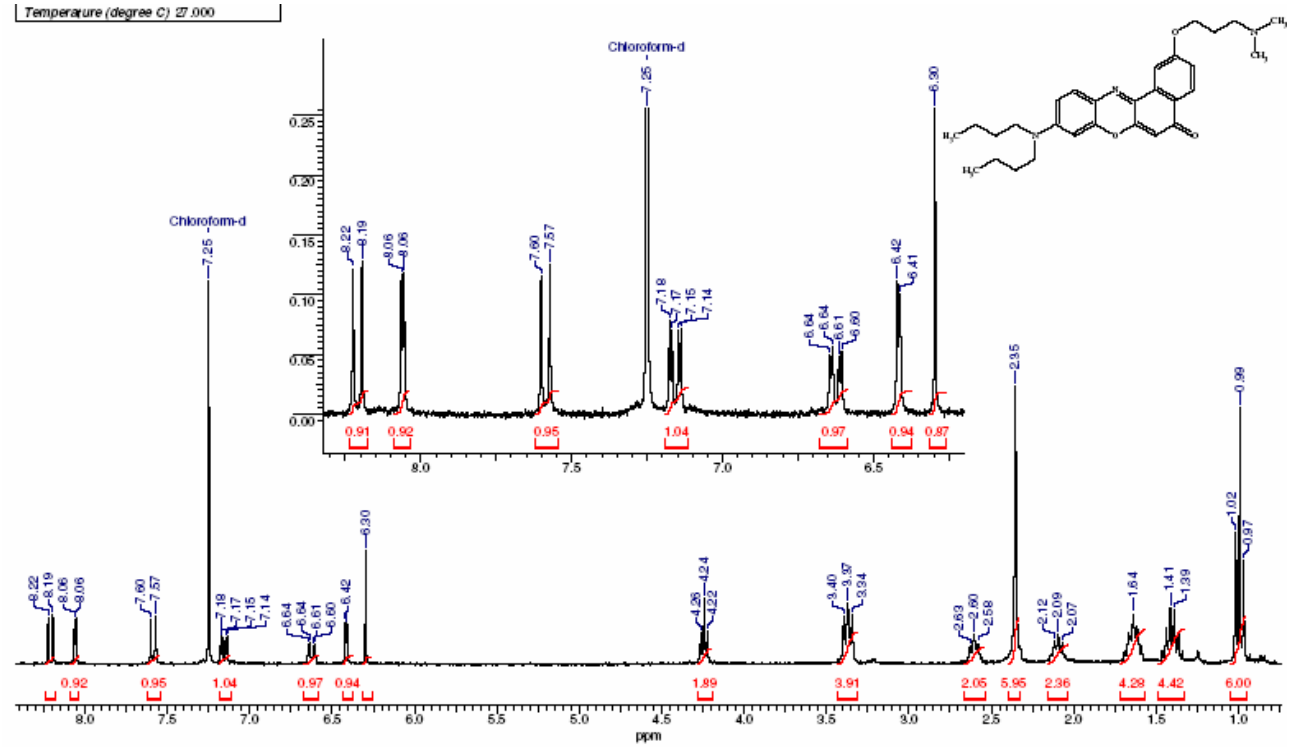

Figure 7.11. ^{1}H NMR spectrum of compound **31a**.

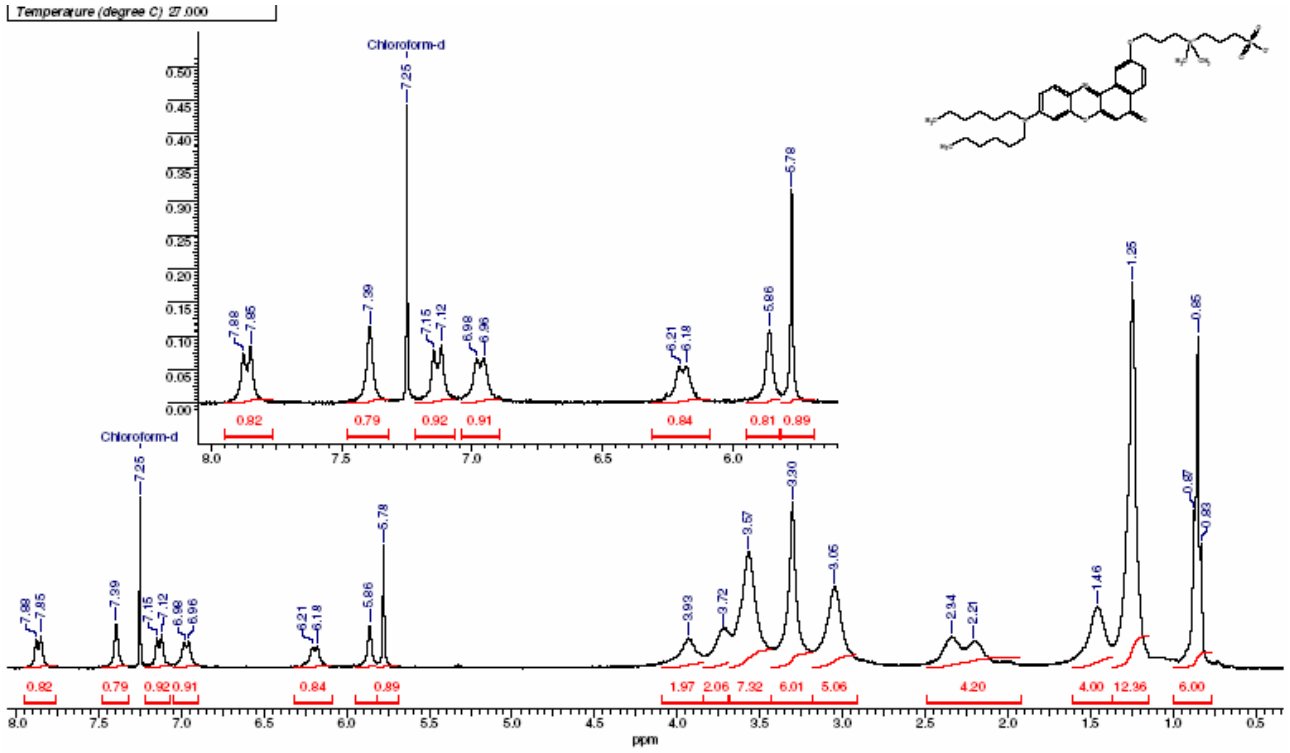

Figure 7.12. ^{1}H NMR spectrum of compound **32b** (Probe **16**).

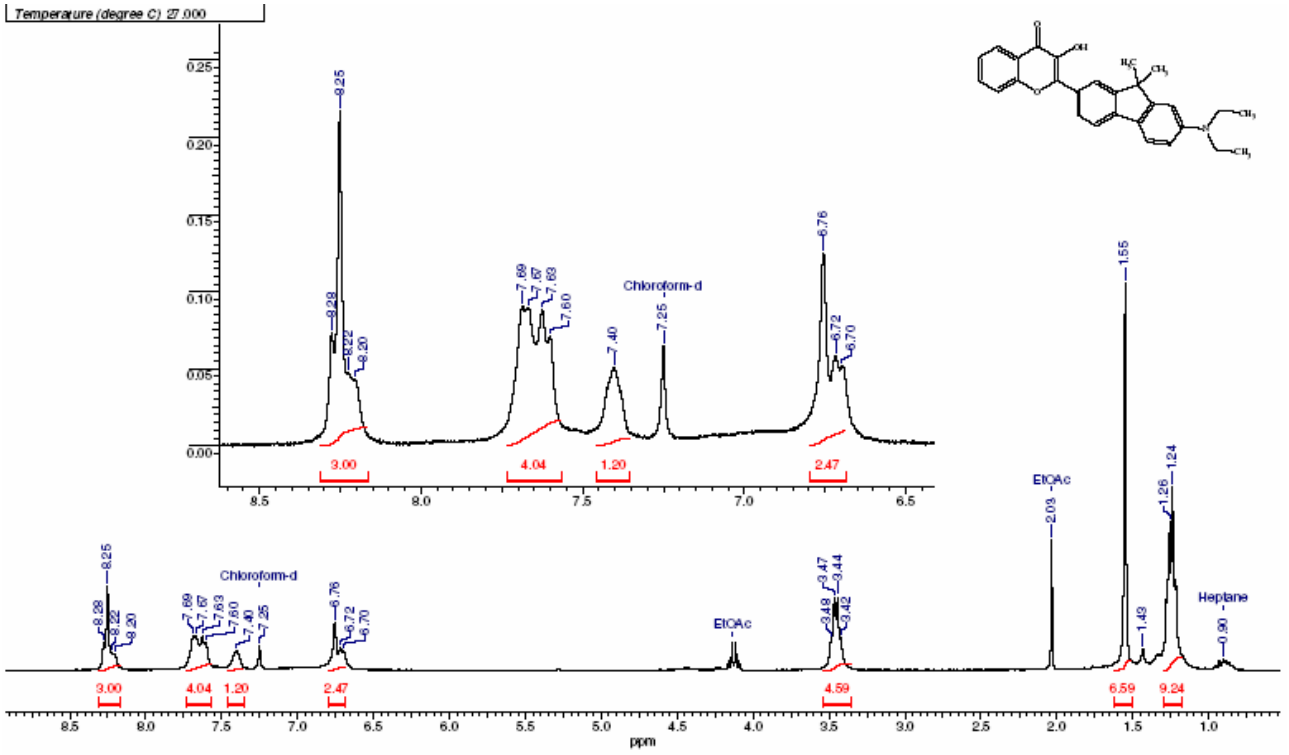

Figure 7.13. ^{1}H NMR spectrum of compound **43**.

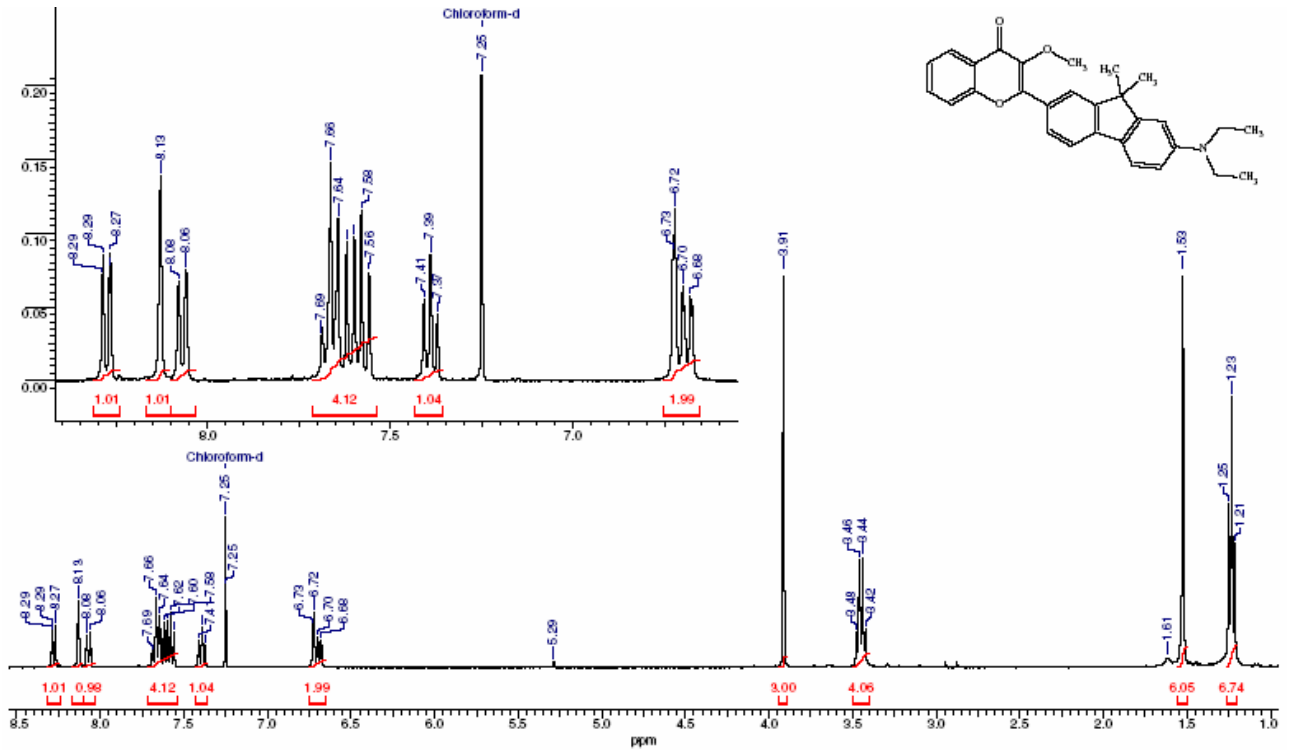

Figure 7.14. ^{1}H NMR spectrum of compound **44**.

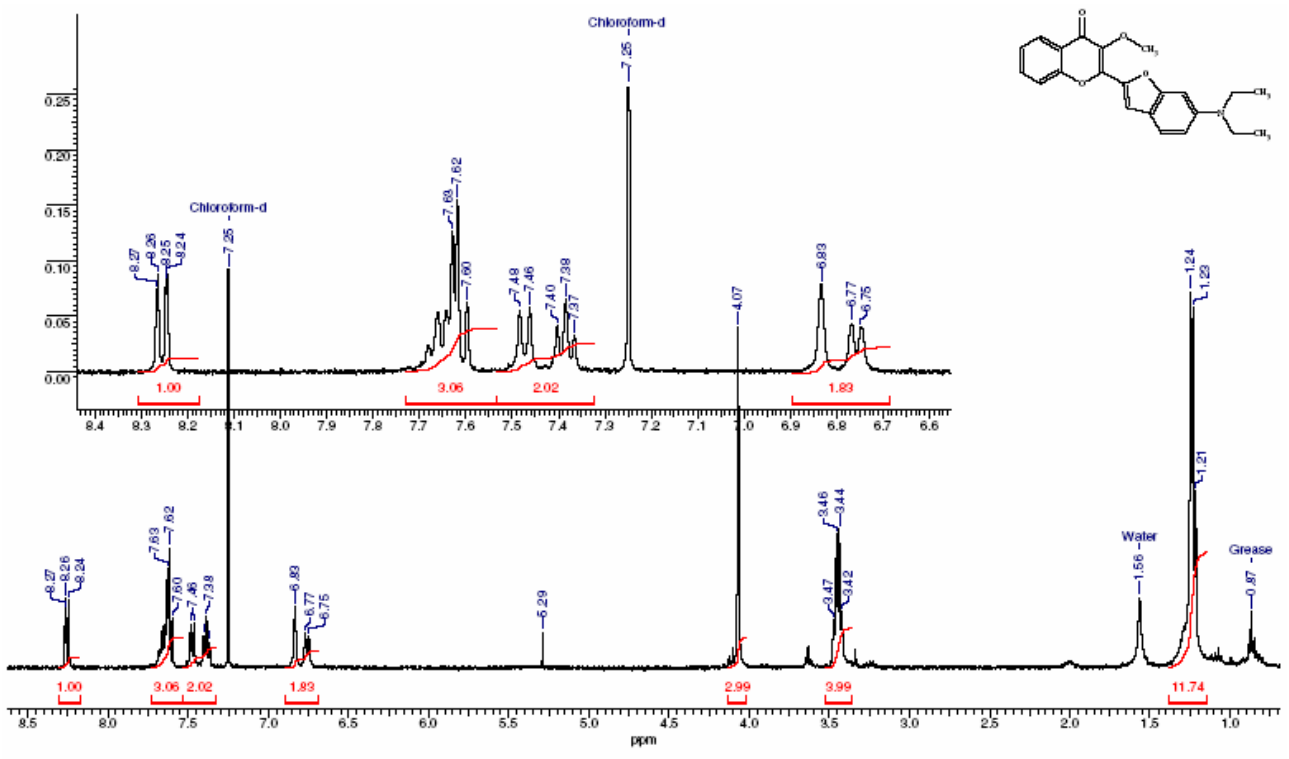

Figure 7.15. ^{1}H NMR spectrum of compound **45**.

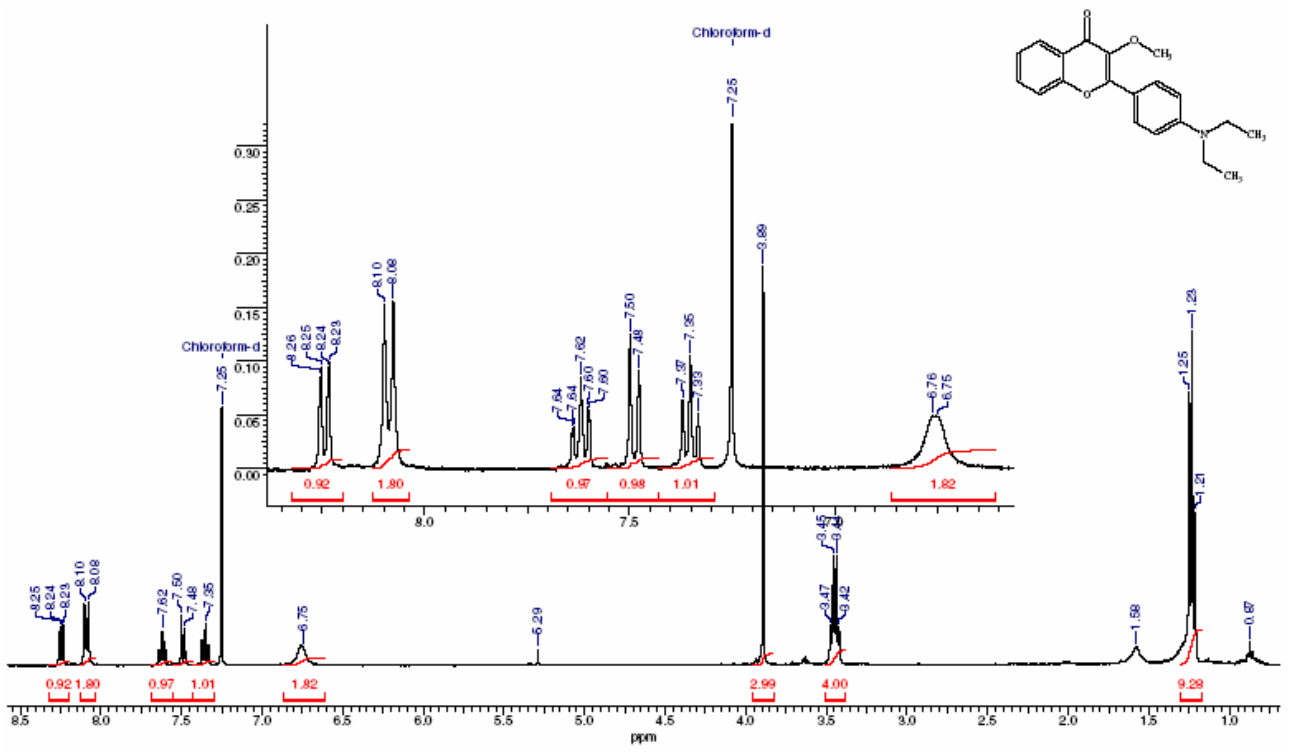

Figure 7.16. ^{1}H NMR spectrum of compound **46**.

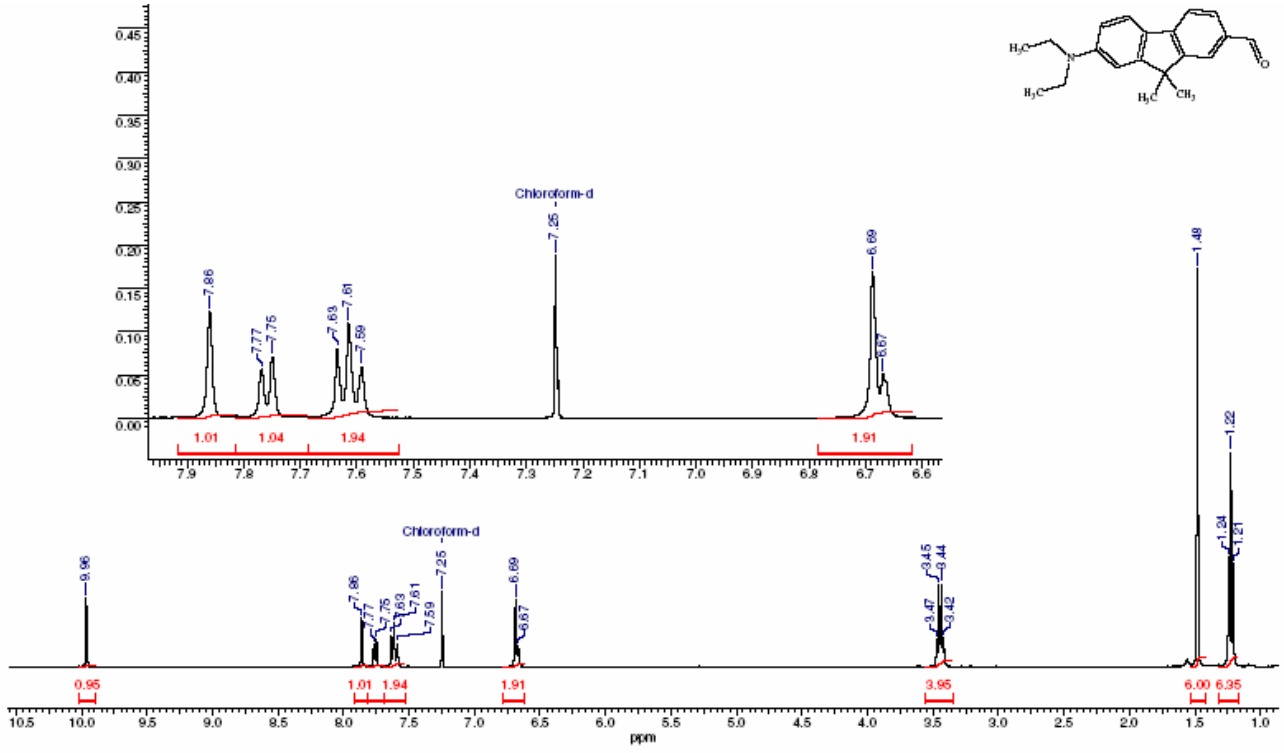

Figure 7.17. ^{1}H NMR spectrum of compound **40** (Probe **19**, FR0).

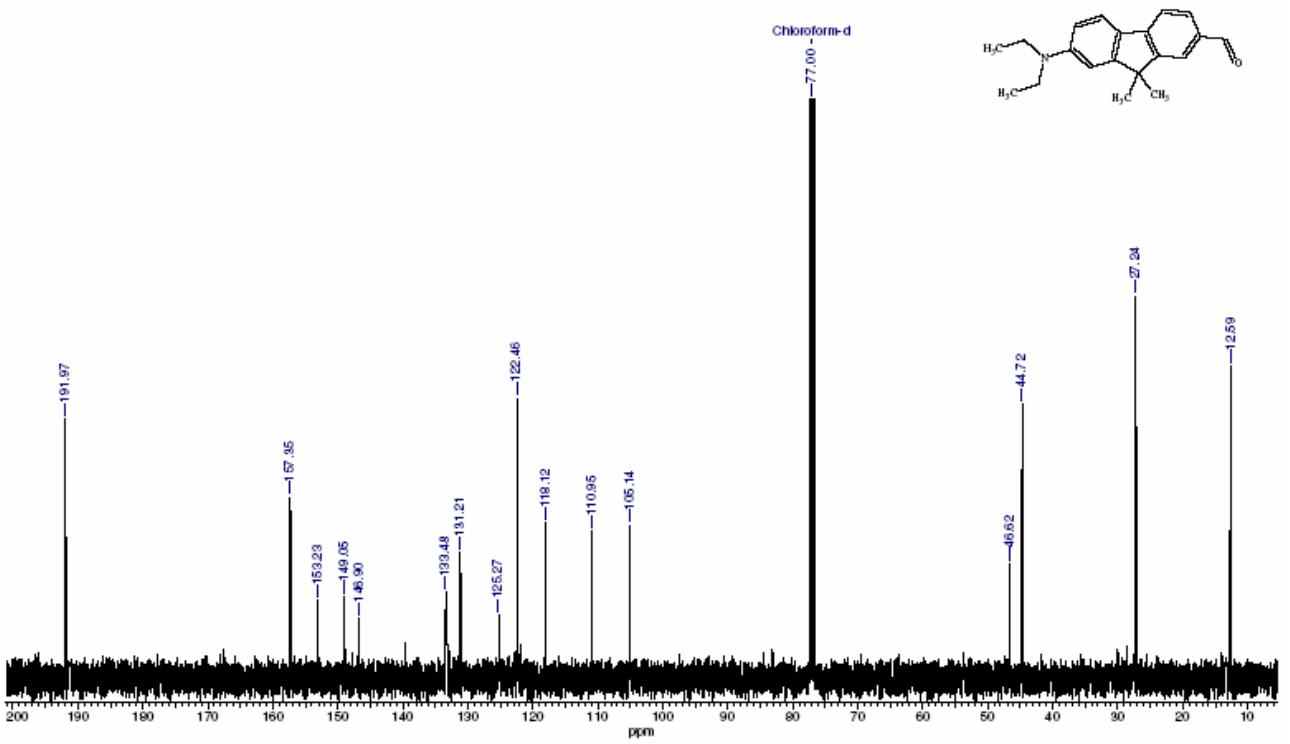

Figure 7.18. ^{13}C NMR spectrum of compound **40** (Probe **19**, FR0).

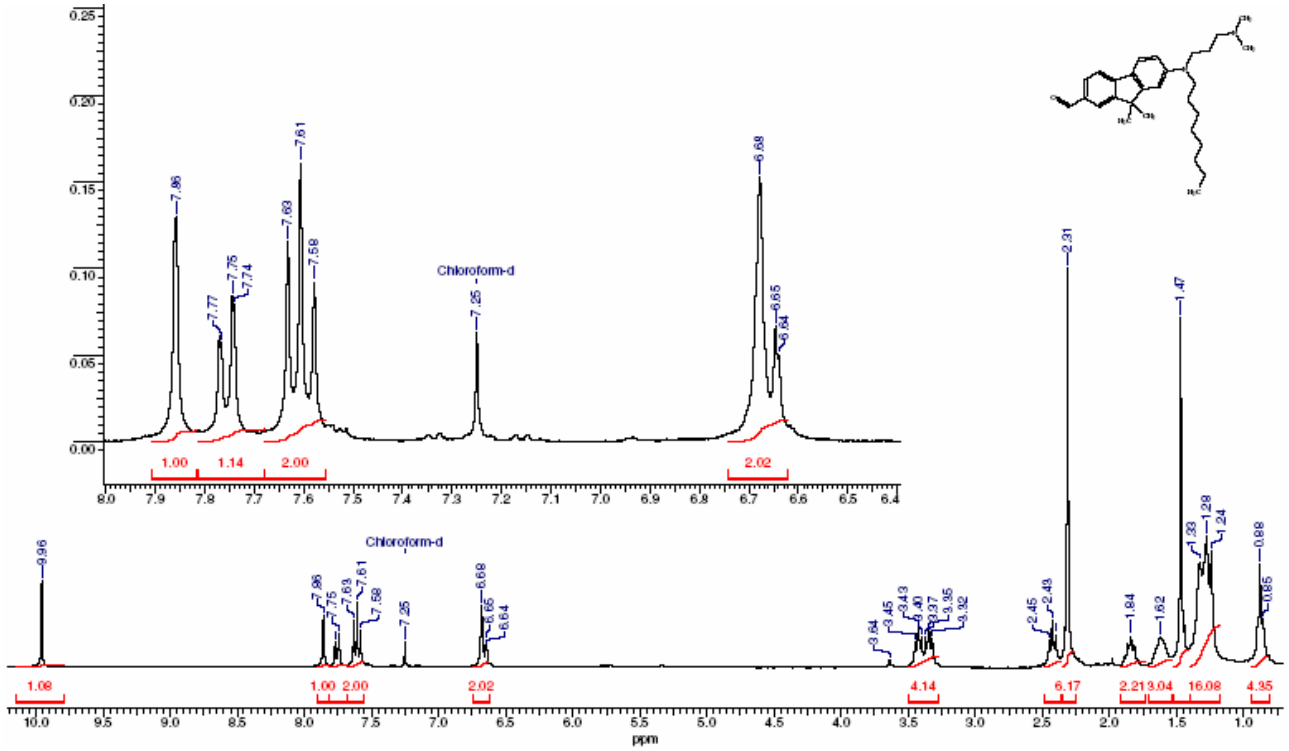

Figure 7.19. ^{1}H NMR spectrum of compound **58**.

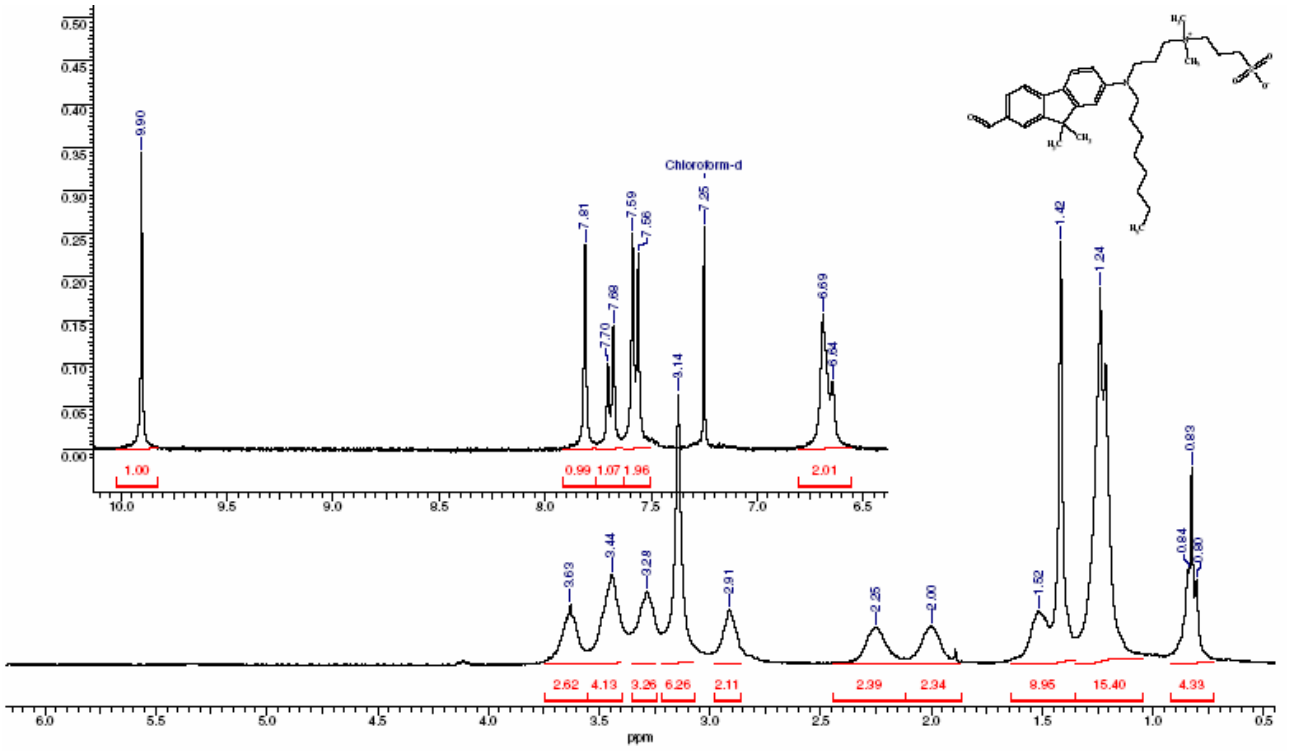

Figure 7.20. ^{1}H NMR spectrum of compound **59** (Probe **24**).

Figure 7.21. Fluorescence solvatochromism of 3-methoxychromone derivative (compound **44**).

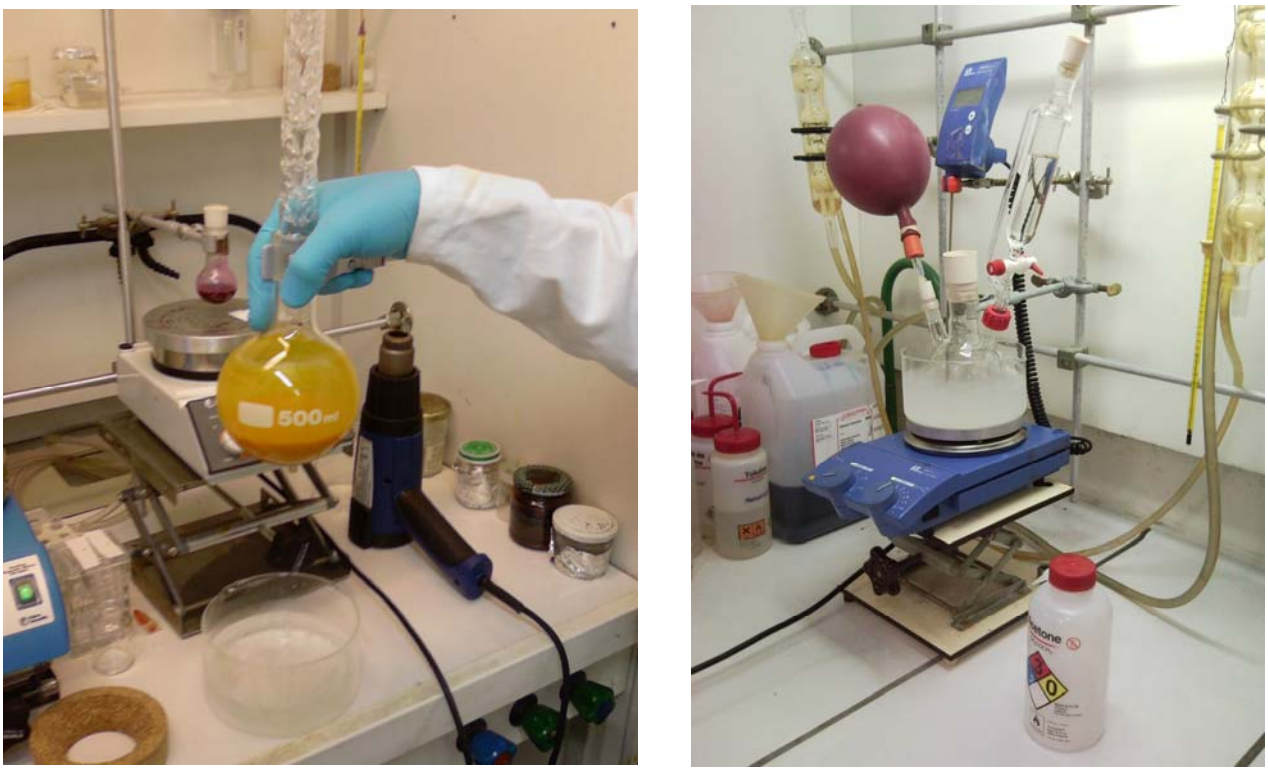

Figure 7.22. Chemical synthesis of compounds.

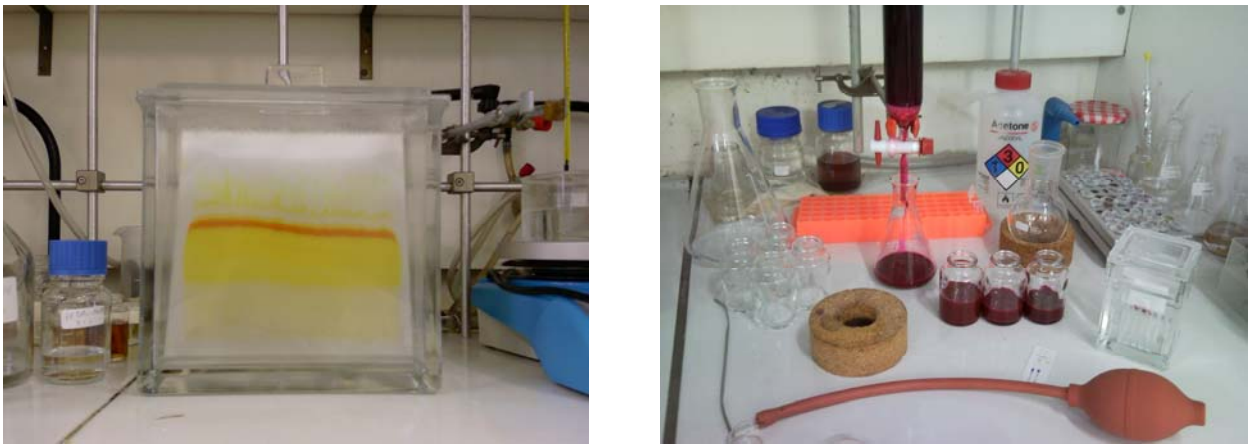

Figure 7.23. Purification of compounds by: preparative TLC (left), column chromatography (right).

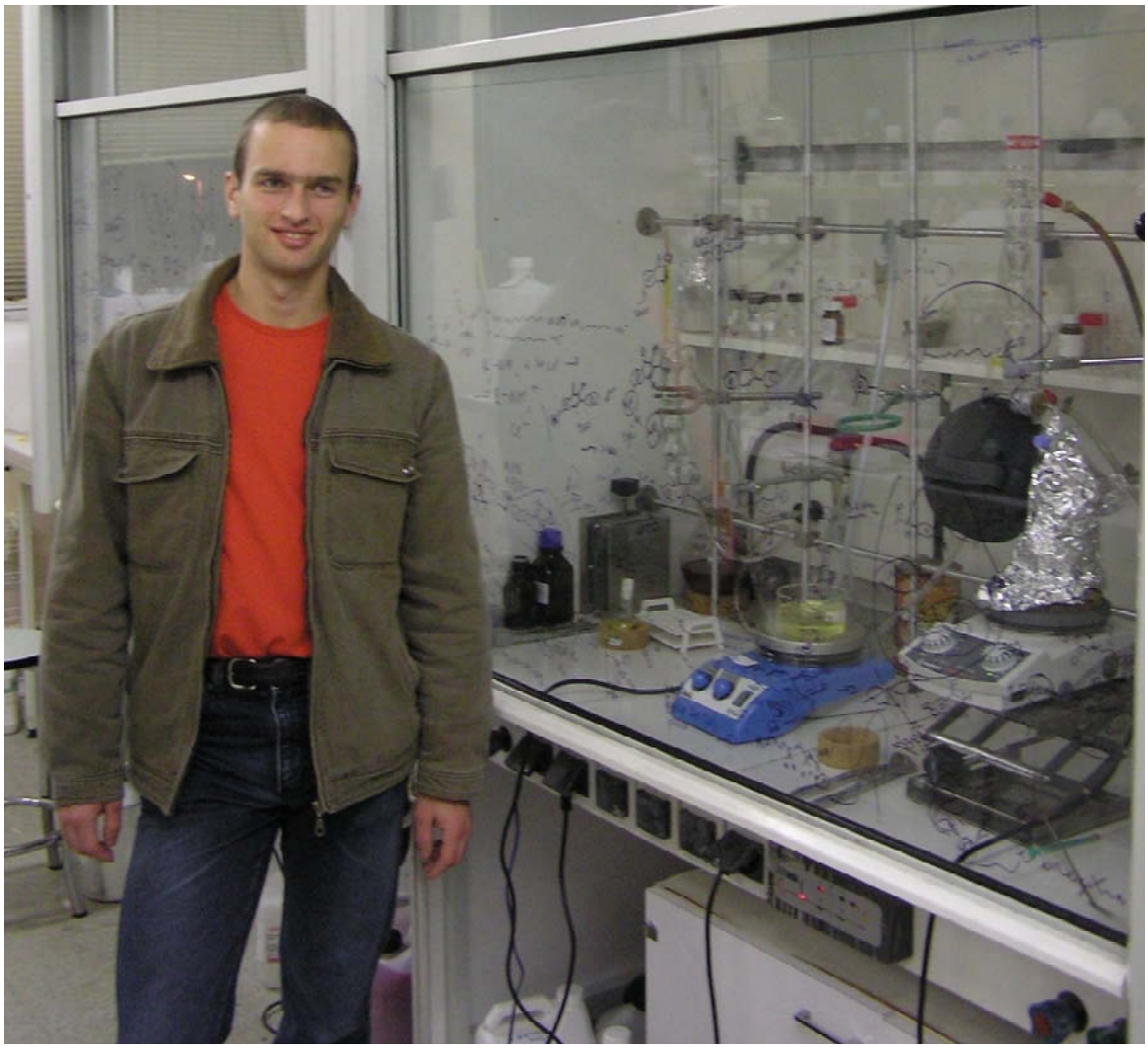

Figure 7.24. Fellow O. Kucherak after a long working day in the lab.

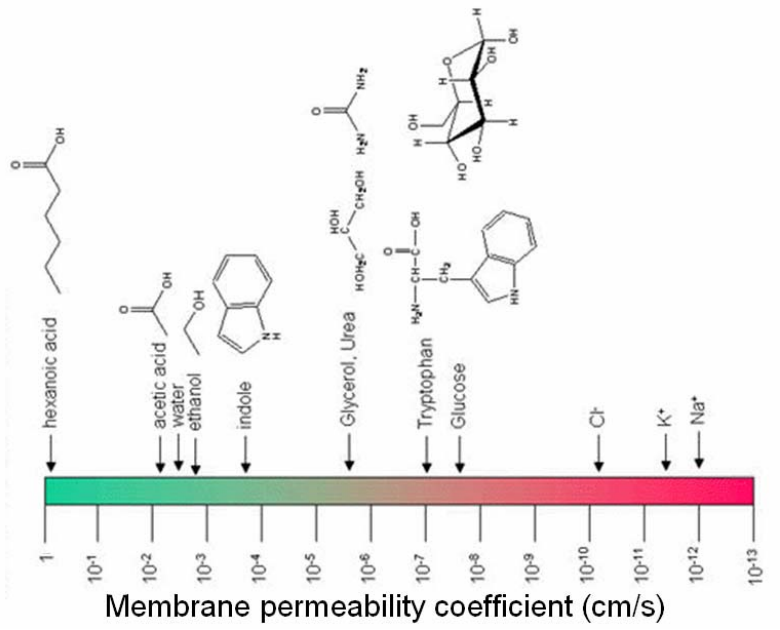

Figure 7.25. Membrane permeability barriers to polar and ionic substances.

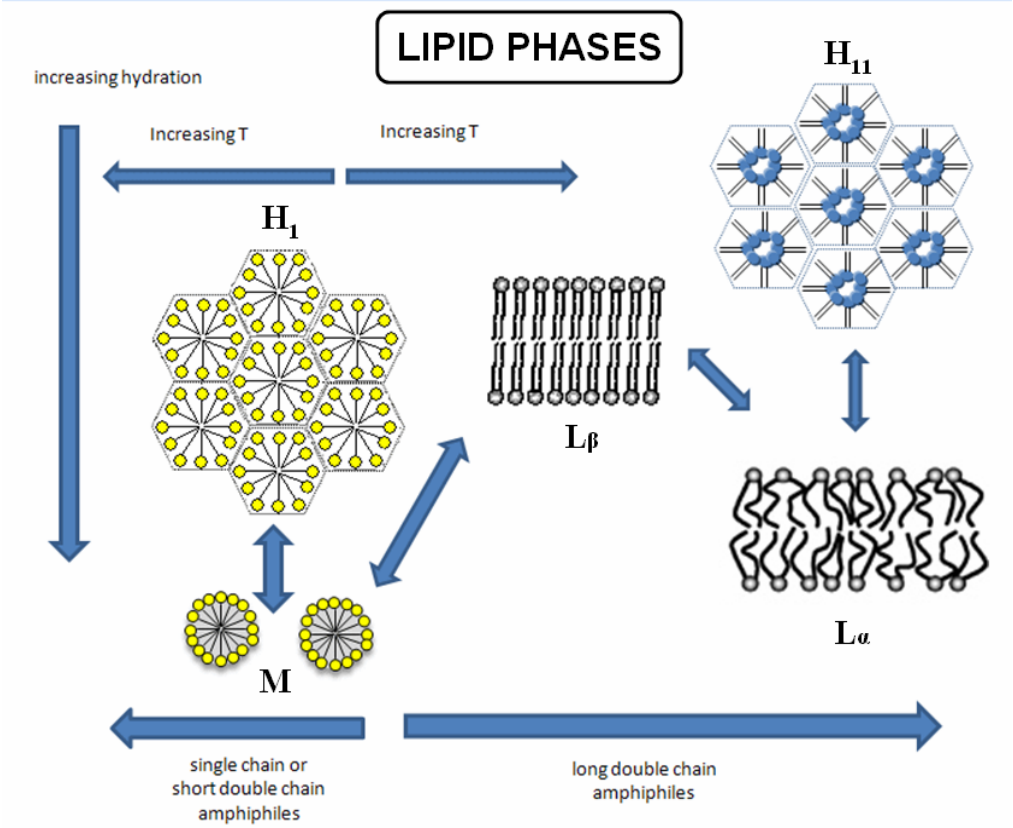

Figure 7.26. The most common types of lipid phases: lamellar liquid crystalline phase (Lα), lamellar gel phase (Lβ), micellar phase (M), hexagonal H_I (cylinders packed in the shape of a hexagon with polar heads facing out into water), hexagonal H_{II} (cylinders packed as hexagon with chains pointing out as in reverse micelles)

Résumé

Les sondes fluorescentes sont d'importants outils pour l'étude des processus biologiques. Ainsi, la première sonde ratiométrique capable de détecter l'apoptose (F2N12S) a récemment été développée au laboratoire. Cette sonde, qui se fixe sur le feuillet externe des membranes plasmiques des cellules, détecte la perte de l'asymétrie lipidique transmembranaire résultant de l'apoptose. Le but du présent travail est de développer des sondes fluorescentes pour l'apoptose présentant des caractéristiques améliorées permettant de palier certains défauts de F2N12S. Nous avons tout d'abord effectué une étude systématique de F2N12S sur membranes modèles et cellules afin de mieux comprendre ses mécanismes de réponse à l'apoptose. Nous avons découvert que l'apoptose induit non seulement une modification de la charge surfacique du feuillet externe, mais également de son hydratation et de son état de phase, expliquant ainsi la réponse de la sonde. Ceci a été confirmé par des expériences d'extraction du cholestérol, induisant des modifications des spectres de fluorescence similaires à celles observées lors de l'apoptose. Ensuite, nous avons synthétisé une vingtaine de nouvelles sondes membranaires, qui ont été classées en trois catégories en fonction de leur réponse obtenue sur membranes modèles. Une première catégorie montre une sensibilité presque nulle vis-à-vis de l'état de phase, mais nettement améliorée vis-à-vis de la charge surfacique (>3 fois), comparée à F2N12S. Une seconde catégorie montre une meilleure sensibilité à l'état de phase comme à la charge surfacique. Une troisième catégorie, dérivée du Rouge Nil, est sensible seulement à l'état de phase. De façon surprenante, les sondes uniquement sensibles à la charge surfacique ne montrent qu'une très faible réponse à l'apoptose, ce qui n'est pas le cas des deux autres types de sonde, sensibles à l'état de phase et qui montrent une réponse spectrale significative à l'apoptose. En se basant sur ces résultats, nous avons proposé des principes généraux pour la conception de sondes membranaires fluorescentes. Enfin, nous avons décrit deux nouvelles classes de fluorophores sensibles à l'environnement basés sur les résidus fluoréne et 3-methoxychromone afin d'élaborer de nouvelles sondes membranaires. Ces nouveaux fluorophores ont montré des propriétés spectroscopiques intéressantes, telles qu'une forte luminosité, une excellente photostabilité et un solvatochromisme exceptionnel. Les premières tentatives pour convertir ces fluorophores en sondes membranaires ont été décrites. Nous escomptons que les résultats obtenus stimulent la recherche pour obtenir de nouveaux outils moléculaires pour l'imagerie de fluorescence des membranes cellulaires.

Abstract

Fluorescent dyes are of great importance for investigation of biological processes. Recently, the first ratiometric fluorescent probe for apoptosis detection (F2N12S) was developed in our laboratory. This probe, being bound to the outer leaflet of the cell plasma membrane, detects the loss of the transmembrane lipid asymmetry that occurs on apoptosis. The aim of the present work was to develop improved fluorescent apoptosis probes that will overcome the drawbacks of F2N12S. Primarily, we performed systematic studies of F2N12S in model membranes and cells to better understand the mechanism of its response to apoptosis. We found that in addition to surface charge, the membrane hydration and phase state are changed on apoptosis, thus explaining the spectroscopic response of the probe. This conclusion was confirmed by experiments with cholesterol extraction from cell membranes, which showed similar changes in the fluorescence spectra as those observed on apoptosis. On the second step, we have synthesized about 20 new membrane probes, which were classified into three types according to the experiments in model membranes. The first type of dyes showed nearly no sensitivity to the phase state while their sensitivity to the surface charge was much higher (>3-fold) as compared to F2N12S. The second type showed improved sensitivity both to the surface charge and to the phase state of the lipid bilayers. The third type, which was based on Nile Red, was sensitive only to the phase state. Surprisingly, the probes that were sensitive only to the surface charge showed very poor response to apoptosis while the other two types of probes, that were sensitive to the lipid phase state, revealed a significant spectroscopic response to apoptosis. Basing on these results we proposed general principles for the design of fluorescent membrane probes. Finally we described two new classes of environment-sensitive fluorophores on the base of fluorene and 3-methoxychromone units for further construction of new advanced membrane probes. These new fluorophores showed attractive spectroscopic properties, such as high brightness and photostability as well as an exceptional fluorescence solvatochromism. The first attempts to convert these fluorophores into membrane probes were also described. We expect that the obtained results should stimulate the research in the field of biological membranes and the development of new molecular tools for fluorescence imaging.